Configurational properties of polyphenylene precursor polymers

John Richard Holland

CONFIGURATIONAL PROPERTIES OF POLYPHENYLENE PRECURSOR POLYMERS.

October 1993

John Richard Holland

University of Durham

Supervisor

R.W.Richards

University of Durham

Abstract

The configurational changes of a soluble precursor polymer, poly(5,6-dimethylcarboxycyclohexadi-1,3-ene) have been studied during it's conversion to poly(phenylene) by thermal aromatisation. This was performed principally in solution in N-methylpyrrolidinone and chloroform, by size exclusion chromatography, viscometry and scattering techniques.

The results show the polymer is initially a random coil, and during aromatisation stiffens to a wormlike chain, the intermediate to the rodlike molecule. This is evidenced by increased persistence length and increased dependency of size on molecular weight.

The conversion to a stiffer molecule is accompanied by chain scission, more pronounced for high molecular weight polymers, and agglomeration, with consequential increased polydispersity and scatter in results. At 30% aromatisation aggregates dominate the behaviour of the solution, and at 40% the polymer becomes insoluble. Results from each technique differ according to the relative sensitivity to the two species present.

Aggregates exist as low as 10% aromatisation, suggesting the formation of contiguous phenylene nuclei, dispersed phenylene would not cause aggregation. When separated from the solution the aggregated species was found to be only slightly more aromatised than the free chain equivalent, and chemically very similar, suggesting aggregation arises from the arrangement rather than the quantity of phenylene monomers.

The scattering behaviour of lightly aromatised polymer conformed to a wormlike chain model, while the aggregated polymer's scattering is close to that of a star model, suggesting a fringed micelle structure with a core of closely packed phenylene blocks, and arms preferentially composed of precursor polymer, with randomly dispersed phenylene. The insolubility of partially aromatised poly(DHCD-DMC) is common to other studies of polymers with conjugated backbones in which change from a good to a poor solvent causes a change from random coil to aggregated stiff chains.

Acknowledgements

Thanks are due to the following people and organisations who assisted in the study described within this work.

Primarily thanks are due to Randal Richards for his supervision, support and forbearance.

To ICI PLC for provision of all polymer materials, for financial support, and to Andrew Burgess and Alan Nevin, industrial supervisors, from the Heath Laboratories of ICI at Runcorn, for practical and nutritional support. To SERC for the research funding, to the staff of the Chemistry Department, especially Ray and Gordon the glassblowers and Alan Kenwright on the NMR and Gordon on the SEC.

To the staff of the ILL and Rutherford-Appleton laboratories for assistance with SANS experiments, especially Steve King. Not forgetting my fellow workers at Durham, Gail, Gary, Jim, John and Robin, the Strathclyde irregulars, Mark, Steve and Tall Paul. Last and by no means to my family for their support, especially Gwyn, Owain and William, without whom ...

To Gwyn

INDEX

Declaration

All work contained within this thesis is my own work, unless stated otherwise, and has not previously been submitted for any other qualification

John Richard Holland

October 1993

CHAPTER 1

1.1 POLYPHENYLENE

1.1.1 Introduction

Poly(paraphenylene)(PPP) is a chemically simple polymer(figure 1.1) which would have remarkable thermal, chemical, electrical and mechanical properties, making it a desirable material if it could be synthesised with a high degree of polymerisation. Its structure of 1,4-coupled phenyl rings avoids bridging groups, the esters, carbonyls, amides, imides and hydrocarbons that render the standard aromatic engineering polymers susceptible to thermal, chemical and radiation damage. PPP is therefore suitable for use in more extreme environments than other carbon based polymers.

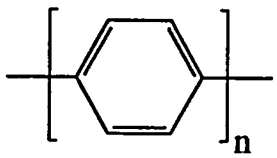

Figure 1.1:Poly(paraphenylene)

The polymer chain is highly conjugated, and it can be doped *via* oxidation, increasing conductivity from that of a very good insulator ($\approx 10^{-10}$S cm^{-1}) to that of a semiconductor ($\approx 10^{2}$S cm^{-1}). It would also be expected that the highly conjugated structure and high crystallinity would give the polymers good mechanical strength. Another application recently developed for PPP utilising its novel properties is in light emitting diodes[1].

There are however a number of possibly insurmountable problems associated with PPP. The polymer degrades below its crystalline melting point, so that melt processing is impossible. It is also insoluble in any known solvent, and the only method that has been applied to its fabrication is sintering[2], which produces a porous product of inferior properties. The synthesis of poly(paraphenylene) is also problematic, and until recently no method of synthesis has produced PPP with regular structure and high molecular weight[3]. Solution methods precipitate oligomers at modest molecular weights (DP≈10),

and solid state methods produce polymers of similarly low molecular weight, partly due to the formation of dense crystallites restricting mobility, which are difficult to purify.

A number of syntheses have been attempted, and they fall into two categories; direct synthesis or precursor routes.

1.1.1 Synthesis Of Polyphenylene

1.1.1a Conventional polymerisation

Kovacic *et al* polymerised benzene cationically with a Lewis acid-oxidant system, $AlCl_3$ and $CuCl_2$[4]

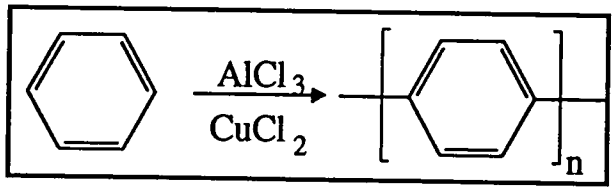

Reaction 1: Kovacic reaction

However the reaction requires large quantities of copper chloride, and the product contains considerable impurities. Copper(II) Chloride can be replaced with other metal halides, though these are far less effective. The polymer is darkly coloured and of low molecular weight, typically 10-15 rings, with many structural defects and some crosslinking.

Yamamoto[5] synthesised PPP by the polymerisation of a parahalobenzene with a coupling reaction with magnesium metal, catalysed by Ni(II);

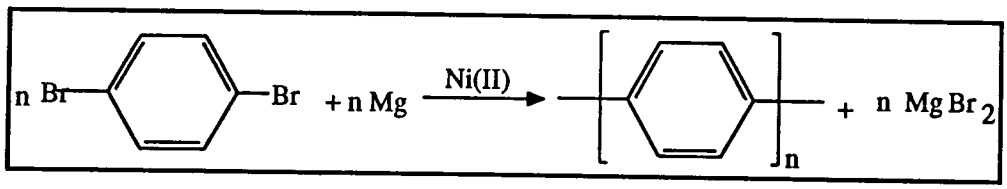

Reaction 2: Yamamoto synthesis

This is similar to the Wurtz-Fittig reaction, but requires milder conditions and can produce high yields at 0°C. The product is cleaner than that of Kovacic, but again only achieves a low degree of polymerisation, in the order of 10 to 12 rings long.

Benzene has been polymerised by electrochemical means[6] in a variety of solvents; SO_2, HF, $LiAsF_6$, CF_3SO_3H. The solution is electrolysed with platinum electrodes and a

poly(paraphenylene) film forms at the electrode. These films are of generally lower conductivity than that from the methods described above, attributed to structural defects. The DP is of the order of 10-14.

The insolubility and intractability of polyphenylene has been approached in two separate ways. One is to put flexible side chains onto the polyphenylene backbone[7,8], which renders the polymer soluble although it does diminish the desirable properties of the material.

1.1.1b Precursor Polymers

Polyphenylene can also be synthesised *via* a precursor polymer which can be fabricated into the required shape and converted to PPP. All methods to this end have centred around non-aromatic cyclohexadiene polymers .The first attempt was that of Marvel[9]. Cyclohexadiene was polymerised with cationic or Ziegler initiators.

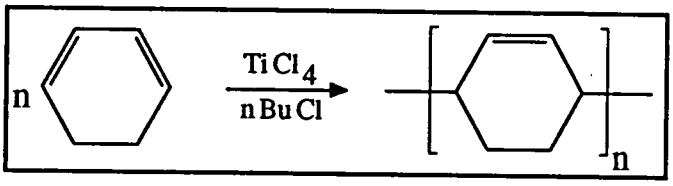

Reaction 3: Marvel synthesis

This polymer could be produced in high yield at molecular masses up to 20,000, and was soluble in benzene, toluene and carbon disulphide. It could be aromatised to polyphenylene by reaction with bromine, followed by pyrolytic debromination, or by reaction with Pd, S, or N-bromosuccinide. The product was a tan coloured polymer, with considerable bromine impurities.

Another, somewhat unusual, precursor method is that due to François and Zhong[10]. Cyclohexadiene was copolymerised with polystyrene using secondary butyl lithium as the initiator. The result is a block copolymer of PS-co-1,4-PCHD with sequences of DHCD up to ≈100 monomer units long. The aromatisation follows the same method as Marvel and a soluble polymer is produced, although with a tendency to agglomeration. This polymer has been cast into films, and pyrolised to pure polyphenylene at 420°C.

The PPP products were estimated to have a DP of 10. The polymers became conducting when doped.

A third route uses disubstituted cyclohexadiene (DHCD) monomer which is free radically polymerised, and can be thermally pyrolysed to PPP without recourse to further reagents, producing volatile by products which are driven off leaving a polymer of high purity. This synthesis has been approached *via* two routes, giving essentially the same product. The method of Stille and McKean[11] follows conventional synthetic chemistry;

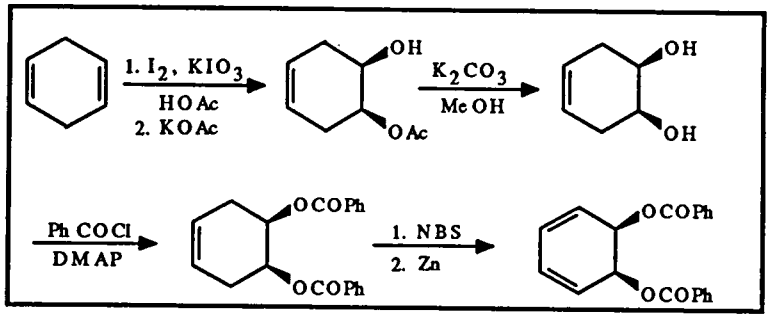

Reaction 4: Stille and McKean synthesis of DHCD derivatives

The diester is the monomer which is free radically polymerised. Ballard *et al* produced the monomer base *via* the bacterial oxidation of benzene[12]. This has the advantage of absolute stereospecificity; and may be the reason why the Ballard group obtained higher molecular weight products for the dicarboxyl derivative(table 1.1).

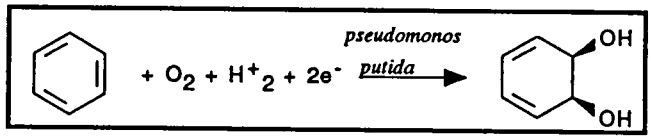

Reaction 5: Ballard *et al* synthesis of DHCD

Derivative	Method	Molecular weight(w-av.)	M_w/M_n	Yield	T_p
Dicarboxyl	Stille/bulk	30,000	1.2	35%	181
Dicarboxyl	Ballard/bulk	140,000	2.4	61%	185

Table 1.1: Comparison of poly(paraphenylene) precursor polymers

Dihydroxycyclohexadiene(DHCD) is derivatised using an acid chloride or anhydride together with a pyridine catalyst. For example the dimethylcarbonate monomer;

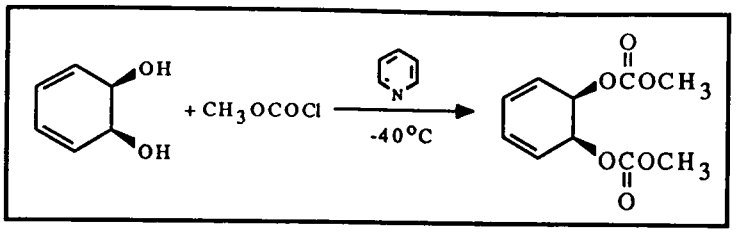

Reaction 6: Derivatisation of DHCD-DMC

This type of monomer has only been successfully polymerised free radically, although another derivative, the trimethylsilane, has been polymerised with transition metal catalysts[13]. Azobis(isobutyronitrile)(AIBN) is the favoured initiator, and the mixture is polymerised in the melt at 50-70° C, a lower temperature than that generally used for free radical reactions to reduce the amount of chain transfer.

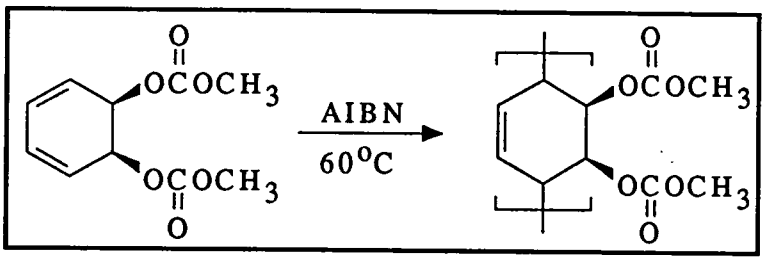

Reaction 7: Polymerisation of DHCD-DMC

The precursor polymer had a degree of polymerisation of the order of 1000's and is soluble in common place solvents, acetone, chloroform and N-methyl-Pyrrolidinone(NMP). The final stage is pyrolytic aromatisation, a generally facile reaction which can be undertaken as a solid, or in NMP. The reaction is base catalysed, either by NMP, or by basic salts in the solid.

The properties of the final polymer depend on the reaction by-products being wholly expelled from the bulk. This can be aided by the selection of a suitable leaving group. A number of substituents were prepared by both groups, including acetate, pivalate, methyl ether, benzoate and methoxycarbonate. The latter is found to be most satisfactory as a leaving group. The acid formed, methoxycarboxylic acid, is unstable and decomposes to methanol and carbon dioxide, small molecules which can more easily diffuse out of the polymer.

The aromatisation reaction does not proceed at an even rate, but has a induction time, the reaction then accelerates abruptly and proceeds at an increasing rate until it is about

70% complete[12]. This is attributed to an autocatalytic effect, whereby the aromatisation of cyclohexane is facilitated by the presence of neighbouring phenylene groups. This would cause reaction to proceed sequentially along the polymer chain, a 'zipping mechanism'. The sequential reaction may be terminated by the effects of chain defects(see following paragraph), the end of the chain or chain scission, and this must be the case or once a chain had started to aromatise it would rapidly continue to completion, the chain would become insoluble and precipitate, however this is not observed in practice.

The polymers of DHCD derivatives were found to contain a proportion of 1,2-bonded units in the polymer backbone, caused by chain transfer reactions. Ballard and Stille quantify the ortho-bonding by proton nuclear magnetic resonance spectroscopy attributing the to it the signal at ≈2.0ppm, both sets of authors found the 1,2 bonds to constitute ≈15% of the main-chain bonds. Ortho-bonding leads to kinks in the chain which are susceptible to fracture during the aromatisation reaction, especially in the solid state. The polymer aromatised in the solid state can be reduced to a degree of polymerisation as low as seven on full aromatisation. This is in the same range as the more conventional methods outlined above, although the advantages of greater purity and intermediate are retained. Full mechanical properties are unlikely to be achieved from this polymer, but studies on polyacetylene suggest molecular weight does not dictate electrical properties[14], and the conductivity obtained, ≈100 s cm^{-1}, is comparable to the highest values obtained by other workers. It is suggested that poly(paraphenylene) oligomers are further polymerised by the presence of the dopant AsF_5[15]. It would appear that although recent work[16,17] suggests some progress has been made, the synthesis of high molecular weight linear polyparaphenylene is still someway off.

1.2 CONFIGURATION OF POLYMER CHAINS

1.2.1 Random Coil Chains

A polymer chain containing a large number of monomer units having a degree of rotational freedom around the main chain bonds can describe an almost infinite number of different configurations, to form a variety of different shapes. However in practice energetic considerations and steric and geometric restrictions mean there is a limited number of more probable configurations. To rationalise the situation a number of molecular models have been developed which can be used to describe polymer configurations.

In the simplest case of a freely jointed chain of n bonds, length l, the configuration of the chain may be treated in terms of the random flight described by Lord Rayleigh[18]. The mean projection, $\langle l_x \rangle$, of a bond on a particular axis, x, will be given by;

$$\langle l_x \rangle = \int_0^l l_x p(l_x) dl_x \qquad (1.1)$$

Where $p(l_x)dl_x$ is the probability that the projection lies between l_x and $l_x + dl_x$, and the mean square value is;

$$\langle l_x^2 \rangle = \int_0^l l_x^2 p(l_x) dl_x \qquad (1.2)$$

which can be shown[19] to reduce to;

$$\langle l_x^2 \rangle = \frac{l^2}{3} \qquad (1.3)$$

The probability that the displacement of one chain end from the other will be dx is given by

$$W(x)dx = \left(\frac{\beta}{\pi^{1/2}}\right) e^{-\beta^2 x^2} dx \qquad (1.4)$$

where $\beta = [1/(2\, n\langle l_x \rangle)]^{1/2} = (3/2nl)^{1/2}$. If this is extended to three dimensions then the probability of finding one chain end being displaced to a finite element (dx,dy,dz) from the other, located at the Cartesian origin, is given by the Gaussian function

$$W(x,y,z)dxdydz = W(x)W(y)W(z) = \left(\frac{\beta}{\pi^{1/2}}\right)^3 e^{-\beta^2 r^2} dxdydz \qquad (1.5)$$

where r is the magnitude of the chain end displacement vector **r**, as shown in figure 1.1

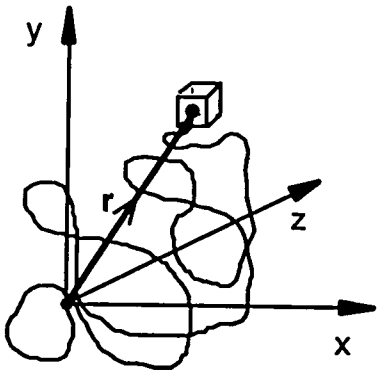

Figure 1.1, Representation of random flight chain

The probability that **r** will have a certain magnitude irrespective of direction is W(x,y,z) × sum of volume elements r from origin, ($4\pi r^2.dr$). The probability, W(r), of the chain end displacement being between r and dr is

$$\mathbf{W(r)dr} = \left(\frac{\beta}{\pi^{1/2}}\right)\mathbf{e}^{-\beta^2 r^2}\,\mathbf{4\pi r^2 dr} \tag{1.6}$$

This probability function is plotted in figure 2. The mean value of r will be given by

$$\langle \mathbf{r} \rangle = \int_0^\infty \mathbf{r W(r)dr} \Big/ \int_0^\infty \mathbf{W(r)dr} \tag{1.7}$$

(1.8)

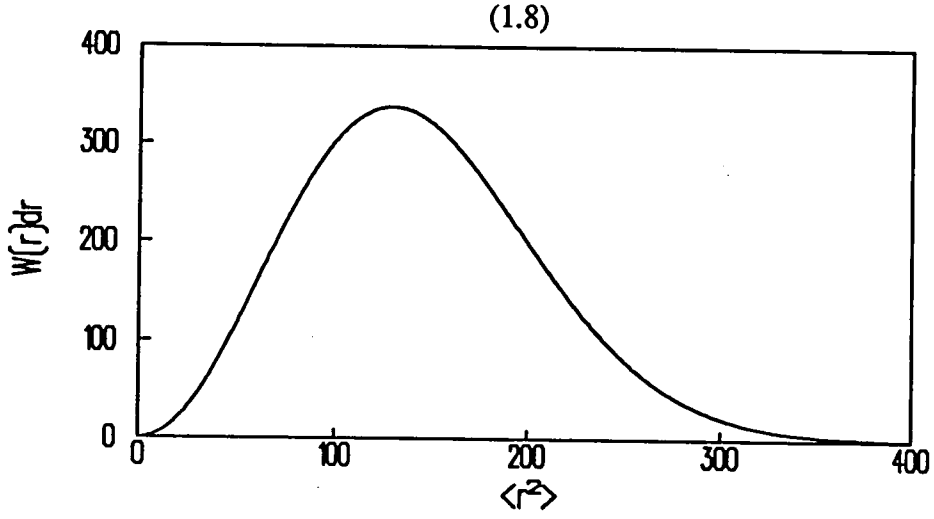

Figure 1.2: Distribution of end to end distance of a Gaussian chain of 10,000 segments of length 2.5Å

The integral of W(r)dr will be unity, therefore by substituting (6) we get;

$$\langle \mathbf{r} \rangle = \frac{2}{\pi^{1/2}\beta} \tag{1.8}$$

And similarly for the mean square value;

$$\langle \mathbf{r^2} \rangle = \frac{3}{2\beta^2} \tag{1.9}$$

Substituting for β in (9) gives;

$$\langle r^2 \rangle = nl^2 \qquad (1.10)$$

The mean square distance of a chain element from the centre of mass, usually termed the mean square radius of gyration, $\langle s^2 \rangle$, can be shown to be[20];

$$\langle s^2 \rangle = \frac{nl^2}{6} \qquad (1.11)$$

so that for the model of the random coil polymer the mean square end to end distance and the mean square radius of gyration are interchangeable, using the relation;

$$\langle s^2 \rangle = \frac{\langle r^2 \rangle}{6} \qquad (1.12)$$

The model of the linear random flight chain is unrealistic and incomplete from the respect of structural restrictions or conformational statistics of polymer chains. It is therefore necessary to consider the cases of short range interference and stiff chains. Bond restrictions for a fixed bond angle of θ causes the chain to expand by $[(1-\cos\theta)/(1+\cos\theta)]^{1/2}$, which is $\sqrt{2}$ for the carbon-carbon single bond. The most significant of the conformational effects is the pentane effect between the first and fifth chains in a sequence between which energy is at a minimum when they lie adjacent.

Kuhn describes a model that more closely approximates to a true polymer chain. This represents the polymer as an equivalent chain of freely jointed segments each of which is the displacement vector of a sequence of N monomer units of restricted rotation.

Kuhn showed that, although as in figure (3) the step lengths differ, the correct statistical distribution of displacement lengths for the whole chain is obtained by replacing the step length with one of the root mean length of the number, n_k, of bonds that it replaces.

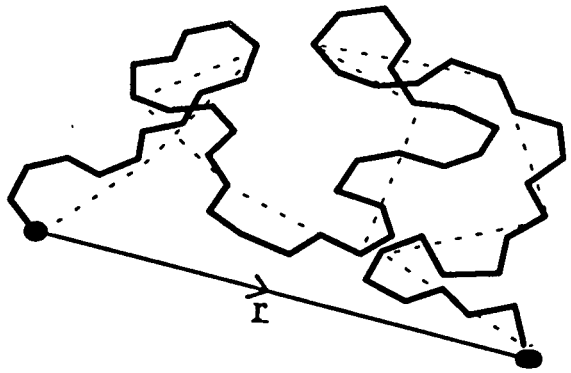

Figure 1.3; Representation of Kuhn model of chain with 5 monomer units per step length

Here again we have the situation of a random flight chain; fixed length and wholly random direction, simply with β changed from $\left(\frac{3}{2l^2n}\right)^{1/2}$ to $\left(\frac{3}{2\lambda^{-2}n_k}\right)^{1/2}$

where the chain consists of n_k segments of length λ^{-1}. The definition of n_k and λ^{-1} is problematic, in effect λ^{-1} could be any small number of statistical units so the condition of a random flight chain still applies. In practice the terms are defined with reference to $\langle r^2 \rangle$ at full extension, L_r. In the simplest case of vinyl polymers[21] we have;

$$L_r = nl.\sin\left(\frac{\theta}{2}\right) \qquad (1.13)$$

where θ is the covalent bond angle of the main chain bonds. For these chains the mean square end to end distance is defined;

$$\left\langle r^2 \right\rangle = nl^2 \frac{1-\cos\theta}{1+\cos\theta}\sigma^2 \qquad (1.14)$$

where σ is a conformation factor, taking into account the effects of steric hindrance to rotation, accounting for the difference in the true value of $\langle r^2 \rangle$, $\langle r^2 \rangle_e$, and the freely rotating model $\langle r^2 \rangle_f$;

$$\left\langle r^2 \right\rangle_e = \left\langle r^2 \right\rangle_f \sigma^2 \qquad (1.15)$$

σ for poly(ethylene) is in the order of 2, and is independent of n for high polymers. The definition of n_k is;

$$n_k = \frac{L_r}{\left\langle r^2 \right\rangle} \quad \text{or by substitution} \quad n_k = \frac{n}{2\sigma^2}(1-\cos\theta) \qquad (1.16)$$

and for l_k;

$$\lambda^{-1} = \frac{\langle r^2 \rangle}{L_r} \qquad \text{or by substitution} \qquad \lambda^{-1} = \frac{2l \sin(\theta/2)}{1+\cos\theta} \qquad (1.17)$$

The parameter characteristic ratio is a function of the ratio $\langle s^2 \rangle / M$, it's value for a random coil chain is constant, i.e.; $C_\infty \propto \langle s^2 \rangle / M$, but $M = m \times n \times a$, where m is the mass per unit of a chain of n units length a, and with eqn. 1.11 this gives;

$C_\infty \propto \frac{a}{m}$, since both a and m are constants for a given chain, C_∞ too is constant for a given chain.

1.2.1a Unperturbed polymers and the effects of excluded volume

Up to this point polymer chains have been considered in isolation. This is an unlikely concept, and for purposes of study a polymer molecule will either be in a solid matrix of polymer or in a solution. The solvent can vary in quality. A good solvent is one in which the interaction between polymer and solvent is energetically favourable compared to that of the polymer with itself. A polymer molecule in a good solvent will tend to expand to maximise its contact with the solvent, leading to an extended configuration and increased $\langle r^2 \rangle$. This is described as a long range effect (cf. steric hindrance and the restrictions on free rotation which are short range but have a similar effect). Polymers in such a condition are said to possess excluded volume, space within the polymer coil that is denied to a segment because it is already occupied by another segment from which it is widely separated on the chain. In contrast a poor solvent is one where the polymer-polymer interaction is favoured over polymer-solvent. A polymer in a poor solvent will adopt the random flight configuration, as short range effects allow. As solvent quality is changed from good to poor so that the polymer-polymer interaction becomes progressively more favourable, at the expense of the polymer-solvent interaction, a point is reached where the strength of the polymer-polymer interaction balances that of perturbation, so that excluded volume vanishes. The polymer is then said to be in an unperturbed state, the theta condition. This can be achieved by changing the temperature of the solvent, or by changing the composition of a mixed solvent. The properties are

denoted by a subscript 0, $\langle r_0^2 \rangle$. The properties of a perturbed polymer (in a good solvent) are related to the unperturbed by an expansion factor, α;

$$\langle r^2 \rangle = \alpha \langle r_0^2 \rangle \tag{1.18}$$

and similarly

$$\langle s^2 \rangle = \alpha \langle s_0^2 \rangle \tag{1.19}$$

The unperturbed dimensions are determined from intrinsic viscosity measurements, or by scattering techniques (light, X-rays and neutrons). It was predicted[17] and subsequently experimentally confirmed[22] that polymer chains in the solid state adopt unperturbed dimensions.

1.2.2 Rigid rod configuration

The rigid rod configuration, where the polymer molecule is represented by a single straight rod is a mathematically more simple case. The mean square end to end distance is obviously the square of the length;

$$\langle r^2 \rangle = l^2 \tag{1.20}$$

The radius of gyration is defined as;

$$\langle s^2 \rangle = \frac{l^2}{12} \tag{1.21}$$

The rigid rod model is however as simplistic and unrealistic as the random flight coil for high polymers and is not a particularly useful model

1.2.3 Wormlike chain models

Between the extremes of the random coil and the rigid rod models lie the vast majority of real polymers, better described by intermediate models. These are generally termed wormlike chains. The concept was first introduced by Kratky and Porod[23] for X-ray studies of vinyl and cellulose polymers. The model they describe is a continually curving chain, which is represented in terms of n segments of length l and bond angle ϕ, not the valence angle. The chain dimensions are defined in terms of the contour length , L, and

the persistence length, a. The contour length is the end to end distance at maximum extension, L=nl. If one end of the chain is taken to be the origin of a three dimensional system with the first segment in the z direction, then the persistence length is the average distance over which the trajectory in the z direction persists. Persistence length is a useful comparative measure of chain stiffness. If the chain is represented in terms of progressively smaller l and larger n, with smaller ϕ between them, while retaining values of a and L, then $\langle r^2 \rangle$is defined as the limit as $n \to \infty$, $l \to 0$, and $\phi \to 0$;

$$\langle r^2 \rangle = 2al - 2a^2\left[1 - e^{-\frac{L}{a}}\right] \qquad (1.22)$$

The limits of (22) give the solutions

$$\lim_{a \to 0} \langle r^2 \rangle = 2aL = 2a.nl \qquad (1.23)$$

equivalent to the Kuhn random coil, with the persistence length = $l_k/2$

$$\lim_{a \to \infty} \langle r^2 \rangle = L^2 \qquad (1.24)$$

equivalent to a rigid rod.

The mean square radius of gyration of the wormlike chain is given by [24];

$$\langle s^2 \rangle = \frac{aL}{3} - a^2 + \frac{2a^3}{L}\left[1 - \frac{a}{L}\left(1 - e^{\frac{L}{a}}\right)\right] \qquad (1.25)$$

by substituting;

$$L = \frac{M}{M_L}$$

where M is mass and M_L is mass per unit contour length, (25) can be approximated for less stiff chains[25] to;

$$\left(\frac{M}{\langle s^2 \rangle}\right)^{1/2} = \left(\frac{3M_L}{a}\right)^{1/2}\left(1 + \frac{3aM_L}{2M}\right) \qquad (1.26)$$

therefore a plot of $(M/\langle s^2 \rangle$ vs. m^{-1} yields a and M_L .

The KP wormlike chain is an intermediate to the coil and rod, and can adequately describe either. It is also a useful model that can describe a wide range of real polymers. The characteristic ratio, C_∞ ($\propto \langle s^2 \rangle / M$) of a random coil chain can be shown to be independent of molecular weight. Molecular weight is proportional to the number of monomer units, n., so;

$$\frac{\langle s^2 \rangle}{n} = \frac{l^2}{6} \tag{1.27}$$

The molecular weight dependence for a wormlike chain from (25) is plotted in figure (4)

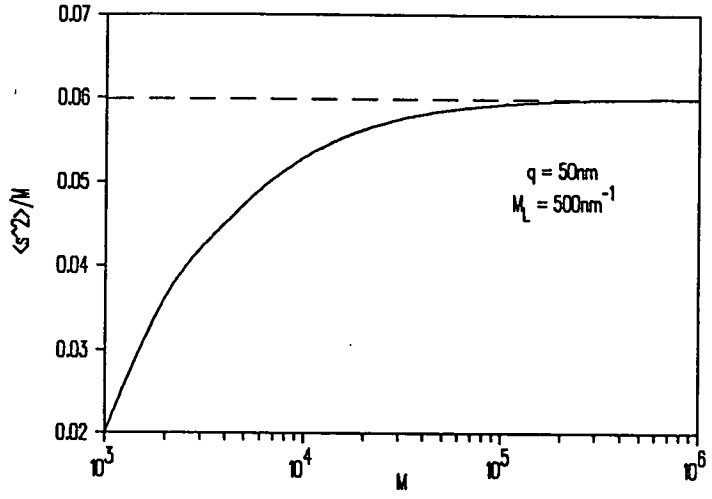

Figure 1.4, Molecular weight dependency of C_∞ for a wormlike chain(solid) and random coil(dashed).

At low molecular weights the behaviour is that of a rod, where C_∞ is proportional to M and C_∞ increases with increasing M up to the asymptotic value of an equivalent random coil. Again the KP chain can be seen as an intermediate model behaving as a rigid rod at low molecular weights and as a random coil at very high molecular weights.

1.2.3a Wire model of a wormlike chain

Several authors calculate properties of the wormlike chain by treating it as a very thin elastic wire[26,27,28] with a finite energy of bending, but without torsional energy. The wire is treated as a space curve, if c is the partial contour length measured from one end of the chain the unit tangent vector at a contour point c is $\mathbf{u}(c)$. The bending energy stored per unit of contour length at c when the chain undergoes a small deformation from the rest state will be;

$$U(c) = \frac{\gamma_0}{2}\left|\partial \mathbf{u}(c)/\partial c\right|^2 \tag{1.28}$$

where γ_0 is the bending force constant. From this Saito[25] et al show that the mean over all possible configurations is;

$$\langle \mathbf{u}(c) \cdot \mathbf{u}(c') \rangle = e^{(-2\lambda|c-c'|)} \tag{1.29}$$

where λ^{-1} is the Kuhn statistical step length. This is defined in terms of γ_0 as;

$$(2\lambda)^{-1} = \frac{\gamma_0}{k_B T} \tag{1.30}$$

where k_B is Boltzmann's constant and T absolute temperature.

The mean square end to end distance is expressed as;

$$\langle r^2 \rangle = \int_0^L \int_0^L \langle u(c) \cdot u(c') \rangle ds\, s' \tag{1.31}$$

Substitution of (1.31) gives;

$$\langle r^2 \rangle = \frac{L}{\lambda} - \frac{1}{2\lambda^2}\left[1 - e^{-2\lambda L}\right] \tag{1.32}$$

From equation (1.22) this gives the relationship between a and λ;

$$a = \frac{(\lambda^{-1})}{2} \tag{1.33}$$

which are used interchangeably and also gives a definition of persistence length;

$$\gamma_0 = k_B T a \tag{1.34}$$

1.2.3b The effects of excluded volume

The wire model of Yamakawa and Stockmayer[26] may be usefully to describe the effects of excluded volume of stiff wormlike chains. It should be noted that stiff chains are generally only soluble in good solvents, and that excluded volume effects will only occur with high values of L, i.e. towards the random coil limit.

The chain expansion factor, α_r is defined by increase of mean square end to end distance above the unperturbed value;

$$\alpha_r^2 = \frac{\langle r^2 \rangle}{\langle r_0^2 \rangle} \tag{1.35}$$

α_r is defined as a function of the number of Kuhn segment lengths in the chain;

$$\alpha_r^2 = 1 + k(n_k)z \tag{1.36}$$

where $k(n_k)$ is a function of the number of Kuhn segment lengths, values of which are tabulated in ref. 26, with an asymptotic value of 4/3. z is an excluded volume parameter;

$$z = \left(\frac{3\lambda}{2\pi}\right)^{3/2} B L^{1/2} \tag{1.37}$$

A second expansion factor is defined for the perturbations of radius of gyration α_s^2, defined as;

$$\alpha_s^2 = 1 + \frac{67}{70} k(n_k) z \qquad (1.38)$$

From experimental results of stiff chain polymers it is observed that the results obey equation (25) up to a critical length (in the order of 50 Kuhn lengths) and then deviate[29]. The deviation is ascribed to the effects of excluded volume, but is much greater than that predicted by YS theory, which predicts deviation at about 1 Kuhn segment length. Slightly better agreement was found to the YS theory for less stiff chains[30]. Calculations made on flexible polymers by Yamakawa and Shimada predicted deviation from $\alpha_s^2 = 1$ at values of n_k about 3-5, which fitted well to measurements for flexible polymers in good solvents, but this is still a long way short of 50, and at present the theory of perturbation effects in stiff chains is inadequate. This is especially problematic because stiff polymers tend only to be soluble in good solvents, and so it is not possible to determine theta properties in solution.

1.2.4 Experimental determination of chain parameters

To characterise real polymer systems in terms of the chain models outlined above it is useful to be able to determine the chain parameters for particular polymers from experimental data. There have been many methods proposed to this end, especially for the wormlike models.

1.2.4a Random coil model

The random coil model is reasonably straightforward, and its parameters can be determined with relative ease. Properties which may be determined include molecular weights (M_n, M_w and M_z), radii of gyration $\langle s^2 \rangle$, intrinsic viscosity $[\eta]$, diffusion coefficient D, and the scattering function $P(\theta)$. The characteristic ratio may be determined directly and its dependence on molecular weight examined (for a true random coil C_∞ is independent of M), and $\langle r^2 \rangle$ can be calculated from (12). If the conditions are known it is possible to collect data at the theta condition and to determine the unperturbed dimensions, and then to calculate expansion factor α at a given temperature. The unperturbed dimensions can be calculated from the two parameter plots using $[\eta]$ data (for a comprehensive treatment of this see chapter 4)

The diffusion coefficient-molecular weight dependency can be determined in terms of the relationship;

$$D = K''M^{-\nu} \tag{1.39}$$

where K'' is a constant , and ν is an exponent given by;

$$\nu = \frac{1+b}{3} \tag{1.40}$$

where b has the value 0.5 for a random coil and 1 for a rigid rod.

The scattering function $P(\theta)$ of a random coil polymer is given by;

$$P(\theta) = \left(\frac{2}{\upsilon^2}\right)\left[e^{-\upsilon} + \upsilon - 1\right] \tag{1.41}$$

where $\upsilon = Q^2\langle s^2 \rangle$,Q is the scattering vector;

$$Q = \frac{4\pi}{\lambda}\sin\left(\frac{\theta}{2}\right) \tag{1.42}$$

where λ is the wavelength of the radiation scattered, be it visible light, X-rays, or neutrons, and θ the angle at which it is measured. This gives the plot shown in figure 1.5.

By fitting (41) to scattering data it is possible to determine $\langle s^2 \rangle$. Light scattering data by virtue of the high λ, is only able to cover a small range of Q. While this is sufficient to calculate $\langle s^2 \rangle$ it is necessary to view a wider range, such as that possible in neutron scattering, to see the full function as seen in figure 1.5. In reality the plateau does not continue indefinitely. a real chain shows stiffness at some scale, so that even the most flexible chain will show an upturn to rigid rod behaviour. Conversely most stiff polymers will behave as coils at very high molecular weight. It is therefore pertinent to remember that if a polymer is to be treated as a random coil the correct molecular weight range should be studied, and that care should be exercised in extrapolation outside of this range.

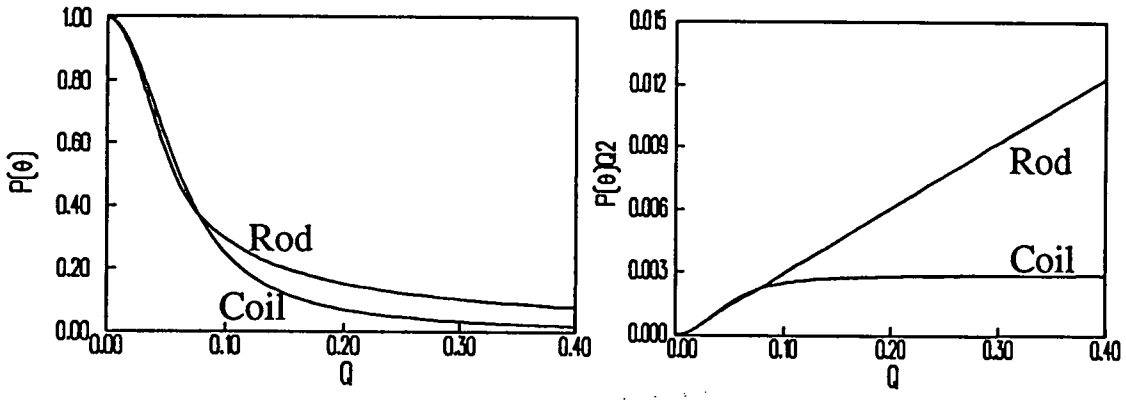

Figure 1.5: Plot of equations 1.41 and 1.43, i, intensity plot, ii, Kratky plot

1.2.4b Rigid-rod model

As with the random coil, the rigid rod model is fairly straightforward to characterise from experimental data. From M and $\langle s^2 \rangle$ the characteristic ratio can be determined, and the molecular weight dependency determined. The scattering vector for a rigid rod polymer is given by;

$$P(Q) = \frac{1}{x}\int_0^x \frac{\sin(2x)}{2x} \cdot dx - \left[\frac{\sin x}{x}\right]^2 \qquad (1.43)$$

where $x=\sqrt{3}.Q^2\langle s^2\rangle^{1/2}$.

This is illustrated in figure 5 along with that of a random coil, in two forms $P(\theta)$ vs Q, an intensity plot and $P(\theta)Q^2$ vs Q, the so called Kratky plot, which clearly delineates the differences. True rigid rods and random coils can be easily discriminated by this presentation if a sufficient range of Q is accessible. Rigid rod behaviour is observed from wormlike polymers at high Q values corresponding to short length scales.

1.2.4c Wormlike chain model

Determination of the parameters of a wormlike chain is much more problematic than that of the rod and the coil. The models cover a much wider range of configuration, and what holds for more flexible polymers may not hold for stiffer molecules. This can be clearly seen in the effects of excluded volume. The wormlike chain is defined in terms of a and L, a can be measured but L is not directly measurable, and must be derived from experimental data.

The method of Murakami[31] provides the most reliable method to determine a and M_L from M and $\langle s^2\rangle$ equation 1.26 by a plot of $(M/\langle s^2\rangle)^{1/2}$ vs 1/M.

For more rigid polymers an alternative has been proposed by Zhang *et al*[32] ;

$$\left(\frac{M^2}{12\langle s^2\rangle}\right)^{2/3} = M_L^{4/3} + \frac{2}{15}\frac{M^{1/3}}{a} \qquad (1.44)$$

While these equations hold for stiff polymers, for more flexible polymers it becomes necessary to correct for excluded volume, and will hold only as far as the coil limit.

1.2.4d Intrinsic viscosity

Intrinsic viscosity data of wormlike chains can be combined with molecular weight to extract the chain parameters. A number of methods have been proposed, and the most effective are those based on the theory of Yamakawa and Fujii[33]. The Onseen Burgers procedure of hydrodynamics is applied to a continuous wormlike chain. This yielded the relationship;

$$[\eta] = \frac{\Phi_0 L_r^{3/2}(\lambda^{-1})^3}{M} \qquad (1.45)$$

where $L_r = L/(\lambda^{-1})$, and Φ_0 is the Flory universal viscosity constant, $\approx 2.87 \times 10^{23}$ mol^{-1}. The diameter, d, of the chain is;

$$d = \left(\frac{4M_L}{\pi \rho_2 N_A}\right)^{1/2} \qquad (1.46)$$

where ρ_2 is the density of polymer and N_A is Avagadro's number. Reduced contour length d_r is given by; $d_r = d/(\lambda^{-1})$.

Procedures based on this method rely on plotting M/[η] vs $M^{1/2}$ and extrapolating $M^{1/2} \rightarrow 0$[34], and this is restricted to less stiff chains (where the Mark-Houwink coefficient, a<<0.9) and even in this case it may lead to ambiguity. Bohdaneckỳ modified (45) in terms of a relationship for Φ_0[35],

$$\Phi_0 = \Phi_{0\infty}\left[B_0 + \frac{A_0}{L_r^{1/2}}\right]^{-3} \qquad (1.47)$$

where $\Phi_{0\infty}$ is the viscosity constant at the limit of infinite chain length, B_0 is a constant of 1.05 and A_0 is defined by;

$$A_0 = 0.46 - 0.53 \log(d\lambda) \qquad (1.48)$$

Combining (45) and (47) suggests that a plot of $(M^2/[\eta])^{1/3}$ vs. $M^{1/2}$ will have slope B_η and intercept A_η, where these are defined ;

$$A_\eta = \frac{A_0 M_L}{\Phi_{0\infty}^{1/3}} \quad \text{and} \quad B_\eta = \frac{1.05}{\Phi_{0\infty}^{1/3}}\left(\frac{2a}{M_L}\right)^{-1/2} \qquad (1.49a\&b)$$

M_L and a can be extracted from A_η *via* the relationships;

$$\frac{d_r^2}{A_0} = \frac{4\Phi_{0\infty}}{1.215\,\pi N_A}\left[\frac{\bar{\nu}}{A_\eta}\right]B_\eta^4 \qquad (1.50)$$

$$\log\left(\frac{d_r^2}{A_0}\right) = 0.173 + 2.158 \log d_r \quad (d_r \leq 0.1) \qquad (1.51)$$

$$= 0.795 + 2.78 \log d_r \quad (0.1 \leq d_r \leq 0.4) \qquad (1.52)$$

where $\bar{v}$ is the partial specific volume. It is then possible to derive the wormlike polymer chain parameters, $(\lambda)^{-1}$ from viscosity data. In practice it is found that the plots of $(M^2/[\eta])^{1/3}$ vs. $M^{1/2}$ tend to deviate downwards at high molecular weights. This can be attributed to the effects of excluded volume as the chains reach the coil limit, and the method of Bohdanecký provides no procedure to compensate for this. Bohdanecký tabulates the limits of validity of equation (47) in terms of reduced chain diameter, and within this range chains that exhibit excluded volume can only be characterised below the coil limit.

The values of a determined from viscosity were low in comparison with those from other methods, it is suggested that this can be corrected by using a lower value of $\Phi_{0\infty}$, about 2.1×10^{23} would make good the deficiency. This may be justified in observations made by Yamakawa *et al*[36] in a study on atactic PMMA where $\Phi_{0\infty}$, was found to be low, $\approx 2.3 \times 10^{23}$, which was attributed to chain stiffness.

1.2.4e Scattering function

The distinctive scattering behaviour of wormlike chains, especially when plotted in the Kratky format, was first disseminated by Kratky and Porod in their pioneering X-ray studies of stiff chain polymers. A typical theoretical curve is shown in figure 6 together with those for the equivalent rod and coil. It can be seen that in common with other properties the scattering function of the wormlike chain is intermediate to the extremes of the rod and coil.

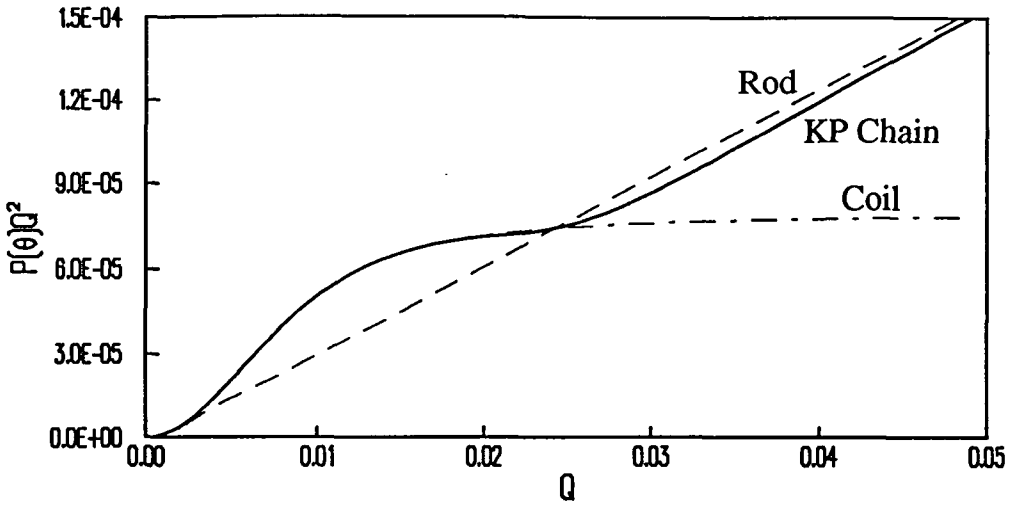

Figure 1.6: Comparison of Kratky-Porod scattering with rod and coil

The scattering vector is inversely proportional to the length scales that it probes, hence the overall dimensions of the molecule are probed at low Q values. At high values of Q where short length scales are probed the scattering function becomes asymptotic with that of the rigid rod, and the stiff local configuration is described. The region from the origin to the plateau is the Guinier region, where $P(\theta)=1+Q^2\langle s^2\rangle/3$, and is independent of configuration, hence radius of gyration can be extracted from a plot of $1/P(\theta)$ vs Q^2. Kratky and Porod predicted that the transition point from coil to rod could yield the persistence length. This may be done by extrapolation of the asymptotes of the coil and rod, the intersection being equal to $6/\pi a$. This provides a useful direct method of determining a, but it is found that not all polymers display a distinct plateau region in their scattering profile.

The scattering function of an isotropic wormlike chain without excluded volume is given by;

$$P(\theta) = \frac{2}{L^2}\int_0^L (L-a)I(Q;a).da \qquad (1.53)$$

Where I(Q;a) is the Fourier transform of the distribution function, G(r;a). A number of authors have presented forms of this equation which can be used to model the scattering behaviour of KP chains. Yamakawa derives an approximation to (53)[37];

$$P(\theta)=P_0(Q;L)\Gamma(Q;L) \qquad (1.54)$$

where $\Gamma(Q;L)$ is a scaling factor in terms of L and a, requiring numerical values tabulated in ref. 35, and $P_0(Q;L)$ is a combination of the rod and coil scattering functions;

$$P_0(Q;L) = [1-(Q,L)]P_{(c^*)}(Q;L) + \chi(Q,L)P_R(Q,L) \qquad (1.55)$$

where $\chi = e^{\left(-\pi\langle s^2\rangle Q/2L\right)^{-5}}$, $P_{(c^*)}$ the scattering function for a coil of radius of gyration $\langle s^2\rangle$, and P_R the scattering function for a rod of length L.

A second expression for the scattering function is that due to Koyama[38];

$$P(\theta) = \int_0^{L_r}(L_r - x)\exp\left[-\frac{1}{3}\left(u^2 x f(x)\right)\right]\frac{\sin\left(uxg(x)\right)}{uxg(x)}dx \qquad (1.56)$$

where $L_r = 2L/(\lambda^{-1})$, $u = Q(\lambda^{-1})/2$, $x = 2t/(\lambda^{-1})$, and;

$$xf(x) = \frac{2\langle r^2\rangle}{(\lambda^{-1})^2} - \frac{x^2 g(x)^2}{2} \qquad (1.57)$$

$$x^2 g(x)^2 = \frac{2\langle r^2\rangle}{(\lambda^{-1})}\sqrt{10}\left[1 - \frac{3\langle r^4\rangle}{5\langle r^2\rangle^2}\right]^{1/2} \qquad (1.58)$$

where; $2(\langle r^2\rangle/\lambda^{-2}) = x - 1 + e^{-x}$, and

$(\langle r^4\rangle/\lambda^{-4}) = 5x^2/3 - 52x/9 - 2(1-e^{-3x})/27 + 8(1-e^{-x}) - 2xe^{-x}$.

The two functions are compared in fig. 1.7, it can be seen that eq.1.55 displays the characteristic plateau of Kratky and Porod, which is not such a prominent feature of eq.1.56.

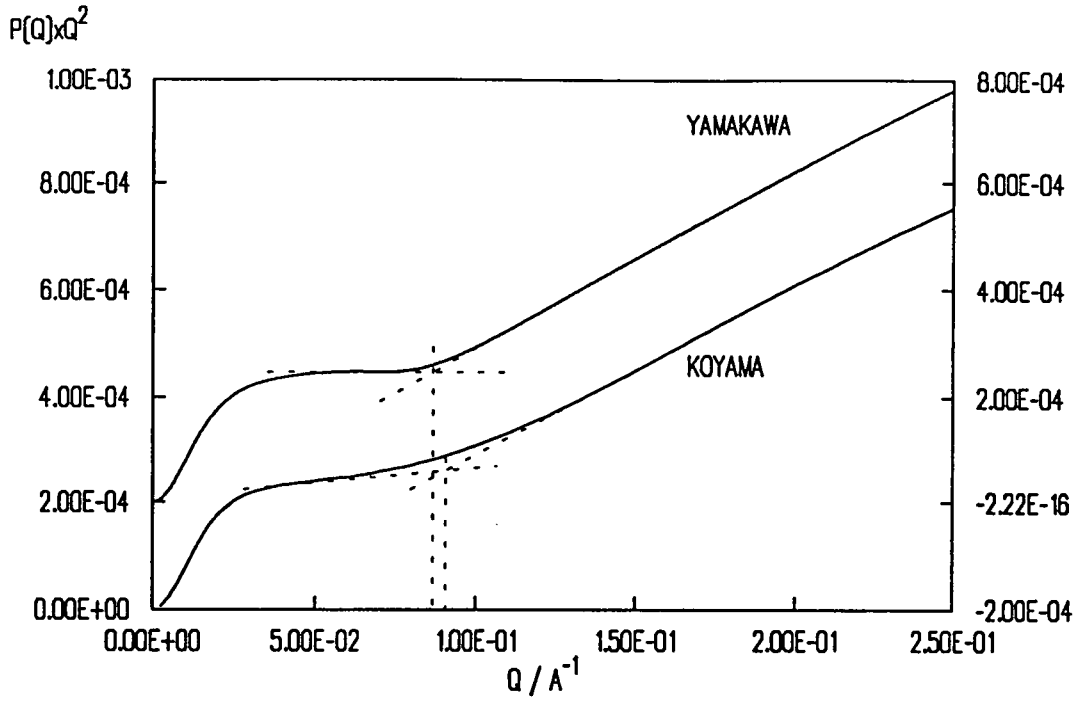

Figure 1.7:Comparison Of Yamakawa And Koyama KP Model Scattering Functions with L=1000Å, a=25Å (Yamakawa shifted $2x10^{-4}$ on Y-axis for clarity, upturn corresponds to 21.2Å for Koyama and 22.4 for Yamakawa)

Koyama also includes an excluded volume expansion factor α, defined as

$$\alpha^2 = \frac{\langle \lambda^{-1} \rangle \langle r^2 \rangle}{t} \tag{1.59}$$

this redefines the second and fourth moments of end to end distance thus;

$$\langle r^2 \rangle = \frac{\alpha^2}{\lambda^{-1}} \left[t - \frac{\alpha^2}{2\langle \lambda^{-1} \rangle} \left(1 - e^{-2\langle \lambda^{-1} \rangle / \alpha^2} \right) \right] \tag{1.60}$$

$$\langle r^4 \rangle = \frac{\alpha^2}{3\langle \lambda^{-2} \rangle} \left[5t^2 - \frac{26\alpha^2 t}{3\langle \lambda^{-2} \rangle} - \frac{\alpha^4}{18\langle \lambda^{-2} \rangle} \left(1 - e^{-2\langle \lambda^{-1} \rangle / \alpha^2} \right) + \frac{2\alpha^4}{\langle \lambda^{-2} \rangle} \left(1 - e^{-2\langle \lambda^{-1} \rangle / \alpha^2} \right) - \frac{\alpha^2}{\langle \lambda^{-1} \rangle} t e^{-2\langle \lambda^{-1} \rangle / \alpha^2} \right] \tag{1.61}$$

Analytical expressions have been derived for P(θ) under more specific conditions, for example Sharp and Bloomfield[39] derive an expression for P(θ) valid close to the coil limit;

$$P(\theta) = \frac{2}{u^2}\left(e^{-u} - 1 + u\right) + \frac{4}{15L_r} + \frac{7}{15L_r u} - \left(\frac{11}{15L_r} + \frac{7}{15L_r} \right) e^{-u} \tag{1.62}$$

where $u=LaQ^2/3$ and $L_r=L/2a$. Equation 1.62 is valid for chains where $L_r > 10$. Figure 1.8 shows (62) in comparison with (55).

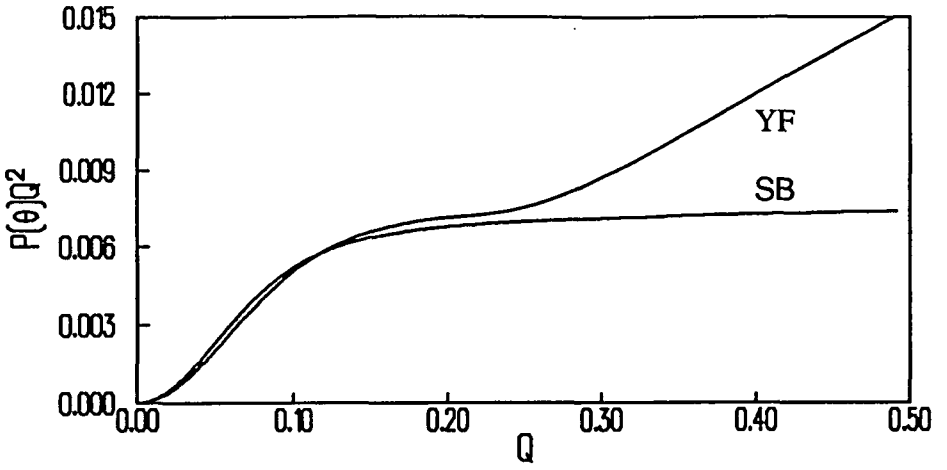

Figure 1.8:Comparison Of Yamakawa And Sharp-Bloomfield Scattering models, L=100Å, a=10Å

The three functions given, (55), (56) and (62) all show the appropriate behaviour of reducing to the rod or coil at the extremes, but are distinctly different. Chain parameters can be extracted by fitting scattering functions to experimental data, by using the most appropriate of the KP chain models.

1.2.5 Other chain models

The models outlined above all assume that the backbone of the chain in question is an homogenous, smoothly curving chain. however if as speculated in section(1.1.1b) the aromatisation reaction zips along the chain this assumption may become false. If the partially aromatised polymer is a block copolymer of poly(DHCD-DMC)-co-PPP it is possible its behaviour may deviate from that of a wormlike chain because it contains both coil and rod-like segments. There are a number of models in the literature which may describe this more adequately.

1.2.5a Broken chains

Several models have been presented describing chains that are not smooth, but in which there are breaks. These are the case of freely hinged rods[40] and the broken wormlike chain[41].

Hermans and Hermans developed a treatment for a zig-zag chain, made up of N freely hinged rigid rods of length A. For this model they derive the scattering function to be;

$$P(\theta)=\frac{2N}{A}\left(\Lambda(\beta)-\left(\frac{2}{\beta^2}\right)\sin^2\left(\frac{\beta}{2}\right)\right)+\frac{2N\Lambda^2(\beta)}{1-\gamma}-2\Lambda^2(\beta)\frac{1-\gamma}{1-\gamma^{-2}} \qquad (1.63)$$

where ;$\gamma=\sin\beta/\beta$, $\Lambda(\beta)=\int_0^t\frac{\sin\beta}{\beta}dt$ and $\beta=QA$

This may be regarded as a special condition of the Muroga equation(65).

The mean square radius of gyration is given by;

$$\langle s^2\rangle=\frac{A^2}{6}\left(N-1+\frac{1}{2N}\right) \qquad (1.64)$$

Both these properties reduce to those of the rod and coil at the extremes.

The broken wormlike chain is a model retaining the space curve of the wormlike chain, but with abrupt changes of direction a random intervals along the chain. This chain was modelled in terms of $\langle r^6\rangle$, $\langle r^4\rangle$, R_h, and $P(\theta)$, and was found to be virtually indistinguishable from that of the standard wormlike chain, except in the cases of very abrupt changes of direction (>135°) or in very small mean length between breaks (it is reported that breaks in DNA at 1/2 → 1/5a had very little effect on a[39], and studies on once broken amylose tricarbanilate polymer found the break impossible to detect[42]). The conclusion of ref. 39 is that the broken wormlike chain would be adequately described by a standard wormlike model, and any differences, except in the conditions of large angle or very frequent breaks would not be detected by general experimental techniques. The broken polyphenylene chain, a product of aromatised poly(DHCD-DMC) contains 15% ortho-bonding, equivalent to a mean sequence of 7 phenyl rings between breaks, with a change in direction of 120°. Although this angle is less than that reckoned to cause disruption the mean sequence length may be considered short for a fully aromatised polymer, but the flexible units cannot be accounted for, so it is not likely to be valid for the partially aromatised polymer.

1.2.5b Polymers of flexible and rigid segments

The models discussed here are of a block copolymer of rigid rods joined by flexible coils, and of a single rigid rod with a flexible segment at each end. The former case is presented by Muroga[43] together with experimental results for the helix to coil transition of poly(sodium D-glutamate), in the form of the equation for the scattering vector.

$$P(\theta) = NA^2\left\{2\Lambda(\beta) - \frac{4}{\beta^2}\sin^2\frac{\beta}{2}\right\} + 2NA^2\Lambda^2(\beta)C - 2A^2\Lambda^2(\beta)C\left(\frac{1-(ve^{-w})^N}{1-ve^{-w}}\right) +$$

$$m^2N^2b^2\left\{\frac{2}{Nw} - 2\left(\frac{1-e^{-w}}{Nw}\right)^2\left(\frac{v}{1-ve^{-w}}\right)\left(\frac{1-(ve^{-w})}{1-ve^{-w}}\right) - 2\frac{(1-e^{-w})(1-v)}{Nw^2(1-ve^{-w})}\right\} +$$

$$\frac{2mbA\,\Lambda(\beta)(1-e^{-w})}{w(1-ve^{-w})}\left\{2N - \frac{(1+ve^{-w})(1-(ve^{-w})^N)}{1-ve^{-w}}\right\} \qquad (1.65)$$

where $C=\left(\frac{e^{-w}}{1-ve^{-w}}\right)$, $w=mb^2Q/6$, $\beta=AQ$, $v=\sin\beta/\beta$ and $\Lambda(\beta) = \frac{1}{\beta}\int_0^{\beta}\frac{\sin t}{t}.dt$ for a model of N rods of length A joined by flexible segments of m monomers length b.

Results presented for the equations tend to give a good fit at high Q in the rod limit, but poorer agreement at lower Q. This is partly ascribed to a broad polydispersity. However it is shown that above a certain Q the model is insensitive to polydispersity. The Muroga model might concur with the structure of the partially aromatised polymer which cannot be adequately described by the KP wormlike model. Examples plot of eq. 1.65 are shown in figure (1.9). Figure 1.9 shows that the limiting cases of short rod sections in a chain the scattering resembles that of a wormlike chain, as is the scattering of a single log rod and a single flexible chain (iii-E on figure 1.9). The intermediate cases show a distinctive corrugated effect.

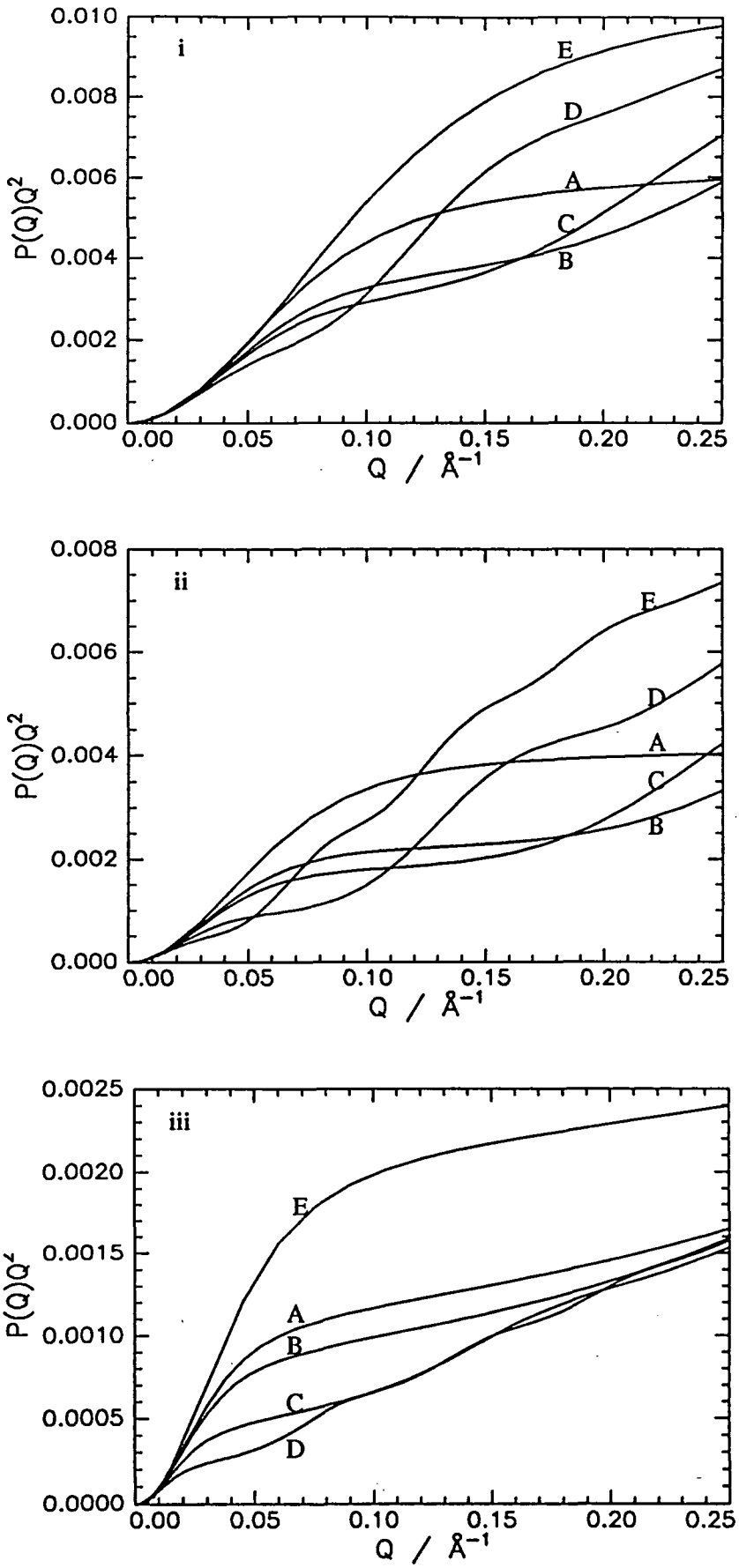

Figure 1.9: Plots of Muroga equation with i;10%, ii; 20%, iii; 50% rod content, and rod length of A;10Å, B; 20Å, C; 25Å, D; 50Å, and E 100Å. Coil segment length 5Å

In figure 1.10 a set of plots is shown, with rod content of 20%, coil segment length of 5Å, and a rod length of 25Å, and varying the contour length of the polymer, showing the effect of polydispersity this shows the curves behave similarly above ~0.1Å, except for the very short chains, which tend towards a single rod. Therefore if a sufficient range of Q is observed the effects of polydispersity can be lessened.

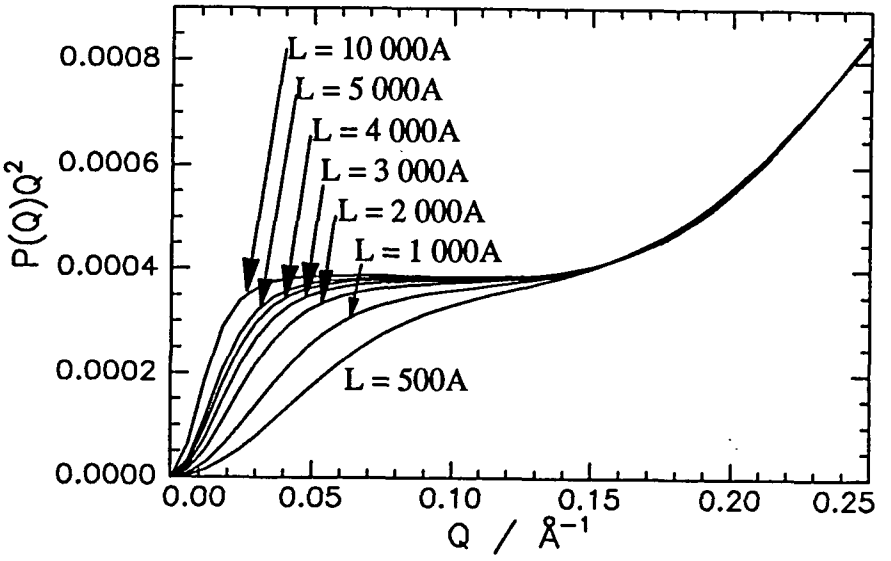

Figure 1.10: Effects of polydispersity on polymer chains.

The model of Huber[44] is a single rod with flexible coils at either end, the expression for P(θ) is a special case of the Muroga model, and this is presented together with an expression for the mean square radius of gyration

$$\langle s^2 \rangle = \frac{1}{(2M+2N)^2}\left[4M^2N^2a^2 + \frac{4N^3b^2}{3} + \frac{16NM^3a^2}{3} + 2MN^2b^2 + \frac{4M^4a^2}{3}\right] \quad (1.66)$$

where the rigid rod consists of 2M+1 segments, length a, and two flexible chains each of N units length b.

The four models presented above are theoretical, and have not been rigorously tested against experimental results. In addition each can only be characterised in terms of a few properties, however they are useful for comparative purposes.

References

1. Bradley,D.D.C.,Brown,A.R.,Burn,,P.L.,Burroughes,J.H.,Friend,R.H., Holmes,A.B.,Mackay,K,Marks,R.N.,*Nature*,**347**,539,(1990).
2. Gale,D.M.,*J.Appl.Poly.Sci.*,**22**,1955,(1978).
3. Brown,E.D.,Kovacic,P.,Wilkie,C.A.,*J.Polym.Sci.,Polym.Lett.*, **23**,453,(1985).
4. Kovacic,P.,Kyriakis,A,*J.Am.Chem.Soc.*,**85**,454,(1963).
5. Hayashi,Y.,Yamamoto,A.,Yamamoto,T.,*Bull.Chem.Soc.Japan*, **51**,2091,(1978).
6. Asada,T.,Nishide,H.,Tsuchida,E.,Yamamoto,K.,*Chem.Lett.*,1541, (1987).
7. Feast,W.J.,Rehan,M.,Schlüter,A-D.,Wegner,G.,*Polymer*,**36**,1054, (1989).
8. Okita,S.Percec,V.,Weiss,R.,*Macromolecules*,**25**,1816,(1992).
9. Marvel,H.,Hartzell,N.,*J.Am.Chem.Soc.*,**81**,448,(1959).
10. François,b.,Zhong,X.F.,*Synth.Met.*,**28**,E35,(1989).
11. McKean,D.R.,Stille,J.K.,*Macromolecules*,**20**,1787,(1987).
12. Ballard,D.G.H.,Courtis,A.,Shirley,I.M.,Taylor,S.C.,*Macromolecules*, **21**,294,(1989).
13. Conticello,V.P.,Gin,D.L.,Grubbs,R.H.,*J.Am.Chem.Soc.*, **114**,3167,(1992).
14. Shacklette,L.W. *et al*,*J.Chem.Phys.*,**73**,4098,(1980).
15. Chien,J.C.W.,Karasz,F.E.,Sclen,M.A.,*Makromol.Chem.,Rapid Commun.*,**1**,217,(1984).
16 Conticello,V.P.,Gin,D.L.,Grubbs,R.H.,*J.Am.Chem.Soc.*,**114**,3167, (1992).
17 Conticello,V.P.,Gin,D.L.,Grubbs,R.H.,*Polym.Mat.Sci.Eng.*,**67**,87,(1992).
18. Lord Rayleigh, *Phil.Mag.*,**37**,321,(1919).

19. Flory,P.J.,'*Principles of Polymer Chemistry*' ,Cornell Press, Ithaca, New York, 1953.
20. Debye,P.,*J.Chem.Phys.*,**14**,639,(1946).
21. Yamakawa,H.,'*Modern Theory of Polymer Solutions*', Harper & Row, New York, 1971.
22. Benoit,H. *et al*, *Macromolecules*,**7**,836,(1974).
23. Kratky,O.,Porod,G.,*Trav.Rev.Chim.Pay-Bas*,**68**,1106,(1949).
24. Benoit,H.,Doty,P.,*J.Phys.Chem.*,**57**,958,(1953).
25. Murakami,H.,Norisuye,T.,Fujita,H.,*Macromolecules*,**13**,345,(1980).
26. Harris,R.A.,Hearst,J.E.,*J.Chem.Phys.*,**44**,2595,(1966).
27. Saito,N,Takahashi,K.,Yunoki,Y.,*J.Phys.Soc.Japan*,**22**,219,(1967).
28. Stockmayer,W.H.,Yamakawa,H.,*J.Chem.Phys.*,**57**,2843,(1972).
29. Fujita,H.,'*Polymer Solutions*',Elsevier,Amsterdam,1990.
30. Shimada,J.,Yamakawa,H.,*J.Chem.Phys.*,**83**,2607,(1985).
31. Fujita,H.,Murikami,H.,Norisuye,T.,*Macromolecules*,13,345,(1980).
32. Fujita,H.,Liu,W.,Norisuye,T.,Zhang,L.,*Biopolymers*,**13**,345,(1980).
33. Fujii,M.,Yamakawa,H.,*Macromolecules*,**7**,128(1974).
34. Berry,G.C.,Tanner,D.W.,*J.Polym.Sci.,Polym.Phys.Ed.*,**12**,941(1974).
35. Bohdanecky,M.,*Macromolecules*,**16**,1483(1983).
36. Yamakawa,H.*et al*,*Macromolecules*,**24**,5614(1991).
37. Yamakawa,H.,Yoshizaki,T.,*Macromolecules*,**13**,1518,(1980).
38. Koyama,S.,*J.Phys.Soc.Japan*,**34**,1029(1974).
39. Bloomfield,V.A.,Sharp,P.,*Biopolymers*,**6**,1201(1968).
40. Hermans,J.,Hermans,J.J.,*J.Phys.Chem*,**62**,1543(1958).
41 Mansfield,M.L.,*Macromolecules*,**19**,854(1986).
42. Matsuo,K.,Pfannemüller,B.,Schmidt,M.,Ziegast,G.,*Macromolecules*, **17**,710(1984).
43. Muroga,Y.,*Macromolecules*,**21**,2751,(1988).
44. Huber,K.,*Macromolecules*,**22**,2750(1989).

2 EXPERIMENTAL

2.1 Reagents and solvents

In all cases except where the contrary is indicated reagents and solvents used in reactions and for working up were of analytical grade

2.2a Preparation of hydrogenous polymer: Monomer

The monomer, 5,6-cis-dimethylcarboxycyclohexa-1,3-diene(1) was prepared from 5,6-cis-dihydroxycyclohexa-1,3-diene DHCD(2). This is obtained by biological oxidation of benzene by a genetically manipulated micro-organism, *Pseudomonas putida*[1]. The raw material was supplied in the form of yellow, musty smelling crystals. This was purified by recrystallisation from ethyl acetate using decolourising charcoal to remove coloured components which would affect the optical properties of the polymer.

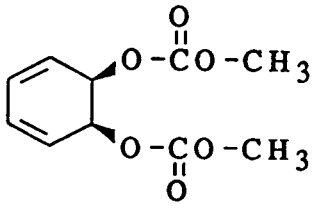

(1)

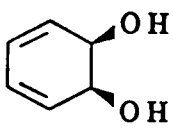

(2)

Ethyl acetate was heated to 30 to 35°C, DHCD added to give a solvent: solute ratio of 3:1, and the mixture stirred until all the crystals dissolved and decolourizing charcoal was added. The mixture was stirred for a further 15 minutes. After settling the solution was filtered through a sintered glass funnel, and the process repeated. The clarified solution was stood at -10°C to recrystallize the solute, the crystals were filtered and rinsed with chilled ethyl acetate. Purification of further impure crystals reused the mother liquor from the first batch to reduce loss of material. The combined purified DHCD was finally vacuum-dried at 40°C. The dried product smelt somewhat phenolic, indicating some decomposition had taken place. An NMR spectrum revealed about 3 mole% of phenol.

Final yield was 520g from a starting mass of approximately 700g.

To produce a monomer capable of free radical polymerisation it was necessay to produce a derivative of DHCD, by substituting the two hydroxyls.

Derivatisation of the monomer can be represented by the equation

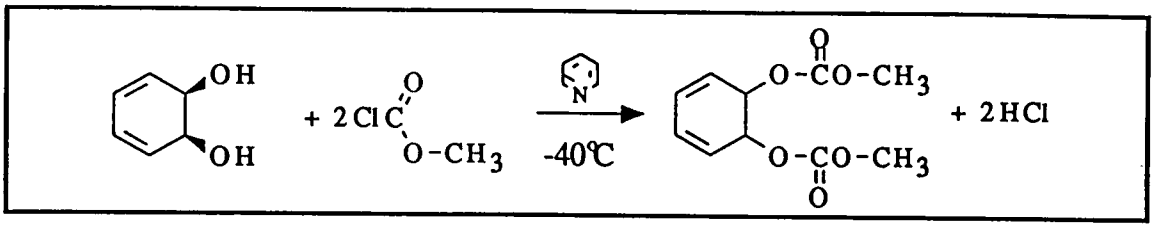

Figure 2.1: Derivatisation Of The Monomer, DHCD-DMC.

The derivative is a dimethoxycarbonyl, DHCD-DMC. DHCD (200g) and pyridine (367g) were stirred on a magnetic stirrer hotplate until an homogenous solution formed and then poured into a 10l flange-necked flask containing methylene chloride (5l). The flask was immersed into a freezing bath at -55°C, and the DHCD solution cooled to -40 to -45°C with vigorous stirring.

Methyl chloroformate (MCF) (GPR grade, 371g) was added very slowly to the solution from a dropping funnel, ensuring that no rise in temperature occured. The initially clear solution became yellow and then cloudy as MCF was added, and pyridine hydrochloride precipitated. Upon completion stirring was ceased and the reaction vessel left to warm to ambient temperature. The yellow colour vanished and the pyridine salt separated and rose to the top of the solution. The salt was filtered out and the liquid split into 3 portions for ease of manipulation.

Each aliquot was washed by shaking 3 times with 10% sodium bicarbonate solution (500ml) or more if necessary until effervescence ceased, followed by a final rinse with demineralised water to remove any remaining sodium. The washed solutions were recombined and concentrated on a rotary evaporator.

The derivatisation was repeated with a further 200g of DHCD, yielding in total 730g of crude liquid product. An NMR spectra of the material(fig. 2.2a) was run on this and showed it contained both pyridine and phenolic impurities.

The crude product was purified by vaccum distillation on a short path still. The first pass at 40°C, 0.4mbar pressure, the product being removed as the volatile fraction. The

pressure was then reduced to 0.02mbar and the residue passed through again at the successively higher temperatures of 80, 90, 100°C, the non volatile fraction being returned each time to be further distilled. The final non-volatile fraction was discarded, although it contained product to avoid degradation products forming and contaminating the product.

The yield of product was 438g of clear liquid, with about 15% aromatic impurity. This was removed by double recrystallization from isopropanol at 35°C, and a final washing with iced isopropanol. An NMR spectra of the wet crystals(figure 2.2b) showed them to be free of aromatics. They were vacuum dried at 20°C overnight. Final yield was 368g of white crystals.

2.2b Polymerisation

The monomer was polymerised in bulk by free radical initiation. DHCD-DMC(368g) was placed in a round bottomed flask and azobis(isobutyronitrile) initiator (2.75g) added, giving a molar ratio of 100:1. The flask was placed in a thermostated oil bath at 50°C to melt the crystals, then magnetically stirred under high vacuum to degas for 30 minutes, followed by flushing with nitrogen. Degassing and flushing was thrice repeated to remove all traces of oxygen.

The polymerisation was left for about 120 hours, the first 70hrs at 50°C, 24hrs at 55°C, and finally 24hrs at 60°C. The polymer was a hard brittle water-clear mass. This was removed by smashing the flask, and was broken up into fragments. It was dissolved in chloroform (2l) over 3 hours, and made up to 3l, split into 3 portions, and each precipitated into hexane (GPR grade, 4l) with vigorous stirring. After 30 minutes stirring the precipitate was filtered off and each batch washed 3 times with 1:5 chloroform-hexane mixture (900ml). The fractions were recombined, stirred for 30 minutes with 1:4 chloroform-hexane, filtered and washed twice with 1:5 chloroform-hexane, and finally vacuum dried at 100°C.

Final yield was 248g, a conversion of 67% from monomer, compared with 65% reported. The low overall yield of 30.5% from purified DHCD is due to the amount of DHCD that aromatised to phenol.

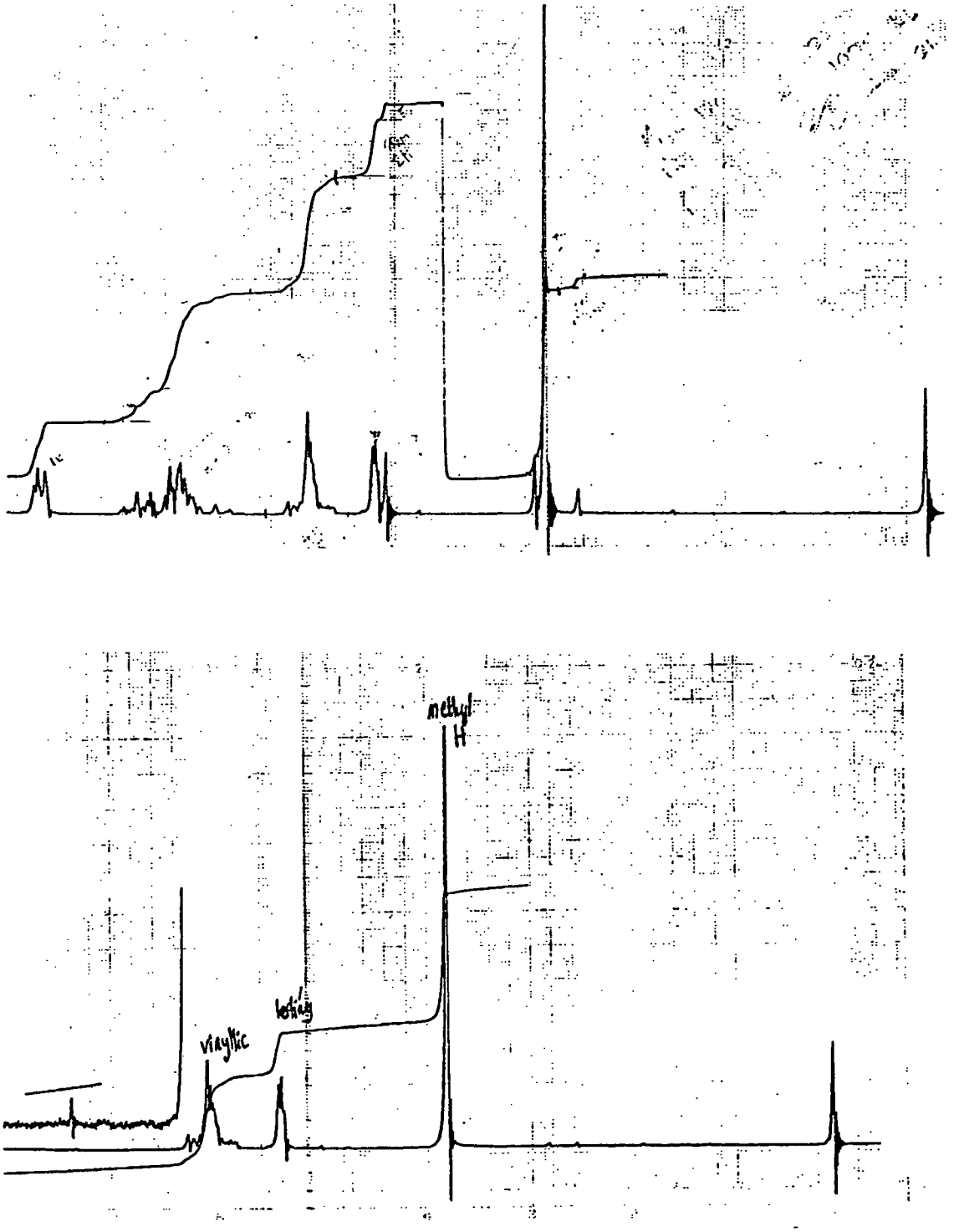

Figure 2.2: NMR spectra of crude and purified products.

2.3 Preparation of deuterated polymer

The preparation of deuterated polymer was essentially the same as for hydrogenous polymer, except performed on a smaller scale.

Deuterated DHCD was prepared by feeding deuterated benzene to the bacteria in heavy water. The monomer was supplied by ICI Chemicals and Polymers Division, Runcorn, and was used as supplied. Deuterated DHCD was weighed into a 50ml flask with AIBN initiator (0.054g) giving a molar ratio of 100:1. The reaction mixture was melted by immersing the flask in an oil bath at 55°C. The traces of dissolved oxygen were removed by successively vacuum degassing the flask then flushing through with nitrogen four times. It was sealed under nitrogen and left to polymerise for five days, increasing the temperature to 60°C after three days. The polymer was a similar transparent brittle solid to the hydrogenous polymer, and was similarly processed.

The polymer was broken up and dissolved in chloroform (55ml) and made up to 80ml. The solution was precipitated into hexane (325ml) with vigorous stirring, the precipitate collected on a sintered glass filter, and stirred for 30 minutes in a 1:4 mixture of chloroform and hexane. This was filtered, washed twice with 1:5 chloroform-hexane mixture (25ml), and finally vacuum dried at 50°C for 24 hours.

The yield was 6.56g, or 65.6%, about the same as for the hydrogenous polymer. A GPC chromatogram was run on the polymer. It has a much lower polydispersity and higher molecular weight than the hydrogenous polymer, due to the lower probability of hydrogen abstraction, and hence chain transfer.

Because of the narrow polydispersity and high molecular weight of the deuterated polymer it was not possible to obtain a range of fractions with sufficient spread of molecular weight for the neutron scattering studies. To produce a wider range of molecular weights the polymerisation was conducted with a higher proportion of initiator, and at a higher temperature. The results are tabulated below.

	initiator ratio	temperature /°C	M_w	Polydispersity
1	1:100	60	870000	1.775
2	1:30	90	296200	4.676

Table 2.1: Comparison Of Deutero-polymerisations.

2.4 Fractionation of polymer

To produce a series of fractions of polymer of sufficiently narrow polydispersity for neutron scattering, i.e. M_w/M_n below 1.5, and to produce a range of molcular masses so that molecular weight dependence of properties could be determined the single polydisperse polymer synthesised was fractionated.

Fractionation was conducted by the method of fractional precipitation, by the stepwise addition of a non-solvent to a solution of polymer. With successive addition of solvent the less soluble higher molar mass polymer precipitates, and can be removed. The fractionation of poly(DHCD-DMC) was carried out with the polymer dissolved in acetone, using methanol as the non-solvent. A narrower polydispersity will be obtained if a dilute solution is used in this case 2% w/v. The apparatus used is shown in fig.2.3.

Poly(DHCD-DMC) was dissolved in acetone (1l), filtered, and fully immersed in the thermostated bath at 25°C±0.02°C as shown. The stirrer was set to a moderately fast rate and methanol added, this was found to be most conveniently done using a series of pipettes of various volumes. Methanol was added slowly into the stirring vortex until permanent turbidity appeared, the solution was then left for an hour or so, by which time it had clarified. Further methanol was then added until a permanent precipitate formed, the temperature was then raised to 30°C and once the precipitate had dissolved stirring was ceased, and the bath was allowed to cool naturally to 25°C once more, and the precipitate collected.

This was done either by pipetting it out from under the supernatant, or running it into a collection vessel underneath, the former method was preferred since the precipitate was

generally a gel, and removed less of the solution. Once collected the precipitate was dissolved in a small amount of acetone, precipitated into a large excess of methanol, filtered, washed and dried under vacuum for at least 24 hours.

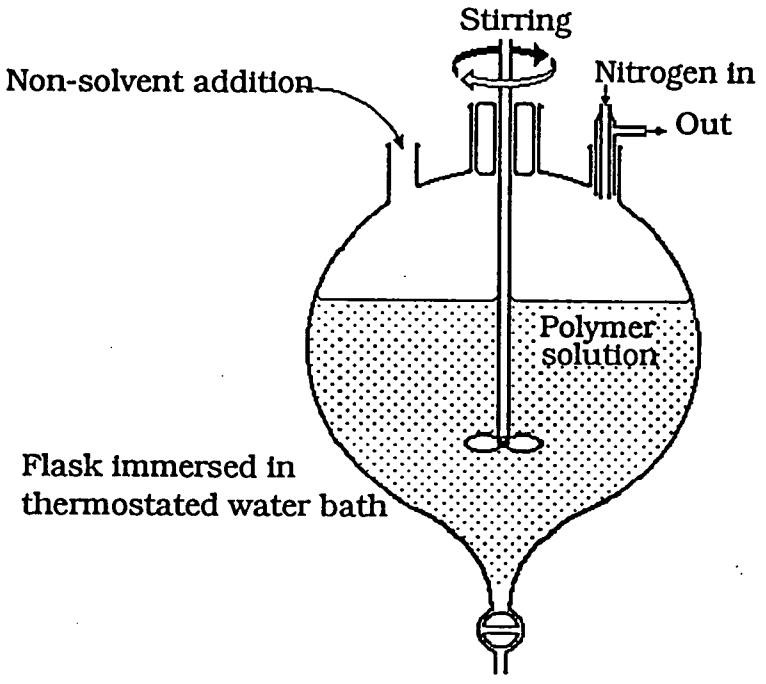

Figure 2.3: Fractionation Apparatus.

Precipitation was continued by this method until large volumes of methanol (≈200ml) produced no precipitate. The solvent mixture was then evaporated under reduced pressure, and the remaining polymer collected as the final fraction. It was noted that at higher molecular weights the precipitates were mobile gels, and lower molecular weights the precipitates were stiff gels or solid precipitates.

Four fractionations were conducted, two with hydrogenous polymer, and two with deuterated polymer, using the same method but scaled down to 5 grammes.

Results

The reults from fractionations are given in tables 2.2 to 2.5

Fraction	Vol. precipitant /cm^3	Mass /g	M_w	Polydispersity
raw	-	20	200000	2.291
A'	255	0.8610	488500	1.405
B'	5	0.9875	374400	1.412
C'	4	0.8196	344200	1.342
D'	5	2.6781	230100	1.478
E'	4	1.4748	253200	1.232
F'	8	1.2110	207400	1.214
G'	12.5	1.2241	201000	1.199
H'	25	2.2481	164100	1.192
I	50	3.3062	112500	1.225
J	50	1.6272	67400	1.106
K	150	0.7509	39400	1.100
L	residual	0.7305	19100	1.260
total		17.919		

Table 2.2: Fractionation (1).

Fraction	Vol. precipitant /cm^3	Mass /g	M_w	Polydispersity
raw	-	20	200000	2.291
A	260	3.7355	405500	1.579
B	10	1.6848	308000	1.345
C	10	2.1259	260000	1.346
D	20	2.9184	178000	1.325
E	25	1.9306	125000	1.226
F	50	2.8058	119500	1.305
G	50	3.0515	84000	1.265
H	residual	0.3359	41000	1.123
Total		18.5884		

Table 2.3: Fractionation (2).

Fraction	Vol. Precipitant /cm^3	Mass /g	M_w	Polydispersity
raw	-	5	870000	1.775
d-AA	41.5	0.2224	1369400	1.72
d-AB	1.5	0.4532	1242900	1.89
d-AC	1.0	0.5401	1208200	1.64
d-AD	1.0	0.8276	1000000	1.50
d-AE	2.0	0.8098	628200	1.48
d-AF	5.0	0.4573	408600	1.42
d-AG	20	0.8471	202100	1.43
d-AH	residual	0.2382	51230	1.27
Total		4.3959		

Table 2.4: Fractionation Of Deuterated Polymer (1).

Fraction	Vol. Precipitant /cm^3	Mass /g	M_w	Polydispersity
raw	-	6.6	296200	4.676
d-A	48	1.1205	639000	1.224
d-B	4	1.2145	226600	1.530
d-C	6.5	1.6310	122700	1.845
d-D	residual	0.9953	40800	1.249
Total		4.9613		

Table 2.5: Fractionation Of Deuterated Polymer (2).

2.5 Aromatisation

2.5.1 Solid State

Poly(DHCD-DMC) may be thermally aromatised to polyphenylene according to the reaction scheme.

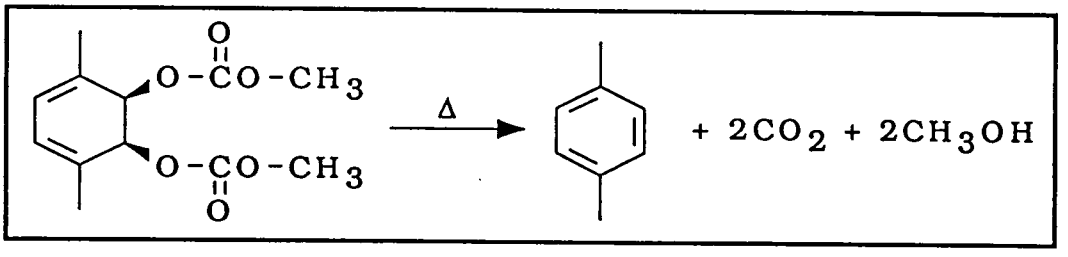

Figure 2.4: Aromatisation reaction.

It was originally intended that the configuration changes of the aromatisation reaction be studied in the solid state.

In order to assess suitable reaction temperatures a set of thermogravimetric analyses were run on the polymers. This technique measures loss of mass with temperature or time. These were performed on a Stanton Redcroft T760 instrument. All samples were heated in a steady steam of oxygen free nitrogen. A small amount of polymer was placed in the balance pan of the instrument, and then lowered into the furnace, which was initially set at 100°C in order to drive off any remaining volatiles. After 15 minutes the heating was increased at the maximum rate (90°C/min) to the required temperature. Output was plotted on a chart recorder as mass *vs* time.

Samples were run over a range of temperatures from 200°C to 500°C, and the results are shown in table 2.1. This established that between 300°C-400°C would be suitable for aromatisation. 350°C was chosen as most suitable to fully aromatise and 300°C to slowly aromatise to intermediate degrees of aromatisation. Above 400°C PPP appeared to be unstable and decompose, causing excessive weight loss. The reaction products were yellow coloured powders or aggregates.

Temperature /°C	Heating Time /minutes	weight loss /%	aromatisation /%
200	60	0	0
250	60	0.5	0.8*
300	173	53.4	80*
350	62	66.5	100
400	25	66.6	100
450	25	71.4	107

* reaction unfinished

Table 2.6: Solid State Aromatisation

2.5.1a Sample preparation

The only solid state aromatisation samples prepared were for a neutron scattering experiment. This required discs of polymer 20mm in diameter, totalling 1mm in thickness. In order to facilitate the escape of the volatile by-products of the reaction (methanol and carbon dioxide, fig. 2.4) the samples were prepared from thin films of polymer

Solutions of 5% w/v polymer in chloroform were prepared and cast into films in PTFE casting dishes in a fume hood. The dishes were covered so that evaporation was slow, requiring about 12 hours to form a rigid film. These were cut into discs and dried at 40° C under vacuum for 24 hours. The films, ranging from 0.05 to 0.1mm thick were stacked 1mm thick in the quartz-windowed, brass scattering cells and aromatised in situ. The cells were placed in a vacuum oven, evacuated, and the chamber filled with dried nitrogen, evacuated and once more filled with nitrogen. The cells were then placed in a tube furnace of similar diameter at 250°C with a slight stream of nitrogen gas. The samples were then aromatised for the appropriate time, allowing a few minutes for the cells to reach temperature. Unfortunately the films tended to foam in the aromatisation reaction, presumably due to the volatile by-products, in extreme cases extruding out of the cell. Even at lower temperatures it was found impossible to produce anything better than a foamed product, and often just a powder.

Subsequently it was decided that due to the impossibility of making void free solid state samples needed for SANS the study would be limited to solutions of the polymer.

2.5.2 Solution aromatisation

Poly(DHCD-DMC) may be aromatised in solution in the solvent N-Methyl Pyrrolidinone (NMP). The solvent has a number of advantages; it is a good solvent for the precursor polymer, which remains soluble up to 40% aromatisation. It has a high boiling point (202°C) which allows the high temperature required for the aromatisation reaction, and it is basic, which catalyses the reaction. It has the disadvantage of being hydroscopic, and is unstable in the presence of both water and oxygen, and this must be handled under a dry inert atmosphere.

The reaction in NMP proceeds between 150°C and 200°C. For this work 175°C has been generally used, as it produces a reasonable rate of reaction but is well below the boiling point of NMP.

Throughout this study all NMP that was used has been dried over anhydrous $MgSO_4$, distilled under reduced pressure, and stored under dried nitrogen, solutions and solvent have generally been handled by methods used for air and moisture sensitive compounds where possible.

In the first attempt at aromatising a solution of poly(DHCD-DMC) 10ml of 5% w/v solution of the polymer was made up in NMP, purged with nitrogen gas, and placed together with a magnetic stirrer bug in a two necked 25ml round necked flask, one neck of which was stoppered with a natural rubber septa in order to allow sampling. The flask was placed in an oil bath at 175°C and 1ml of sample withdrawn at 15 minute intervals, beginning at 15 minutes since it was assumed that the reaction would follow the kinetics in (Ref Chapter 1), with an induction period, although the reaction actually proceeded faster than this. The nature of the aromatising solution changed from a clear, colourless solution, initially though a faint red/brown colour, then once aromatisation accelerated became progressively deeper yellow, and showed a blue iridescence when held up to the light. The apparent viscosity of the solution increased with reaction, and became liable to gel at higher concentrations (above about 40% aromatisation). Above 40% reaction the polymer once precipitated could not then be redissolved in NMP, although it would

dissolve in chloroform to ≈60%. Above 85-90% aromatisation the polymer precipitated during reaction, and was then insoluble in chloroform, hexafluoropropanol, acetone, dimethylsulphoxide or toluene.

The samples from the reaction were used to devise a convenient instrumental method to determine the extent of aromatisation. the patent exemplification method is given from infra-red absorptions characteristic of the carbonyl and phenyl entities (1750cm^{-1} and 810cm^{-1} respectively) as;

$$\%\mathbf{Aromatistion} = \frac{10xA_{810}}{10xA_{810} + A_{1750}} \qquad (2.1)$$

However this was performed by a specular reflectance technique on a FTIR instrument, a technique not available for the study, and attempts to reproduce this from transmission techniques, using both the solutions in a KBr cell, or films cast onto KBr discs proved unsuccessful, partly at least due to the high background level. By contrast TGA proved a more successful technique, and after calibration it was found that by pyrolysing a dry sample of precursor polymer at 350°C for 2 hours the correct weight loss to within 1% could be reproducibly obtained. Therefore this was chosen as the method to analyse samples. The method used was as outlined above in Section 2.5.1. The percentage aromatisation was then calculated by

$$\%\mathbf{Aromatisation} = \frac{3xPM - IM}{2PM} \qquad (2.2)$$

Where PM was the final pyrolysed mass, and IM the initial mass.

Many of the subsequent attempts to repeat the reaction proved unsuccessful, and after two hours reaction the solution had turned dark brown from solvent decomposition and aromatisation gone no further than a few percent. On scrutinization this proved to be due to the drying of the nitrogen gas used in the various stages, especially as a purge, including a H_2SO_4 bubbler, presumably tiny acid droplets interfered with the catalytic effect of NMP, and caused it's decomposition. On replacing the drying apparatus with a single column of alternating layers of 3Å molecular sieve and KOH granules the reaction proceeded without difficulty.

On repetition of the aromatisation reaction it was found that the kinetics were somewhat irregular (figure 2.5) and that reaction times varied considerably .The preparation of samples at a given degree of aromatisation by reaction time proved unsatisfactory, and so this was done instead by measuring the volume of CO_2 gas evolved.

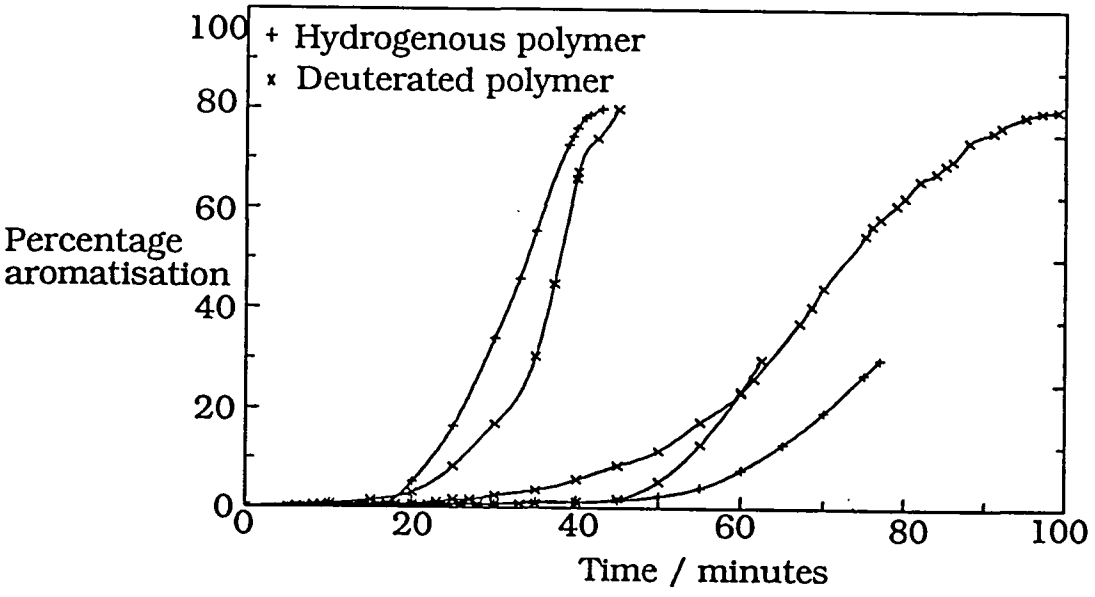

Figure 2.5: Representative aromatisation reaction profiles.

The apparatus constructed for this is shown in figure 2.6. It was constructed using approximately 0.25mm internal diameter HPLC tubing, with a HPLC 3-way valve.

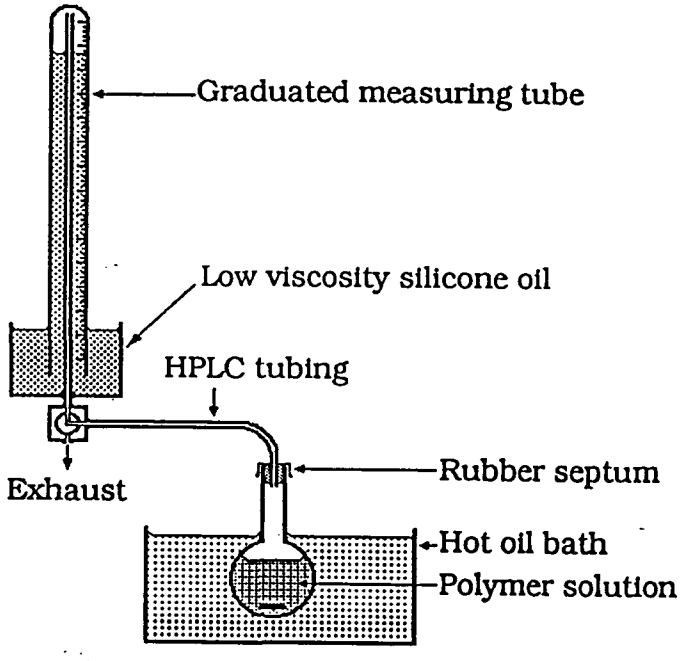

Figure 2.6: Aromatisation apparatus.

A number of aromatisations were performed, measuring the gas evolved and constructing a calibration curve.

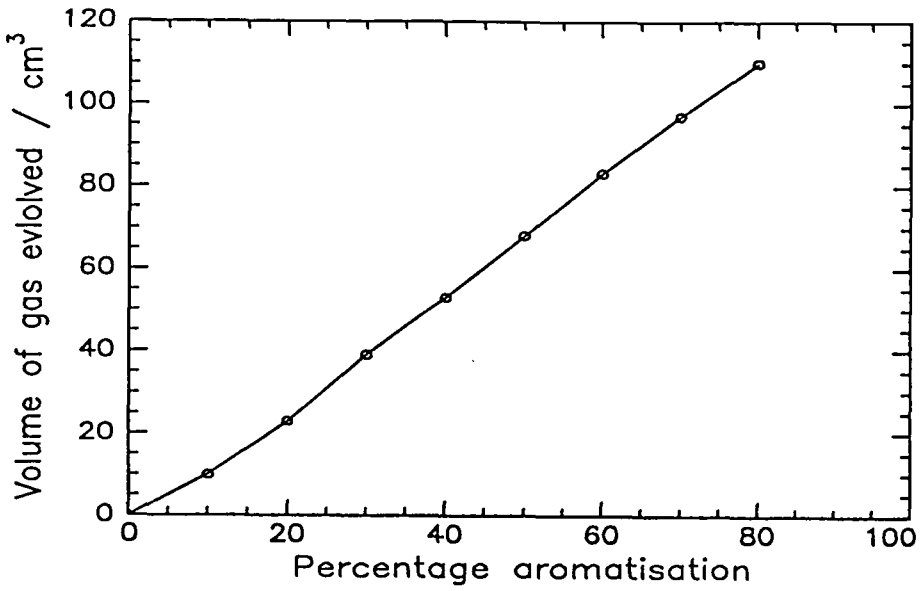

Figure 2.7: Aromatisation reaction calibration curve: Gas evolved from 5% solution of poly(DHCD-DMC) in NMP containing 0.1g polymer.

2.5.2a Sample preparation

Aromatisation was performed by the following procedure: Dried poly(DHCD-DMC) was weighed into the reaction vessel and a PTFE stirrer bug added. This was then sealed with an uncoloured natural rubber septum. The vessel was purged for 15 min by inserting two needles into the septum, one connected to a dried nitrogen supply, at very low pressure to avoid blowing out the polymer. The appropriate volume of solvent to make a 5% solution was transferred to the reaction vessel using a graduated syringe. The nitrogen and exhaust needles were again inserted and nitrogen bubbled through the solution with vigorous stirring for 10 minutes, the needles withdrawn and the solution stirred until fully dissolved. The reaction vessel was then attached to the gas collection apparatus, by inserting the inlet tube into the septum, and sealing the top with vacuum grease. The apparatus was then lowered, to immerse the reaction vessel in an oil bath, thermostatically controlled to 175°C±3°C on a stirrer-hotplate, with slow stirring, generally there was a small amount of degassing as the solution warmed up, and before reaction began this was exhausted. Once this had stopped the valve was turned to

connect the reaction to the gas meter. The reaction was stopped once the appropriate volume had been collected. This was done either by quenching in methanol, or if the reaction exceeded the limit of solubility, by plunging the sealed vessel into liquid air until the solution started to freeze. Solid polymer was filtered, dried under reduced pressure and stored in a fridge, samples in solution were stored under nitrogen in a desiccator in a fridge.

2.6 Verification of deuteration

To confirm that virtually all of the hydrogen in the polymer was the ^{2}H nucleiand that this was not lost by an exchange process with solvents during any stage of the study a number of NMR spectra were obtained of the deutero-monomer, and an aromatised polymer recovered after use in two SANS experiments. The solutions were made up with known concentrations in deutero-chloroform. Two spectra were run on each sample, Firstly in deutero-chloroform, then this was spiked with a small aliquout of trichloroethylene, and further spectra run (Bruker 400MHz instrument). By means of comparing the proton peak areas for the spiked and unspiked samples it was possible to determine how much of the ^{1}H isotope was present in the samples. The spectra are shown in figures 2.8 and 2.9. It was calculated that the monomer was in excess of 99.5% deuterated, the aromatised polymer in excess of 99% deuterated, a satisfactory result showing the deuterated polymer was stable to the conditions of preparation.

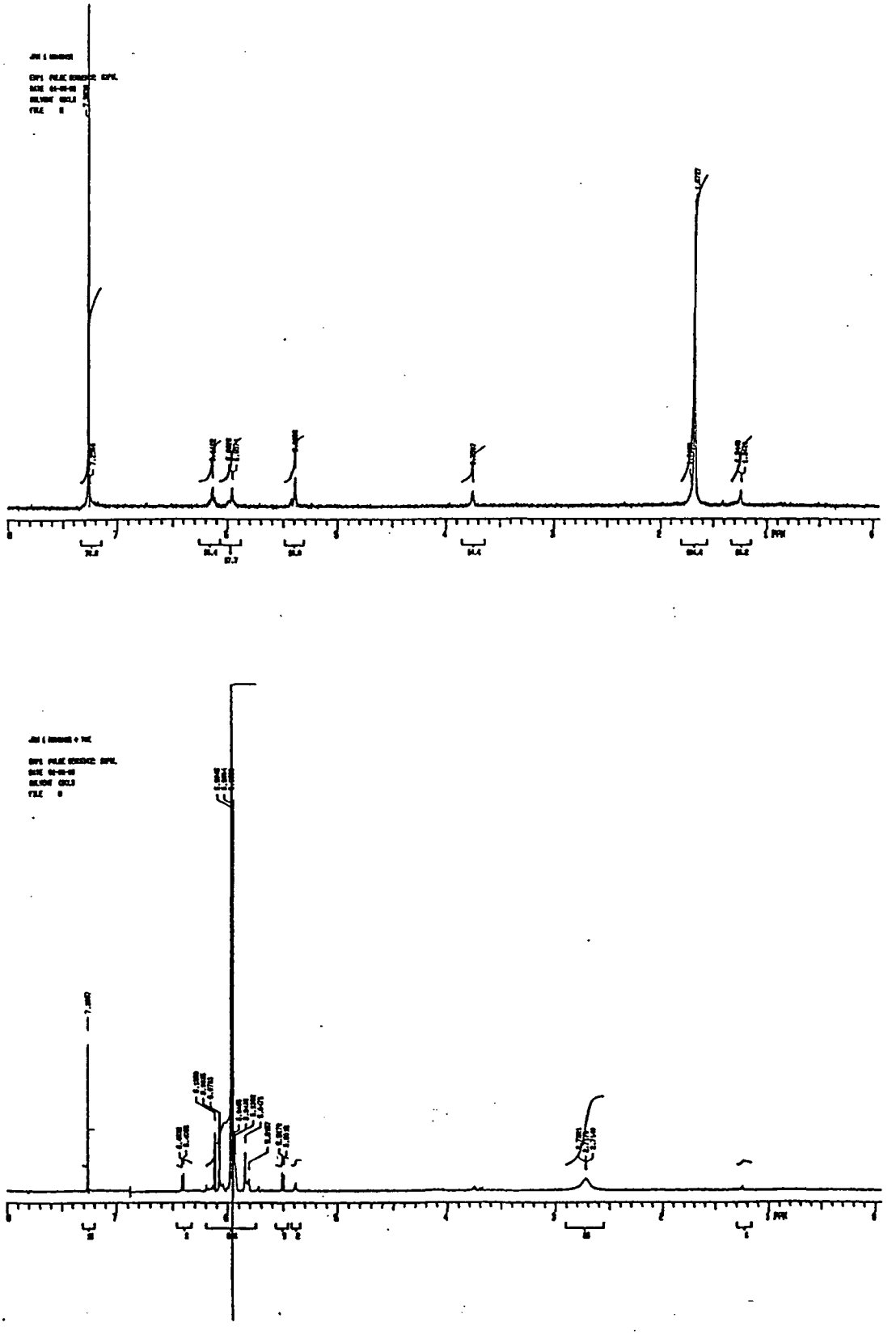

Figure 2.8: NMR spectra of a;monomer, b;monomer+trichloroethylene

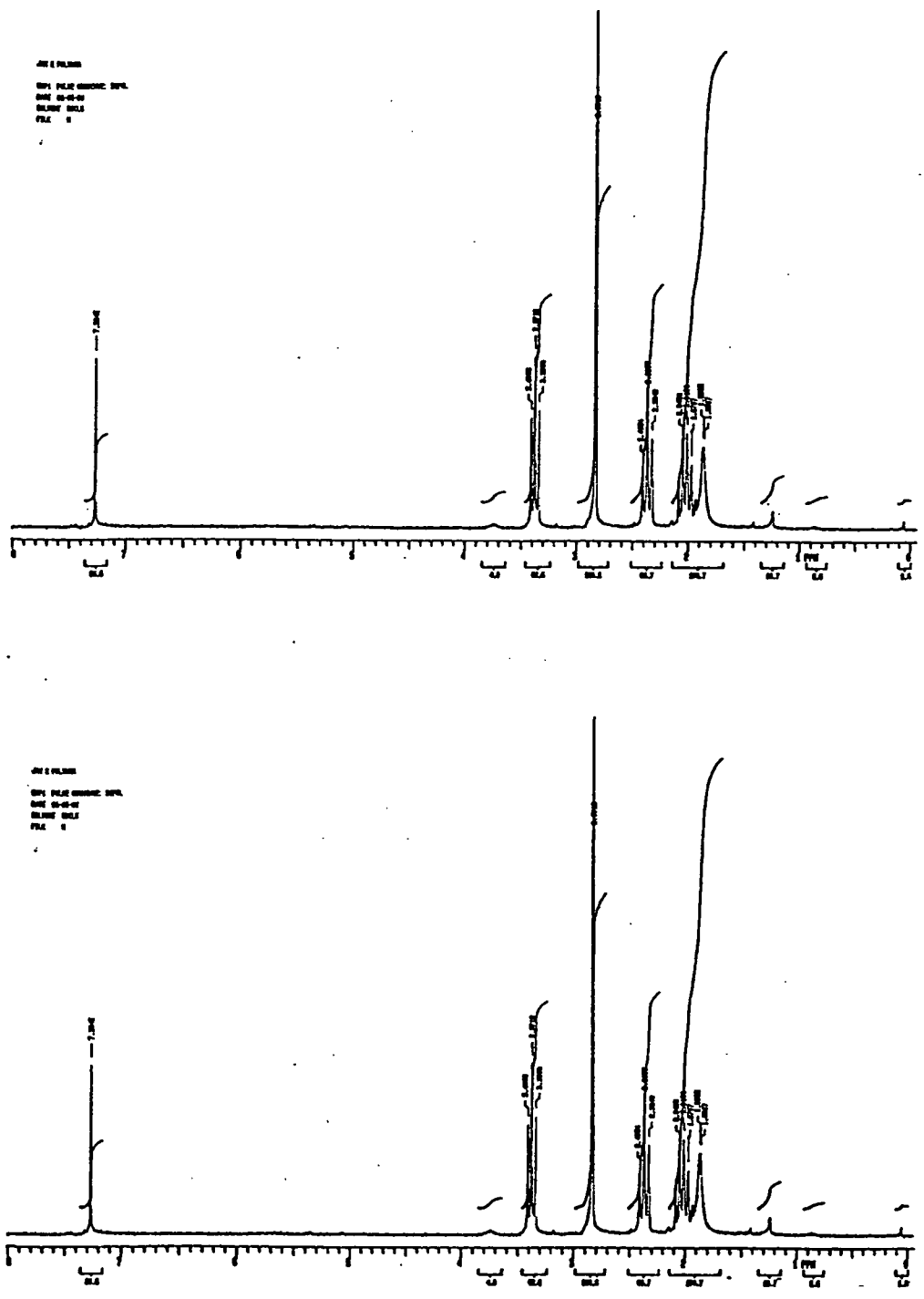

Figure 2.9: NMR spectra of aromatised polymer, a;polymer, b;polymer+ trichloroethylene

2.7 References

1, Ballard,D.G.H,Courtis,A.,Shirley,I.M.Taylor,S.C.,*Macromolecules*,22, 294,(1989).

CHAPTER 3

MOLECULAR WEIGHT CHANGES WITH AROMATISATION

3.1 Introduction

Changes in the molecular weight of poly(DHCD-DMC) with aromatisation were followed by the use of size exclusion chromatography (SEC). Additionally to establish a link with chemical changes a partially aromatised sample was fractionated and chemically analysed by a range of methods.

3.2 Size exclusion chromatography

Size exclusion chromatography is a chromatographic method for separating polydisperse polymers for analysis of molecular weight distribution[1,2]. As the name suggests the method relies on the differences in size for the mechanism of separation.

The stationary phase is a porous material and the mobile phase a solution of the polymer. The type of stationary phase varies, it can be either a rigid cross-linked polystyrene gel, a porous glass or porous silica particles. Inorganic packing tends to contain surface sites which can lead to interaction with eluted polymers, contributing an enthalpic factor into the otherwise entropically controlled process of size exclusion, and these sites need to be deactivated. In general unless high temperatures are required polymer gels are the preferred choice of stationary phase. The polymer gels have been developed so that a high degree of resolution is readily available.

The eluted polymer solution passes through a column packed with small beads of porous polystyrene gel, and the molecules of polymer diffuse in and out of the pores. The residence time of the molecule in the pore is related to its size, smaller molecules will reside longer than larger ones. This is the result of the longer path length that a smaller molecule can describe since more of the pore is available to it, thus small molecules will be retained longer on the column whilst large molecules will elute sooner. There are limits to the method, above a certain size molecules will be unable to diffuse into the pores, these excluded molecules will remain in the interstitial volume and elute from the column without further separation, and hence cannot be distinguished in terms of their

size. Very small molecules have free access to the stationary phase into which they can permeate and will elute at the solvent front, and again they are not distinguishable. These limits are called the limit of total exclusion and the limit of total permeation respectively. Intermediate sized molecules can diffuse into some of the pores, depending on their size, this is the region of selective permeation where molecules can be distinguished(figure 3.1).

The volume of solvent required to elute a molecule from a column is V_R, if the flow rate is f_v then the retention time on the column, t_R, will be;

$$t_R = \frac{V_R}{f_v} \tag{3.1}$$

V_0 is the interstitial volume of the column, and V_p is the total volume of the pores, the total permeation volume when the solvent front emerges from the column is;

$$V_t = V_0 + V_p \tag{3.2}$$

In liquid chromatography the degree of retention is given in terms of the capacity factor K';

$$K' = \frac{V_R - V_T}{V_T} \tag{3.3}$$

where K' will be zero for total permeation and typical values for partial permeation are 0 to -0.5. Positive values of K' will only be obtained in the case of interaction up to a maximum of 1 for total interaction with the column packing, which should be avoided in SEC. The general LC capacity factor is replaced by a specific SEC capacity factor K". This is defined as;

$$K'' = \frac{V_R - V_0}{V_0} \tag{3.4}$$

The limits of K" are now zero for total exclusion and unity for total permeation. The separation of a solute in terms of V_R will be given by;

$$V_R = V_0 + K''V_i \tag{3.5}$$

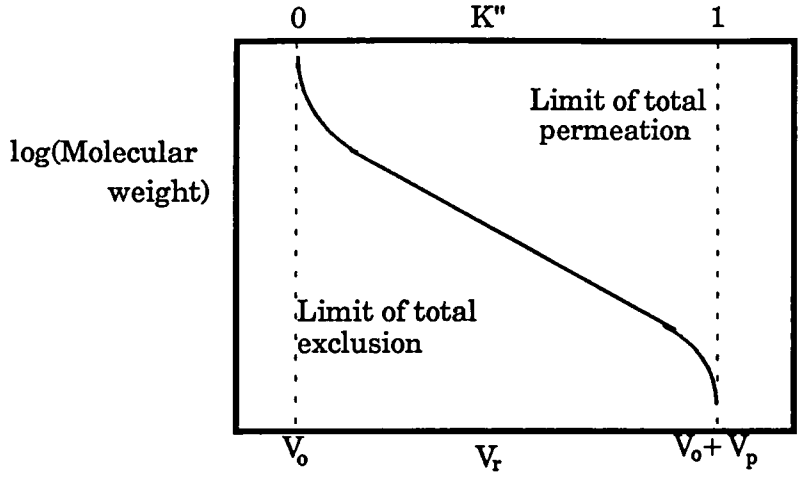

Figure 3.1, Limits of SEC method

The resolution, R_s, of two peaks A and B in GPC is given by

$$R_s = \frac{2(V_A - V_B)}{w_A + w_B} \tag{3.6}$$

where V_A and V_B are the respective peak retention volumes, and w_A and w_B are the respective tangential baseline widths of a monomodal species with a Gaussian distribution. A value of 2 or more indicates full separation with no overlap and full resolution, values of one or less indicate peak overlap and only partial resolution. Resolution is not vital in SEC of high molecular weight polydisperse polymers, where the distribution of molecular weight is required, although it is often useful to be able to resolve broad bimodal distributions. If the peak has a width of four standard deviations, 4σ, at 99% of the distribution the specific resolution for a 1cm column is given by[3];

$$R^*_{sp} = \frac{0.576}{\sigma D_2 \sqrt{L}} \tag{3.7}$$

where L is the length of the column and D_2 the slope of the calibration curve in figure 3.1. R^*_{sp} provides a useful comparative measure for the performance of columns.

The peak capacity, n, of a column, that is the number of peaks with resolution of unity, in a given elution volume in SEC is given by;

$$n = 1 + 0.25N^{1/2} \ln \frac{V_T}{V_0} \tag{3.8}$$

where N is the number of theoretical plates (an analogy to a fractionation column given by $N=(t_R/\sigma)^2$). In HPLC this is given by

$$n = 0.25N^{1/2}K' \tag{3.9}$$

The resolution for SEC with a similar number of plates is therefore considerably less. For a typical SEC column of 40000 theoretical plates n is in the order of 20 to 50, for a similar HPLC column n will be ≈500.

SEC is not an absolute method, and the molecular weights are taken from a calibration curve, usually constructed with narrow distribution ($M_w/M_n \approx 1.01$-1.1) standards. Anionically polymerised polystyrenes are the most common choice. A typical calibration curve is shown in figure 3.2.

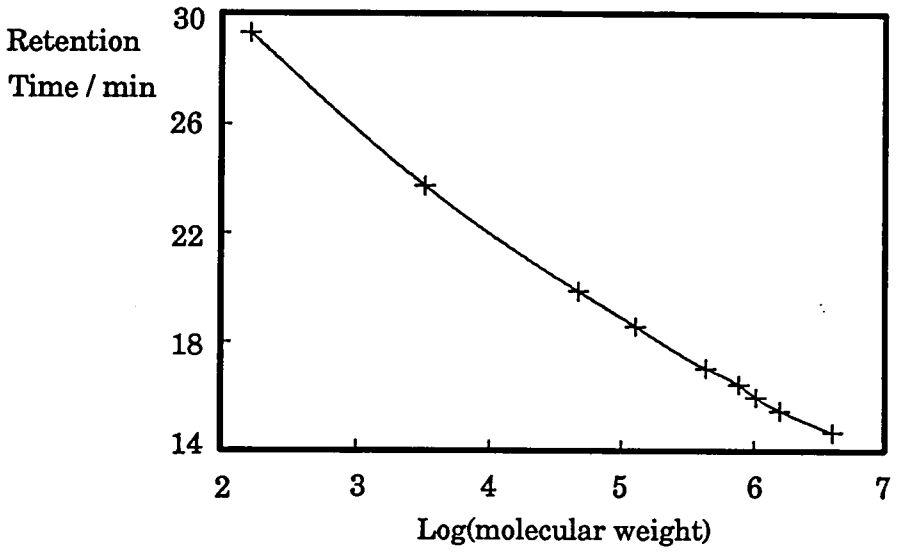

Figure 3.2, Typical SEC calibration curve

However it can be seen that in practice the calibration will only apply to samples of the calibrant polymer. The retention time is dependent on the size of the molecule, and a given molecule of one polymer will not adopt the same configuration as a molecule of a different polymer of the same molecular weight, both steric and solvent effects will differ, and so then will size. A somewhat crude correction is the application of a Q factor, for any vinyl polymer it is assumed ;

$$Q = \frac{\text{monomer unit mass}}{2.52} \qquad (3.10)$$

This is then used to scale results, but this still assumes the same extended chain configuration.

A more satisfactory correction is to use the method of universal calibration. Grubisic et al[4] proposed that hydrodynamic volume of a polymer be used as the calibration variable. This is related to the molecular mass by the equation;

$$[\eta]M = 2.5N_A R_H \qquad (3.11)$$

where $[\eta]$ is the intrinsic viscosity and N_A the Avagadro number. Therefore if a calibration curve is constructed of $[\eta]M$ *vs* t_R an absolute calibration should be obtained, and in practice this is found to hold for a very wide range of polymers[5] over a broad range of molecular weights.

Intrinsic viscosity is related to molecular mass by the Mark-Houwink equation;

$$[\eta] = KM^a \qquad (3.12)$$

where K and a are constants. The exponent a is related to the configuration thus;

a = 0.5 random coil in the theta condition

$0.5 < a < \approx 0.8$ random coils in a good solvent

$\approx 1 \leq a \leq 2.0$ rodlike molecule

a = 0.33 sphere

Hence the universal calibration applies not only to the random coil configuration, but also to rodlike and spherical molecules. In order to use this method it is necessary to know the molecular weight dependency of the viscosity of the eluted polymer and if it is not a polymer with tabulated values the absolute molecular weights and the intrinsic viscosities must be determined beforehand.

Size exclusion is the dominant mechanism in polymer separation, and ideally is the only one, however other effects will play a rôle to some extent. Interaction has already been mentioned. There should ideally be no interaction between polymer and stationary phase, however this is not always the case. Surface effects can be significant when the stationary phase is inorganic, especially when the eluted polymer is polar, leading to an increase in V_R. This is not an important effect with polystyrene gels, however polymer incompatibility with the gel can arise, and will lead to lower values of V_R, as the polymer is more strongly excluded from the gel.

Dispersion effects will arise in an eluted solution leading to a broadening of the chromatogram. There are several contributory factors in these effects which need to be balanced to achieve minimum dispersion. The effects are determined in terms of plate height H, the rate of change of peak variance relative to the distance migrated. For maximum resolution H should be minimised. Plate height in SEC can be treated in a similar manner to liquid chromatography[6]. The total dispersion arises from four effects which will be treated as independent of each other.

i)Eddy diffusion, caused by the splitting of streamlines as the mobile phase moves around particles of gel leaving turbulent zones. The effects of turbulence around joints in the pipework of the instrument should be minimised by it's construction. Eddy diffusion is independent of flow rate;

eddy diffusion = A, where A is the coefficient of eddy diffusion.

ii)Molecular diffusion in the longitudinal direction of the mobile phase;

longitudinal diffusion = Bu^{-1}, where B is the coefficient of longitudinal diffusion and u is the flow rate .

iii)Mass transfer between streamlines in the mobile phase of different relative velocities;

mass transfer in mobile phase = $C_m u$, where C_m is the coefficient of mass transfer.

iv)Mass transfer between mobile and stationary phase = $C_s u$ where, C_s is the coefficient of mass transfer.

The total effect is the sum of the individual effects, in practice however eddy diffusion and mass transfer in the mobile phase are interdependent and are coupled;

$$H = \frac{B}{u} + C_m u + \Sigma\left(\frac{1}{A^{-1} + (C_m u)^{-1}}\right) \qquad (3.13)$$

For high polymers diffusion coefficients are small, and eddy diffusion tends to dominate, the effects of diffusion based processes(including mass transfer) becoming more significant with lower molecular mass. The competing effects can be illustrated using a van Deempter plot(fig.3.3).

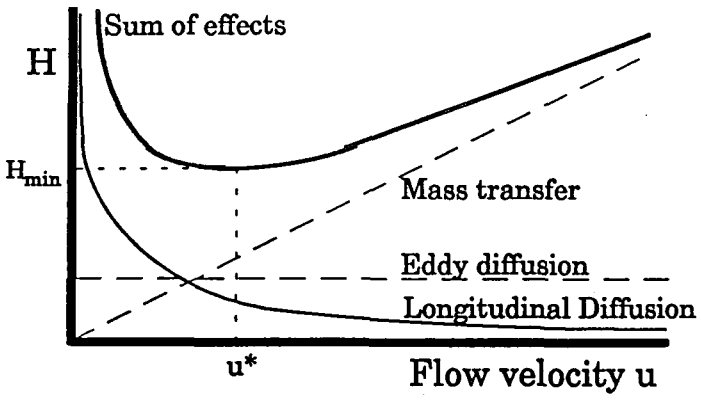

Figure 3.3: A van Deempter plot showing competing effects in size exclusion chromatography

3.2.1 Apparatus and instrumentation: Columns

In section 3.2 it was stated that the most commonly used stationary phase was crosslinked synthetic polymer gels. These are generally polystyrene/divinylbenzene suspension polymerised to small porous particles, evenly sized and spherical to optimise permeability and reduce pressure drop. Pore size is varied to accommodate different ranges of molecular weights. These are packed into columns in the order of 300mm long and 8mm in diameter.

3.2.2 Pumping system and elutent

To measure molecular weights precisely it is necessary that the flow of elutant through the columns is constant, so that elution times for a particular species do not differ. It is also necessary that the flow is not pulsed, as this leads to background fluctuation in the detector. A convenient method to compensate for small changes in the flow rate is the use of an internal marker. Samples are injected into the solvent stream using a valve loop, switchable from a bypass, so the sample can be injected into the loop without solvent flow, reducing dispersion. It is important that the sample injected is not significantly more viscous than the solvent as this can lead to further dispersion. The solvent used as elutent should fulfil three criteria, it should be a good solvent for the eluted polymer, it should provide sufficient contrast to the polymer for the method of detection, and it must wet the polymer gel so that the pores are accessible.

3.2.3 Detector

The detector for the eluted polymer is placed at the end of the line after the columns. A range of instruments are used for this purpose. The most common is the differential refractometer, it measures the change in refractive index of the solvent stream caused by the dissolved polymer, a property common to most solvent/polymer combinations. If there is no difference in refractive index between the polymer and solvent another method must be used. The method also suffers from modest sensitivity to low concentrations, and high sensitivity to temperature and pressure changes.

UV spectrophotometers are also widely used, these rely on an absorbing group on the polymers, and an absence of strong absorption at the same waveband in the solvent. It is usually possible to tune the wavelength to suit the absorbing group. The method is sensitive to the absorbing polymer, requiring only small cell volumes, and is insensitive to changes in temperature and pressure. IR spectrophotometers are also used as detectors, again a suitable waveband must be chosen so the polymer absorbs strongly and the solvent has little or no absorption. The method is insensitive to changes in mobile phase composition, and to temperature fluctuations, but has a low sensitivity and requires large cell volumes. Less common detectors include viscometers, used in conjunction with a refractometer to give absolute values of molecular weight. Absolute weights can also be directly obtained by using a low angle laser light scattering detector, although this requires the dn/dc values for the polymer which must be determined if unknown. These two detectors are expensive and hence not widely used.

3.3 Experimental

SEC measurements were performed in solution in chloroform. The apparatus was a Waters model 590 pump and valve loop injector unit, with 3 Polymer Laboratories PLgel columns of 5μm diameter particles one each of 10^2, 10^3, and 10^5 Å pore size. The detector unit in general use was a Waters model R401 differential refractometer, and for detection solely of phenylene a Perkin-Elmer model LC55 UV spectrophotometer. This was set to 260nm for calibration purposes and to 320nm for phenylene. Detector signals were collected on a Polymer Laboratories data capture unit, and fed into a personal computer where it was analysed using Polymer Laboratories software[7]

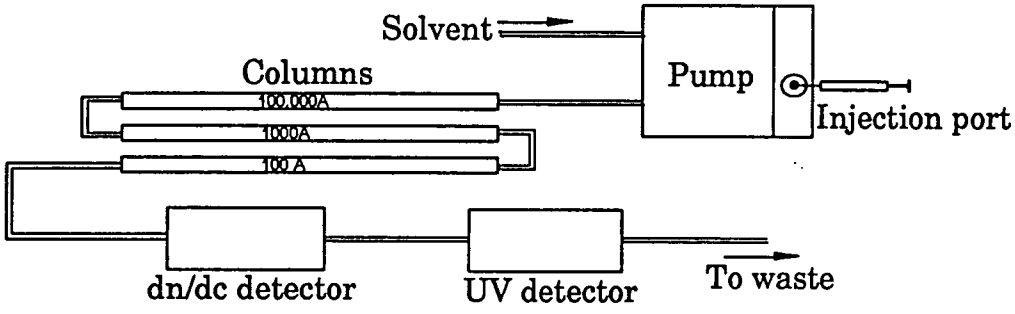

Figure 3.4: Size Exclusion Chromatography Apparatus

Calibration was performed using narrow polydispersity Polymer Laboratories polystyrene standards, over the molecular weight range of 162 to $4x10^6$. Toluene was used as an internal marker for the refractive index detector and acetophenone for the UV detector.

Samples were made up in the range ≈ 0.5 - 0.1%, except for those of very high molecular weight standards which were in the order of 0.02%[8], by dissolving the sample in 2ml of distilled chloroform. A single drop of flow marker was added to the solution and filtered through a 0.2μm Millipore PTFE membrane filter. The sample (200μl) was introduced into the valve loop, and injected into the solvent stream whilst simultaneously initiating the software. This technique could be undertaken with a difference of a fraction of a second, for elution times of 15 to 25 minutes, which should ensure a high degree of precision.

3.4 Results

The results obtained from SEC for each fraction are tabulated below;

Percentage Aromatisation	M_p	M_n	M_w	M_z	M_w/M_n
0	415500	302500	405500	518000	1.34
10	257500	191000	304000	470000	1.59
20	180500	129500	273000	576000	2.11
30	157000	91500	357500	969000	3.90
40	92500	69000	569500	2275000	8.30

Table3.1: Fraction A

Percentage Aromatisation	M_p	M_n	M_w	M_z	M_w/M_n
0	324000	234000	308000	382000	1.32
10	186500	124000	206000	389000	1.61
20	152000	98000	207500	442000	2.12
30	132000	80500	241500	594000	3.01

Table 3.2: Fraction B

Percentage Aromatisation	M_p	M_n	M_w	M_z	M_w/M_n
0	239000	208000	260000	323500	1.25
10	157500	116000	208500	384500	1.59
20	150000	81500	205000	495500	2.51
30	132500	76500	192000	473500	2.51
40	51500	37500	215000	846500	5.72

Table 3.3: Fraction C

Percentage Aromatisation	M_p	M_n	M_w	M_z	M_w/M_n
0	167000	141500	178000	216000	1.25
10	183000	92000	149500	196500	1.45
20	152500	96000	198500	454000	2.07
30	109500	68500	197000	518500	2.89
40	55500	39500	266000	975500	6.73

Table 3.4: Fraction D

Percentage Aromatisation	M_p	M_n	M_w	M_z	M_w/M_n
0	120500	110500	125000	142000	1.133
10	128500	99000	158500	310500	1.61
20	116000	71500	146500	377500	2.04
30	87000	59500	142000	373000	2.39

Table 3.5: Fraction E

Percentage Aromatisation	M_p	M_n	M_w	M_z	M_w/M_n
0	118500	83000	119500	142000	1.43
10	108500	74500	110000	186000	1.48
20	91000	61500	139500	432000	2.26
30	68000	49000	117500	342500	2.41
40	52500	36000	154000	605000	4.29

Table 3.6: Fraction F

Percentage Aromatisation	M_p	M_n	M_w	M_z	M_w/M_n
0	80000	74000	84000	94500	1.14
10	64500	54500	80500	166000	1.47
20	60500	49000	84500	227500	1.73
40	47500	32000	152000	650000	4.72

Table 3.7: Fraction G

Percentage Aromatisation	M_p	M_n	M_w	M_z	M_w/M_n
0	1923000	1225000	2312000	3658000	1.89
20	189000	105500	243000	482000	2.29
30	65500	153000	147000	606500	9.61
40	66000	44000	242000	842000	5.50

Table 3.8: Fraction H

Percentage Aromatisation	M_p	M_n	M_w	M_z	M_w/M_n
0	29500	17100	26500	37600	1.55
10	27500	17500	26000	35000	1.48
20	26000	15500	26000	50000	1.66
30	25500	18750	107250	385000	5.72
40	22000	15500	62000	343500	4.00

Table 3.9: Fraction L

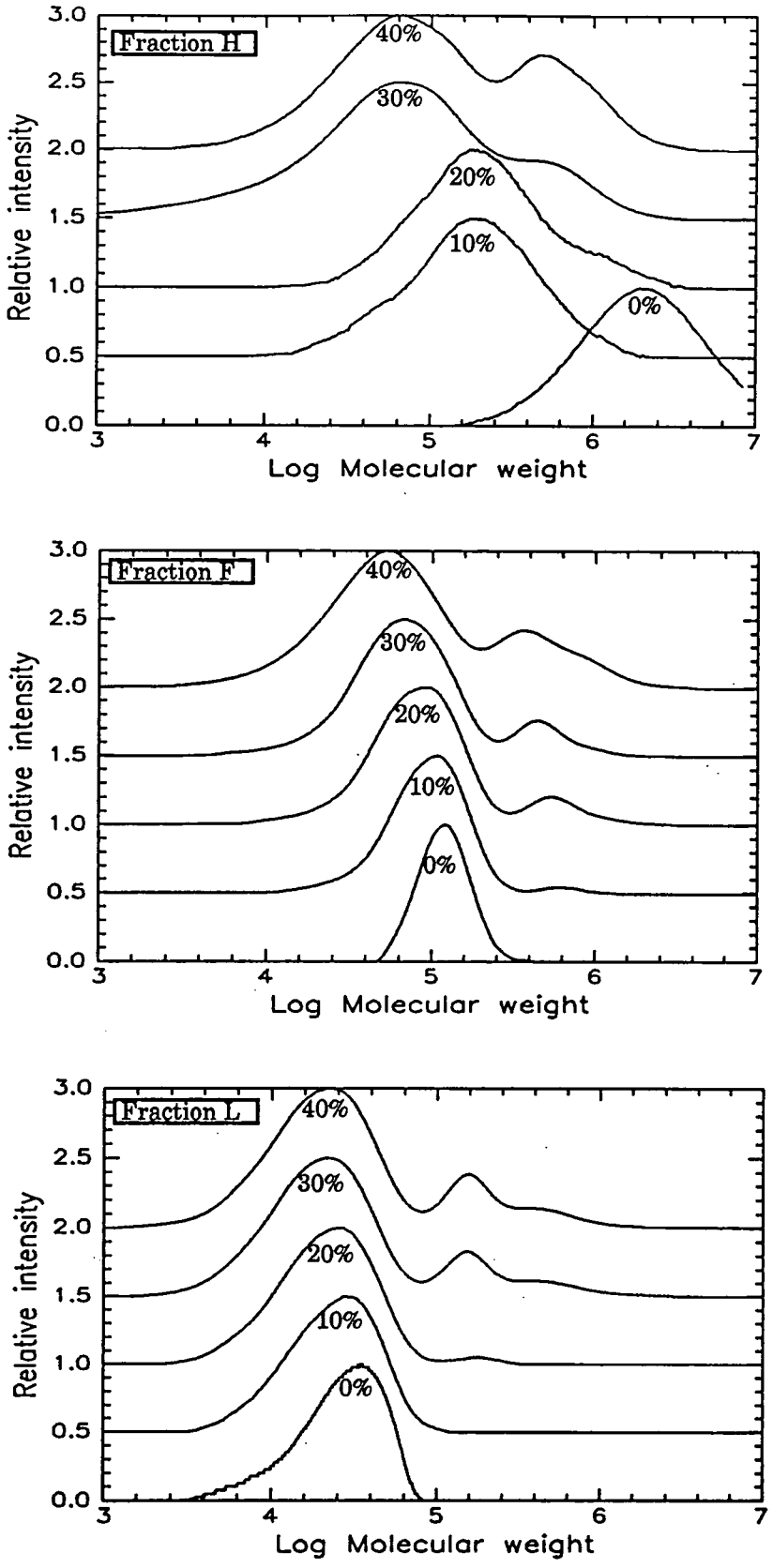

Figure 3.5: Chromatograms of Fractions H, F and L, from 0 to 40% aromatisation

Figure 3.5 shows typical sets of SEC chromatograms. A feature is the appearance of a second peak at the high molecular end of the distribution. This is presumably due to the formation of an aggregated species in the solution. The second peak has been analysed to determine the peak molecular weight and the area that lies under the peak (table 3.10).

Sampl	M_{pmain}	$M_{psecondary}$	Ratio M_{ps}/M_{pm}	Percentage in secondary peak
B10	186500	940000	5.04	2.3
C10	157500	723000	4.59	6.2
E10	128500	799000	6.22	4.8
F10	108500	630000	5.81	2.1
G10	64500	484000	7.50	3.3
Mean			5.8±1.2	4±2
B20	152000	798000	5.25	4.5
C20	150000	807000	5.38	10.9
D20	152500	872000	5.72	9.1
E20	116000	664000	5.72	7.5
F20	91000	546000	6.00	11.0
G20	60500	398000	6.58	6.9
L20	26000	175000	6.73	1.8
Mean			5.9±0.6	8±3
A30	157100	774500	4.93	30.7
B30	132000	748000	5.66	19.7
C30	132500	694000	5.24	13.7
D30	109500	606000	5.53	19.7
E30	87000	538000	6.18	11.7
F30	68000	449000	6.60	12.2
H30	65500	417000	6.37	15.3
L30	51500	152000	2.95	19.0
Mean			5.4±1.1	18±6
A40	92500	771000	8.34	26.4
C40	51500	423000	8.21	29.6
D40	55500	458000	8.25	32.8
F40	52500	367000	6.99	24.4
G40	47500	289000	6.08	29.1
H40	66000	496000	7.52	32.2
L40	22000	153000	6.95	20.7
Mean			7.5±0.8	28±4

Table 3.10: Results from bimodal SEC samples

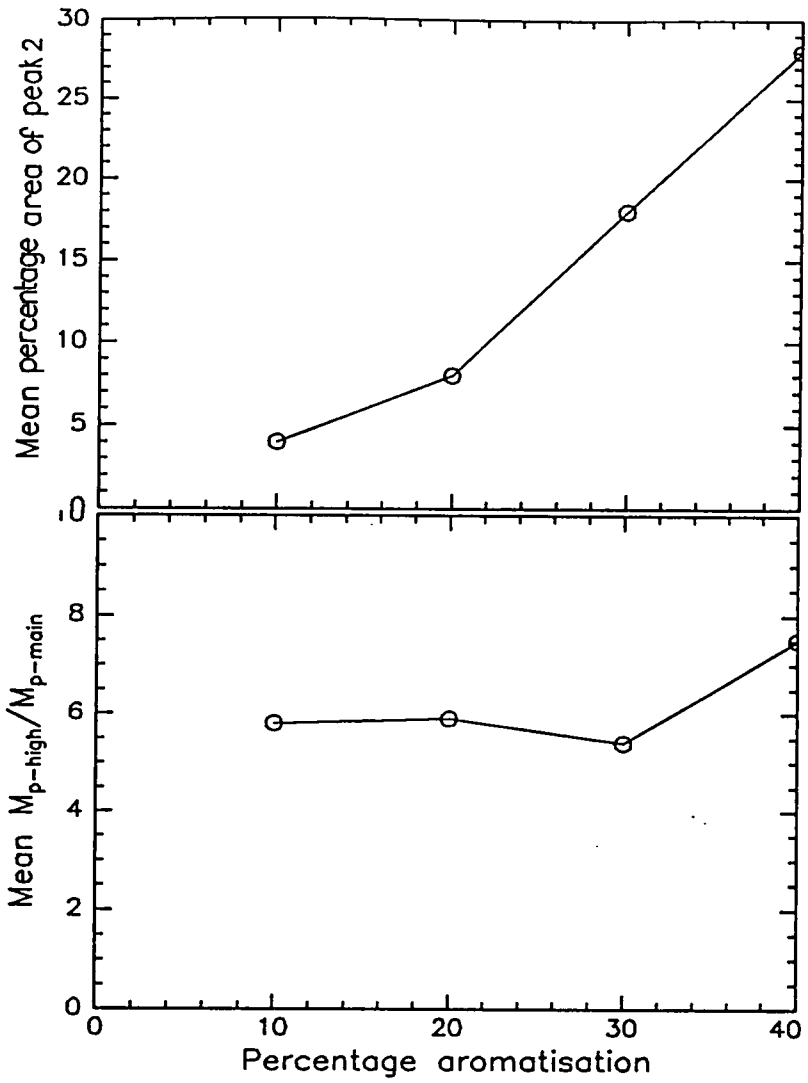

Figure 3.6: Change in properties of second peak in distribution with aromatisation

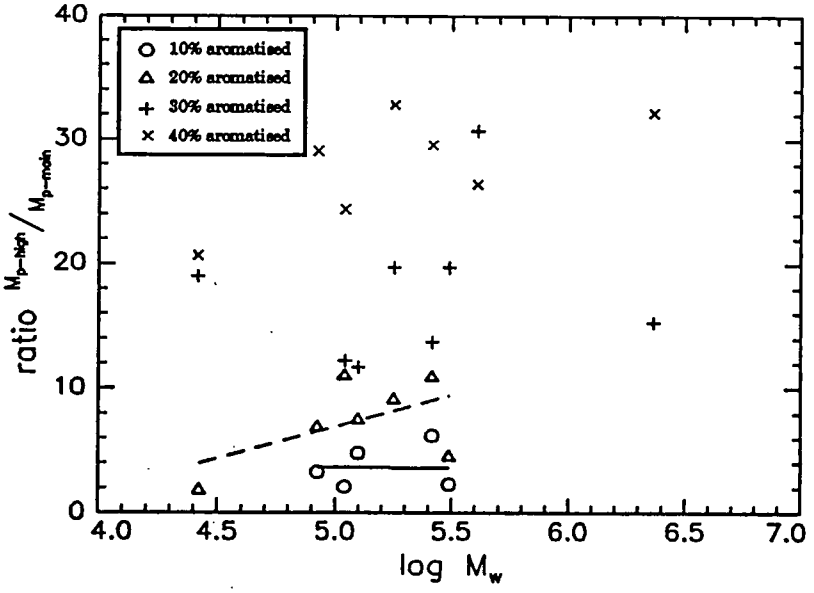

Figure 3.7: Change in molecular weight peak ratio with molecular weight

A further set of samples were prepared and analysed by SEC. These were prepared from the unfractionated polymer, and were aromatised up to 50%. This was to determine the relative amounts of phenylene in the two peaks in the chromatograms, using a UV spectrophotometer, coupled to the apparatus, providing dual detection. While the refractive index detector is sensitive to both poly(DHCD-DMC) and PPP, poly(DHCD-DMC) in $CHCl_3$ is insensitive to radiation above 280nm while partially aromatised polymer absorbs strongly with peaks at 260nm and 300nm. The spectrophotometer was set at 320nm where there was no distinguishable signal from the precursor, but strong absorption from the aromatised polymer(fig.3.8).

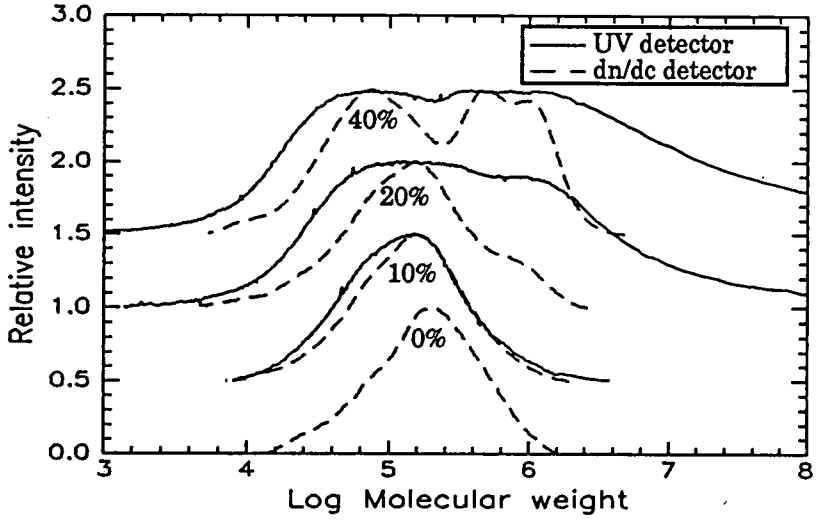

Figure 3.8: UV spectra of unaromatised and partially aromatised polymer

From the chromatograms using the UV detector the peaks are seen to tail out into the low and high molecular weight ends. The detection of phenylene in these tails suggest that the aromatisation reaction which reduced them causes chain scission and aggregation. The results from these samples are tabulated below, although results from the UV detector are not tabulated because in some cases (marked §) the signal extended well beyond the limits of total exclusion, because of very large aggregates which are formed and total permeation, possibly because of interaction of the aromatised species with the column, or the presence of very small fragments from the aromatisation.

Sample	dn/dc			UV		
	$M_n / 10^3$	$M_w / 10^3$	PD	$M_n / 10^3$	$M_w / 10^3$	PD
U0%	109	237	2.19	---	---	---
U10%	80	187	2.34	82	177	2.16
U15%	84	194	2.32	107	270	2.52
U20%	67	223	3.30	110	347	3.15
U25%	56	234	4.23	51	§	
U30%	73	235	3.20	53	§	
U35%	73	416	5.71	45	§	
U40%	71	373	5.25	73	§	
U50%	89	528	5.90	38	§	

Table 3.11: Results from dual-detector SEC

A number of the chromatograms recorded contained multiple peaks, detailed below

Sample	dn/dc			UV		
	$M_{p\,main}$ /10^3	$M_{p\,sec.}$ /10^3	Ratio $\frac{s}{m}$	$M_{p\,main}$ /10^3	$M_{p\,sec.}$ /10^3	Ratio $\frac{s}{m}$
UF15	161			157	861	5.5
UF20	154			155	835	5.4
UF25	109	500	4.6	108	535	5.0
UF30	122	522	4.3	108	458	4.2
UF35	75	442(1060)	5.9 (14)	74	279(839)	3.8 (11.3)
UF40	74	591(956)	8.0 (13)	72	377(1134)	5.2 (15.8)
UF50	71	358(973)	2.5 (14)	65	722	11.1

Table 3.12: Peak molecular weights for bimodal chromatograms(figures in parentheses represent molecular weights of a tertiary peak).

3.5 Discussion

The SEC analysis of the partially aromatised polymer has revealed some information on the mechanism of the aromatisation reaction. From the changes in M_n and M_p it is seen that there is a drop in molecular mass during the reaction. This will occur to some extent because of the loss of substituents, but the effect is greater than that from stoichiometry alone, as can be seen in figure 3.9 where the theoretical loss is shown together with the actual loss.

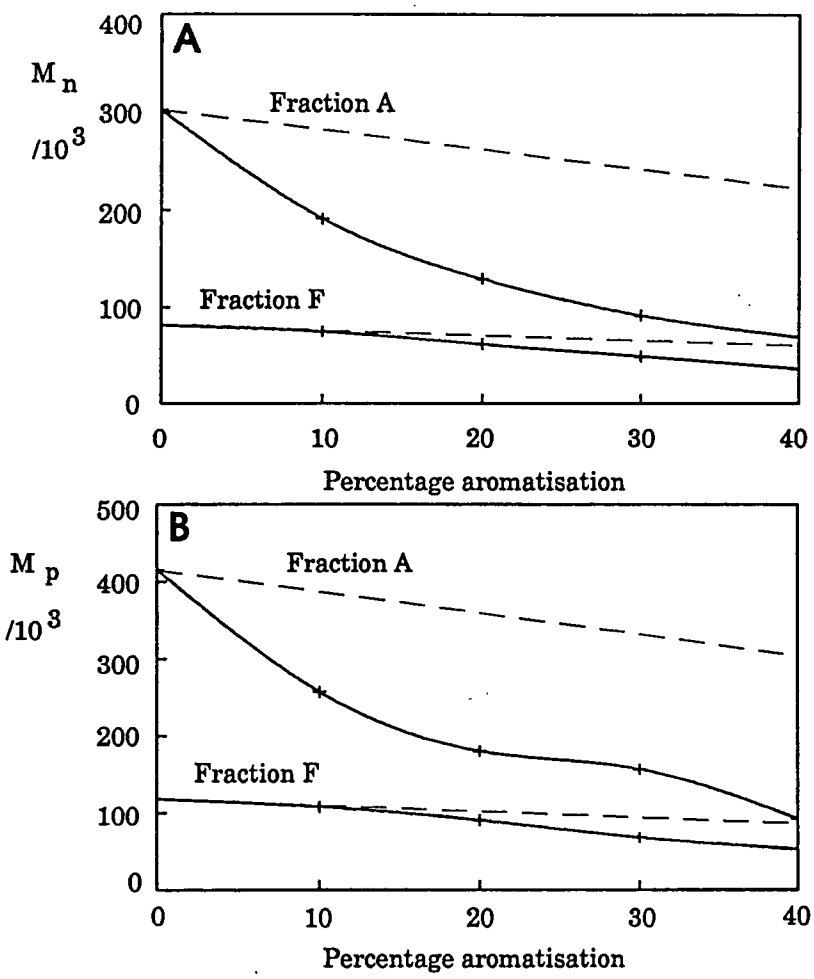

Figure 3.9: Changes in molecular weight with aromatisation

A: number average molecular weight, B: peak molecular weight

(Dashed lines represent stoichiometric loss on aromatisation).

The additional drop in molecular weight can be attributed to chain scission during the aromatisation reaction, and to the induction period of the reaction. The varying times of the induction period (figure 2.5) could account for some of the differences in changes with aromatisation.

Number average molecular mass is by definition (see Appendix 2) sensitive to molecules of low molecular weight, and insensitive to molecules of high molecular weight. It will therefore be affected by the fragments from chain scission, whilst remaining largely unaffected by the formation of high molecular weight aggregates. Peak molecular weight is the value at the maximum of the distribution, and reflects the condition of the bulk of the polymer. It is seen in fig. 3.9 that chain scission has occurred in both fractions A and F, although the effect is more pronounced in the higher molecular weight fraction. This is due to steric effects, the longer wormlike chain adopting a more coiled configuration will experience a greater steric strain as it stiffens than the shorter chain, which will tend towards a straighter configuration. It is thought that the strain causes the rupture of the 1,2-bonded units, although most scission occurs between 0 and 10% reaction.

Weight average molecular weight (defined in Appendix 2) is sensitive to the larger molecules in the polymer, and is affected by the formation of the aggregates in the solution. Therefore M_w generally increases with reaction, after an initial drop caused by chain scission. The rise in M_n as M_w increases leads to an inevitable increase in polydispersity.

The high molecular weight peak in the aromatised polymer is due to the formation of aggregates, caused by the clustering of insoluble phenylene segments in the aromatised polymer. These aggregates must also contain a proportion of poly(DHCD-DMC) to maintain solubility. The aggregates may be of a micelle type structure with a PPP core and a halo of poly(DHCD-DMC)(fig. 3.10) From the ratio of peak molecular weights an approximate aggregation number can be calculated, as in table 3.12. This is approximately 6, rising to about 8 at 40% conversion, the polymers UF40% and UF50%(table 3.12) have two high molecular peaks, with aggregation numbers of approximately 8 and 13, and 5 and 14 respectively, it would appear that there is an

increase in the aggregation number with aromatisation, perhaps the result of longer sequences of PPP allowing larger clusters to form.

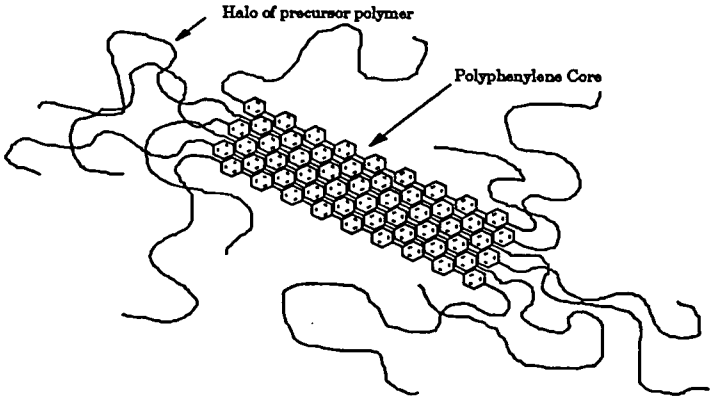

Figure3.10: Possible micelle type structure with aggregation number of 6

If the partially aromatised polymer forms micelle-like aggregates then it is probable that the polyphenylene exists as blocks rather than randomly dispersed units, and the presence of aggregates down to 10% reaction provides some evidence for a 'zipping' mechanism for the reaction forming a blocky polymer. It is otherwise extremely unlikely that blocks could form if 10% of the cyclohexadiene nuclei had aromatised randomly.

Measurements with the UV detector{fig 3.8} show that the phenylene is distributed evenly through the aromatised polymer (differences in relative peak intensities appear to be due largely to the signal saturating because of the far greater sensitivity of the UV detector) and the distribution generally follows the overall trend of the dn/dc detector. It is noted however that at higher degrees of aromatisation there are small amounts of very high molecular material, consistent with the formation of aggregates increasing as the reaction proceeds and more polyphenylene is formed. Phenylene remains distributed throughout the whole molecular weight range, and even at 50% reaction a large proportion of it is in the peak of unassociated molecules, although it is not possible to determine whether or not these have intramolecularly aggregated.

When a polymer solution passes through a SEC apparatus the polymer molecules are subjected to shear forces. These may be of a sufficient magnitude to cause the polymer to form aggregates, as there is no evidence from QELS measurements (see Chp 6) of

bimodality, even at 40% conversion, but this could be the result of insufficient resolution. SANS measurements made under shear show no evidence of significant changes, but this may simply be due to insufficient shear in the experiment. One possibility that could account for the spurious formation of micelles in SEC is that under normal circumstances the aromatised molecules prefer to aggregate intramolecularly, and they only cluster together in a shear field. If these micelles are not an artifice of the method then it can be seen that they will form as low as 10% aromatisation, this supports the idea that the reaction proceeds via a 'zipping' mechanism, the autocatalytic effect causing cyclohexene units to aromatise sequentially along the chain forming blocks of PPP, because contiguous blocks of PPP would cause the chains to aggregate far more readily than randomly distributed ones, especially if they constitute only 10% of the polymer units.

Micelles formed by amphiphilic surfactants in aqueous solution have been observed to disperse and reform rapidly in pressure- and temperature perturbation type experiments. It has been deduced from SEC measurements on block copolymers that because they eluted as sharp peaks after very long elution times(≈5hrs)[9] the situation must be very different for polymer micelles, and the cores will be shielded by the halo of soluble polymer. This would be especially pertinent in the present case where the extreme insolubility of the PPP blocks favours the polymer-polymer interaction and the core is likely to be dense, especially if composed solely of paraphenylene. Therefore once formed the micelles remained stable and eluted together, but because the molecules were polydisperse the peaks were not very sharp.

The more or less even distribution of PPP throughout the molecular weight range is slightly unexpected. It would be imagined that all the poly(phenylene) formed, or at least the bulk of it would aggregate if it formed as blocks, as it is assumed to. The reasons for this could be either that a high proportion remains intramolecularly aggregated, or that up to a certain length of PPP block the polymer is freely soluble. and a critical block length is required for micelles to form, which has not been achieved, perhaps because of ortho bonded units interrupting the reaction, or that a proportion of the reaction is

random and does not propagate to neighbouring units. Whatever the reason the result, so far as SEC is concerned there are two species in the solution of partially aromatised polymer, single chains and micellar aggregates. This problem has been addressed to some extent in the following section. In terms of its properties a micelle is more closely akin to a spherical entity, albeit inhomogenous, than a single chain, and this will modify its physical properties, such as the relationships between size and molecular weight, a mixture of both a micelle and a single chain will be considerably more complex than either singly.

3.6 Analysis of aromatised polymer

Partially aromatised samples of poly(DHCD-DMC) tended to show bimodality in size exclusion chromatograms. This was thought to be due to the existence of two species in the polymer, one that exists as single molecules and one liable to aggregation, which may be more highly aromatised. To clarify the situation a single sample at 30% aromatisation was prepared. This was then fractionated and a range of tests done on each fraction, to establish differences that might exist.

A total of 1.3g of aromatised polymer was obtained. This was fractionated by non solvent addition, because the polymer was insoluble in acetone, and liable to further reaction in NMP. Chloroform was used as a solvent, and hexane as non-solvent. A 1% solution of polymer was used, and after several attempts 3 fractions of approximately equivalent weight were obtained, and the following analyses were performed;

3.6.1 Size exclusion chromatography

SEC measurements were made on the unfractionated polymer, and on the three fractions. The original polymer and the three fractions were dissolved in distilled chloroform along with a drop of toluene as a flow marker, filtered and run through the Waters instrument described in section 3.3. The resulting chromatograms (fig. 3.11) quite clearly show the separation of the two species in the solution into two fractions, sample 1 is almost entirely the high molecular weight peak, and sample 3 almost entirely the low molecular mass peak. Fraction 2 is a mixture of the two. The molecular weights are tabulated in table 3.13

Sample	M_p /10^3	M_n /10^3	M_w /10^3	M_w/M_n
Unfractionated	74(449*)	53	145	2.74
Fraction 1	714	384	589	1.53
Fraction 2	134	88	202	2.30
Fraction 3	65	49	79	1.60

* second peak

Table 3.13: Results of SEC analysis of fractionated aromatised polymer

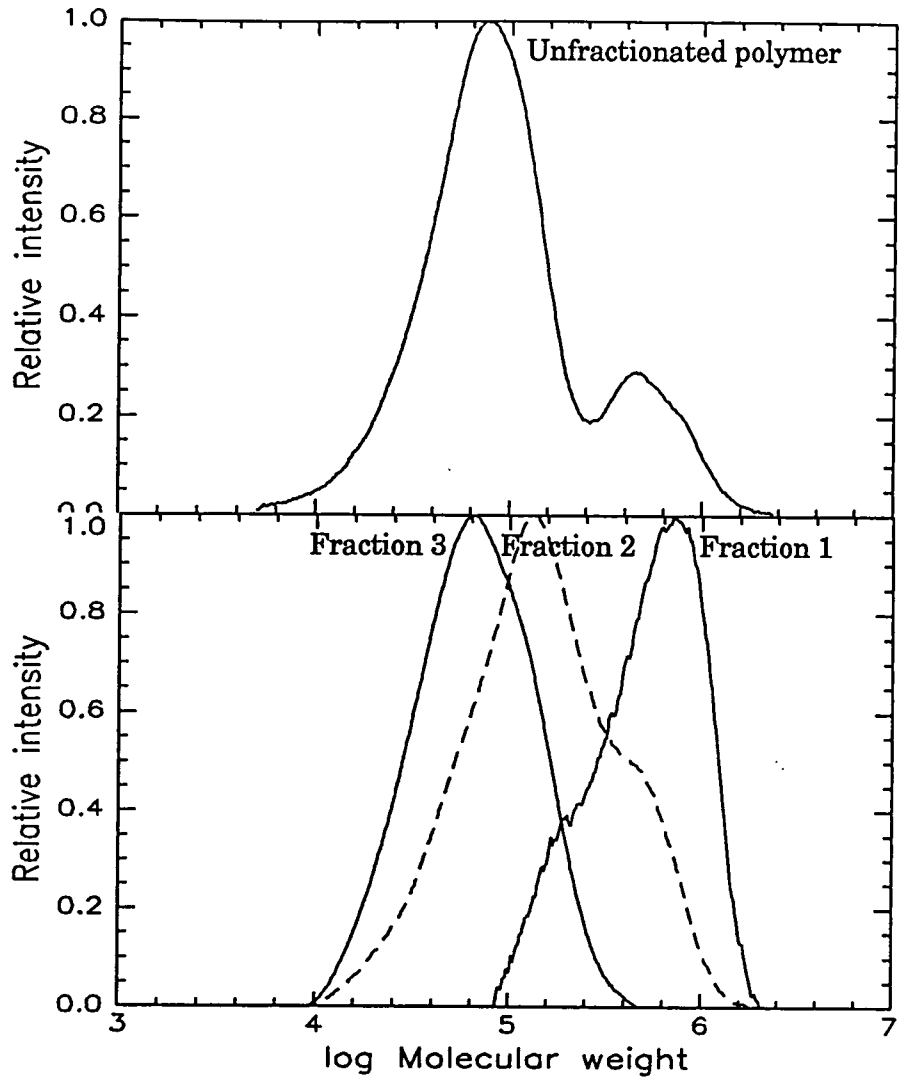

Figure 3.11: Molecular weight distributions of aromatised polymer, showing results of fractionation

3.6.2 Thermogravimetric analysis

TGA is used simply to determine the extent of aromatisation of the fractions. The samples are pyrolysed to full aromatisation, and the weight loss used to calculate the % aromatisation(section 2.5.1). The original polymer and the three fractions were run, and the results are tabulated below.

Sample	Initial mass /g	Final mass /g	Aromatisation /%
Unfractionated	4.42	1.85	30.5
Fraction 1	3.25	1.37	31.4
Fraction 2	4.03	1.68	30.1
Fraction 3	2.99	1.23	28.5

Table 3.14: TGA analysis of partially aromatised polymer

3.6.3 Elemental analysis

The method of determining the percentage of carbon and hydrogen, and by default oxygen, the sample is a method of determining percentage aromatisation in the sample. The theoretical proportions of carbon and hydrogen can be calculated, and then the theoretical aromatisation can be determined from experimental data. Four samples were submitted, the three fractions, and an unaromatised polymer as a test of the method. The theoretical percentage carbon is 52.6%, and hydrogen, which is constant for any percentage aromatisation, 5.26%. The results are tabulated below:

Sample	Hydrogen /% ±0.03	Carbon /% ±0.09	Aromatisation /%
Unaromatised	5.37	52.88	0
Fraction 1	5.26	66.75	33.6
Fraction 2	5.33	66.20	32.3
Fraction 3	5.29	65.54	30.7

Table 3.15: Elemental analysis of partially aromatised polymer

3.6.4 Fourier transform infra-red spectroscopy

FTIR spectra were run on the fractions to detect chemical changes in the sample, especially those relating to the carbonyl absorption at about $1750cm^{-1}$, and the phenyl absorption around $810cm^{-1}$.

Spectra were run both by transmissions with thin films cast from chloroform, and, when the technique became available, by attenuated total reflection from films cast from chloroform onto a thallium salt KRS3 crystal. The transmission spectra had a very high background, and films sufficiently thin to reduce this could not be cast, as they lost their integrity, and so the ATR spectra are used instead.

The absorptions of the relevant peaks are tabulated in 3.16, corrected for background. When the method used in the ICI patent[10] to determine percentage aromatisation from FTIR (equation 3.14) was used it was found to severely overestimate percentage aromatisation. This could be corrected if the value of the multiplier γ was altered (table 3.16), choosing a value of 30% aromatisation for the second fraction.

$$\% \text{ Arom} = \frac{\gamma A_{810cm^{-1}}}{\gamma A_{810cm^{-1}} + A_{1750cm^{-1}}} \qquad (3.14)$$

for ICI patent γ=10, if 30% arom. for fraction 2, then γ=2.939

This method is however highly irregular, and little weight can be placed on the results, although the order of the results corresponds to that from the other techniques. The difference may be due to instrumental and sample variables, the samples for the ICI method were sputtered with gold for measurement for instance. If however the spectra are compared it can be seen that they are virtually identical (figure 3.12).

Sample	A_{810}	A_{1750}	$\frac{100 \times A_{810cm^{-1}}}{A_{810cm^{-1}} + A_{1750cm^{-1}}}$	$\frac{100 \times \gamma A_{810cm^{-1}}}{\gamma A_{810cm^{-1}} + A_{1750cm^{-1}}}$
Fraction 1	0.435	2.584	15.5	33.1
Fraction 2	0.421	2.559	14.1	30.0
Fraction 3	0.373	2.603	12.5	27.2

Table 3.16: FTIR analysis of partially aromatised polymer

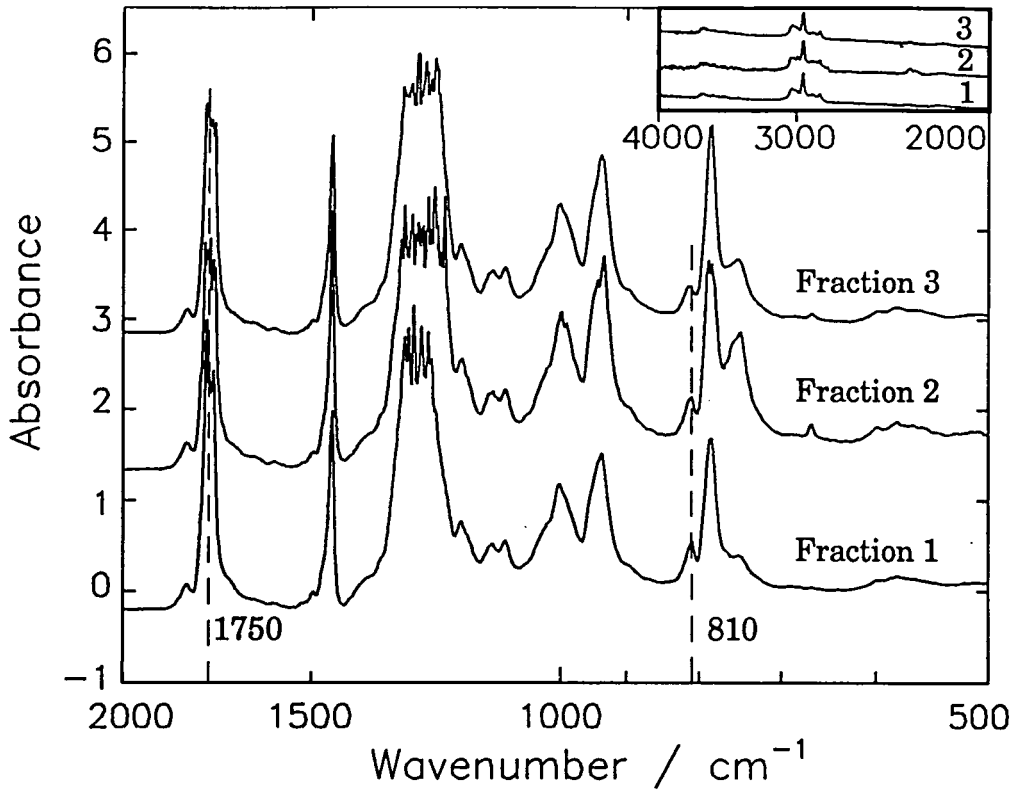

Figure 3.12: FTIR spectra of aromatised polymer showing peaks used for calculation. (inset box-extended spectra).

3.6.5 Nuclear magnetic resonance spectroscopy

NMR, like FTIR should reveal chemical differences in the fractions. Samples were submitted for proton and carbon 13 NMR. The proton spectra were very poor, and no suitable spectra could be obtained. Carbon 13 spectra were obtained from 5% deuterochloroform solutions in 13mm diameter tubes. The spectra obtained are shown in figure 3.13. The assignments and differences are tabulated in table 3.17.

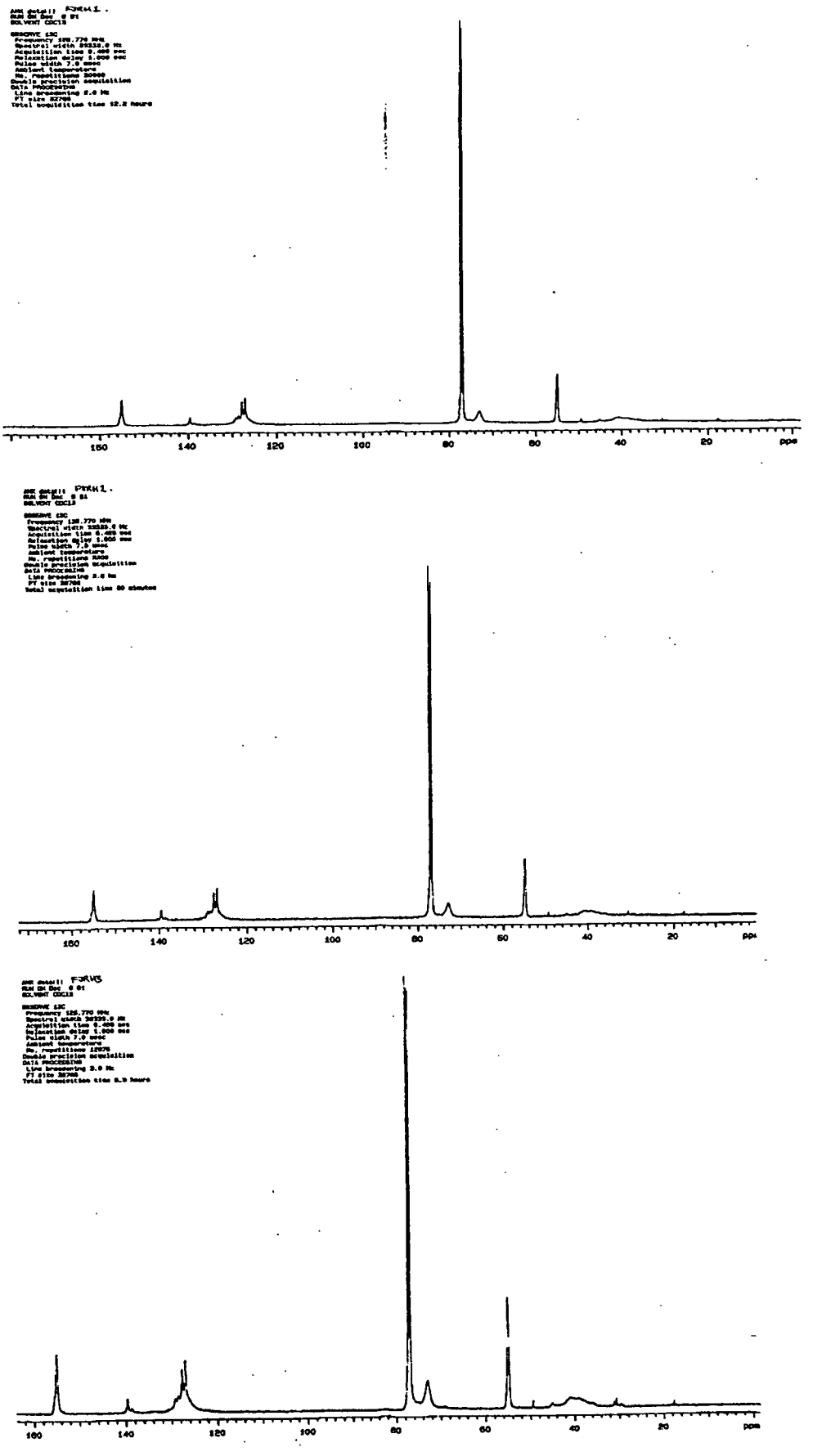

Figure 3.13: ^{13}C NMR of partially aromatised polymers

It is likely that the signal from long polyphenylene segments would be very much attenuated because of their lack of mobility if they have aggregated as the SEC measurements would suggest. A similar effect has been noted with PS-co-PPP[11]. In common with the FTIR spectra there appears to be little difference between the three fractions

^{13}C site	Assignment /ppm	Peak
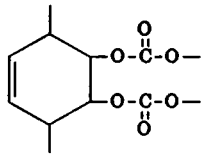	155	sharp
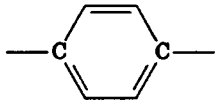	140	sharp
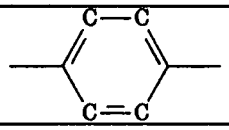	129	medium
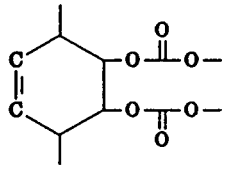	127	sharp
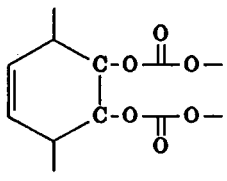	73	medium
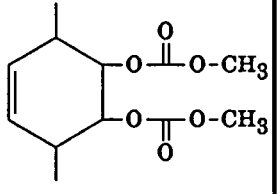	55	sharp
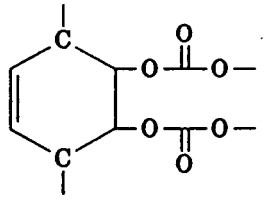	40	broad

Table 3.17: NMR assignments for partially aromatised polymer(figure 3.13)

3.6.6 Mass spectrometry

Samples of the polymer fractions were submitted for mass spectrometry, together with an unaromatised polymer. It was hoped that some idea could be gained of the amounts of aromatisation and chain scission that have taken place in the polymers by comparison of the characteristic peaks of precursor, phenylene and initiator peaks, since presumably the fragments detected will predominantly originate from chain ends. However in practice this has proved unfeasible, the spectra obtained from the methods available were of poor quality, and not reproducible, and also there is some uncertainty in interpretation since the precursor residue will have exactly three times the mass of phenylene, so it becomes impossible to distinguish sequences of either entity. Spectra from fractions 1 and 3, and the unaromatised polymer are shown below. One prominent difference is the dearth of peaks from fraction 1, compared to fraction 3 and the unaromatised precursor polymer.

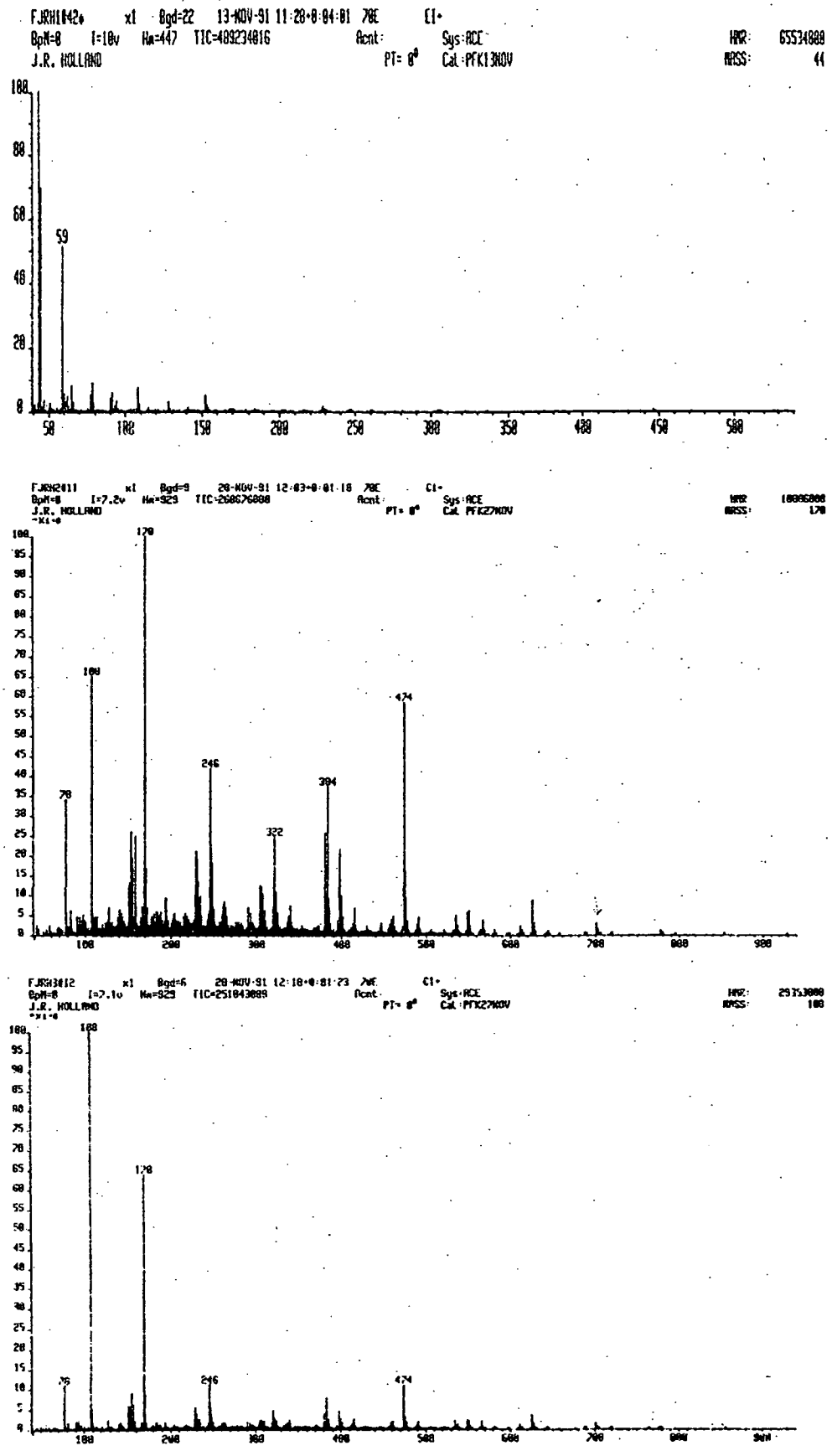

Figure 3.14: Mass spectra of fraction a;1, b; 2, and c; 3.

3.6.7 Discussion

The fractionation of the partially aromatised polymer has successfully separated the two species observed in SEC chromatograms, and revealed some of the differences between them. The possibility of separating these two species is evidence for the bimodality observed in SEC being real, not a result of the conditions of the technique.

The two fractions most widely resolved, 1 and 3 do not display any significant chemical differences as far as NMP and FTIR can detect. The differences which do exist are subtle, and indicate different proportions of PPP and poly(DHCD-DMC) moieties, rather than the existence or exclusion of a particular group in one or other of the fractions.

SEC shows a considerable difference in molecular weight between the two, fraction 1 being ≈8 times heavier than fraction 3. Elemental analysis and TGA show a real, if small difference in the degree of aromatisation of each sample, fraction 1 being more aromatised than fraction 3, this presumably being the cause of the aggregation. Fraction 1 is the least soluble, as it was first to precipitate, fraction 3 the most soluble, this would also be expected as fraction 1 contains a greater proportion of PPP, if only apparently 3%. The fractions also formed distinctly different solutions when dissolved in chloroform, 5% solutions in $CDCl_3$ were prepared for NMR. Fraction 1 formed a very viscous solution, almost a gel, deep yellow in colour, fraction 3 formed a fluid solution, pale yellow in colour.

Leaving aside fraction 2, which is intermediate to fraction 1 and 3, the results for the fractions show polymers which, while not being significantly different beyond a few percent aromatisation in terms of chemistry, are significantly different in terms of physical properties. Fraction 1 is composed of a heavy species, presumably an aggregate, ≈8 times the size of fraction 3.

The reasons for this could be several, there may be a critical point, just beyond 30% aromatisation where the chains lose the ability to exist as free chains, and thermodynamic considerations force them to aggregate. Some evidence for this may be seen in the viscometric data (chapter 5) where the watershed between single chain and aggregated behaviour lies between 20 and 30% reaction, and it is around this point that a similar effect

is observed in ILS. However size exclusion chromatograms for polymers at 10% and 20% conversion often contain aggregated polymer (table 3.10), while those at 40% contain a significant proportion of single chains.

Another possibility is that the aromatisation reaction is sufficiently random that while one section of the polymer is aromatised in short blocks, other chains experience the sequential reaction along extensive lengths, which make the polymer more susceptible to aggregation. As the reaction proceeds a greater proportion joins that polymer with long sequences and aggregates. The cause of short and long sequences could be the distribution of the ortho-bonded kinks in the chain.

A third possibility is that all the less aromatised polymer, the single chains of fraction 3 have aggregated intramolecularly, again possibly because of the distribution of PPP block lengths. If this is the case both the classes of aggregate are stable within the SEC column and its associated shear fields. There is also little dispersion and reformation in solution, it has proved possible to resolve the two peaks quite successfully by fractionation, and in the same form as they are measured by SEC.

The methods of analysis used in this study show that the chemical differences in the two polymer species are restricted to small differences in the degree of aromatisation, and that there is instead some structural difference between them. The most likely cause of this is the different lengths of PPP sequences, and that once a molecule contains a sufficiently long sequence, or possibly sequences of PPP it will form supramolecular aggregates, and it is the arrangement, not the amount, of poly(paraphenylene) in a moderately aromatised polymer which causes it to aggregate.

3.7 References

1, Holding,S.,Hunt,B.J., *Size Exclusion Chromatography*, Blackie, Glasgow, 1989.

2, Dawkins,J.V.,Ch in '*Comprehensive Polymer Science*',vol 1,Ed Booth,C.,Price,C.,Pergammon Press,Oxford,1989.

3, Bly,D.D,Kirkland,J.J.,Stoklosa,H.J.,Yau.W.W.,*J.Chromatogr.*,**125**,219, (1976).

4, Benoit,H.,Grubisic,Z.,Rempp,P.,*J.Polym.Sci.*,**B5**,753,(1967).

5, Bruzzone,A.R.,Cooper,A.R.,*J.Polym.Sci.,Polym.Phys.Ed.*,,**11**,1423,(1973).

6, Giddings,J.C.,Mallik,K.L.,*Anal.Chem.*,**38**,997,(1966).

7, *'GPC data station operating manual'*, Polymer Laboratories, Church Stretton, 1991.

8, GPC polymer standards guide, Polymer Laboratories, Church Stretton.

9, Price,C.*et al,Polymer Communications*,**23**,650,(1982).

10, Ballard,D.G.H.,Courtis,A.,Shirley,I.M.,European patent 0076605,1983.

11, Francois,B.,Zhong,X.F.,*synth.metals*,28,E35,(1989).

CHAPTER 4

INTENSITY LIGHT SCATTERING

4.1 Introduction

Intensity light scattering is an invaluable method for measuring the dimensions and thermodynamic properties of a solute, and unlike SEC there is no theoretical limit to the molecular mass which can be measured, from small molecules up to viruses with molecular masses of thousands of millions. It involves the measurement of the scattered light from a solution over a range of angles.

Intensity light scattering has been used in this study to measure the size and second virial coefficient of partially aromatised polymer in solution in two solvents chloroform and NMP.

4.2Theoretical Considerations

A précis of the technique is provided here. More thorough introduction discussions of the method are available in a number of texts[1,2]. When light interacts with a particle of polarisability α, whose size approximates to that of the wavelength of light, the particle behaves as an oscillating dipole. This oscillating dipole becomes a secondary source of radiation, radiating a plane polarised wave of identical wavelength in all directions. The intensity of the light at the point P in the plane perpendicular to the dipole shown diagrammatically in figure 1 is given by the expression;

$$I_\theta = \frac{16\pi I_0 \alpha^2}{\lambda^4 r^2} \cdot \sin^2 \frac{\theta}{2} \qquad (4.1)$$

For a system containing N particles in a volume V scattered intensity per unit volume is given by;

$$I_\theta = \frac{16\pi^4 I_0 \alpha^2}{\lambda^4 r^2} \cdot \frac{N}{V} \cdot \sin^2 \frac{\theta}{2} \qquad (4.2)$$

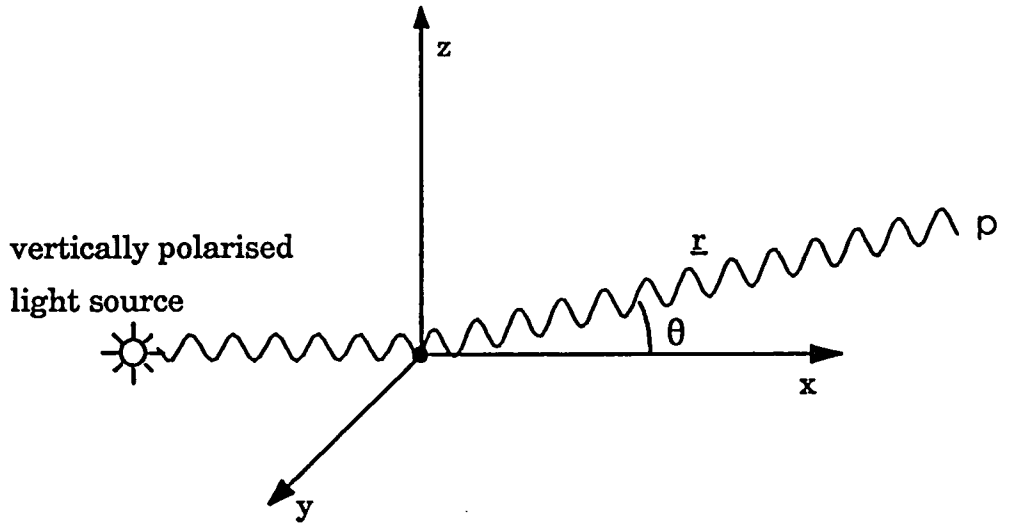

Fig 4.1: Scattering of plane polarised light by a point scatterer.

The polarisability is related to the refractive index, so for a solution of N particles, refractive index n, in a volume, V, of solvent with refractive index n_0

$$\alpha = \frac{1}{2\pi n_0}(n-n_0)\frac{V}{N} = \frac{1}{2\pi n_0}\left(\frac{dn}{dc}\right)\frac{M}{N_A} \tag{4.3}$$

where M is molar mass of particles, N_A is Avogadro's number, and dn/dc is the specific refractive index increment of the solution. Taking θ as 90° (2) becomes;

$$I_{90} = \frac{16\pi^4 I_0}{\lambda^4 r^2}\cdot\frac{N}{V}\left(\frac{1}{2\pi n_0}\left(\frac{dn}{dc}\right)\frac{M}{N_A}\right)^2 \tag{4.4}$$

but concentration, c, is MN/N_AV, therefore;

$$I_{90} = \frac{4\pi^2 c}{\lambda^4 r^2}\cdot\frac{I_0}{n_0^2}\left(\frac{dn}{dc}\right)^2\frac{M}{N_A} \tag{4.5}$$

It is also convenient at this point to remove the dependence on observer distance, r, by the use of the Rayleigh ration Rθ;

$$R_\theta = \frac{I_\theta r^2}{I_0} \tag{4.6}$$

Equation 5 can now be rewritten as;

$$R_{90} = \frac{4\pi^2}{\lambda^4 N_A n_0^2}\left(\frac{dn}{dc}\right)^2 cM \tag{4.7}$$

further reduced to;

$$R_{90} = HcM \tag{4.8}$$

where H is termed the optical constant, and consists of all the terms at the front of (4.7);

$$H = \frac{4\pi^2}{\lambda^4 N_A n_0^2}\left(\frac{dn}{dc}\right)^2 \qquad (4.9)$$

The additional scattering in polymer solutions is due to local fluctuations in composition, and hence refractive index because of Brownian motion (section 6.2). This excess scattering was related by Debye[3] to the change in concentration associated with osmotic pressure, Π;

$$R_{ex} = \frac{32\pi^3}{3\lambda^4}\cdot\frac{RTc}{N_0}n^2\left(\frac{dn}{dc}\right)^2 \Big/ \left(\frac{d\Pi}{dc}\right) \qquad (4.10)$$

replacing the osmotic pressure term by the differential of the series;

$$\frac{\Pi}{c} = RT\left(\frac{1}{M} + A_2c + A_3c^2 + \ldots\right) \qquad (4.11)$$

gives the expression

$$\frac{Hc}{\Delta R_{90}} = \frac{1}{M} + A_2c + A_3c^2 + \ldots \qquad (4.12)$$

The virial coefficients beyond the second are generally of negligible value, and can therefore be ignored.

For large particles (diameter $\geq \lambda/20$) in solution there are changes in the scattering caused by interference between light scattered by different parts of the molecule and the scattering can no longer be regarded as that from a point source. Light reaching the observer becomes out of phase and there is a second form of scattering produced, with an angular dependence, known as Debye scattering (cf. scattering from small particles which are effectively point sources, known as Rayleigh scattering). The principle of Debye scattering is shown in (2), where light from two points on the scattering particle, A and B is viewed.

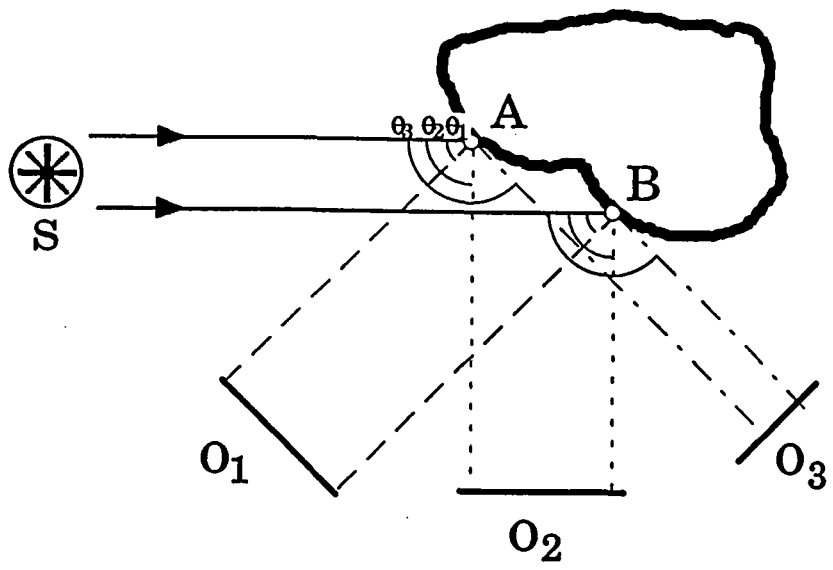

Figure 4.2: Diagrammatic representation of Debye scattering.

In this case light arriving at observer O_3 from A has a longer pathlength from S than that from B, and this difference in pathlength changes with angle so that the difference in path is less at O_2, and still less at O_1. The angular dependence is described by the particle scattering function, P(Q), defined as;

$$P(Q) = \frac{\text{Rayleigh Ratio for large particle}}{\text{Rayleigh Ratio at zero angle}} \qquad (4.13)$$

The particle scattering function is then used as a correction factor for the Debye equation;

$$\frac{Hc}{\Delta R_{90}} = \frac{1}{MP(Q)} + 2A_2c + \ldots \qquad (4.14)$$

The particle scattering function depends on the shape of the scattering molecule[4] and is generally expressed in terms of the scattering vector Q;

$$Q = \frac{4\pi}{\lambda}\sin\left(\frac{\theta}{2}\right) \qquad (4.15)$$

where θ is the scattering angle, and the mean square radius of gyration, $\langle s^2 \rangle$;

Scattering functions for simple models are given in (16), (17) and (18);

Sphere: $$P(Q) = \left[\frac{3}{u^3}(\sin u - u\cos u)\right] \qquad (4.16)$$

where u=Qd/2, d=diameter of sphere.

Gaussian coil $$P(Q) = \frac{2}{v^2}\left[e^{-v} + v - 1\right] \qquad (4.17)$$

where $v=Q^2\langle s^2 \rangle$.

Rigid rod

$$P(Q) = \frac{1}{x}\int_0^x \frac{\sin(2x)}{2x} \cdot dx - \left[\frac{\sin x}{x}\right]^2 \qquad (4.18)$$

where $x=\sqrt{3}.Q\langle s^2\rangle^{1/2}$.

4.2.1 Determination of molecular weight

The method most widely used to analyse data from intensity light scattering is that of Zimm[5] where the particle scattering function;

$$P(Q) = 1 - \frac{Q^2\langle s^2\rangle}{3} \qquad (4.19)$$

is substituted into (14). Equation (19) is applicable to all shapes of molecules in the region of low Q, since the scattering functions tend to converge as Q→0(fig. 4.3). Data is plotted and *via* a double extrapolation method {fig. 4}, plotting the left hand quantity in (eq. 4.14) against $\sin^2(\theta/2)$+kc, a reduced form of Q with a spacing factor added for clarity. Measurements are made on a polymer solution over a range of angles (and hence Q) and at a series of dilution's. By extrapolation from measured data of angle and concentration to the zero angle and concentration is possible to extract molecular mass, radius of gyration and second virial coefficient from the scattering data.

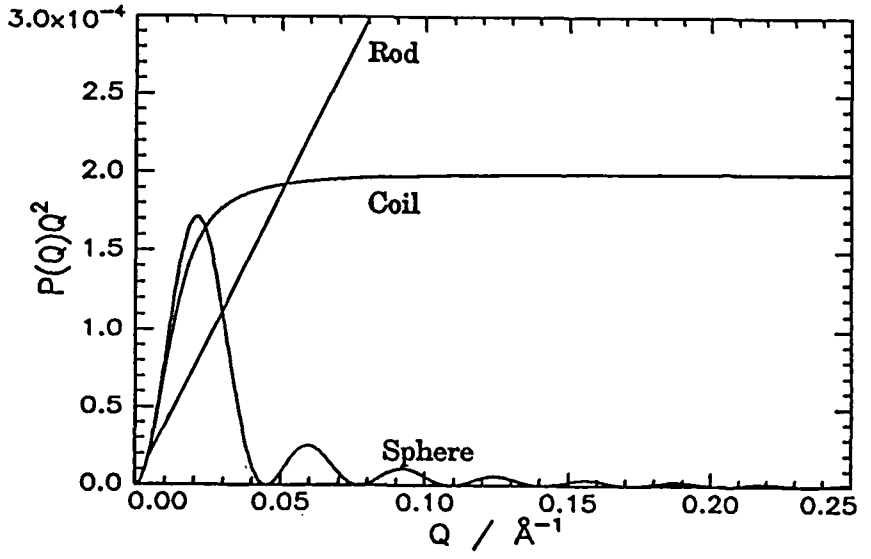

Figure 4.3: Comparison of Kratky plots of scattering functions of rod, coil and sphere.

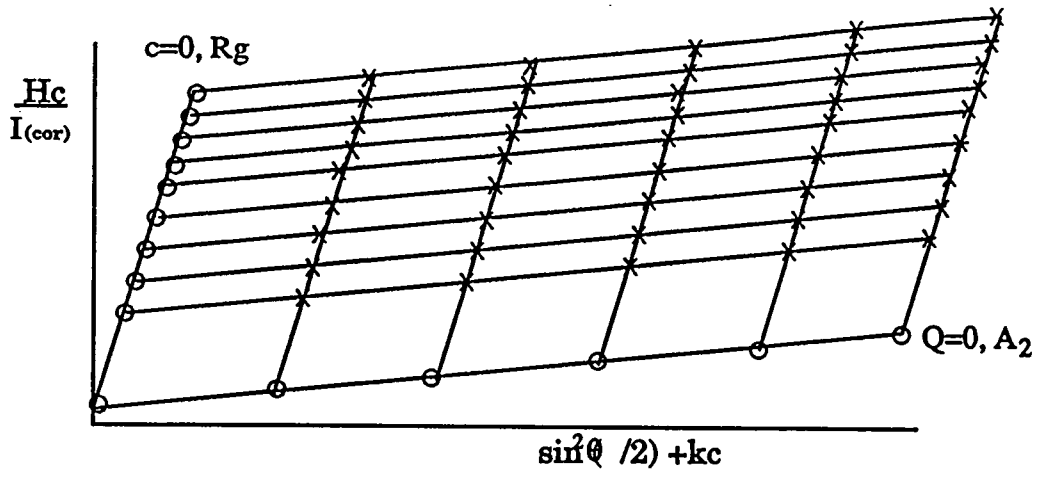

Figure 4.4: Diagrammatic Zimmplot showing data (×) and extrapolated points (○).

Extrapolating angular data to zero give Q=0, and hence P(Q) = 1, under this condition;

$$\left(\frac{Hc}{\Delta R_{90}}\right)_{I=0} = \frac{1}{M} + 2A_2c \qquad (4.20)$$

Extrapolating the counts at zero angle for each concentration therefore gives second virial coefficient from the slope and the reciprocal of the molecular mass from the y-intercept.

Conversely if the excess scattering of each concentration is extrapolated to zero for each angle it should give a line which obeys the condition for eq. (4.13) with c = O;

$$\left(\frac{Hc}{\Delta R_{90}}\right)_{c=0} = \frac{1}{M}\left[1 + Q^2\langle s^2\rangle\right] \qquad (4.21)$$

And now $\langle S^2 \rangle$ can be obtained from the gradient and 1/M from the intercept, which should of course correspond to the value from extrapolating Q to zero. This method has been found to hold good for very many polymer systems over the range of molecular weight of 10^4 to 10^7.

The Zimm plot provides a method to calculate absolute values of molecular weight, to be able to extract this information it is necessary to know the refractive index of the solvent at the appropriate wavelength, the refractive index increment for the solvent-polymer combination and R_{90} for a standard against which the data can be normalised. The Rayleigh ratio can be calculated for vertically polarised light vertically polarised detector can be calculated from the relationship[6];

$$R_{90} = \frac{8\pi^2}{\lambda^4} kT \cdot \frac{\beta_T}{\alpha_p^2} n^2 \left(\frac{dn}{dT}\right)_p^2 \qquad (4.22)$$

Where k is Boltzmann's constant, T absolute temperature, β_T the coefficient of isothermal compressibility and α_p the coefficient of volume expansion.

In light scattering techniques specific refractive index increment is the contrast factor and the intensity of the excess scattering is dependant upon it, therefore it is necessary that (dn/dc) be of sufficient magnitude ($\geq 0.05 cm^3 g^{-1}$) to ensure a reasonable signal. It is also important that the specific refractive index increment be determined as accurately as possible, since the term is squared in the determination of molecular weight.

4.2.2 Effect of polydispersity

The treatment of molecular weight to this point has assumed the scattering species is of a single molecular mass, however this is not found in practice and is useful to consider the case of a polydisperse polymer. The Debye equation for such a polymer is;

$$\frac{Hc}{\Delta R_{90}} = \frac{1}{M_w P_z(Q)} + 2A_{2app} c \qquad (4.23)$$

where A_{2app} is the apparent second virial coefficient.

The molecular weight is now the weight average value (see appendix 2). and the particle scattering function becomes;

$$P_z(Q) = \frac{1}{M_w} \sum_i M_i P_i(Q) w_i \qquad (4.24)$$

Where $P_i(Q)$ is the scattering function for the i^{th} molecular weight constituting weight fraction w_i of the total polymer. A series expansion of $P_z(Q)$ gives a mean value for the radius of gyration;

$$P(Q) = 1 - \frac{Q^2 \langle s^2 \rangle_z}{3} + \ldots \qquad (4.25)$$

where;

$$\langle s^2 \rangle_z = \frac{1}{M_w} \sum_i \langle s^2 \rangle_i M_i w_i \qquad (4.26)$$

so that $\langle s^2 \rangle_X$ is the z-average value, proportional to the z-average molecular weight (appendix 2). To use M_w and $\langle s^2 \rangle_z$ together it is necessary to apply a correction factor to

one or other quantity, since M_w is a more useful quantity it is found more convenient to apply the correction to $\langle s^2 \rangle_z$.

The form of the correction factor used will depend on the nature of the molecular weight distribution. Among the distributions proposed the two generally treated are Schulz-Zimm[7] and the log normal distributions[8]. The Schulz-Zimm distribution was devised for free radically polymerised systems and hence is chosen in this case to represent the polymers in this study which were polymerised free radically. The correction factor for z-average radius of gyration for a polymer with the Schulz-Zimm distribution and a Mark-Houwink coefficient of α (see section (5.2)) is given by[9];

$$\langle s^2 \rangle_w = q \langle s^2 \rangle_z \qquad (4.27)$$

where $q = \dfrac{3h+3}{3h+2\alpha+5}$ and $h = (M_n / M_w - 1)^{-1}$

The second virial coefficient in equation (22) is an apparent value with an angular dependence. Extrapolation to $\theta = 0$ gives a true thermodynamic value which is a complex mean, termed the "light scattering average".

4.3 Experimental

Intensity light scattering measurements were performed on a Malvern 4700 photon correlation spectrometer, shown diagrammatically in figure 4.5.

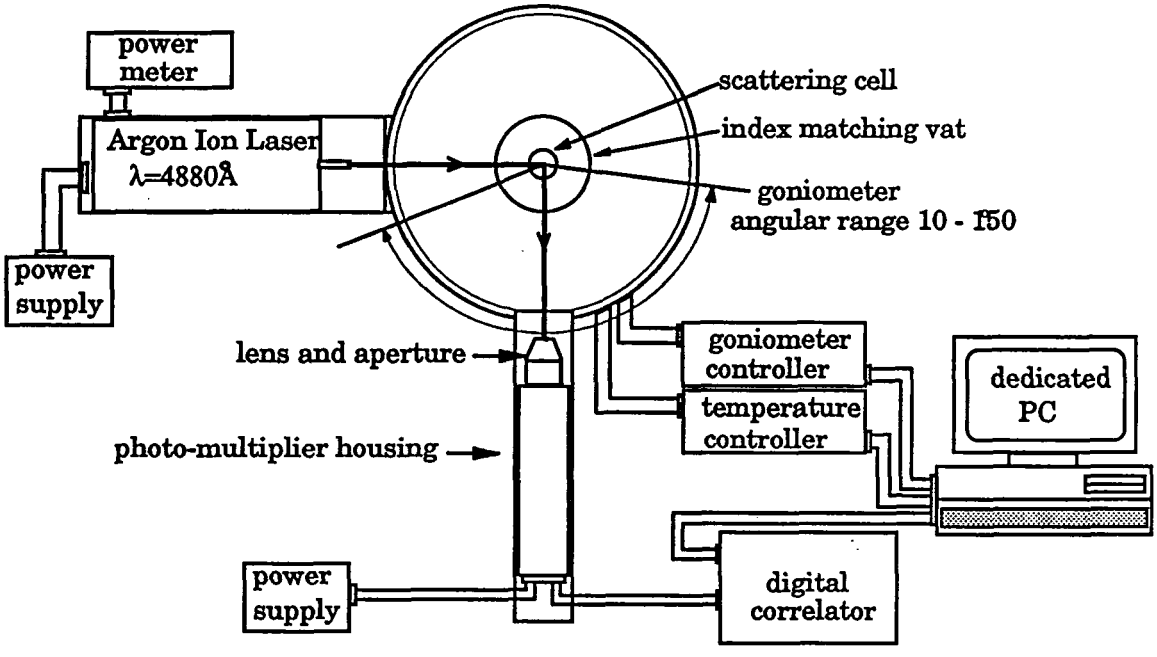

Figure 4.5: Malvern 4700 Photon Correlation Spectroscopy Apparatus.

The experimental set-up was installed upon an optical table with gas damping to reduce vibration effects.

4.3.1 Optical alignment

This procedure is fully described in the instrument manual[10]. Intensity light scattering requires precise alignment of the incident beam along the optical axis of the instrument, and through the centre of the glass cell.

The first stage is to line up the beam through two pinhole attachments on the photomultiplier arm set to 0°, this ensures the beam is parallel to the table and follows the optical axis of the set-up. The alignment of sample cell is confirmed by inserting a thin steel wire enclosed in a metal cell of the same dimensions as the scattering cells. If the beam is central it strikes the wire, causing a bright diffraction pattern. The laser lens L is focused by insertion of an opaque plastic strip into the beam, producing a

characteristic 'boiling' pattern when focused. The photomultiplier is focused by coarse adjustment of the diaphragm, then inserting a strongly scattering latex into the beam and sliding the PM tube along the arm (set to 40°) to focus the image of the beam sharply . Finally alignment is verified by measuring the scattered intensity of a Rayleigh scatterer (toluene) over the full range of θ. The counts at each angle normalised to those at 90° according to eq 4.28 should be 1±0.05 at correct alignment(fig. 4.6).

$$I_n = \frac{I_\theta}{I_{90}} \cdot \sin\theta \qquad (27)$$

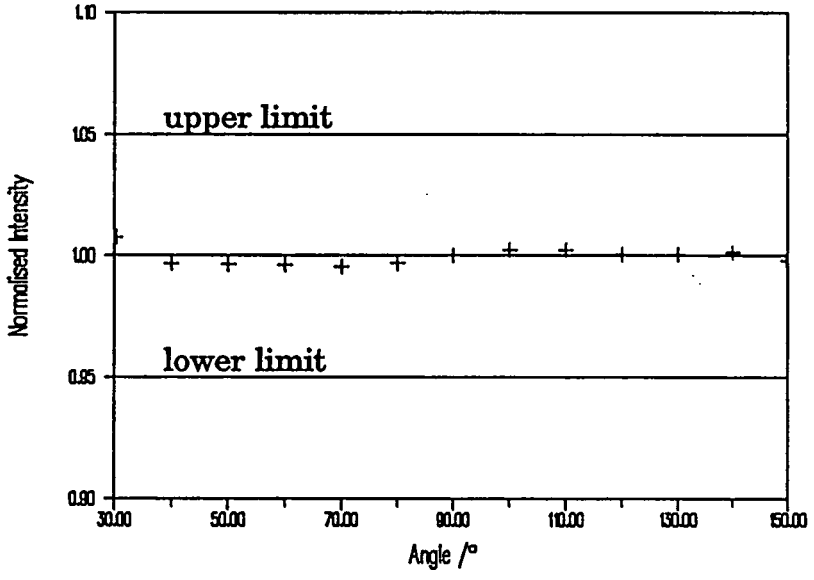

Figure 4.6: Typical normalised counts for a range of angles.

Data was collected using proprietary software, and analysed using proprietary and software developed in the laboratory. The light source was an Ion Laser Technology model 5490 argon ion laser producing an output of ≈50mW at the 4880Å wavelength. Samples were contained in large diameter (28mm) cylindrical glass cells. These were of the "Burchard" type, precisely manufactured from high quality optical glass (Hellma). Toluene was used as the primary standard. Analysis grade toluene was dried over $MgSO_4$ for 24hrs, then distilled directly into the cell, the first cell full was used as a wash and discarded, the second aliquot was distilled into the cell and twice filtered through a 0.2μm PTFE membrane filter, satisfactorily removing all dust. The Rayleigh ratio was calculated from equation (20) to be $32.84\times10^{-6}cm^{-1}$ at 4880Å, slightly higher than

experimentally determined values of $31.0 \times 10^{-6} m^{-1}$ [11] and $29.5 \times 10^{-6} cm^{-1}$, [12]. A measurement made on a sample of a narrow dispersity polystyrene in MEK produced satisfactory values of M_w and $\langle s^2 \rangle^{1/2}$ (±1%) using the median value of $31.0 \times 10^{-6} cm^{-1}$, and this has been used in all measurements.

4.3.2 Sample Preparation

All polymer solutions were made up from freshly dried and distilled solvent, using volumetric grade B glassware. Before use solutions were left for at least 24hrs to reach equilibrium, to prevent photochemical decomposition, chloroform solutions were stored in the dark. Solutions were then filtered to remove dust, the solution was poured from the flask into a gas tight syringe with a filter holder containing a 0.2μm pore size PTFE membrane filter disk, The solution pumped through at a slow rate ($\approx 2 \rightarrow 5 cm^3 min^{-1}$) directly into the light scattering cell, rinsed lightly around the cell, and returned to the syringe and filtered once more into the cell. Two passes were generally sufficient to remove dust from the samples, and if not then further filtering simply exacerbated the problem. Contrary to expectation the more polar solvent NMP proved considerably more easy to filter than chloroform.

All measurements were conducted in a purpose-built light scattering laboratory devoid of natural light, and illuminated by dimmed tungsten filament bulbs to reduce background light. Intensity measurements were made over the angular range of 30° to 150°, in steps of 10°, and using 5 polymer solutions, together with the pure solvent and toluene as the primary standard.

4.3.3 Determination of Refractive Index

The refractive index of NMP at 4880Å could not be found in the literature and was measured using a Bellingham and Stanley Pulfrich critical angle refractometer, using sodium and mercury vapour lamps to provide illumination over a range of wavelengths. The refractive index from which the value at 4880Å was interpolated from a Cauchy dispersion(4.29).

The sample of NMP used was dried over $MgSO_4$ for 24hrs and vacuum distilled prior to use. To avoid hydration of the hygroscopic solvent the solvent in the cell was replaced

after measurement at each wavelength. All measurements were made at the ambient temperature (≈25°C).

λ /Å	n	Error in n last figure ±
4047(Hg)	1.4949	14
4358(Hg)	1.4875	10
5461(Hg)	1.4697	8
5791(Hg)	1.4676	16
5890(Na)	1.4677↔	4

↔cf. text value[13] of 1.4684 at 20°C

Table 4.1: Values of refractive index of NMP from Pulfrich refractometer.

The Cauchy dispersion gives refractive index as a function of wavelength;

$$n = A + \frac{B}{\lambda^2} \qquad (4.29)$$

where A and B are constants.

The interpolated value of NMP at 4880Å, as shown in figure 4.7, was determined as 1.4775.

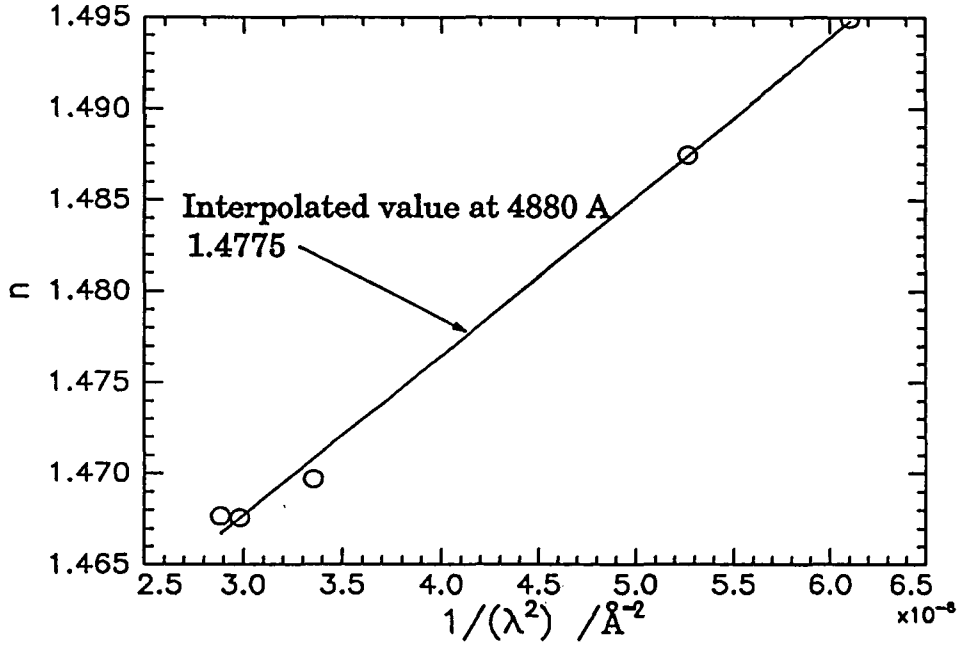

Figure 4.7: Cauchy dispersion of NMP refractive indices.

4.3.4 Determination of Specific Refractive Index Increment

The differential refractometer was used to determine the specific refractive index increment of polymer solutions, necessary to extract molecular mass and second virial coefficient from Zimm plots.

The measurements were all made on a Wyatt Optilab Model 903 refractometer set to 4880Å, using proprietary software to collect and analyse data on an Opus PC. All measurements were taken at 25°C, the instrument being thermostated using a Haake water circulator.

Measurements were made on poly(DHCD-DMC) over a range of degrees of aromatisation, in both the solvents used for the light scattering study, i.e. chloroform and NMP. The techniques used for the measurements in each solvent were different, as a result of the different viscosities. A solution in NMP was considerably more viscous than an equivalent chloroform solution. All solutions for refractometry were made up using freshly distilled, dried solvent. All solutions were made up at approximately 1% concentration w/v in 25ml volumetric flasks, and aliquots pipetted out to make solutions at approximately 0.8, 0.6, 0.4 and 0.2% concentration.

Calibration of the instrument was by using a solution of known refractive index, in this case an aqueous solution of KCl. The dn/dc of aqueous KCl was interpolated[14] as 0.2129 at 4880Å. A 1% stock solution was made using water (distilled, 250ml) and dried KCl (BDH Analar, 2.5g) and diluted to a total of 6 concentrations, which were run through the measuring cell by a gravity feed and the cell calibration constant determined. Chloroform solutions of the partially aromatised polymer at 0, 10, 20, 30 and 40% aromatisation were prepared and run through the cell using the same gravity feed arrangement as for the aqueous solutions, and the specific refractive index increments determined by extrapolation to zero concentration. A typical result, and the data determined are shown in figure 4.8.

Solutions of the same polymer in NMP were also prepared, but it was found that due to the greater viscosity the solutions would not flow under gravity, and were instead injected into the cell using a 5ml syringe via a Luer-lock connection. This caused the

cell, which proved very sensitive to pressure to give aberrant results, and care was needed to ensure that pressure remained constant while readings were being made. Typical data and the results are shown below (figure 4.9).

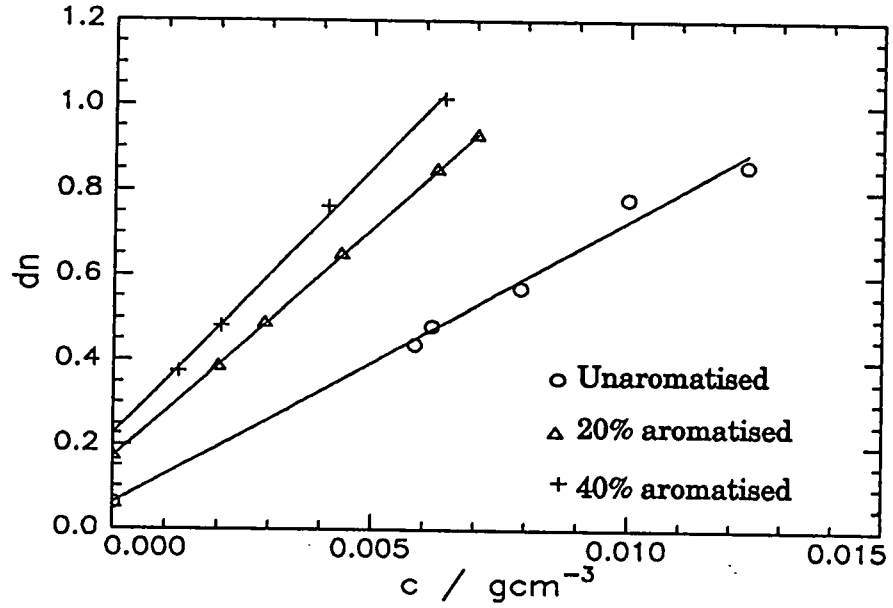

Figure 4.9b: Typical plots of refractive index increment measurements, solvent NMP.

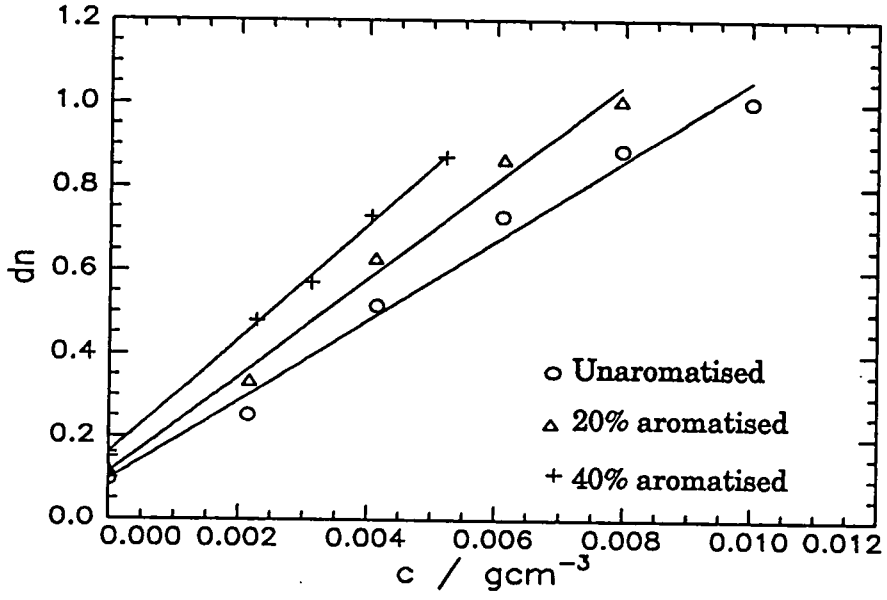

Figure 4.9b: Typical plots of refractive index increment measurements-solvent: chloroform.

	0%	10%	20%	30%	40%
NMP	0.060	0.090	0.139	0.180	0.206
Chloroform	0.100	0.111	0.123	0.138	0.151

Table 4.2: Specific refractive index increments.

4.3.5 Determination of Partial Specific Volume

The partial specific volume of the partially aromatised polymers in each solvent was measured using an Anton Paar model DMA601 density measuring cell together with an Anton Paar DMA60 controller. This instrument measures fluid densities by the change in the wavelength of sound waves through the liquid.

It was calibrated against two known fluids, in this case air, for which the density at various barometric pressure is documented[11], and degassed, purified water (Elgastat UHQ water). Measurements were made on solutions of partially aromatised polymer at 0, 10, 20, 30 and 40% aromatisation in chloroform and NMP. A stock solution of 5% was made up by dissolving the polymer in 1ml of dried, distilled solvent, which had been thoroughly vacuum degassed, in a 10ml volumetric flask, and again thoroughly degassing under vacuum. The solution was then carefully made up to the mark. As all subsequent dilution was done with degassed solvent no further degassing of the solution was deemed necessary.

The measuring cell consisted of a fine horizontal glass U-tube, which was sealed at either end using natural rubber septa. The assembly was thermostated to 25.0±0.1°C using a circotherm. To make the measurement a small amount of sample (≈0.5cm^3) was injected into the U-tube, allowed 5 minutes to equibrilate, then a number of measurements of 30 seconds duration made, until 10 consistent reading were obtained, and these were averaged. Five concentrations of polymer were measured, together with the solvent. These readings, with those from air and water were used to calculate solution density, according to the instrument manual

Aromatisation	solvent*	concn. w/v				
		1%	2%	3%	4%	5%
0%	1.4809	1.4802	1.4800	1.4796	1.4789	1.4787
10%	1.4794	1.4788	1.4780	1.4773	1.4768	1.4760
20%	1.4803	1.4796	1.4793	1.4782	1.4771	1.4768
30%	1.4788	1.4781	1.4775	1.4767	1.4761	1.4755
40%	1.4795	1.4790	1.4789	1.4782	1.4789	1.4790

**literature value = 1.4832 at 20° C*

Table (4.3a): Solution densities of partially aromatised polymer in chloroform.

Aromatisation	solvent*	concn. w/v				
		1%	2%	3%	4%	5%
0%	1.0303	1.0355	1.0312	1.0387	1.0409	1.0431
10%	1.0310	1.0338	1.0362	1.0380	1.0409	1.0430
20%	1.0293	1.0318	1.0345	1.0362	1.0377	1.0394
30%	1.0303	0.0341	1.0350	1.0372	1.0396	1.0412
40%	1.0267	-----	1.0312	1.0338	1.0362	1.0393

**literature value = 1.0260 at 25° C*

table (4.3b): Solution densities of partially aromatised polymer in NMP.

Partial specific volumes ν_2 were then calculated from the relation

$$\nu_2 = \frac{1}{\rho_0} + \frac{1/\rho_s - 1/\rho_0}{w} \qquad (4.30)$$

where ρ_0: solvent density

ρ_S: solution density

w : Weight fraction of polymer

percentage aromatisation	NMP ν_2	Chloroform ν_2
0%	0.749	0.699
10%	0.744	0.707
20%	0.818	0.709
30%	0.801	0.707
40%	0.722	0.695

Table (4.4) solution densities and partial specific volume in chloroform and NMP.

Partial specific volumes can be used in the Gladstone-Dale relationship, in conjunction with refractive index increment to calculate the refractive index of the polymer, providing a useful cross-check of the refractive index increment

$$\frac{dn}{dc} = \nu_2(n_p - n_s) \qquad (4.31)$$

where n_s and n_p are the refractive indices of the solvent and the polymer respectively, and dn/dc is the specific refractive index of the solution substituting values from tables (4.3) and (4.4) give the following results;

Aromatisation	NMP	Chloroform
0	1.522	1.519
10	1.545	1.527
20	1.591	1.536
30	1.622	1.547
40	1.626	1.555
100	1.833*	

**solid film, source = ICI technical literature*

Table 4.5: Refractive index of aromatised polymer.

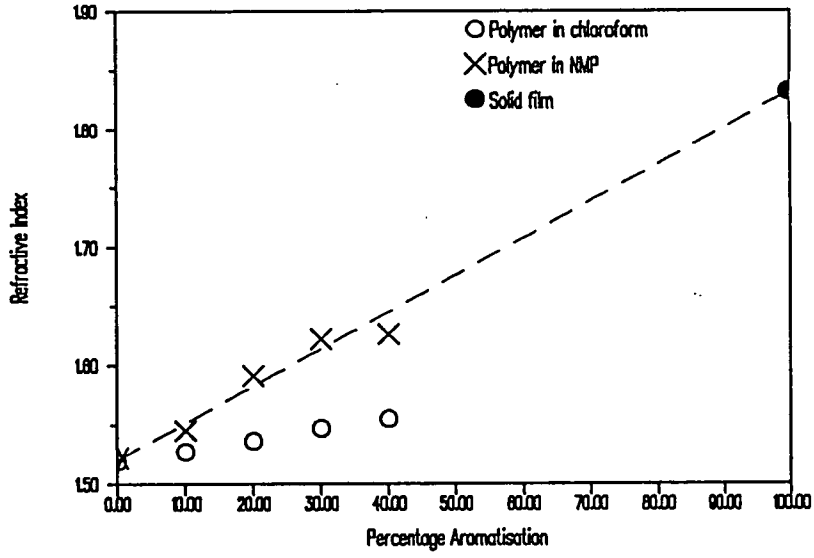

Figure 4.8: Comparison of apparent refractive indices of dissolved polymer. The dashed line represents the linear relationship between polyphenylene and the precursor.

4.3.6 Data Analysis

The data from intensity light scattering was analysed by the method of Zimm (section 4.2.1). Data collected for the five concentrations was first corrected for background by subtraction of solvent scattering, and reduced to the Raleigh ratio from multiplication by the ratio of the Rayleigh ratio of toluene by the scattering from toluene;

i.e. $$R_{sample,\theta} = R_{toluene} \frac{\left(I_{sample} - I_{solvent}\right)}{I_{toluene}} \cdot \frac{n_{solvent}}{n_{toluene}} \qquad (4.32)$$

Where $R_{toluene}$ can be found in the relevant literature. The resulting data is then plotted as;

$$\frac{Hc}{I_{cor}} \quad vs \quad \sin^2\left(\frac{\theta}{2}\right) + kc \qquad (4.33)$$

where H is the optical constant(section 4.2), c the concentration, and k an arbitrary constant for purposes of spatial clarity. A least squares fit line is fitted to the concentration and angular sets of data, to extrapolate to zero concentration and angle. These lines are then extrapolated to the y-axis, where they should intercept at the same point. In some cases it proved necessary to remove points at the low angles, 30°, 40° and 50°. This had two causes, dust in the sample would create excess scattering, and for strongly scattering highly aromatised samples and polystyrene in MEK used to check the alignment in some cases the scattering must have saturated because the signal was attenuated.

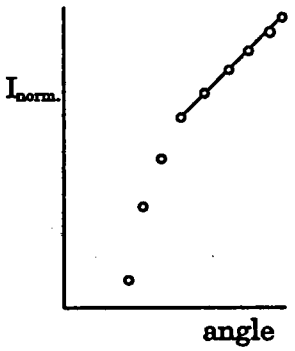

Fig 4.9:a Excess scattering caused by dust.

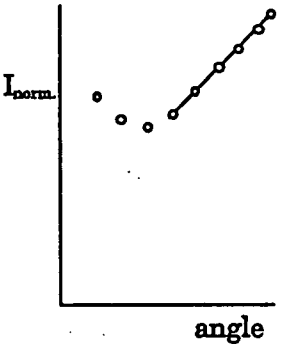

b attenuated scattering caused by saturation.

The reciprocal of the intercept of the y-axis gives the molecular weight, the gradient of the lines of concentration data.

4.4 Results

	M_w	$\langle s^2 \rangle_z^{1/2}$ /Å	$\frac{M_w}{M_n}$	$\langle s^2 \rangle_w^{1/2}$ /Å	A_2 /cm^{3}g^{-1}
	(±5%)	(±5%)		(±5%)	(±10%)
H	1220000	980	1.89	800	0.00099
A	242000	330	1.34	290	0.00116
D'	92000	210	1.37	190	0.00111
C	85000	190	1.32	170	0.00112
I	83000	200	1.24	180	0.00139
D	79000	160	1.25	140	0.00131
F	65000	170	1.29	150	0.00140
G	26000	88	1.14	83	0.00166
L	10000	60	1.55	51	0.00224

Table 4.6: Unaromatised polymer in NMP.

	M_w	$\langle s^2 \rangle_z^{1/2}$ /Å	$\frac{M_w}{M_n}$	$\langle s^2 \rangle_w^{1/2}$ /Å	A_2 /cm^{3}g^{-1}
	(±5%)	(±5%)		(±5%)	(±10%)
B	66000	240	1.79	190	0.00132
E	59000	220	1.61	180	0.00093
A	54000	210	1.59	170	0.00169
C	45000	160	1.73	130	0.00147
F	37000	150	1.48	130	0.00165
D	37000	140	1.62	120	0.00177
L	24000	100	1.48	85	0.00177

Table 4.7: 10% aromatised polymer in NMP.

	M_w	$\langle s^2 \rangle_z^{1/2}$ /Å	A_2 /cm^{3}g^{-1}
	(±5%)	(±5%)	(±10%)
F	49000	210	0.00073
B	48000	220	0.00121
C	46000	210	0.00131
D	35000	170	0.00102
E	29000	180	0.00125
H	27000	190	0.00149
G	26000	140	0.00207
L	23000	120	0.00086

Table 4.8: 20% aromatised polymer in NMP.

	M_w	$\langle s^2 \rangle_z^{1/2}$ /Å	A_2 /cm^{3}g^{-1}
	(±5%)	(±5%)	(±10%)
A	106000	190	0.00149
B	100000	190	0.00152
D	47000	150	0.00217
E	42000	120	0.00188
C	39000	130	0.00192
F	31000	160	0.00208

Table 4.9: 30% aromatised polymer in NMP.

	M_w	$\langle s^2 \rangle_z^{1/2}$ /Å	A_2 /cm^{3}g^{-1}
D	128000	240	0.00044
H	110000	340	0.00038
A	98000	270	0.00092
L	84000	150	0.00025
C	70000	210	0.00058
F	37000	140	0.00072

Table 4.10: 40% aromatised polymer in NMP.

	M_w	$\langle s^2 \rangle_z^{1/2}$ /Å	$\frac{M_w}{M_n}$	$\langle s^2 \rangle_w^{1/2}$ /Å	A_2 /cm^{3}g^{-1}
	(±5%)	(±5%)		(±5%)	(±10%)
B	159000	320	1.340	260	0.00131
C	116000	260	1.318	210	0.00146
D	78000	220	1.250	180	0.00162
E	76000	220	1.250	170	0.00118
G	14000	94	1.340	75	0.00354
L	10000	68	1.687	48	0.00512

Table 4.11: Unaromatised polymer in chloroform.

	M_w	$\langle s^2 \rangle_z^{1/2}$ /Å	$\frac{M_w}{M_n}$	$\langle s^2 \rangle_w^{1/2}$ /Å	A_2 /cm^{3}g^{-1}
	(±5%)	(±5%)		(±5%)	(±10%)
B	85000	220	1.79	150	0.00072
D	80000	270	1.62	200	0.00108
C	71000	180	1.75	130	0.00078
F	44000	190	1.48	150	0.00105
L	21000	83	1.48	63	0.00179

Table 4.12: 10% aromatised polymer in chloroform.

	M_w	$\langle s^2 \rangle_z^{1/2}$ /Å	$\frac{M_w}{M_n}$	$\langle s^2 \rangle_w^{1/2}$ /Å	A_2 /cm^{3}g^{-1}
	(±5%)	(±5%)		(±5%)	(±10%)
A	156000	360	2.11	230	0.000480
L	133000	260	2.12	170	0.000308
C	111000	290	2.07	190	0.000477
D	105000	310	2.04	210	0.000432
B	102000	280	2.51	170	0.000356
E	96000	250	2.26	160	0.000440
F	44000	180	1.66	130	0.000501

Table 4.13: 20% aromatised polymer in chloroform.

	M_w	$\langle s^2 \rangle_z^{1/2}$ /Å	$\frac{M_w}{M_n}$	$\langle s^2 \rangle_w^{1/2}$ /Å	A_2 /cm^{3}g^{-1}
	(±5%)	(±5%)		(±5%)	(±10%)
A	289000	340	3.90	190	0.000252
L	234000	200	5.72	110	0.000130
B	221000	300	3.01	180	0.000317
C	206000	270	2.51	170	0.000222
D	162000	210	2.89	130	0.000279
H	131000	330	9.61	180	0.000536
F	75000	260	2.41	160	0.000397
E	71000	220	2.39	140	0.000470

Table 4.14: 30% aromatised polymer in chloroform.

	M_w	$\langle s^2 \rangle_z^{1/2}$ /Å	$\frac{M_w}{M_n}$	$\langle s^2 \rangle_w^{1/2}$ /Å	A_2 /cm^{3}g^{-1}
	(±5%)	(±5%)		(±5%)	(±10%)
D	407000	290	6.73	160	0.000350
L	219000	180	4.00	100	0.000122
C	215000	210	5.72	120	0.000318
A	205000	260	8.30	140	0.000291
H	199000	290	5.50	160	0.000389
G	142000	200	4.72	110	0.000225
F	114000	190	4.29	110	0.000394

Table 4.15: 40% aromatised polymer in chloroform.

Ideally all z-average radii of gyration should have been corrected for polydispersity, however the only PD values available are from SEC with chloroform as the solvent. Aromatised polymers displayed a bimodal distribution in chloroform but the distribution in NMP was not known, therefore only at low aromatisation, where bimodality in chloroform was slight, has the $\langle s^2 \rangle^{1/2}$ correction been applied.

The changes in molecular weight which are observed by ILS are similar to those observed by SEC, that is there is a greater decrease than stoichiometric loss of carboxyl side groups alone between 0% and 20%, a loss equivalent to 13.33%. Fraction A decreases by 78% at 10% aromatisation, and fraction C decreases by 47% at 10%, and 46% at 20% aromatisation, the loss is more severe for those fractions of higher molecular weight, so that fraction G remains the same at 20%, while fraction F has decreased by 24%, and the lowest, fraction L, actually increases significantly. This increase was also observed in SEC and is due to the formation of aggregates. The decrease in molecular weight is caused by chain scission, and the increased susceptibility of the higher molecular weight fractions may be due to the greater steric strain as the longer chains straighten out. Beyond 20% aromatisation there is a general rise in the molecular weights caused by the aggregation of the aromatised polymer, observed in SEC, however in the case of ILS it is not possible to resolve the contributions of the single and aggregated chains. A the aromatisation reaction proceeds there is a loss of the initial order of the fractions, due to the random nature of the aromatisation process.

The results were plotted as log plots in order to determine the molecular weight dependency of radii of gyration and second virial coefficient *via* the relationships

$$\langle s^2 \rangle_w^{1/2} = x\, M_w^{y} \qquad \text{and} \qquad A_2 = \delta M_w^{-\gamma}$$

The following results were obtained for the relation between mean square radius of gyration and molecular weight

Percentage Aromatised	z - av		w - av	
	x	*y*	*x*	*y*
0	0.218	0.587	0.257	0.572
10	0.015	0.869	0.020	0.829
20	0.032	0.820	—	—
30	2.779	0.401	—	—
40	0.230	0.604	—	—

Table 4.16a: Molecular weight-radii of gyration relationship from Zimm plots solvent NMP.

Percentage Aromatised	z - av		w - av	
	x	*y*	*x*	*y*
0	0.532	0.534	0.296	0.566
10	0.075	0.714	0.103	0.655
20	1.080	0.479	0.874	0.464
30	31.99	0.179	32.04	0.136
40	6.51	0.291	5.120	0.262

Table 4.16b: Molecular weight-radii of gyration relationship from Zimm plots solvent chloroform.

The results for the second virial coefficient relationships are shown in tables 4.17a & b

Percentage Aromatised	w - av	
	δ	γ
0	0.0079	0.161
10	0.0215	0.244
20	0.0486	0.356
30	0.0368	0.276
40	0.0509	0.408

Table 4.17a: Molecular weight - second virial coefficient relationships for partially aromatised polymer in NMP.

Percentage Aromatised	w - av	
	δ	γ
0	0.441	0.498
10	0.389	0.545
20	0.003	0.168
30	0.073	0.452
40	0.008	0.279

Table 4.17b: Molecular weight - second virial coefficient relationships for partially aromatised polymer in chloroform.

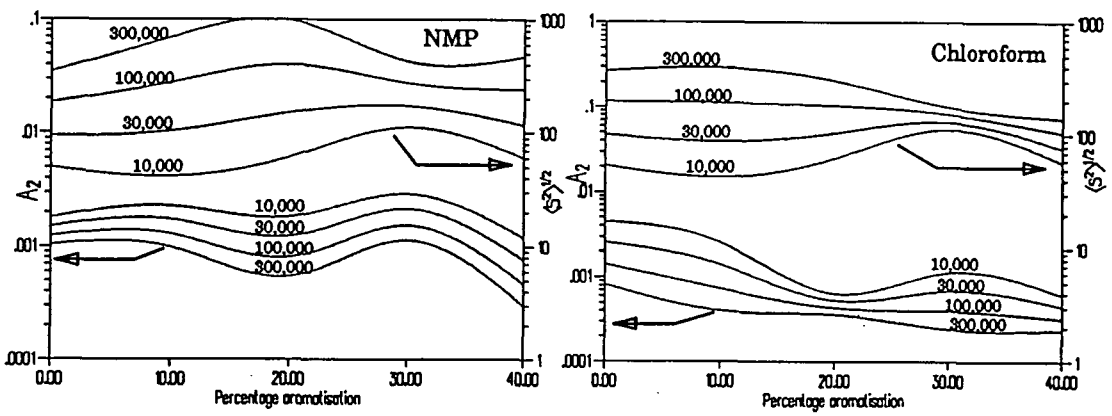

Figure 4.10: Measured properties, $\langle s^2 \rangle^{1/2}$ and A_2 from relationships in tables 4.16 and 4.17 over a range of molecular weight.

The trend seen in the exponents from the molecular weight *vs* radii of gyration relationships from chloroform and NMP solutions are similar to some extent. Initially $y \approx 0.55$, signifying the average conformation of the chains is that of a random coil, slightly expanded from the theta dimensions by excluded volume interactions. The value of y increases to a value of ≈0.8 and could be due to either improved thermodynamic interactions between polymer and solvent, or increasing chain extension, and is attributed to the latter. This is because the aromatisate, poly(phenylene), is insoluble, and will presumably decrease the effective quality of the solvent. If this were the case a concomitant decrease in A_2, a measure of the polymer/solvent interactions, would be expected. Although second virial coefficient data is significantly scattered it does appear that second virial coefficient falls during the aromatisation.

The exponent y of the $\langle s^2 \rangle^{1/2}$ *vs* M_w relationship rises to a peak value ≈0.7-0.8 at intermediate aromatisation and then drops, in each case down to a value lower than that

of the theta state i.e. y=0.5. This suggests that there is a change in the configuration of the polymer chains, from extended coils at low aromatisation to an aggregate, whose behaviour is closer to that of a sphere (y=0.33) than a single chain. The uncertainty in the value of y is greater for these more highly aromatised polymers because of the greater scatter of data in the plots.

For both solvents there is an anomalous low value at 30% aromatisation, seen also in viscosity data, for which no adequate explanation can be advanced. There is a difference between the solutions in NMP and chloroform, the values of y in NMP are higher, so NMP is the better solvent, and aggregation is more severe in chloroform.

The plots of A_2 *vs* M_w are much more difficult to interpret than those of $\langle s^2 \rangle$ because of the scatter in the plots. This is partly due to the lesser degree of certainty of the values (±10%, twice that of $\langle s^2 \rangle$ and M_w) but as A_2 is an indicator of the thermodynamic condition of the polymer it may well be very sensitive to the aggregation phenomena suggested above. This might sample especially be the case with preparation, A_2 may have been affected by the dissolution and filtering through micropore filters. It is also noted by other authors that a regular variation in A_2 with M_w for a variety of polymer solvent systems could not be obtained, for which no satisfactory reason could be given[15,16].

Values of the exponent γ for randomly coiled polymers are given theoretically as 0.15[17] and 0.25[18], lines for both of which are overlaid on the plots. Although there are no firm relationships connecting behaviour of second virial coefficients from light scattering measurements with their configuration it is possible to infer trends from the data. These do not necessarily follow the pattern which was expected, A_2 did not necessarily fall as the polymer-solvent interactions declined with rising aromatisation. The second virial coefficient is a thermodynamic quantity related to the interaction between polymer and solvent. It can be defined in terms of the Flory interaction parameter χ_1 ;

$$A_2 = \frac{\bar{v}_2^2}{N_A V_1}(1/2 - \chi_1) \qquad (4.34)$$

where $\bar{\upsilon}_2^2$ is the specific volume of the polymer, N_A is Avagadro's number, and $V_1$is the partial molar volume of the solvent. Where the polymer is in a good solvent interaction is high and A_2 will have a large value, where the solvent is poor interaction will be less and A_2 will have a lower value, at the theta point A_2 =0.

For the unaromatised polymer in NMP the exponent γ of the molecular weight dependency of A_2 is between the literature values of 0.15 and 0.25, and could therefore be described as a solution of randomly coiled molecules in a good solvent, with a similar situation at 10% aromatisation. Above this the exponents do not conform to these limits, as a result of changes in configuration and solubility. The molecular weight dependency of A_2 becomes greater with increasing aromatisation (except 30%), possibly an effect of aggregation if larger molecules are more liable to aggregate than smaller ones. For a rigid rod type molecule there should be little or no size dependency. It is also seen in fig 4.11 that there is no significant fall in A_2 at 10%, a slight fall at 20%, a rise 30%, then falling to the lowest values at 40% aromatisation. This would be expected as the inclusion of insoluble phenylene units in the chain reduces the overall polymer-solvent interaction.

The high values of A_2 for the 30% aromatised polymer is an anomaly, which points to a fundamental difference in the 30% aromatised polymer. Whether this is the result of sample preparation or a fundamental difference in the polymer is not clear.

The second virial coefficients of chloroform solutions behave somewhat differently. The exponent γ for the unaromatised polymer at 0.5 is much greater than that of a random coil in a good solvent obtained in NMP, although the relationship of M_w and $\langle s^2 \rangle^{1/2}$ is much the same, γ at 10% aromatisation is also high 0.55, more than at 0%, while the values from 20 and 40% are lower than this, 0.17 and 0.28 respectively. These results are very much affected by scatter, and are over narrow ranges of molecular weight, making interpretation uncertain.

In molecules undergoing a fringed micelle formation it would be expected that the dependence of A_2 on molecular weight would decrease as parts of the molecule become

confined in a dense core from which solvent is excluded, and polymer-solvent interaction is reduced for the molecule overall.

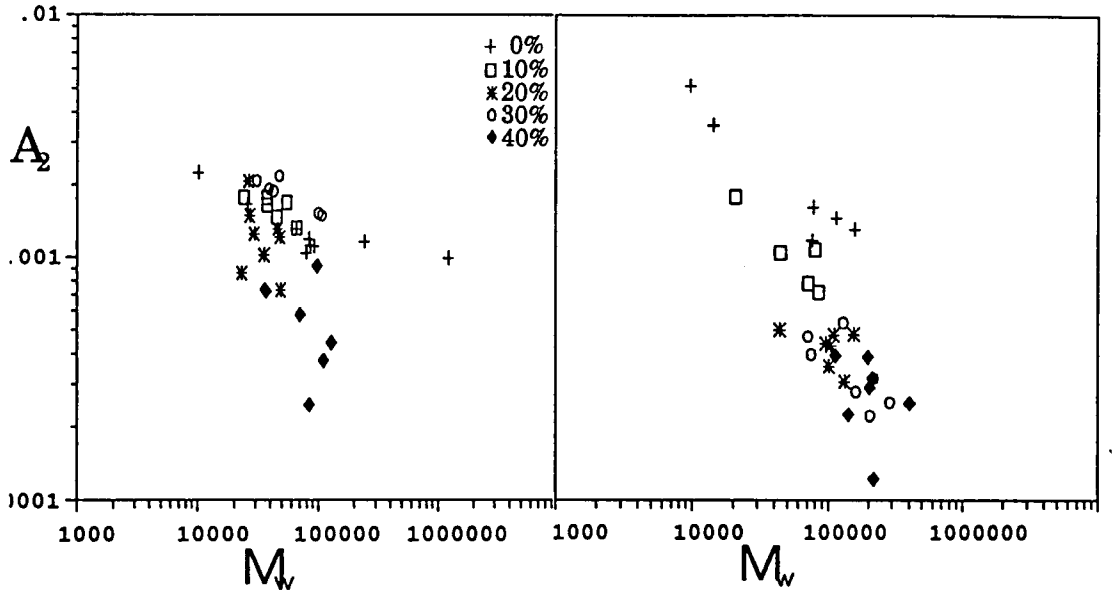

Figure 4.11: Comparison of A_2 in NMP(left) and chloroform.

If comparison is made between values of A_2 in NMP and chloroform it is seen that the A_2 of unaromatised polymer is greater in chloroform, but once aromatisation begins the situation is reversed, and A_2 is greater in NMP. Chloroform would therefore appear to be a superior solvent for the precursor polymer, but NMP is better for the aromatised polymer, hence the earlier onset of aggregation observed with chloroform solutions.

4.4.1 Determination of Persistence Length

The data from ILS can also be manipulated in a number of other ways to extract further information. Persistence length can be determined using two plots, depending on the size of the molecules in the sample.

Murakami uses the approximation

$$\left(\frac{M}{\langle s^2\rangle}\right)^{\frac{1}{2}} = \left(\frac{3M_L}{a}\right)^{\frac{1}{2}}\left(1+\frac{3aM_L}{2M}\right) \qquad (4.35)$$

where a is the persistence length and M_L is the molecular weight per unit contour length. This is valid to ±1% for $M/4aM_L > 1$, that is for longer or more flexible molecules.

Alternatively for shorter or stiffer molecules where $M/4aM_L < 1$ Zhang *et al* replace (4.35) with

$$\left(\frac{M^2}{12\langle s^2\rangle}\right)^{\frac{2}{3}} = M_L^{\frac{4}{3}} + \frac{2M}{15}\left(\frac{M_L^{\frac{1}{3}}}{a}\right) \qquad (4.36)$$

Plots according to both the Murakami and Zhang approximations have been constructed and are shown in figure 4.26, and the results are tabulated in table 4.18. A number of the data sets could not be satisfactorily plotted and are consequently not included in the results

method/ solvent		**0% arom.**	**10% arom**	**20% arom**
Zhang	**a /Å**	85	238	318
NMP	**M_L /Å^{-1}**	69	70	50
($M_w \leq 4aM_L$)	**$4aM_L$**	24000‡	80000	64000
Murakami	**a /Å**	35	193	244
NMP	**M_L /Å^{-1}**	40	69	46
($M_w \geq 4aM_L$)	**$4aM_L$**	21000	53000‡	45000‡
Zhang	**a /Å**	87	82	70
chloroform	**M_L /Å^{-1}**	48	61	50
($M_w \leq 4aM_L$)	**$4aM_L$**	17000‡	20000‡	14000‡
Murakami	**a /Å**	68	87	195
chloroform	**M_L /Å^{-1}**	42	69	122
($M_w \geq 4aM_L$)	**$4aM_L$**	11000	24000	95000

Table 4.18: Persistence lengths from ILS data (those $4aM_L$ values marked ‡ indicate that the range of the data used was substantially or wholly out of the prescribed range for the analysis used).

4.4.2 Two Parameter Plots

The two parameter plots are those from which the molecular and thermodynamic parameters A and B can be determined[19], from which dimensional parameters can be extracted. Two types of plot using ILS data are used here, the Baumann plot[20] and the Berry plot[21].

The Baumann plot is described by the equation;

$$\left(\frac{6\langle s^2\rangle}{M}\right)^{3/2} = A^3 + BM^{1/2} \qquad (4.37)$$

and the Berry plot by ;

$$1.42\times 10^{-24} A_2 M^{1/2} = -A^3 + 6A\left(\frac{\langle s^2\rangle}{M}\right) \qquad (4.38)$$

where $A^2 = (\langle r^2\rangle/M)$ (an description of A and B is given in section 5.2.1)

The data from ILS was plotted according to these equations, however this data was greatly scattered, and hence the plots are difficult to interpret. In addition data from aromatised polymers gives negative intercepts which are physically unreal, and not tabulated. The asymptotic characteristic ratio, C_∞, can be calculated from the unperturbed dimensions thus[20];

$$C_\infty = \frac{\langle r^2\rangle}{M_w}\cdot\frac{M}{l^2} \qquad (4.39)$$

where M is the mass of the monomeric unit, length l, taken here to be ≈3.5Å for the unaromatised polymer.

polymer	solvent	intercept.	slope	$\langle r^2\rangle/M_w/10^{-17}$ cm^2 g mol^{-1}	C_∞
0%	NMP	1.582	0.00351	13.58	25.26
40%	NMP	0.253	0.0245	4.00	5.79
0%	$CHCl_3$	1.232	0.00744	11.49	21.37
10%	$CHCl_3$	1.122	0.00767	10.80	18.78

Table 4.19: Results from Baumann plots.

polymer	solvent	intercept	slope	$\langle r^2\rangle/M_w/10^{-17}$ cm^2 g mol^{-1}	C_∞
0%	NMP	-0.469	2.620	6.04	11.23

Table 4.20: Results from Berry plot.

It is difficult to draw firm conclusions from these plots where the data is scattered, however the value of the unperturbed dimension, $\langle r^2\rangle/M_w$ from the Berry plot is close to that from viscometry (section 5.4.1), those from the Baumann plots are about double the viscometry value and are therefore regarded as in error. The trend in $\langle r^2\rangle/M_w$, and hence characteristic ratio, C_∞, which could be determined is a decrease as aromatisation increases, possibly an effect of coils collapsing as aggregation occurs, in contrast a stiffer chain will have an increased C_∞ over a flexible one. The stiffness of a polymer chain, as measured by persistence length, and C_∞ are related by the equation[22];

$$C_\infty = \frac{2a}{l} - 1 \qquad (4.39)$$

where l is the length of the monomeric unit.

This would give persistence length, a, for unaromatised polymer as 46Å in NMP and 39Å in chloroform from the Baumann plots and 21Å in NMP from the Berry plot. This compares with 40Å in NMP and 68Å in chloroform from Murakami and Zhang plots.

The negative intercepts are due to the non-adherence by the stiff chains to theory developed for random coil type polymers. A similar phenomena is seen with viscometry data and is more fully discussed in section (5.5).

Characteristic ratio, C_∞, and the persistence length can be calculated from equation (4.38) by constructing a plot of $\langle s^2\rangle$ *vs* M_w and measuring the gradient.

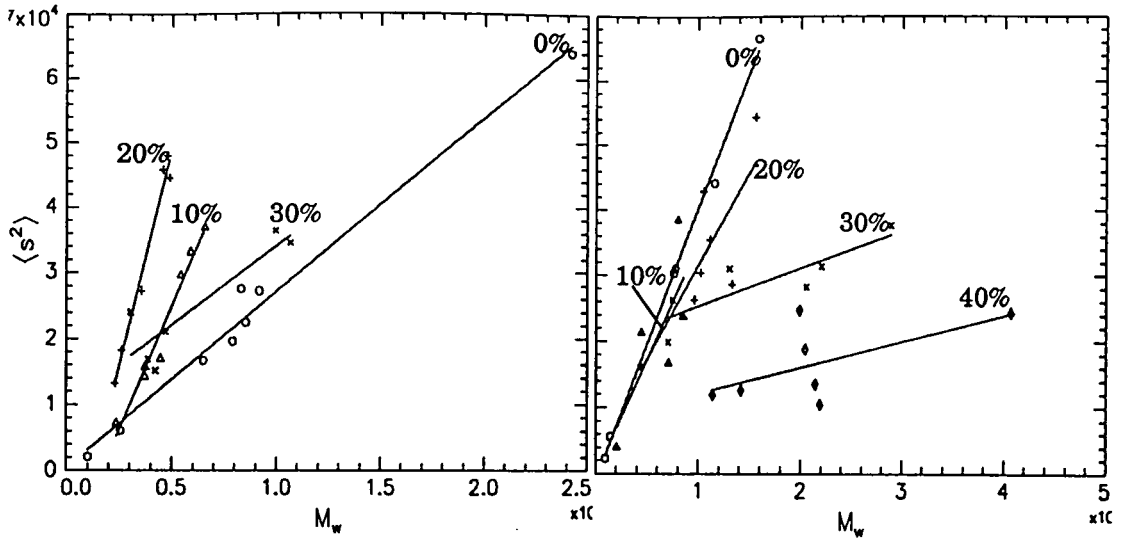

Figure 4.12: Characteristic ratio plots (a) NMP (b) chloroform.

The results for persistence length for 0-10-20% aromatised polymer in NMP are somewhat lower then the values from Murakami and Zhang plots, and may well be more reliable because the plots were less scattered. The same trend is observed, stiffening at low aromatisation, then dropping off as aggregation starts. The opposite is seen in chloroform where the persistence length drops continuously from a rather high value for the unaromatised polymer.

Percentage aromatisation	NMP		chloroform	
	C_∞	a	C_∞	a
0	30	53	47	84
10	79	138	37	67
20	129	227	28	51
30	21	36	5	11
40	--	--	4	9

Table 4.21: Results of characteristic ratio plots.

4.4.3 Characteristic ratio

In section (1.2.1) it is stated that the characteristic ratio of a random coil type polymer is independent of the molecular mass, that is the ratio of ($\langle r^2 \rangle$/M) (and therefore ($\langle s^2 \rangle$/M)) will be constant for any given molecular weight, however, as a real wormlike polymer

chain possesses some degree of stiffness this plateau behaviour is only reached at a certain molecular weight, above which the molecule displays true Gaussian like behaviour. Below this limiting value the molecule displays rod-like behaviour, and the ratio ($\langle r^2 \rangle / M$) increases proportionately with molecular weight from the origin to this point. When the experimental values of ($\langle s^2 \rangle / M$) are plotted against molecular weight some differences in behaviour pertaining to chain stiffness are observed. In each case the data points are plotted, but display some scatter, and are therefore overlaid with the line of the values from the least squares fit to ($\log \langle s^2 \rangle^{1/2}$ vs $\log M_w$).

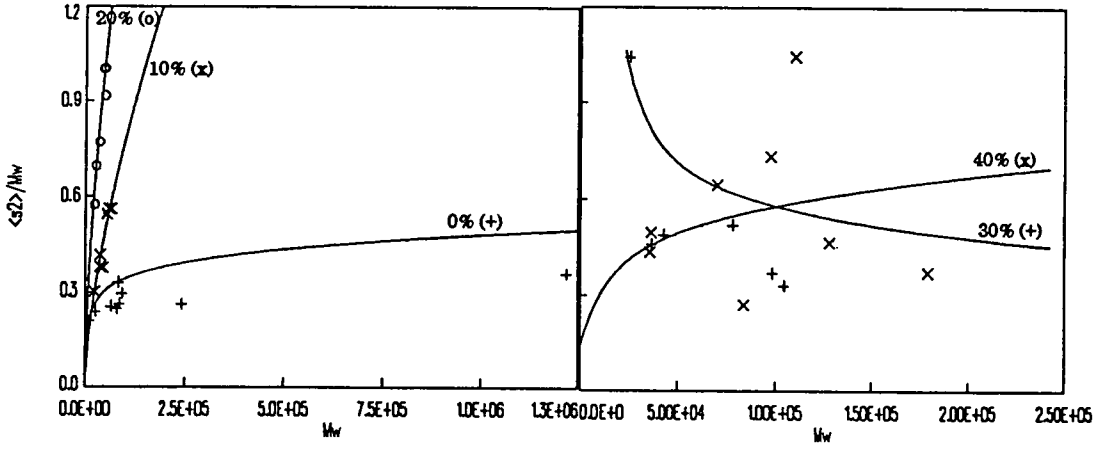

4.13: Molecular weight dependency of characteristic ratio in NMP.

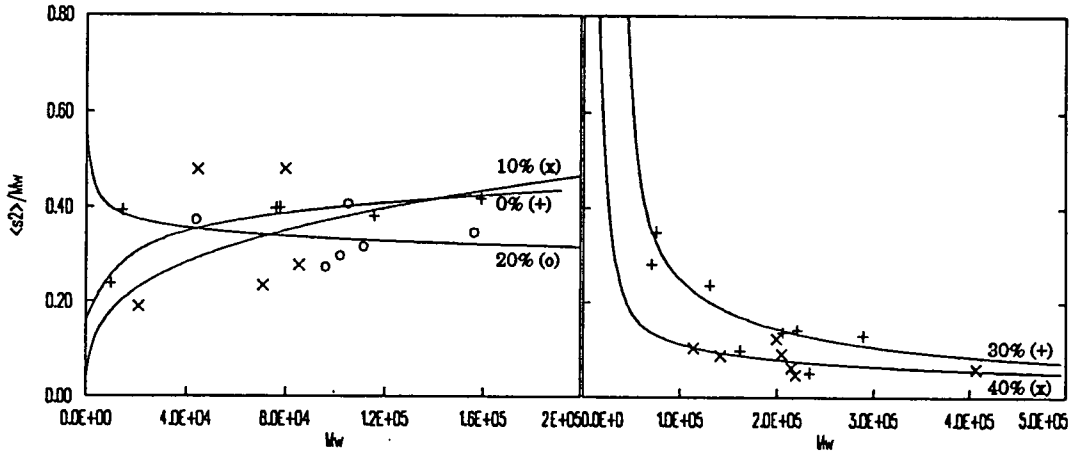

4.14: Molecular weight dependency of characteristic ratio in $CHCl_3$.

If the experimentally determined characteristic ratio is plotted as a function of molecular weight the differences can be more clearly observed. The unaromatised polymer appears

to have reached a constant slope (a true plateau will not be observed because of the effect of excluded volume) over most of it's molecular weight range, indicating that the polymer has a random coil configuration, the curve for polymers at 10% and 20% aromatisation are rising steeply, suggesting the data has been collected over a range where the polymer behaves as a stiff chain. From extrapolation of the fitted lines it can be seen that the rod-like regime of the aromatised polymers extends beyond that of the unaromatised polymer, an indication of increasing chain stiffness with aromatisation. This phenomenon clearly illustrated by a plot of data from polyhexyl isocyanate[23] (fig 4.15) where data has been collected over a range sufficiently broad to show both behaviours, and a transition, marking the fairly abrupt change in the log([η]) vs log(M_w) plot

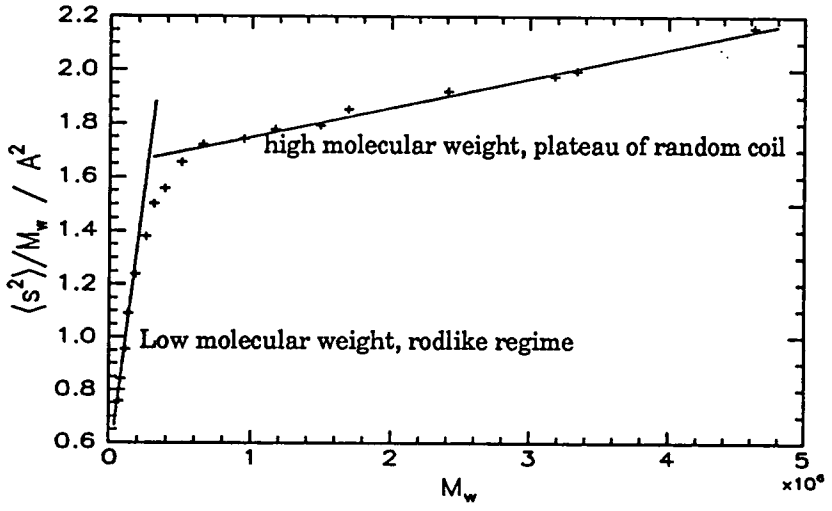

4.14: Molecular weight dependency of characteristic ratio of PHIC in hexane.

4.4.4 Structure of aggregates from Zimm plots

Tanner and Berry[24] describe two possible Zimm plots arising from light scattering by differently aggregated solutions

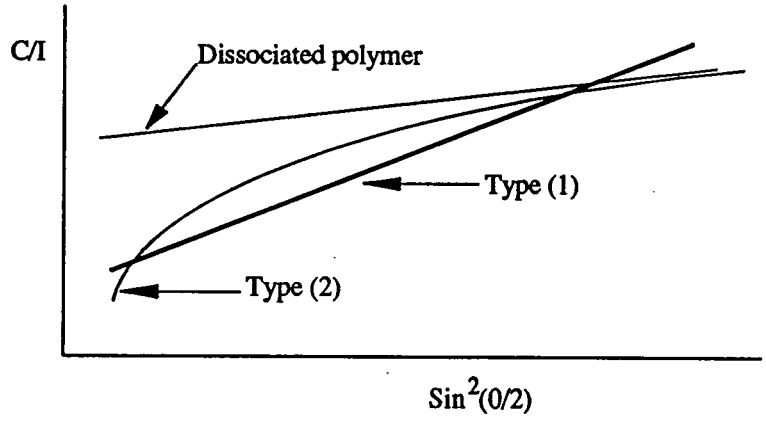

Figure 4.16: scattering patterns from aggregated polymers.

These represent (1) a high M_w but loosely associated aggregate, containing a large proportion of the total polymer, a gel structure. (2) two widely differing sizes of polymers, smaller dissociated molecules responsible for the scattering at high $\sin^2(\theta/2)$ and very large aggregates causing the downturn at low $\sin^2(\theta/2)$.

Two such plots are shown in Figure 4.17, an unaromatised polymer, freely dissociated, and one 40% aromatised in $CHCl_3$, severely aggregated.

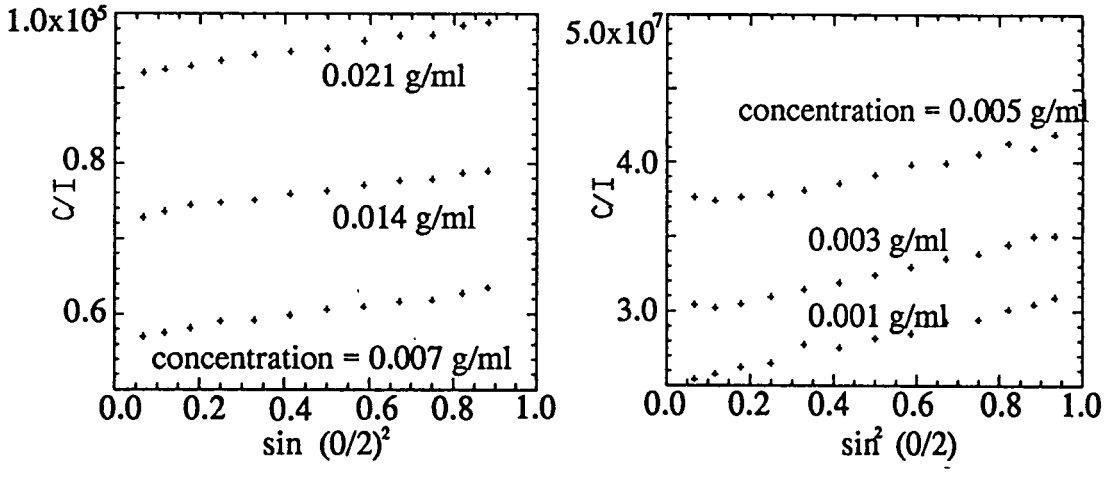

Figure 4.17: Zimm plots of poly(DHCD-DMC) (left) and 40% aromatised polymer.

The dissociated polymer shows the behaviour expected with a linear plot, the aggregated polymer also has a linear plot, a slight upturn at high concentration is caused by the scattering saturating the PM tube, however the lines do not have a steep gradient, and are therefore not type (1), and if a separate species of aggregates exist alongside the dissociated polymer they are not large enough to affect the Zimm plot as type (2). The aggregated solutions may consist of smallish aggregates not greatly larger than the single chains, as is observed in SEC.

4.4.5 Depolarised scattering

A solution of an anisotropic polymer, such as a rigid rod like molecule, will cause plane polarised light to be rotated out of it's plane of polarisation. By filtering out the plane polarised component from the scattered light it is possible to measure this depolarised scattering. In practice this is done by inserting a polarising filter between the sample and the PM tube, perpendicular to the plane of the laser radiation

The depolarised scattering from solutions at 0%, 20%, and 40% aromatised polymer were measured using the PCS apparatus modified as in figure 4.18, and compared with the depolarised scattering from the solvent. The depolarised scattering was ≤0.5% of the

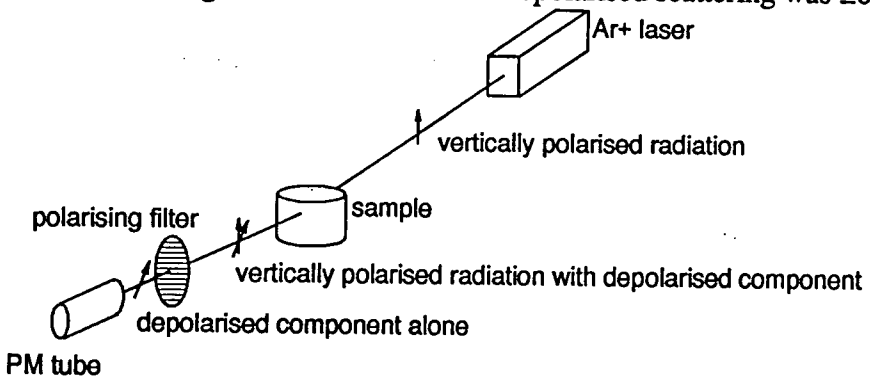

Figure 4.18: Measurement of depolarised scattering.

full scattered intensity, and there was no significant excess scattering from the solutions over the solvent, and in all cases the scattering normalised to unity over the angular range employed in the Zimm plots. From this it was concluded that the polymers in all solutions were essentially isotropic.

It has not been possible to study behaviour of poly(DHCD-DMC) above 40% aromatisation. The limit of solubility of the polymer is 40% aromatisation, above 40% a viscous liquid or a gel is formed with a significant yellow coloration, caused by both the colour of the polymer and degradation of NMP. It is not possible to remove the solvent's contribution as once precipitated the polymer will no longer dissolve. The yellow colour absorbs the Ar^+ radiation at 4880Å, significantly reducing the scattered intensity, preventing the study of it's light scattering behaviour.

4.5 Conclusion

Intensity light scattering shows quite clearly a change in the configuration of poly(DHCD-DMC) during aromatisation to polyphenylene. This is;

coil → stiff chain → aggregate of uncertain structure

It also shows some difference in the behaviour of the two solvents, NMP and chloroform, chloroform is a superior solvent for poly(DHCD-DMC), but is poorer than NMP for the aromatised polymer, and the polymer aggregates more readily in chloroform than NMP. This may be of significance in SEC where discrete peaks corresponding to the free polymer and the aggregate were observed in chloroform. If SEC results were to be extrapolated to ILS then discrete aggregate particles would be expected, at least in chloroform, and possibly in NMP.

This would assume that the aggregates existed in the undisturbed solution after filtering (SEC and ILS solutions were both filtered through 0.2μm membrane filters) and were not an artefact resulting from shear fields within the chromatographic columns.

The presence of high molecular weight aggregates was not detected in the Zimm plots, though this may be due to their smaller size, however they will have an effect on the results from these plots. Zimm plots yield w- and z- average values of the whole population (Appendix 2) which are sensitive to small amounts of a large species. Z-average radii of gyration were corrected for polydispersity, assuming a Schulz-Zimm distribution. This is acceptable for the free radically initiated polymer, but not a distribution of two discrete peaks. The scatter seen in the data, which increases with increasing aromatisation, is due in part to the presence of aggregates, which will be random in nature and distribution if the thermal aromatisation process is random. This would appear to be the case in view of the randomness of the results.

The chain stiffness as characterised by the persistence length, a, has been measured by up to four methods, and they do differ somewhat. Which of these values is correct is uncertain, however in each case results from the same method show the same trend of increasing a

with increasing aromatisation up to 20%, followed by a decrease as aggregation predominates the polymer behaviour.

Aromatisation	a in NMP /Å	a in chloroform /Å
0%	35① 46② 21③ 53④	68① 39② 84④
10%	238⑤ 138④	87① 33② 67④
20%	318⑤ 227④	195① 9④

Table 4.22: Persistence lengths from ILS.

① Murakami plot, ② Baumann plot, ③ Berry plot, ④ $\langle s^2 \rangle$ vs M_w plot, ⑤ Zhang plot.

Although it has not been possible to determine the structure of the aggregates, they are of an insufficient size to cause distortion in the Zimm plots, and are closer to the molecular scale, and they do not display optical anisotropy. Both of which are consistent with the fringed micelle model.

4.6 References

1, Huglin,M.B., *'Light Scattering From Polymer Solutions'* Academic Press, New York, 1972.

2, Kratochvil,P., *'Classical Light Scattering from Polymer Solutions'* Polymer science library 5, A.D.Jenkins(Ed), Elsevier, Amsterdam,1987.

3, Debye,P., *J.Appl.Phys.*,15,338,(1944).

4, Burchard,W, Ch10 in *'Applied Fibre Science'*, Vol 1, ed F.Happey, Academic Press, New York, 1978.

5, Zimm,B.H ,*J.Chem.Phys.*,16,1093,(1948).

6, Huglin,M.B.,*Topics in Current Chemistry*,77,143,(1978)

7, Zimm,B.H., *J.Chem.Phys.*,16,1099,(1948).

8, Booth,C., Colclough,R.O., Ch3 in *'Comprehensive Polymer Science'*, Vol 1, ed. Booth,C. and Price,C., Pergammon Press, Oxford, 1989.

9, Kurata,M., Tsunashima,Y., ChVII in *'Polymer Handbook'* ed. Brandrup,J. and Immergut,E.H., Wiley ,New York,1974.

10, *Automeasure Manual*, version 3, Malvern Instruments, Malvern, 1987

11, DeCeuninck,W., Finsey,R., Moreels,e.,*J.Chem.Phys.*,86,618,(1987).

12, Bender,T.M., Lewis,R.J., Pecora,R., *Macromolecules*,19,244,(1986).

13, Weast, ed, *'CRC Handbook of Chemistry and Physics'*, CRC Press, Boca Raton, 1987.

14, Huglin,M.B.,*Eur Polym.J.*,25,543(1989)

15, Mays,J.M., *Macromolecules*,21,3179,(1988).

16, Gooda, S.R., Huglin, M.B., *Macromolecules*,25,4125,(1992).

17, Kurata,M., Stockmayer,W.H., *Fortschr.Hochpolym.Forsch*, 3,196,(1963).

18, Berry,C., Casassa,E.F., *J.Polym.Sci*,D4,1,(1970).

19, Yamakawa,H., *'Modern Theory of Polymer Solutions'*, Harper and Row, New York, 1971.

20, Bauman,H., *J.Polym.Sci.*B10,1069,(1965).

21, Berry,G.C., *J.Chem.Phys.*,44,4550,(1966).

22, Flory,P.J., '*Statistical Mechanics of Chain Molecules*', Interscience, New York, 1969.

23, Fujtia,H., Murakami,H., Norisuye,T.,*Macromolecules*,13,345,(1980).

24, Berry,G.C., Tanner,D.W., *J.Polym.Sci,Polym.Phys.Ed.*,12,941,(1974).

4.7 Plots of ILS data

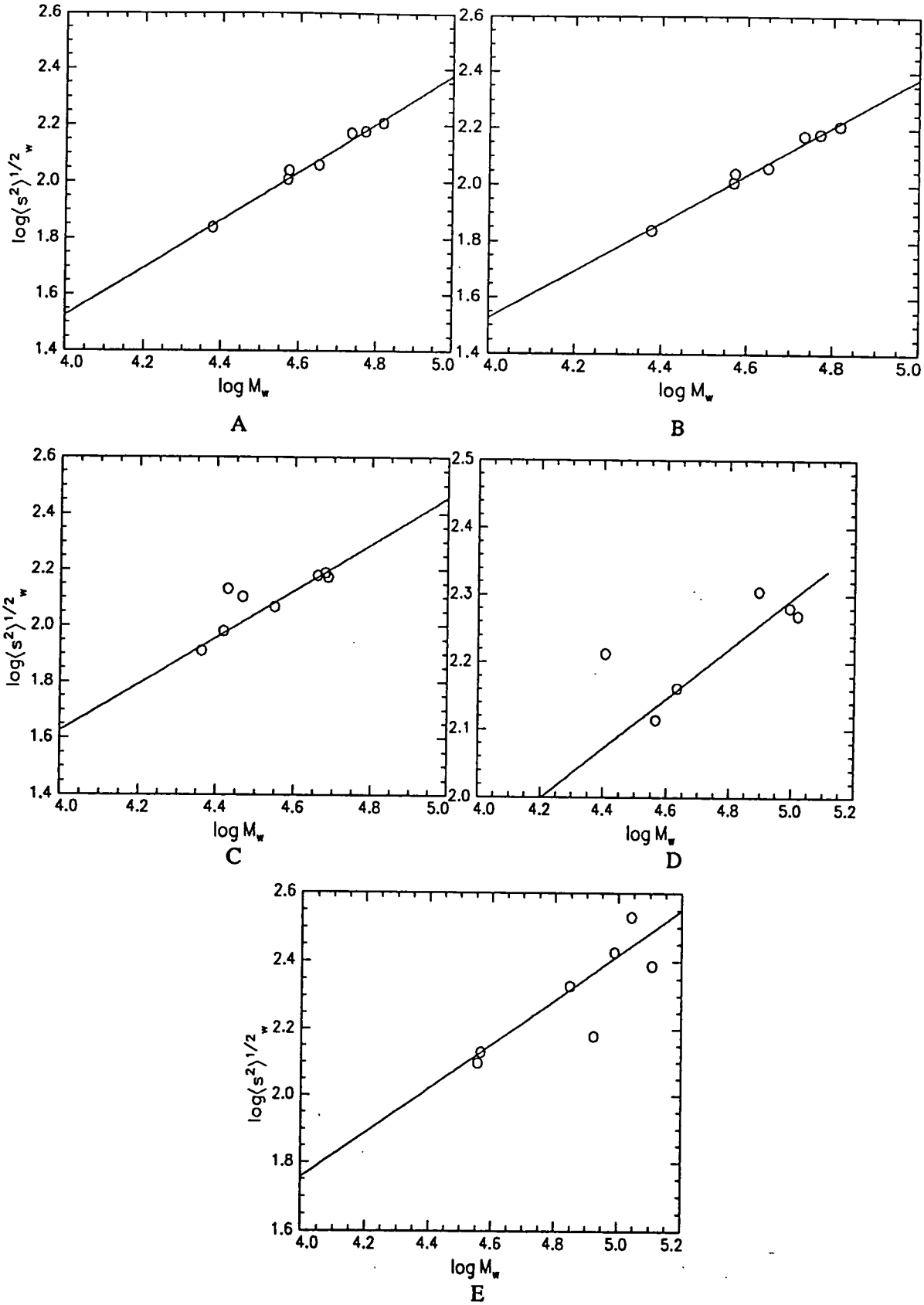

Figure 4.19: Plots of Radius of gyration *vs* Moleclar weight, NMP solution. A;0% aromatisation, B;10% aromatisation, C;20% aromatisation, D; 30% aromatisation, E; 40% aromatisation

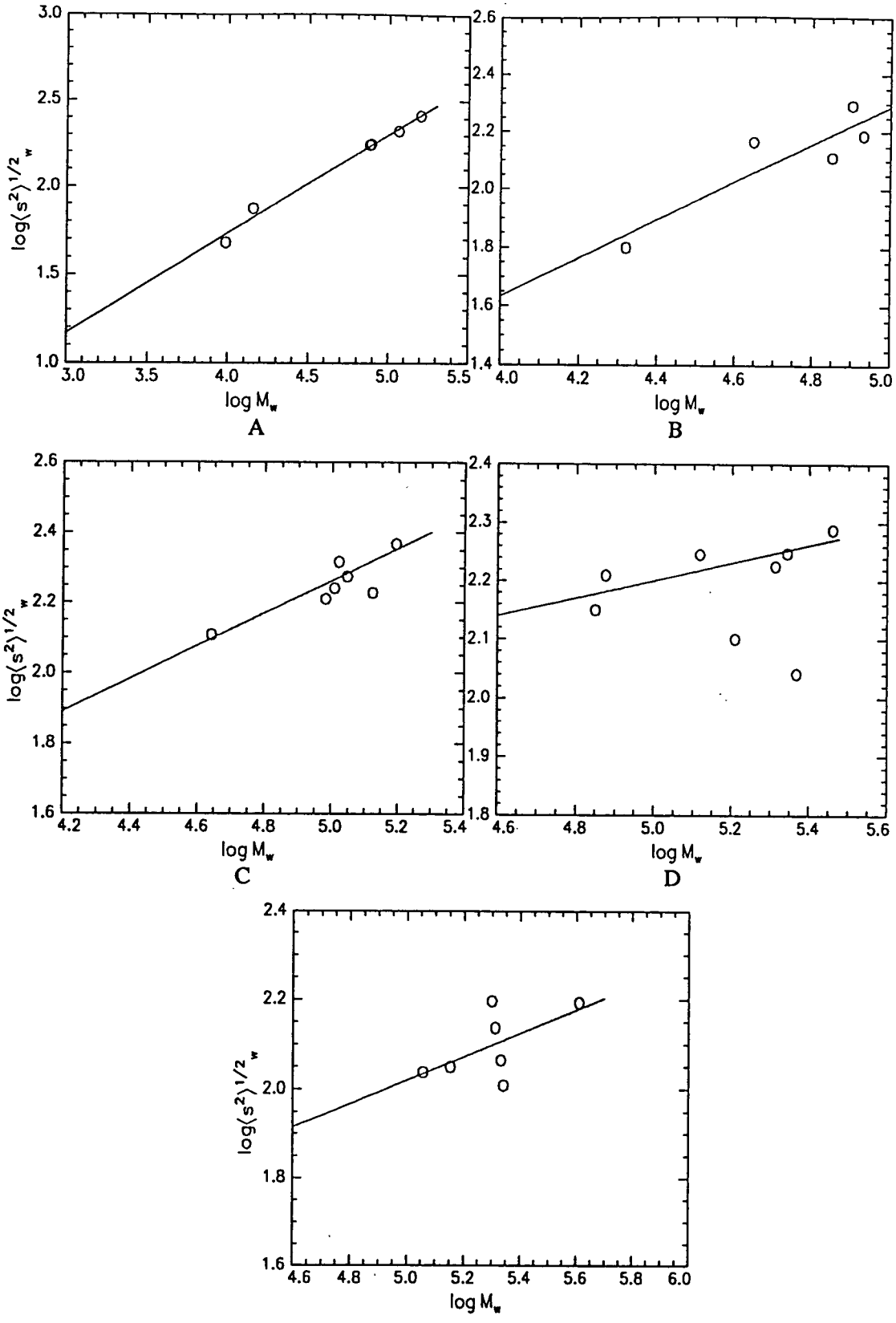

Figure 4.20: Plots of Radius of gyration *vs* Molecular weight, chloroform solution. A;0% aromatisation, B;10% aromatisation, C;20% aromatisation, D; 30% aromatisation, E; 40% aromatisation

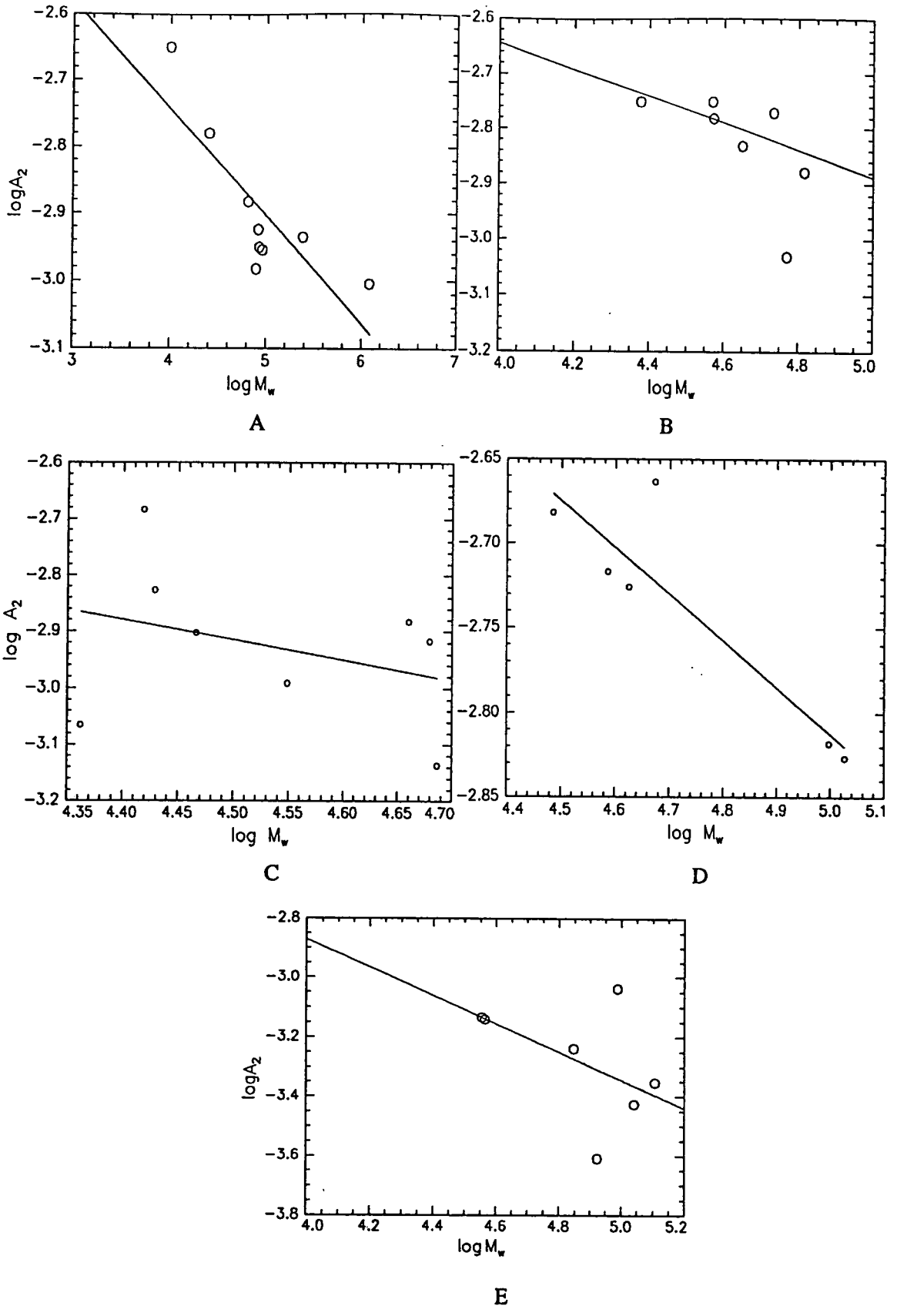

Figure 4.21: Molecular weight dependency of second virial coefficient, NMP solution. A;10% aromatisation, B;10% aromatisation,C;20% aromatisation D;30% aromatisation , E 40% aromatisation.

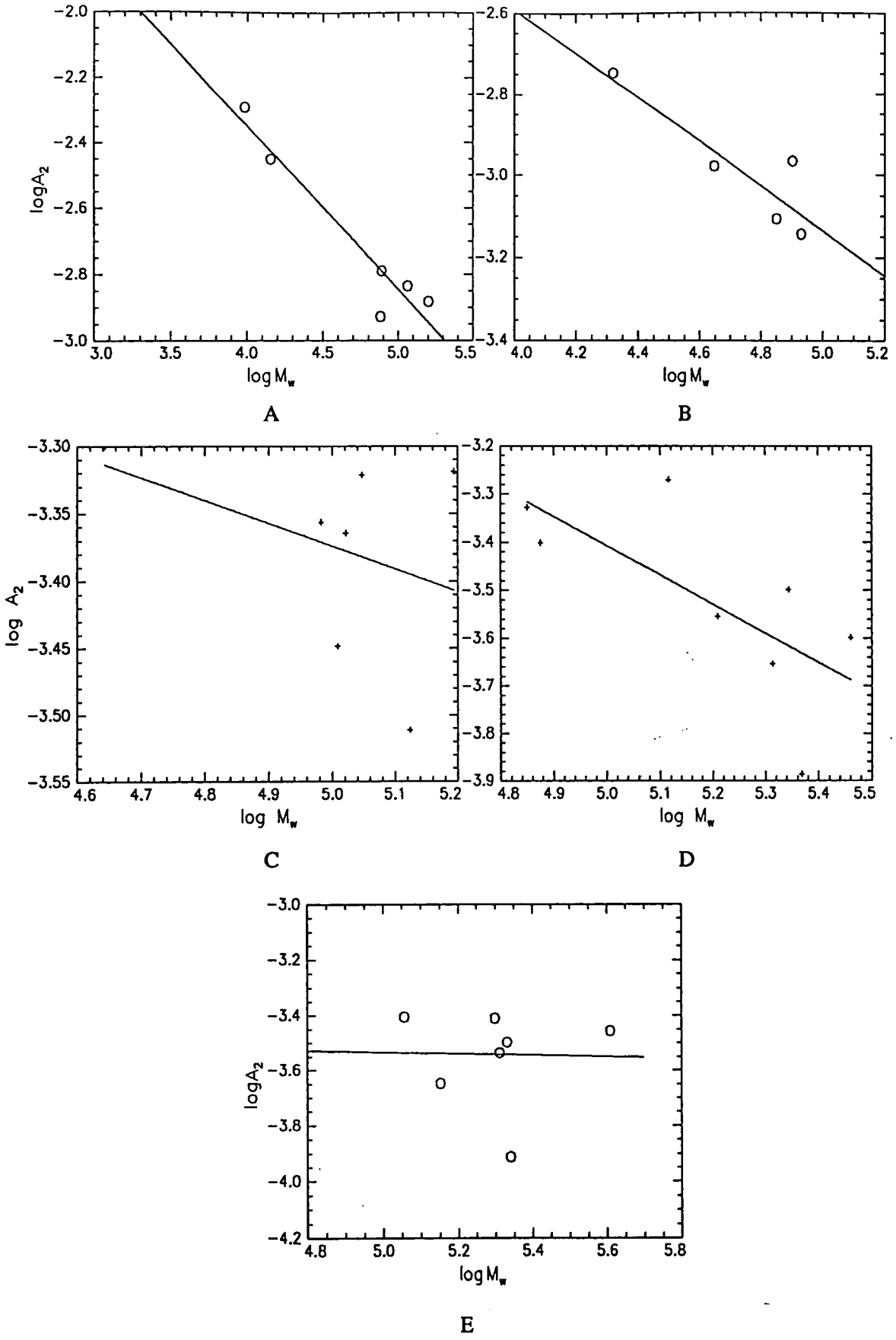

Figure 4.22: Molecular weight dependency of second virial coefficient, $CHCL_3$ solution. A;10% aromatisation, B;10% aromatisation,C;20% aromatisation D;30% aromatisation , E 40% aromatisation.

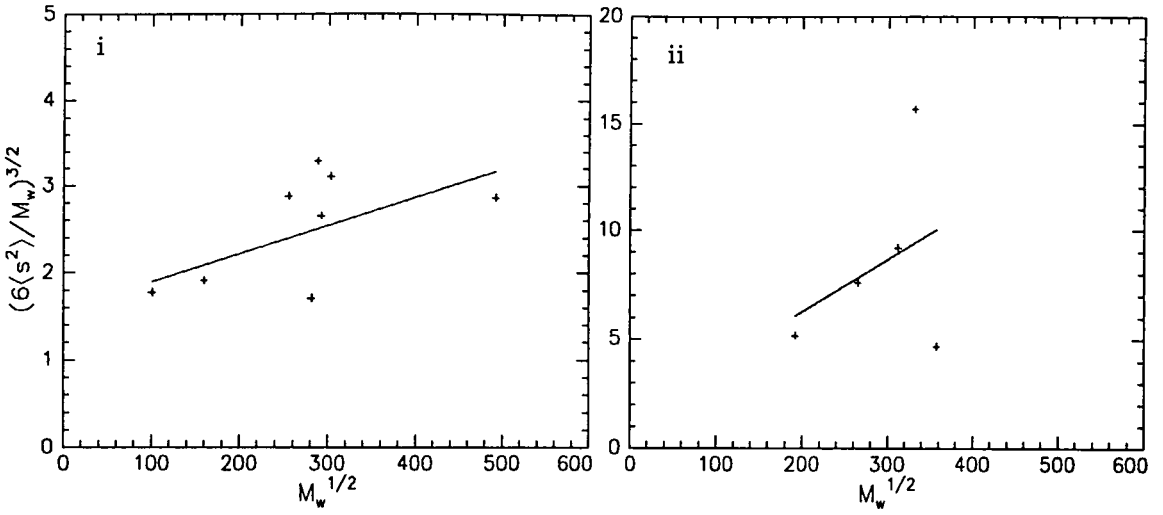

Figure 4.23: Baumann plots of i,unaromatised polymer ii, 40%aromatised polymer, NMP solution.

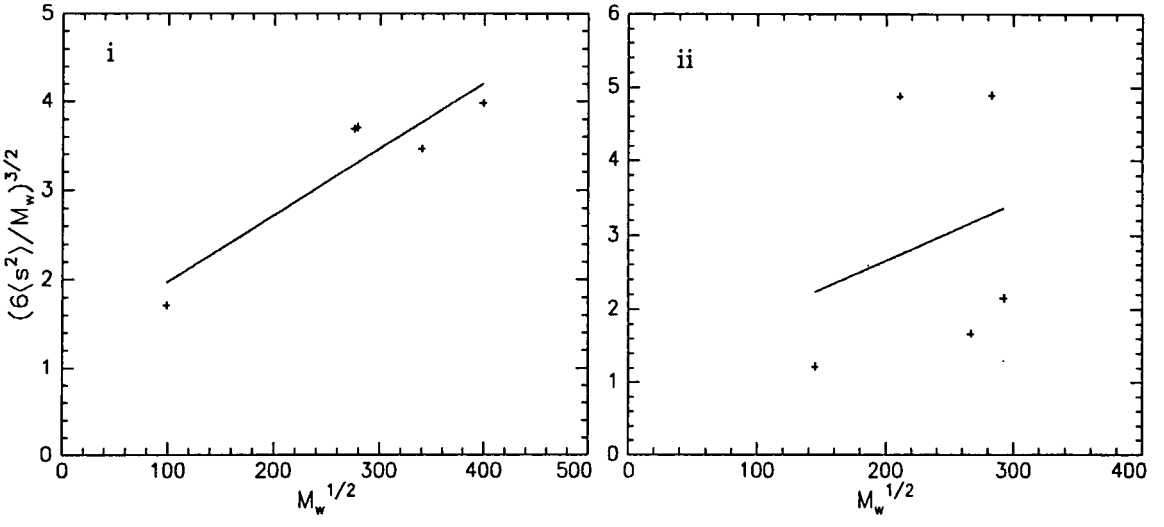

Figure 4.24: Baumann plots of i,unaromatised polymer ii, 10%aromatised polymer, $CHCl_3$ solution.

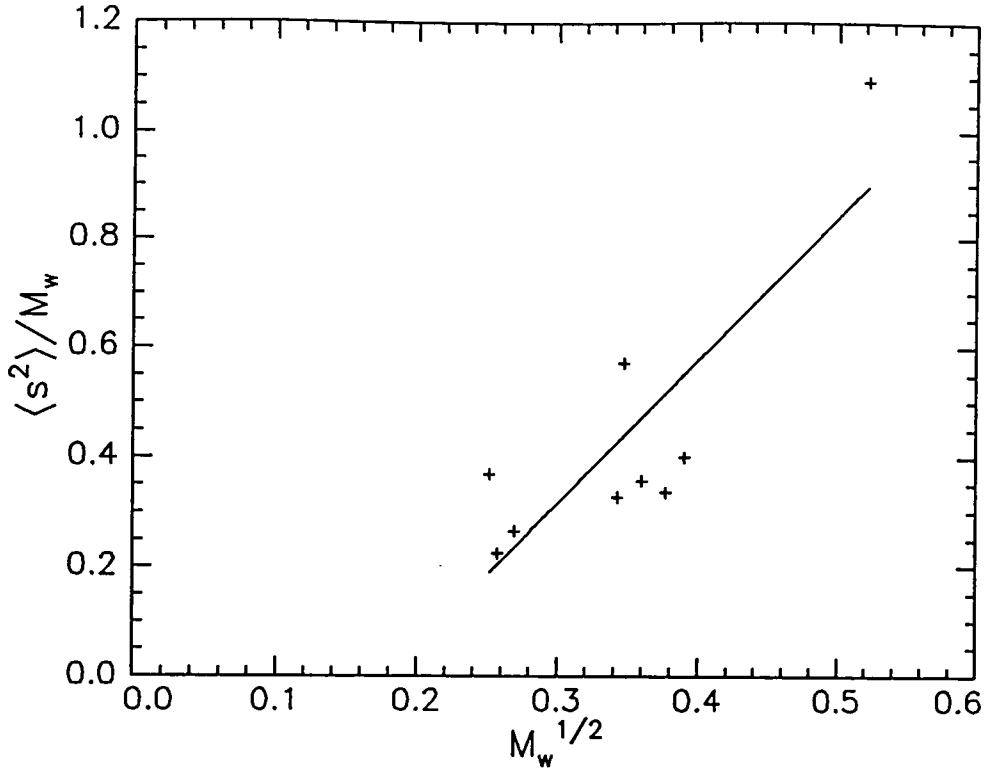

Figure 4.25: Berry plot of unaromatised polymer in NMP solution.

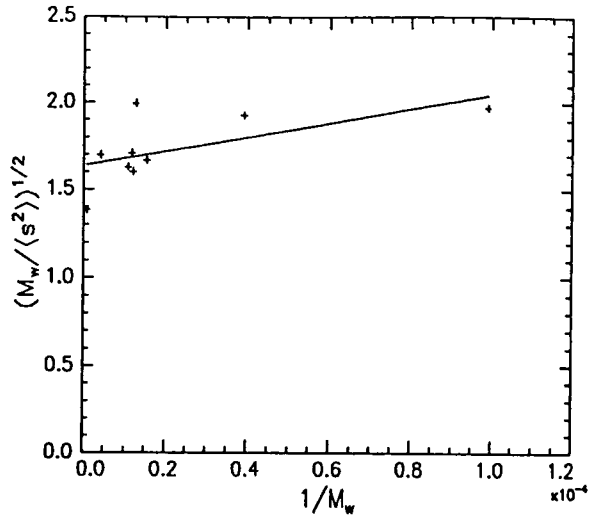

Unaromatised polymer, NMP solution, Murikami plot.

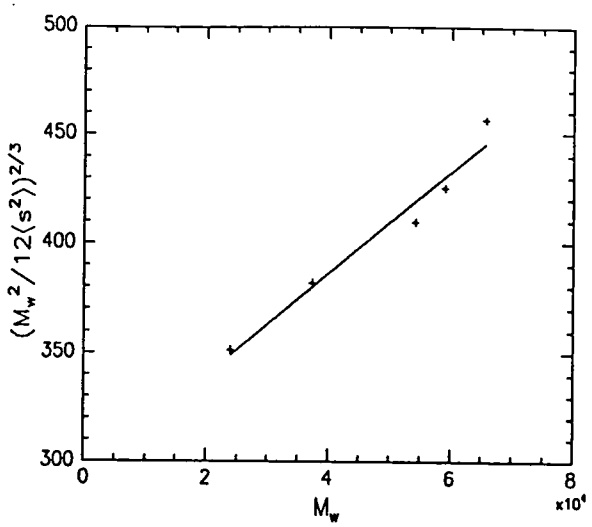

10% aromatised polymer, NMP solution Zhang plot.

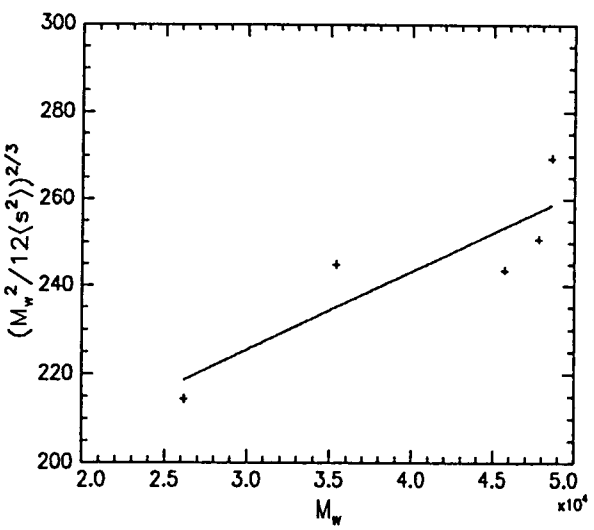

20% aromatised polymer, NMP solution Zhang plot.

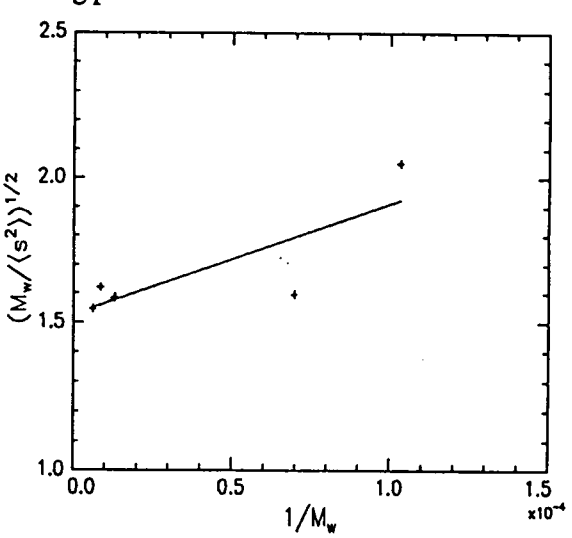

Unaromatised polymer, $CHCl_3$ solution Murikami plot.

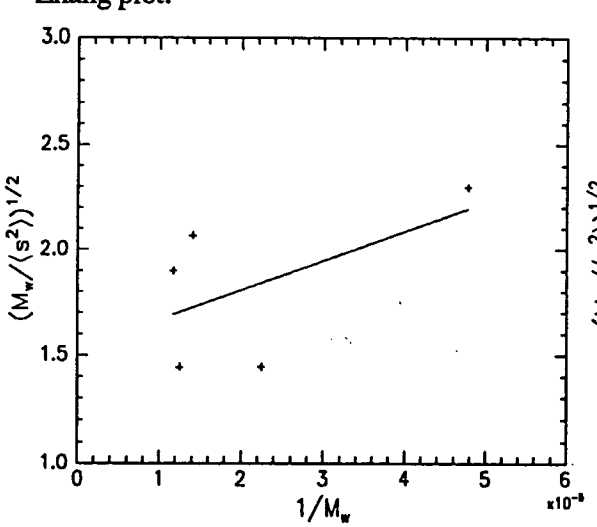

10% aromatised polymer, $CHCl_3$ solution. Murakami plot.

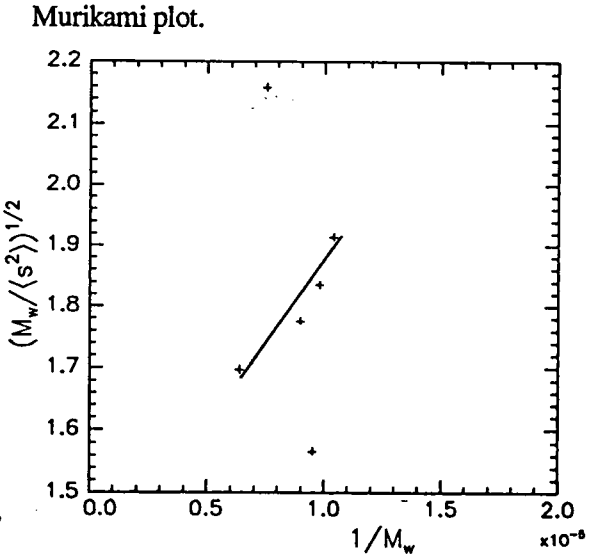

Unaromatised polymer, $CHCl_3$ solution Murikami plot.

Figure 4.26: Persistence length plots from Murakami and Zhang equations (4.34/35).

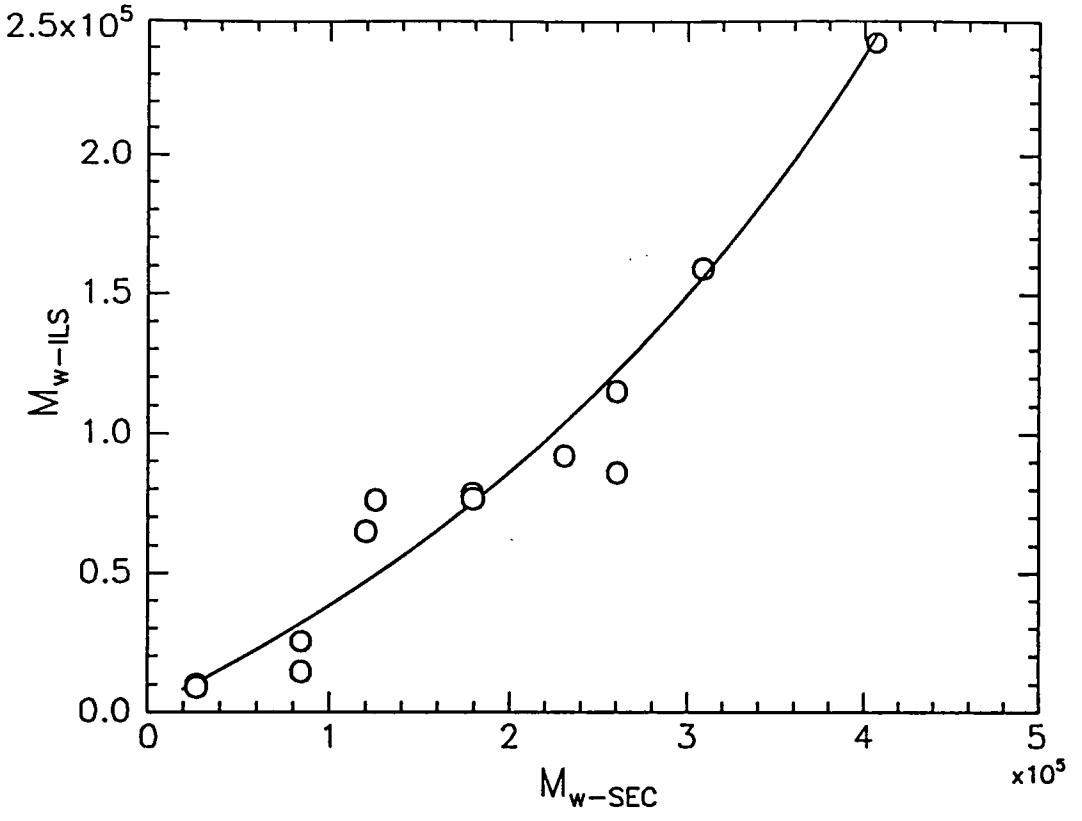

Figure 4.27: Comparison of molecular weights from ILS and SEC.

Fraction D, 0% Aromatisation ; Solvent chloroform

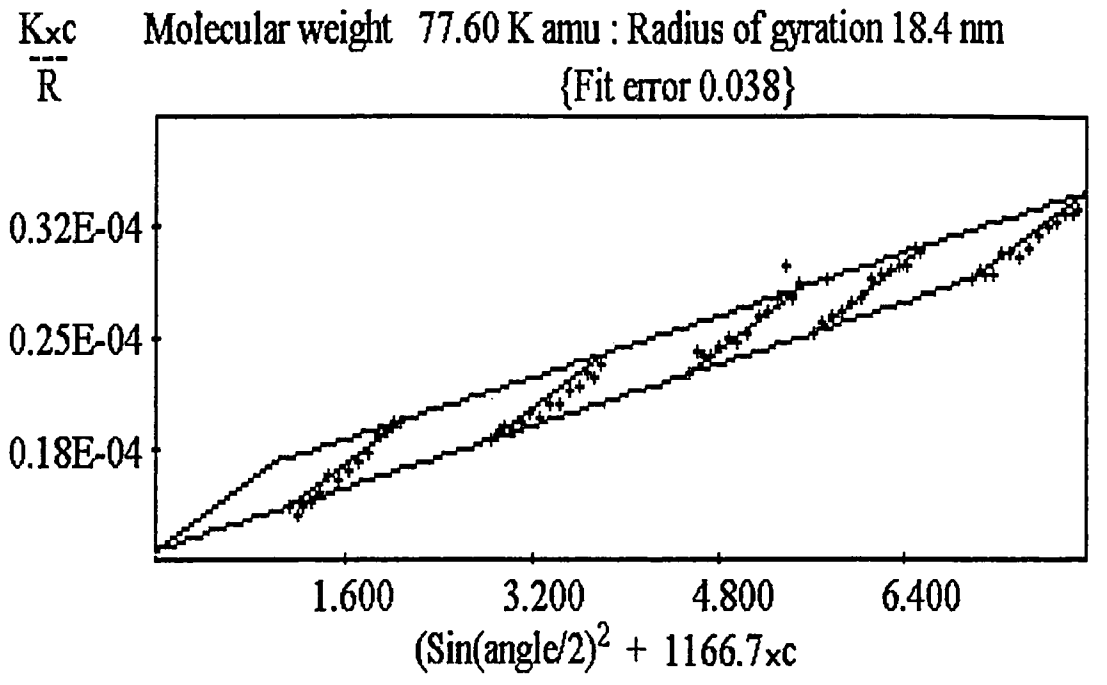

Fraction D, 10% Aromatisation ; Solvent chloroform

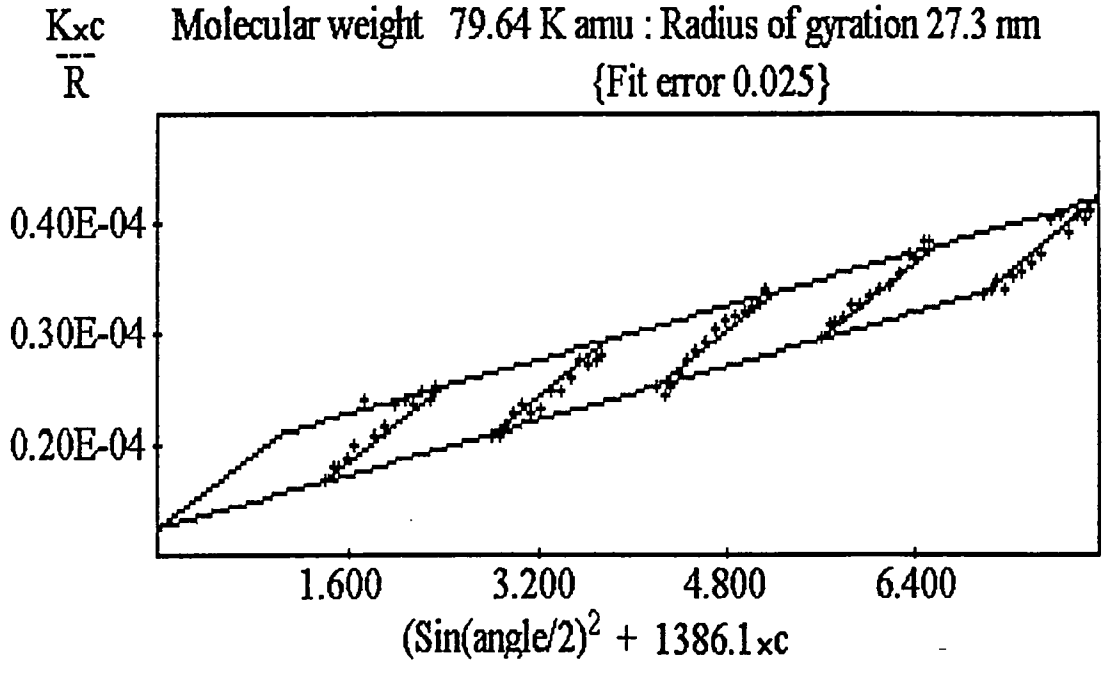

Figure 4.28a: Example Zimm plots from ILS

Fraction F, 20% Aromatisation ; Solvent chloroform

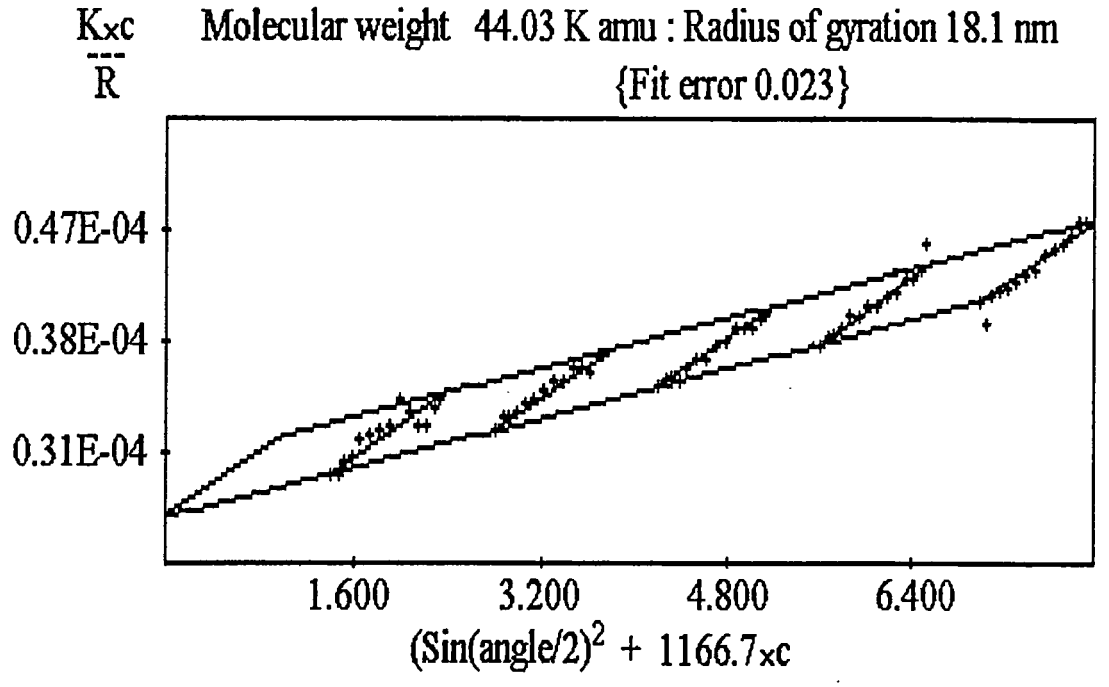

Fraction F, 20% Aromatisation ; Solvent chloroform

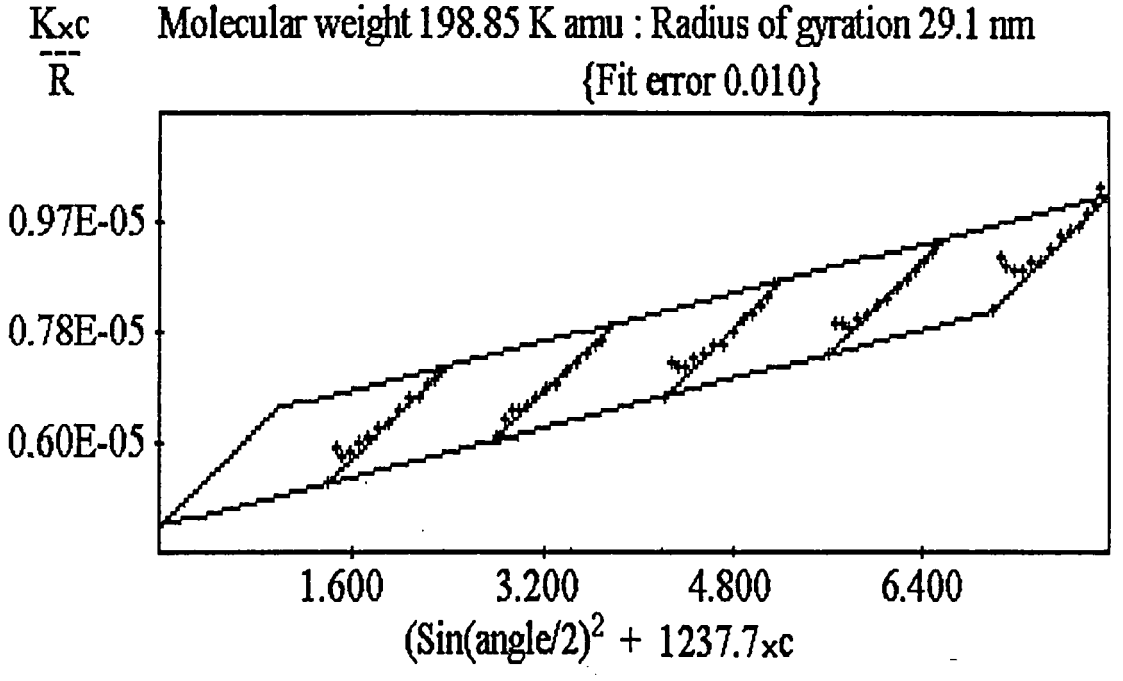

Figure 4.28b: Example Zimm plots from ILS

Fraction H, 40% Aromatisation ; Solvent NMP

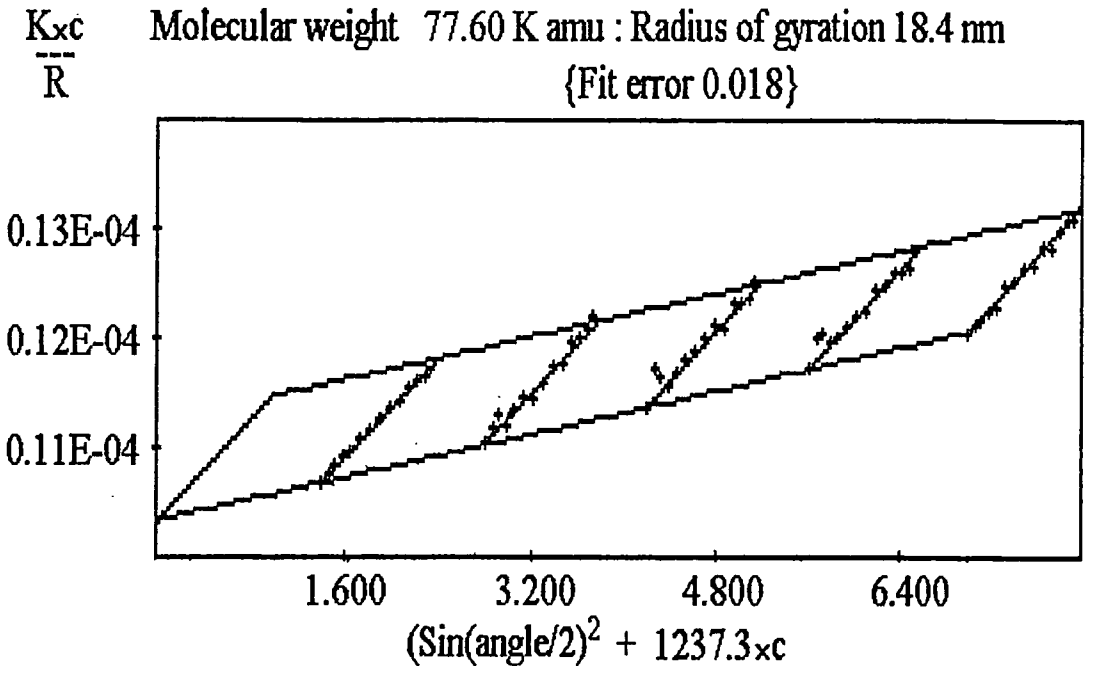

Figure 4.28c: Example Zimm plots from ILS

CHAPTER 5

VISCOSITY MEASUREMENTS

5.1 Introduction

The intrinsic viscosities of dilute solutions of partially aromatised poly(DHCD-DMC) in NMP have been measured and combined with molecular weight measurements to derive configurational parameters and persistence lengths.

5.2 Theoretical Background

It has long been realised that the significant increase in the viscosity of a polymer solution over the solvent should in some manner be related to the molecular weight of the solute species, and from the early stages of polymer science attempts have been made to quantify this relationship[1].

Before considering these relationships it is useful to consider the terms used in viscometry. The principal viscometric parameters are given in table 5.1

Symbol	Definition	Name
η		solution viscosity
η_0		solvent viscosity
c		concentration (/g ml^{-1})
η_r	η/η_0	relative viscosity
η_{sp}	$(\eta-\eta)/\eta_0$	specific viscosity
$[\eta]$	$\lim_{c\to 0}(\eta-\eta)/\eta_0 c$	intrinsic viscosity

Table 5.1: Viscometry parameters.

A convenient empirical relationship has been derived which satisfactorily describes the majority of linear polymers, this is the Mark-Houwink equation[2], describing the dilute solution viscosity in terms of molecular weight, with the two parameters K and α, constants for a given polymer/solvent/temperature combination.

$$[\eta] = KM_v^{\alpha} \qquad (5.1)$$

The value of α depends upon both the quality of the solvent and the configuration of the polymer chain. Typical values of α are

0.5	Random coil in theta condition
$0.5<\alpha<\approx 0.8$	Random coil in good solvent
$\approx 0.8<\alpha<\approx 1.2$	Wormlike chain
$\alpha<\approx 1.2$	Rodlike chain
2.0	True rigid rod

The molecular weight in this case is the viscosity-average, M_V, defined by

$$\overline{M}_v = \left[\frac{\Sigma N_j M_j^{1+\alpha}}{\Sigma N_j M_j} \right]^{1/\alpha} \tag{5.2}$$

This molecular weight is different from both weight and number average values, but is closer to weight average, with which it is sometimes substituted. The positions of these averages for a typical polydisperse polymer are shown in figure 5.1

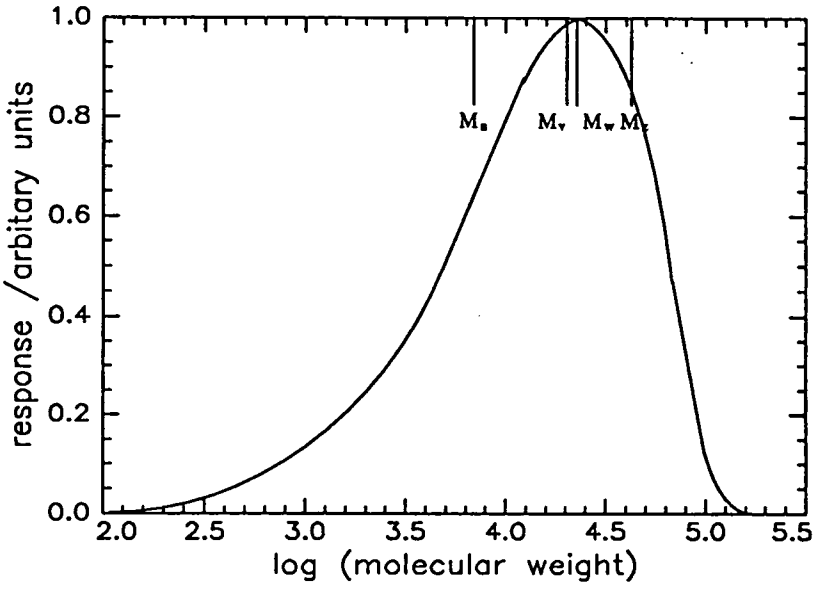

Figure 5.1: Molecular weight averages for a polydisperse polymer ($M_w/M_n = 3.2$).

5.2.1 Theoretical relationships

In order to quantify the hydrodynamic behaviour of polymer solutions a number of assumptions must be made. Because the particles of solvent are much smaller than those of solute it is convenient to regard the solvent as a continuous viscous fluid, however the particles should be small in relation to the measuring apparatus to reduce wall effects. It is also assumed that molecules only interact intramolecularly, and not intermolecularly, if this were not the case then solution viscosity would increase disproportionately over that of the solvent as concentration is increased. In order to achieve this in practice low solute concentrations are used, and then extrapolated to zero concentration

The viscosity of a dilute solution of hard, non-interacting, non-free draining spheres was calculated from hydrodynamic theory by Einstein[3] as;

$$\eta_r = 1 + 2.5\phi \qquad (5.3)$$

Where ϕ is the volume fraction of spheres. This equation can been modified to include wall effects, flexible spheres, and free draining[4] to;

$$\eta_{sp} = 2.5(\mu' - 0.4\mu / \mu' - \mu) \qquad (5.4)$$

Where μ and μ' are the viscosities of the solvent and the excess from the spheres. For a free draining flexible chain made up of segments each segment will contribute equally to the frictional component of the whole entity, so that the overall frictional coefficient, f_o will be proportional to the number of segments x and hence the molecular weight, independent of shape. For Gaussian chains, with large x the mean square radius of gyration $\langle s^2 \rangle_0$ is proportional to x, therefore;

$$[\eta] \propto \langle s^2 \rangle_0 \quad \text{and} \quad [\eta] \propto M$$

This relationship was predicted by Staudinger, but is found to be generally unsatisfactory for real polymer solutions.

Kirkwood and Riseman[5] modelled a chain of Gaussian segment distribution which accounts for the limitation of the free draining model because of solvent polymer

interactions. In this treatment each chain segment has a frictional coefficient, ζ, and for the whole molecule the frictional coefficient is given by

$$f_0 = \frac{6\pi\eta_0\langle s^2\rangle_0^{1/2}}{\left(\frac{8\pi^{1/2}}{3}\right)+\left(\frac{6\pi\eta_0\langle s^2\rangle_0^{1/2}}{x\zeta}\right)} \tag{5.5}$$

However for long chains x is large , and therefore the term containing it becomes negligible and reduces to

$$f_0 = (9/4)\pi^{3/2}\eta_0\langle s^2\rangle_0^{1/2} \tag{5.6}$$

The Kirkwood-Riseman theory was applied to $[\eta]$ by Auer and Gardner[6] and yielded

$$[\eta] = 1.259\,\pi^{3/2}N_A\left(\frac{\langle s^2\rangle_0^{3/2}}{M}\right) \tag{5.7}$$

This compares to equation (5.4), since

$$\phi = 4/3R^3.N_A c/M \tag{5.8}$$

Where R is radius of hard sphere. Combining (5.7) and (5.8) gives

$$[\eta] = 10\,\pi^{3/2}N_A\left(\frac{\langle s^2\rangle_0^{3/2}}{M}\right) \tag{5.9}$$

and means it must be possible to model the viscosity of polymers in dilute solution as impermeable hard spheres of radius $0.875\langle s^2\rangle_0^{1/2}$. This treatment is only applicable to unperturbed dimensions, and ignores excluded volume effects. In good solvents the average configuration is expanded, and the radius of gyration is altered by an expansion factor, α;

$$\langle s^2\rangle = \alpha^2\langle s^2\rangle_0 \tag{5.10}$$

for polymers in the theta condition, and for polymers in good solvents;

$$[\eta] = [\eta]_\theta\alpha^3 \tag{5.11}$$

Equation 5.7 can be modified to;

$$[\eta]_\theta = 6^{3/2}\Phi_0\frac{\langle s^2\rangle_0^{3/2}}{M} \tag{5.12}$$

Φ is a universal constant, whose value has been variously determined between 1.8 and 2.9 x 10^{23}, [7,8]. In order to determine the expansion factor in a particular solvent it is

necessary to know both the expanded and theta dimensions. This could be done by light scattering or by extrapolation of viscosity measurements. For flexible chains in the theta state from equation (5.12);

$$[\eta]_\theta = K_\theta M^{1/2} \qquad (5.13)$$

(5.11) and (5.13) give;

$$\alpha^3 = [\eta]/K_\theta M^{1/2} \qquad (5.14)$$

Rewriting eq.(5.12) with $\langle r^2\rangle_0 = 6\langle s^2\rangle_0$ and $A = (\langle r^2\rangle_0/M)$;

$$[\eta]_\theta = A^3\Phi_0 \qquad (5.15)$$

$$K_\theta = \Phi\left(\langle r^2\rangle_0/M\right)^{3/2} \qquad (5.16).$$

Equations (5.10)-(5.16) suggest that it is possible to quantify the effect of perturbed volume of solute polymers, and calculate the unperturbed dimensions of the polymer from viscometry data, regardless of the nature of the solvent, by extrapolation to zero molecular weight.

There have been a number of equations proposed for this treatment of experimental data. The earliest of these is that of Flory-Fox-Schaefgen[9];

$$[\eta]^{2/3}/M^{1/3} = K_0^{2/3} + 0.858\,K_\theta^{2/3}\Phi_0 B\,M/[\eta]. \qquad (5.17)$$

The constant K_θ can therefore be determined from a plot of $[\eta]^{2/3}/M^{1/3}$ against $M/[\eta]$, the slope yielding an interaction parameter B. This equation however has limitations for good solvents and is no longer generally used. Kurata and Stockmayer[10] proposed a modified equation;

$$[\eta]^{2/3}/M^{1/3} = K_\theta^{2/3} + 0.363\,\Phi_0 B g(\alpha) M^{2/3}/[\eta]^{1/3} \qquad (5.18)$$

with

$$g(\alpha) = 8\alpha^3/(3\alpha^2+1)^{3/2} \qquad (5.19)$$

This is a more cumbersome equation which requires two plots, first to estimate K_θ, from which $g(\alpha)$ is calculated using equations (14) and (19), then replotting incorporating $g(\alpha)$ to extract B. Kurata and Stockmayer used this equation on experimental data and found it to hold well for vinyl polymers, although again deviation can be found with good solvents. A third equation of the type is the Berry viscosity plot[11];

$$\left(\frac{[\eta]}{M^{1/2}}\right)^{1/2} = K_\theta^{1/2} + 0.42\,K_\theta^{1/2}\Phi B\frac{M}{[\eta]} \qquad (5.20)$$

A further modification of the FFS equation was used for the Stockmayer-Fixman equation[12], which is somewhat similar;

$$[\eta]/M^{1/2} = K_\theta + 0.51\Phi_0 BM^{1/2} \qquad (5.21)$$

or in a modified form;

$$[\eta]/M^{1/2} = 1.05K_\theta + 0.287\,\Phi_0 BM^{1/2} \qquad (5.22)$$

(5.21) is valid over the range $0<\alpha^3<2.5$

But these are still found to be erroneous in cases of high molecular weight polymers in good solvents, and will lead to an overestimation of K_θ if high molecular weight data is used. Among equations proposed to overcome this deficiency of the KS and SF equations is the Inagaki-Ptitsyn equation[13];

$$[\eta]^{4/5}/M^{2/5} = 0.786\,K^{4/5} + 0.454\,K^{2/15}\Phi_0^{2/3}B^{2/3}M^{1/3} \qquad (5.23)$$

This equation is applicable to extrapolation procedures using data from high molecular weight polymers in good solvents, in other cases equations (5.18)-(5.21) are to be preferred.

Ideally it would desirable that the molecular weights M of the data plotted in the two parameter plots be monodisperse, in reality this is rarely the case, and so the weight average value, M_w, as determined by light scattering is used.

The ratio $\langle r^2\rangle_o/M$ is obtained from K_θ *via* equation (13a), and from this the characteristic ratio C_∞, can be calculated from the relationship;

$$C_\infty = \left(\frac{\langle r^2\rangle_o}{M_w}\right)\frac{M_b}{l^2} \qquad (5.24)$$

where M_b is the mass per unit skeletal bond length l. The characteristic ratio is a comparative measure of the size of random coil chains, and in general may be regarded as a measure of chain stiffness, but will also be affected by the nature of the solvent[14].

The unperturbed value of $\langle r^2\rangle_o/M$ can be compared to the experimental value from light scattering measurements to calculate the expansion coefficient α.

The second parameter, B, determined from the two parameter plots, is a function of the binary cluster integral, β, and is related to the Flory-Huggins interaction parameter χ;

$$B = \left(\frac{v_2^2}{V_1 N_A}\right)(1-2\chi) \qquad (5.25)$$

where v_2^2 is the partial specific volume of the polymer and V_1 the volume fraction of the solvent.

A theoretical method for determining K_θ has been devised by Van Krevelen and Hoftyzerin[15]. This is an additive function, called the molar intrinsic viscosity function, defined as;

$$J = K_\theta^{1/2} M - 4.2Z \qquad (5.26)$$

where J is $\sum n \times J_{individual,}$, M is the molar mass of the repeat unit and Z is the number of chain atoms in the backbone.

Unit	$J_{individual}$
cyclohexane ring	8.0
phenyl ring	16.3
-OCOO-	27.5
$-CH_3$	3.55

Table 5.2: J values for molar intrinsic viscosity function.

This yields the following values for K_θ substituting cyclohexane ring for DHCD ring (not tabulated)

Percentage Aromatisation	K_θ /$cm^3.mol^{1/2}g^{-3/2}$
0	0.145
10	0.150
20	0.154
30	0.159

Table 5.3: Theoretical values of K_θ for partially aromatised poly(DHCD-DMC).

5.3 Intrinsic Viscosity Measurements

Intrinsic viscosity of the polymers in dilute solution were measured using the apparatus shown in fig.5.2. The aspirating apparatus on top was closed, having previously been flushed with dry nitrogen. in order to ensure that the NMP solvent did not absorb water. The whole apparatus was immersed in a glass-fronted water bath, thermostated to 25.00 ±0.05°C. A volume of solution was pipetted into the bulb, 5ml generally being the minimum amount, the run time for the solution is measured. The solutions, initially approximately 1%w/v were progressively diluted with fresh solvent, agitated by bubbling dry nitrogen through the system and shaking the apparatus, and reduced to four, three, two, and eventually to one fifth of the starting concentration.

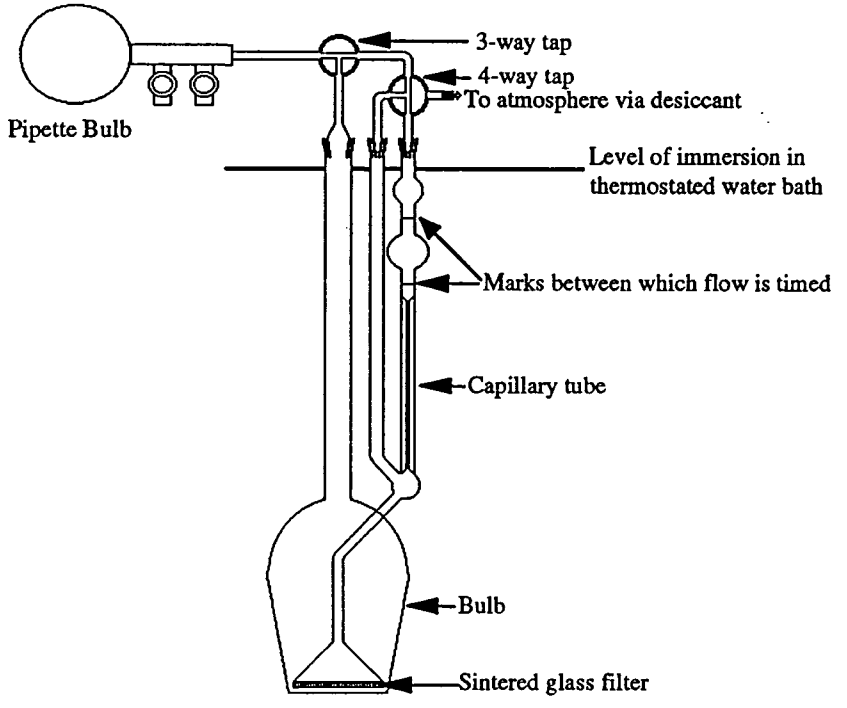

Figure 5.2: Viscometry measuring apparatus.

The run times were measured using a hand held electronic stopwatch measuring to one hundredth of a second. Readings were accepted when three consecutive reading are within 0.05 seconds of each other. These run times were analysed to extract [η] using the equations in table 5.1.

The values of η_{sp} were calculated and plotted against concentration, c, and extrapolated to c=0, the intercept being the intrinsic viscosity, [η]. Example plots are shown in figure 5.3

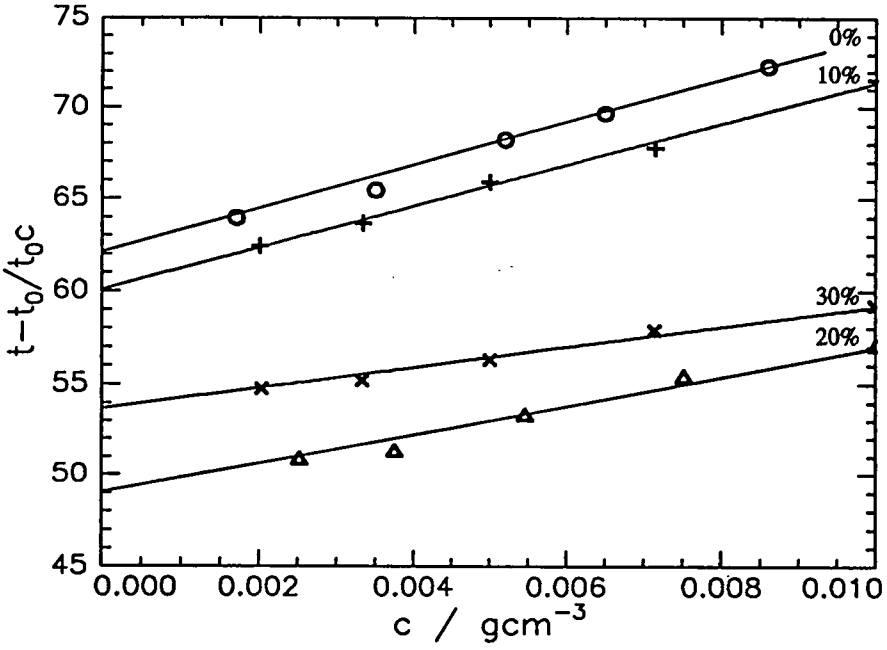

Figure 5.3: Examples of viscosity extrapolation plots for fraction B.

5.4 Results

A series of molecular weight fractions of polymer in solution in NMP were measured, over a range of aromatisation from 0 to 30%. The results are tabulated below.

Sample	0%	10%	20%	30%
	$[\eta]$ /ml g^{-1}	$[\eta]$ /ml g^{-1}	$[\eta]$ /ml g^{-1}	$[\eta]$ /ml g^{-1}
A	95.761	51.792	52.503	53.246
B	62.159	60.057	49.048	53.788
C	57.036	46.825	47.491	36.478
D	49.153	39.843	37.761	37.981
E	47.265	36.592	32.490	37.921
F	45.332	39.476	52.790	38.790
G	25.079	22.932	24.641	--
L	14.112	29.592	21.010	--
I	52.704	--	--	--
C'	52.310	--	--	--

Table 5.4 Intrinsic viscosities of partially aromatised poly(DHCD-DMC) in NMP

These results were combined with the corresponding values of M_w from light scattering to construct Mark-Houwink plots, Stockmayer-Fixman, Kurata-Stockmayer, and Berry two parameter plots, and Bohdaneckỳ persistence length plots.

5.4.1 Mark-Houwink Plots

0% Aromatised polymer

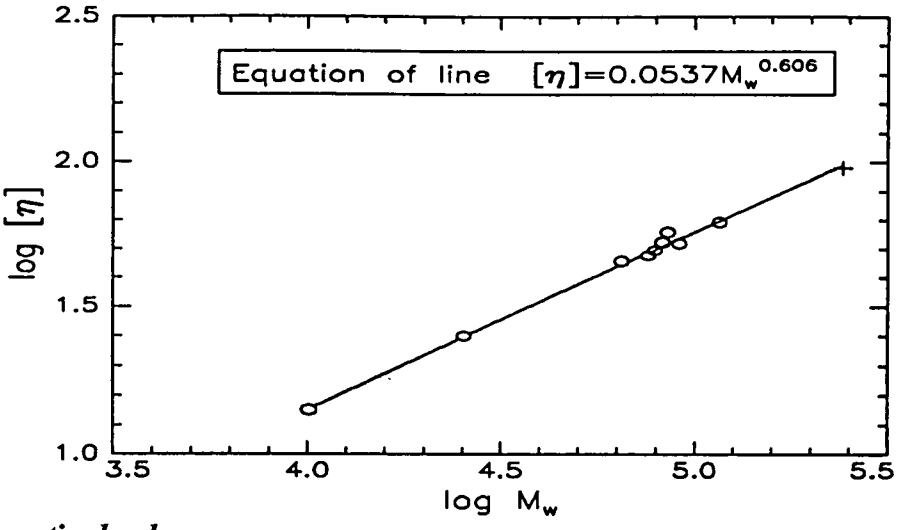

10% Aromatised polymer

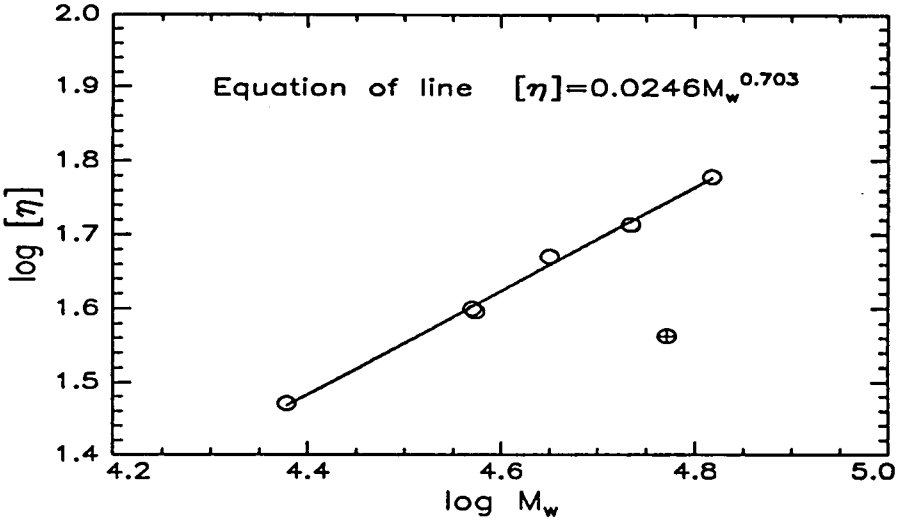

20% Aromatised polymer

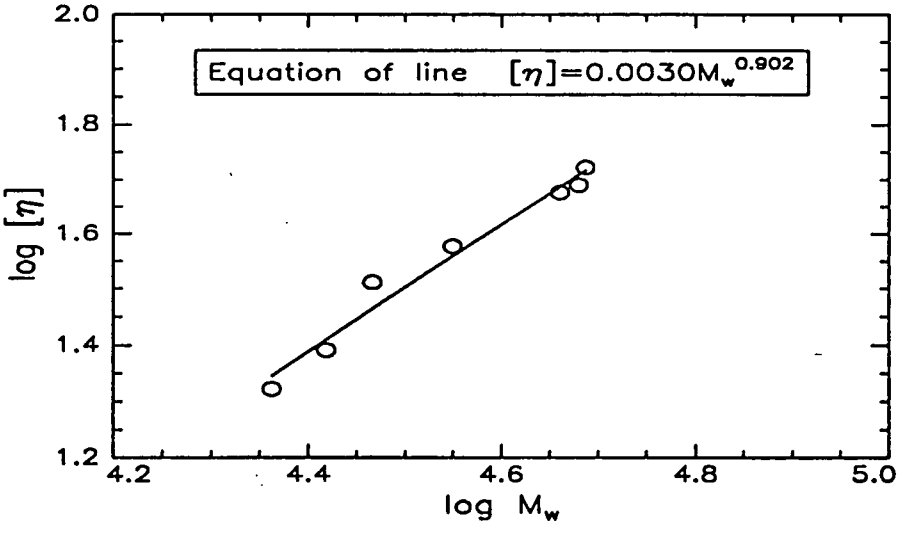

30% Aromatised polymer

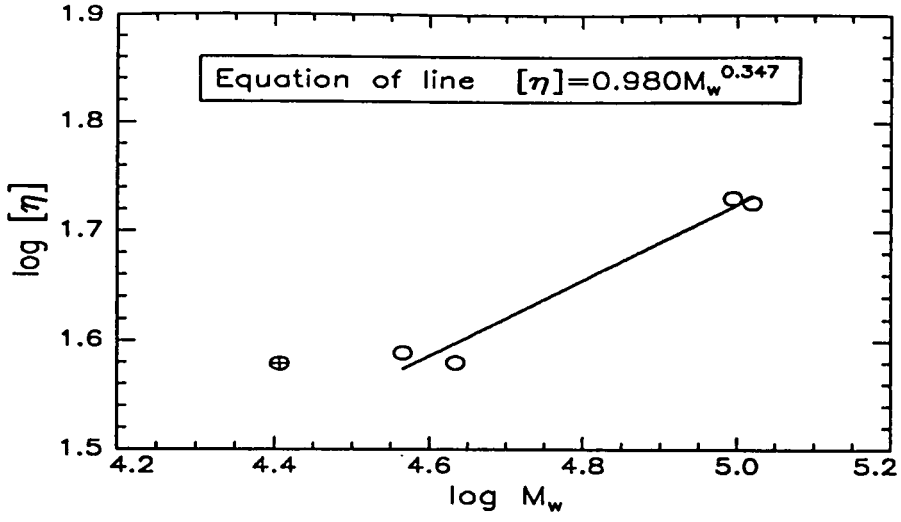

Figure 5.4: Plots of Mark-Houwink equation

Percentage aromatisation	K /ml g^{-1}	α
0	0.0537	0.606
10	0.0246	0.703
20	0.00022	1.145
30	0.980	0.347

Table 5.5 Summary of Mark-Houwink parameters

5.4.2 Two parameter plots

Results from Stockmayer-Fixman plots

0% Aromatised polymer

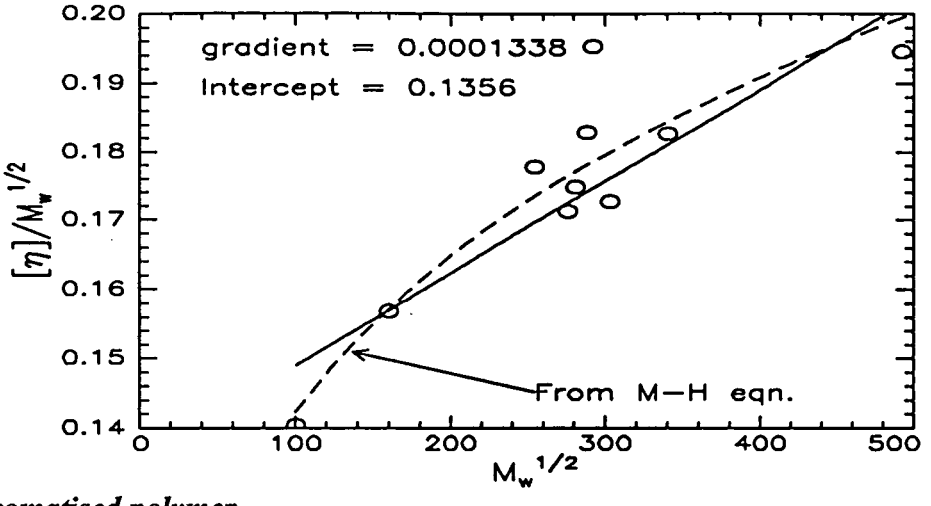

10% Aromatised polymer

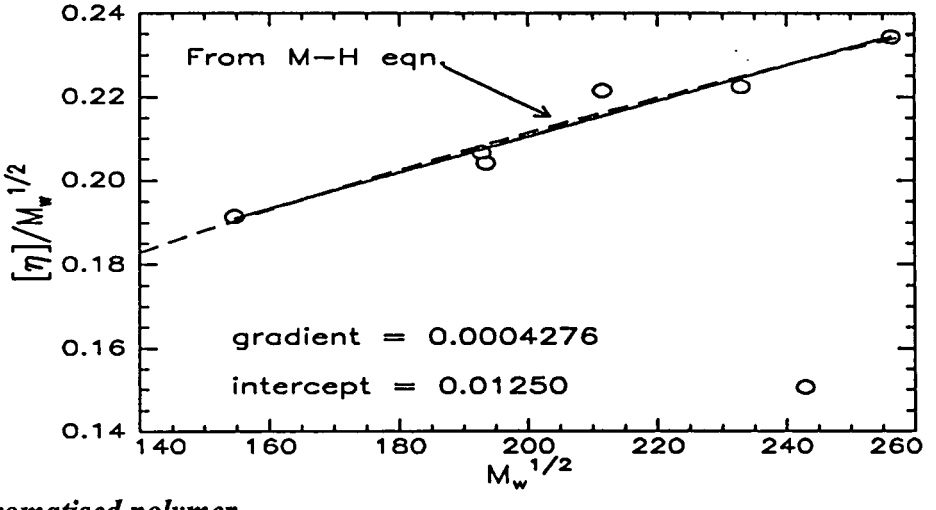

20% Aromatised polymer

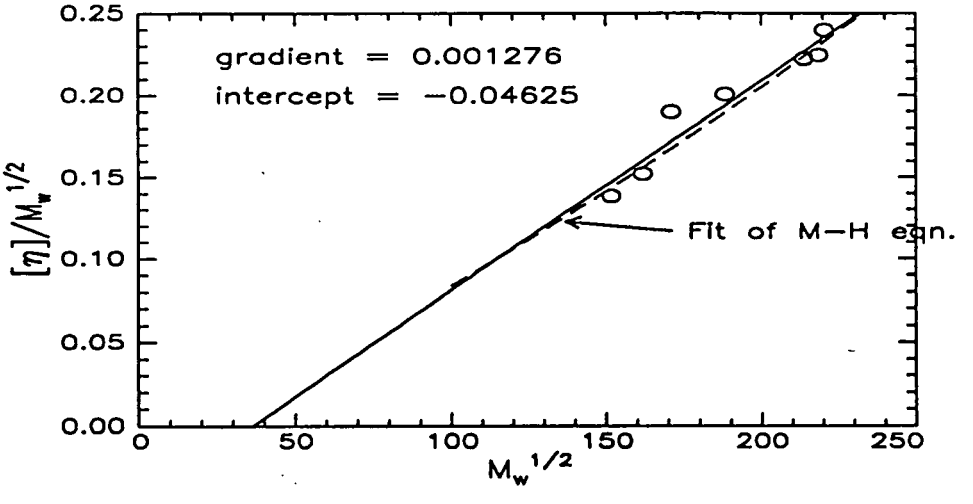

30% Aromatised polymer

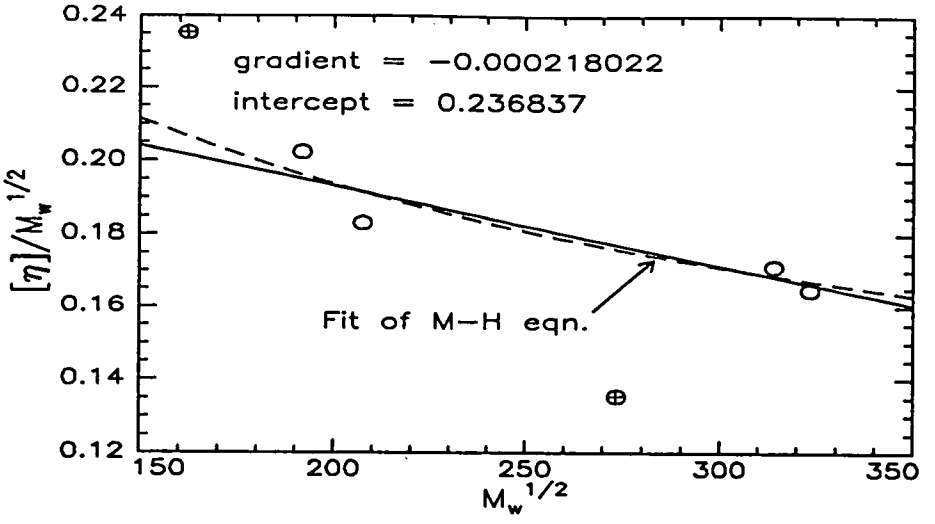

Figure 5.5: Stockmayer -Fixman plots

Results from Berry viscosity plots

0% Aromatised polymer

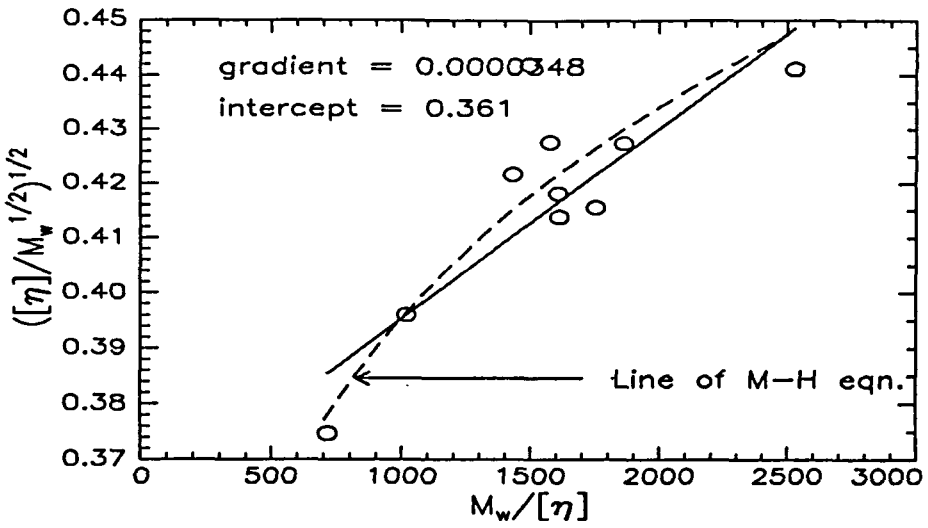

10% Aromatised polymer

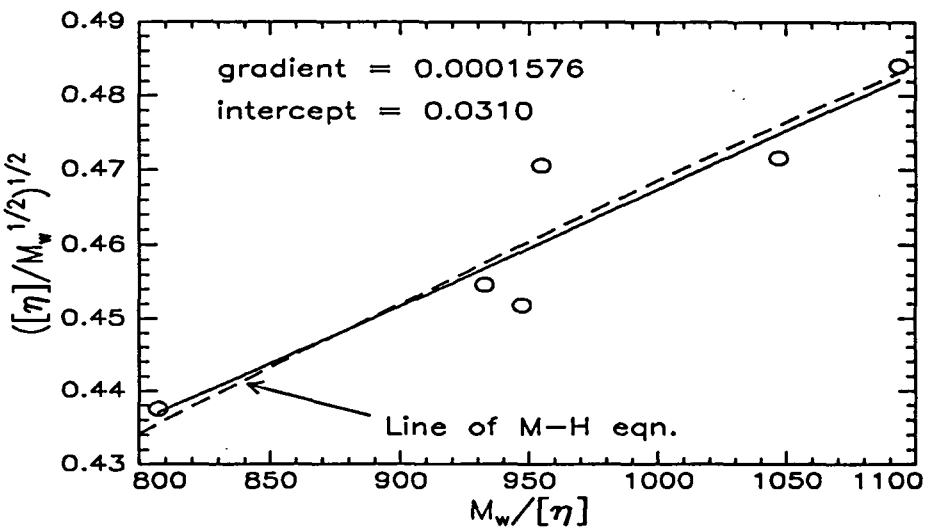

20% Aromatised polymer

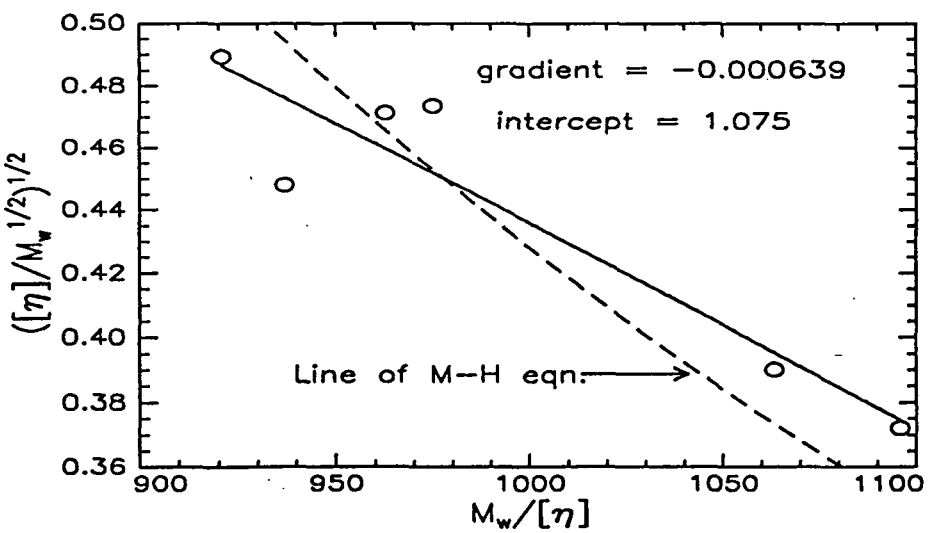

30% Aromatised polymer

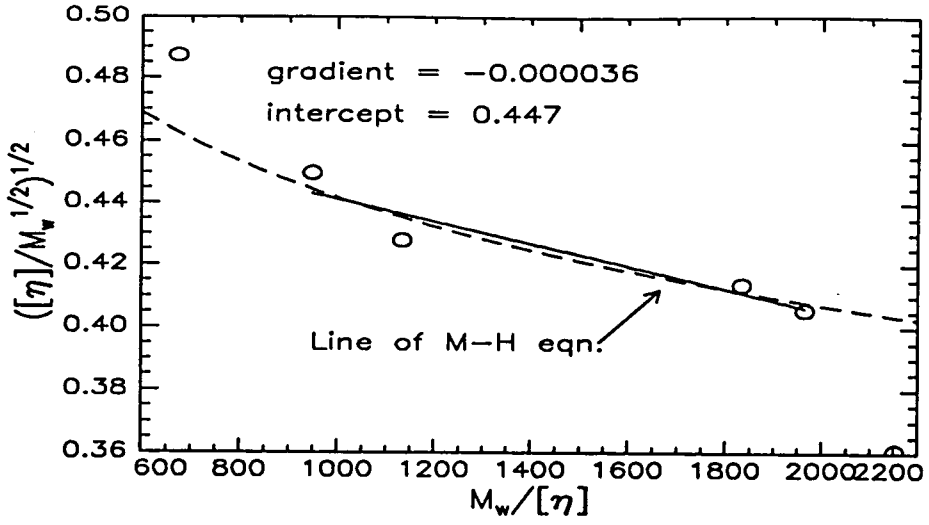

Figure 5.6: Berry viscosity plots

Results from Kurata-Stockmayer plots

Stage 1

0%

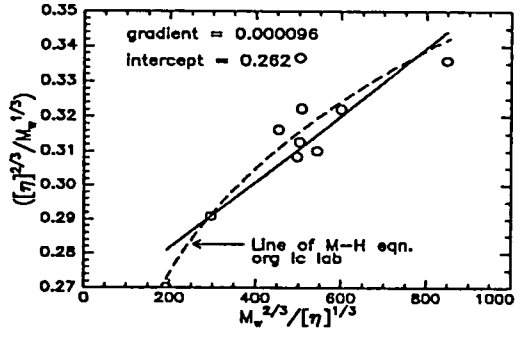

10%

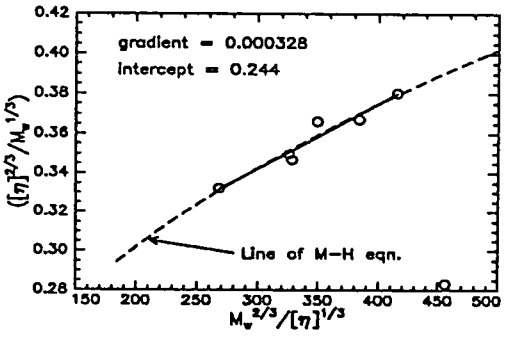

20%

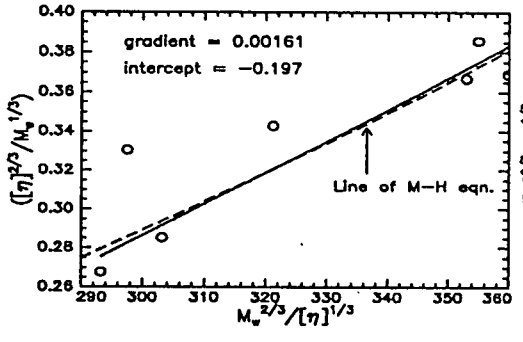

30%

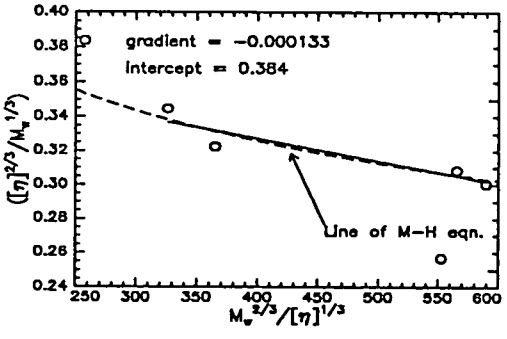

Stage 2

0% Aromatised

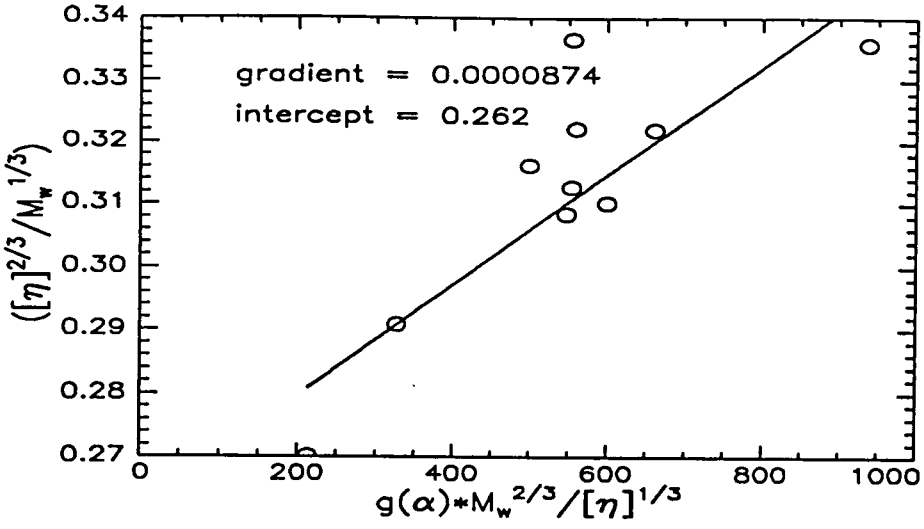

10% Aromatised

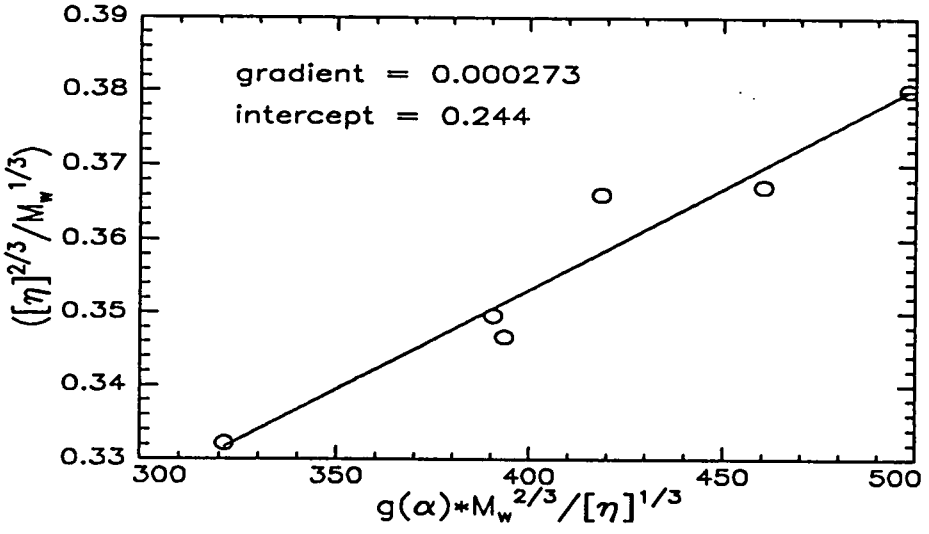

20% Aromatised

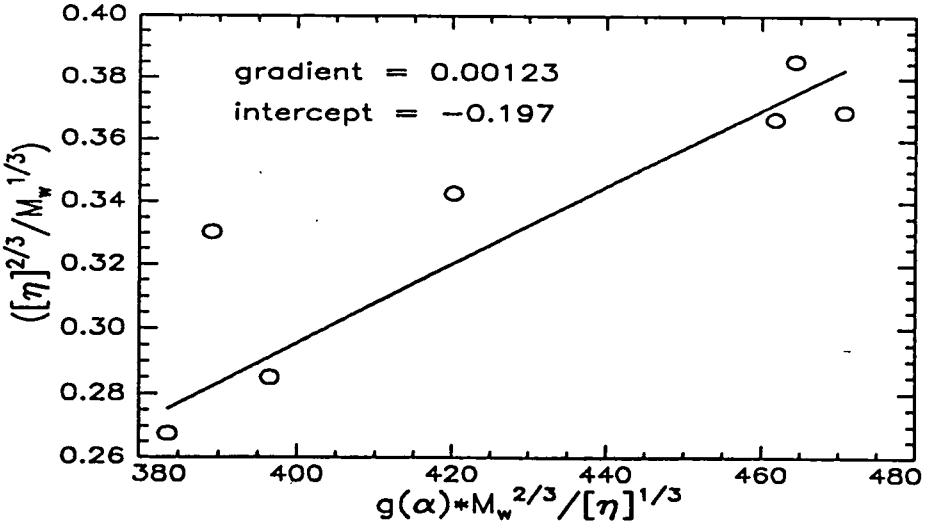

30% Aromatised

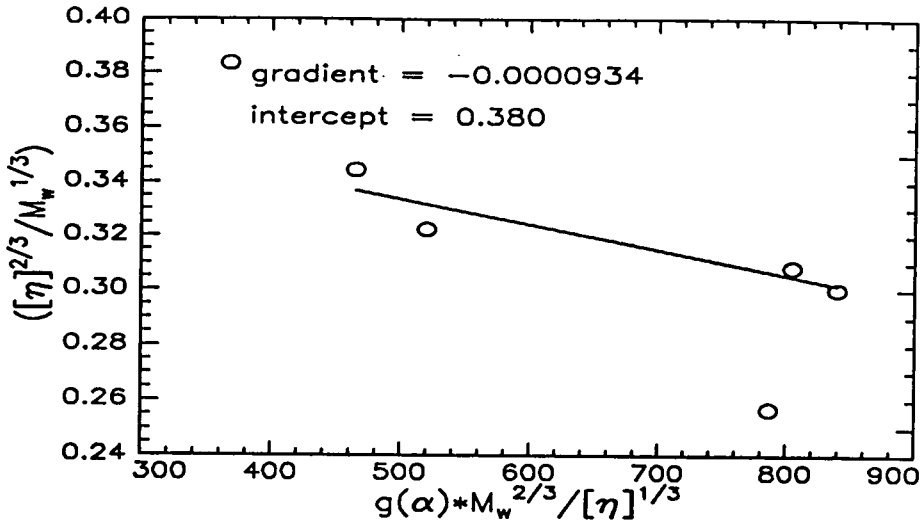

Figure 5.7: Kurata-Stockmayer plots

Results from two parameter plots

	K /ml g^{-1}	B /10^{-27} cm^3	($\langle r^2 \rangle / M_w$) /$10^{-17} cm^2$ g^{-1}	α
SF	0.136	1.05	6.651	---
MSF	0.129	1.86	6.433	---
KS	0.134	0.96	6.598	1.16
Berry	0.130	0.63	6.466	---

Table 5.6: Unaromatised polymer.

	K /ml g^{-1}	B /10^{-27} cm^3	($\langle r^2 \rangle / M_w$) /$10^{-17} cm^2$ g^{-1}	α
SF	0.125	3.35	6.300	---
MSF	0.119	5.96	6.096	---
KS	0.134	3.01	6.164	1.35
Berry	0.130	3.29	5.287	---

Table 5.7: 10% aromatised polymer.

	K /ml g^{-1}	B /10^{-27} cm^3	($\langle r^2 \rangle / M_w$) /$10^{-17} cm^2$ g^{-1}	α
SF	-0.046*	10.01	3.249	---
MSF	---	---	---	---
KS	-0.087*	13.55	4.948	1.70
Berry	1.156	-0.39*	27.75	---

**it is physically impossible for these values to have negative values, therefore fitting to these equations is invalid*

**a negative value of B must be due to a positive value of $\chi \geq 0.5$ (25)*

Table 5.8: 20% aromatised polymer.

	K /ml g^{-1}	B /10^{-27} cm^3	($\langle r^2 \rangle / M_w$) /$10^{-17} cm^2$ g^{-1}	α
SF	0.237	-1.71	9.650	
MSF	0.226	-3.04	9.341	
KS	0.234	-1.03	9.569	0.807
Berry	0.200	-0.052	8.618	

Table 5.9: 30% aromatised polymer.

Percentage aromatisation	C_∞
0	6.38
10	5.67
20	23.78
30	7.58

Table 5.10: Calculated values of characteristic ratio for poly(DHCD-DMC)

5.4.3 Determination of Persistence Length; Bohdanecký plots

In section (1.2.4d) equations (47)-(52) describe the Bohdanecký method for determining persistence length from intrinsic viscosity. A plot is constructed of $(M_w^2/[\eta])^{1/3}$ vs $M_w^{1/2}$, The gradient is B_m and the intercept A_m, which obey the relations;

$$A_\eta = \frac{A_0 M_L}{\Phi_\infty^{1/3}} \qquad B_\eta = \frac{1.05}{\Phi_\infty^{1/3}}\left(\frac{2}{M_L}\right)^{-1/2}$$

Also

$$\frac{d_r^2}{A_0} = \frac{4\Phi_\infty}{1.215\,\pi N_A}\left(\frac{\bar{\nu}B_\eta^4}{A_\eta}\right)$$

and

$$\log\frac{d_r^2}{A_0} = 0.173 + 2.158\log d_r \qquad d_r \le 0.1$$

$$0.795 + 2.78\log d_r \qquad 0.1 \le d_r \le 0.4$$

where $d_r = d/(\lambda^{-1})$ d = chain diameter

Plots have been constructed using the viscometry data determined in this study to extract the three parameters, a, M and dr

Bohdanecký plots

Unaromatised polymer

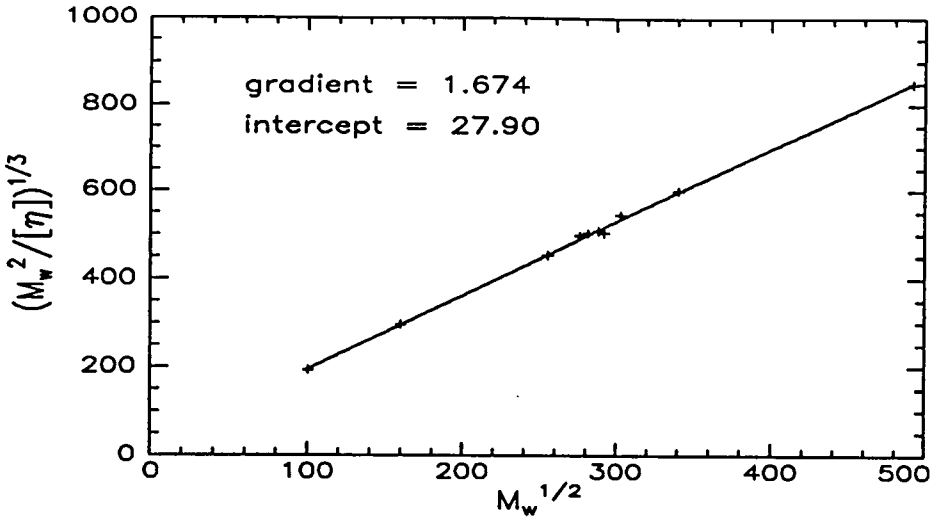

10% aromatised polymer

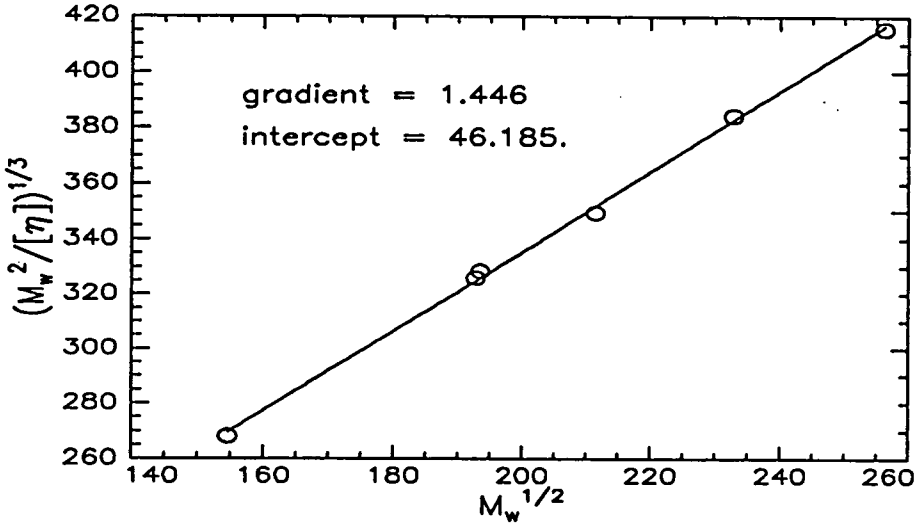

20% aromatised polymer

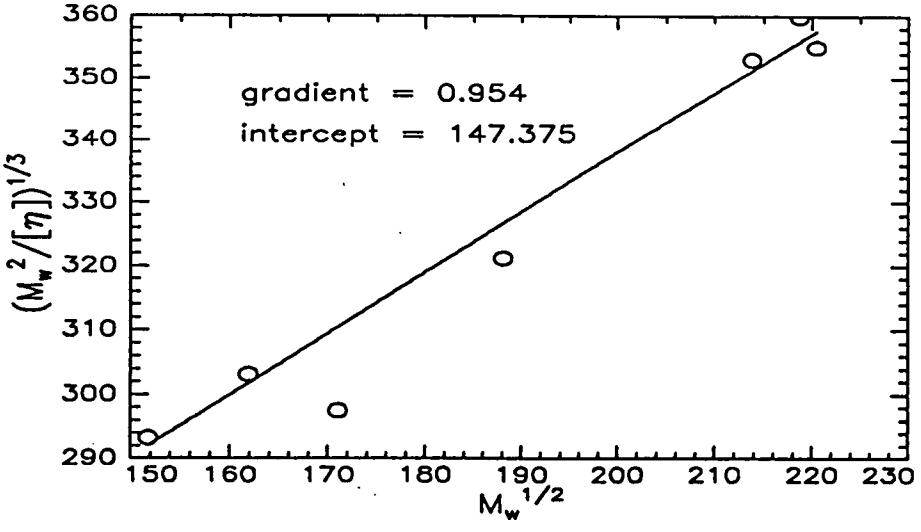

30% aromatised polymer

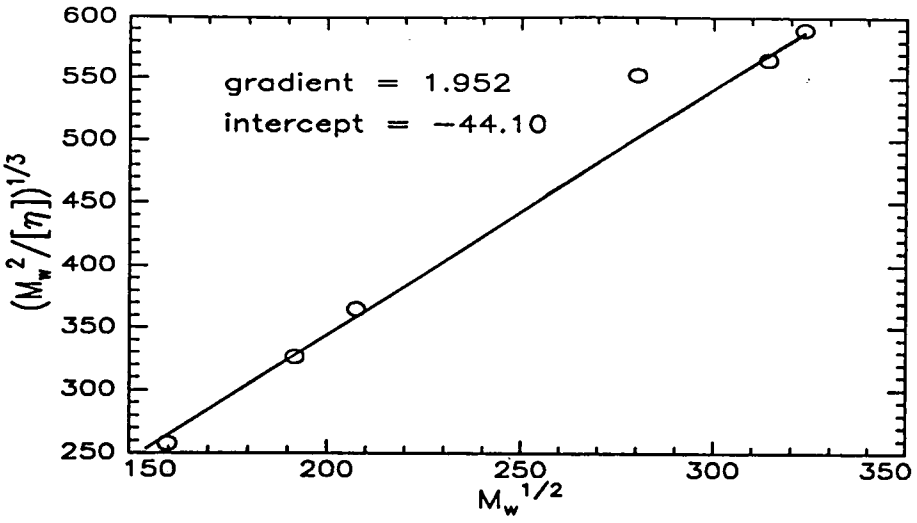

Figure 5.8: Bohdanecký plots

Percentage aromatisation	a /Å	$M_{l.}$ g/Å	monomer length /Å	d /Å
0	20.7	41.7	5.4	12
10	27.1	40.8	5.2	10
20	127	51.5	3.8	9
30	-----	----	----	----

Table 5.11: Results of Bohdanecký plots

5.5 Discussion

The results from viscometry follow the pattern of those from SEC and ILS. The unaromatised polymer in NMP has the properties of a typical random coil molecule, the Mark-Houwink coefficient, α, is quite low at 0.606, and suggests a random coil polymer in only a moderately good solvent. The characteristic ratio, C_∞, is characteristic of a typical random coil molecule, its value of 6.4 compares with that of 6.8[16] for syndio-PMMA, and 6.7[16] for polyethylene. The persistence length of the polymer at 20Å is also typical for a random coil. for comparison the value for syndio-PMMA is 33Å[16] and syndio-PS is 19Å[16] . There is only a slight change between 0 and 10%, but it does follow the trend of the coiled chain becoming more stiff. The Mark-Houwink coefficient increases from 0.6 to 0.7, this being more likely due to the chain stiffening rather than an improvement in the solvent quality, A_2 from light scattering remains about the same(section 4.4), the introduction of phenyl nuclei in the chain should decrease the solubility while increasing it's rigidity, this is borne out by the increase in the persistence length from 21 to 27Å. There is a slight accompanying decrease in the contour length per monomer segment, M_L, from 5.4 to 5.2Å, this might also be expected, shorter phenyl groups incorporated into the chain are bound to slightly decrease the average monomer length. There is a decrease in characteristic ratio accompanying a decrease in the unperturbed dimensions, which is the opposite to that which would be expected, and is at odds with the Kurata plot using ILS data where a significant increase in C_∞ is seen. The reasons for this are not clear, but may be due to the methods having different sensitivities to different species in the solution or to a solvent effect.

There is a pronounced difference in properties between 10 and 20% aromatisation. A sharp increase is seen in the Mark-Houwink coefficient α, which increases to 1.145, now characteristic of a wormlike rather than a flexible chain. This is accompanied by an increase in persistence length to 127Å, which is at the lower limit of typical stiff chains. The high values of the Mark-Houwink coefficient for the stiff chain may be due in some part at least to the limited low molecular weight range, 20-50 $\times 10^3$, over which the data

has been collected. If a wider range of M_w had been available a change in the gradient to that of a random coil, may have been seen. This was not possible because of the chain scission concomitant with the aromatisation reaction. The effect of using a low molecular weight range is clearly observed in the study on PHIC by Murakami et al[17] where for a polymer of a = 420Å a transition is observed from $\alpha = 1.2$ at low molecular weight to $\alpha = 0.77$ at high molecular weight, with a transition at $M_w \approx 600 \times 10^3$. If this effect were to scale proportionally with persistence length, eg in this study at 1/3.5th at that of Murakami et al, then this transition should occur at 170×10^3, above the upper limit of the polymer available. This transition point for stiff chain polymers may also explain the breakdown of the two parameter theory for the 20% aromatised polymer, figure 5.9, where the plots show either a negative intercept or a negative gradient, If the data of Murakami *et al* is plotted as the SF and Berry plot then two regions of behaviour can be observed. The transition point can again clearly be seen, evidenced by the change in slope, and the reversal of the slope in the SF and Berry plots respectively. This transition may be regarded as a change from rod behaviour at low molecular weight to coil behaviour at high molecular weight. At a critical point the chain contains sufficient Kuhn lengths to follow a random path and random coil behaviour similar to that of flexible polymers is now observed. If the transition for PHIC is $M_w = 600{,}000$ the critical number of Kuhn lengths is ten. The critical molecular weight for 20% aromatised poly(DHCD-DMC)(λ^{-1}=250Å) is therefore 130,000. Comparison of the plots of PHIC with those of 20% aromatised poly(DHCD-DMC) show quite clearly that the polymer available is below the critical weight and lies in the rod rather than the coil region. The effect of the aromatisation reaction means it is unlikely that high molecular weight material could be made, and therefore the unperturbed dimensions cannot be determined by viscometric methods. The value for C_∞ given for 20% aromatised polymer is that from the Berry plot which is the only plot which gave a logical value for K, The parameter B was negative, this may indicate a positive value of χ, but it is more likely that the data is invalid.

There are further changes to the system evident at 30% aromatisation, the Mark-Houwink coefficient has now fallen below 0.5, the value for the theta condition, and evidently the polymer no longer exists as either a wormlike or random coil species.

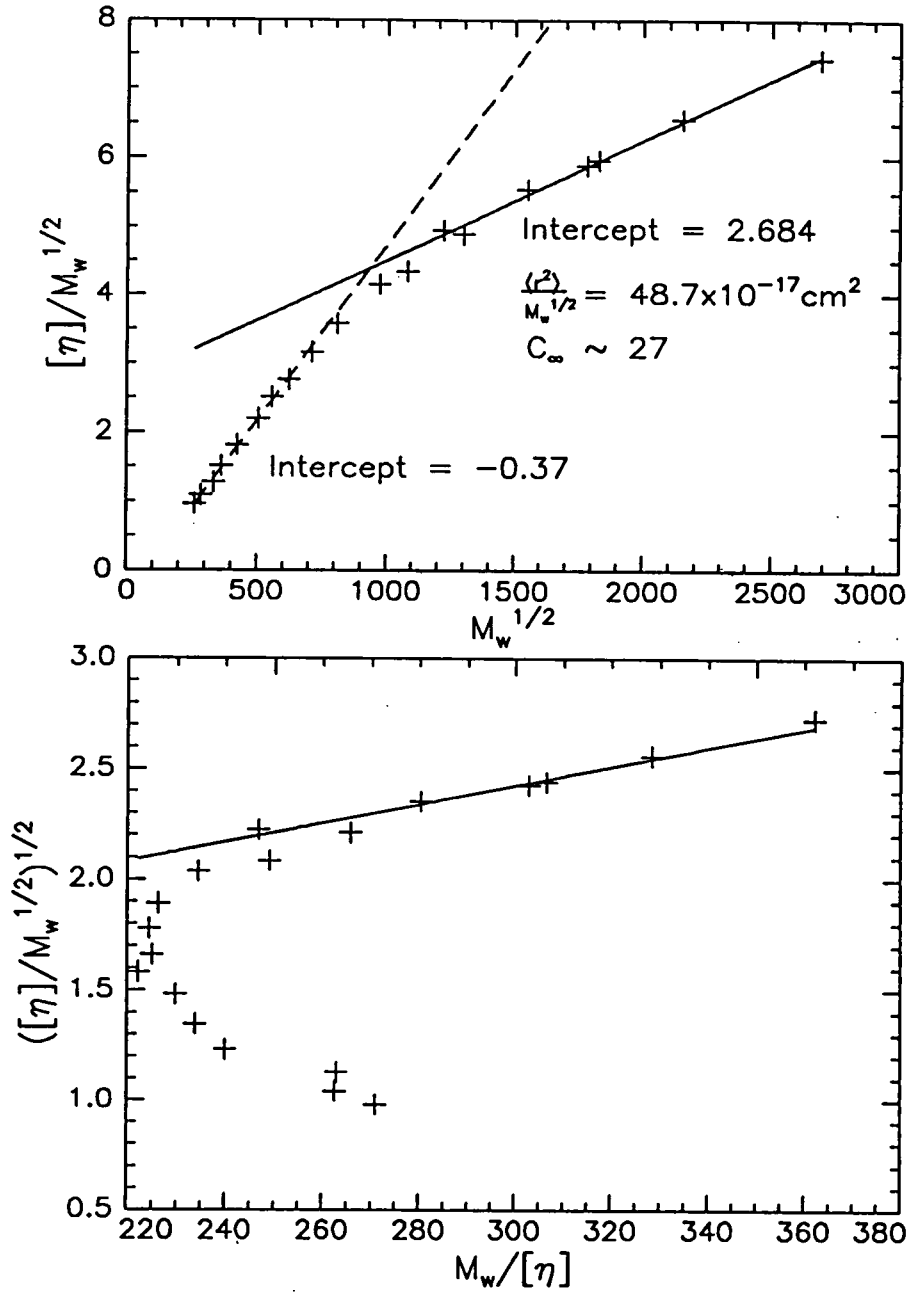

Figure 5.9: Stockmayer-Fixman and Berry plots of poly(hexyl isocyanate) in hexane, data of Murakami *et al*[17].

Literature values for α less than 0.5 are given for branched and block copolymers[18], the latter of which are susceptible to aggregation in selective solvents forming micelle like structures. Aggregation is the cause for low α in this case, light scattering measurements

show an increase in M_w at 30% over that at 20% when the aromatisation reaction should cause it to fall. Aggregates of the fringed micelle type as suggested in (3.5) will be of a more compact form, and hence will have lower viscosities.

The appearance of an aggregated species again brings into question the validity of the two parameter plots which have been derived on the basis of single chains in solution at 30% aromatisation, hence the results obtained should be treated with caution, and no result could be extracted from the Bohdanecky plot at 30%, again an equation which assumes single chain species. If the two parameter plots for this data are valid for 30% aromatised polymer the values of B are negative, and again the Flory-Huggins interaction parameter is large and positive ($\chi \geq 0.5$).

The sharp fall in α indicates that one of the techniques used to determine the data plotted is very sensitive to the presence of the high molecular weight species, viscometry is reported to be relatively insensitive to the presence of a small proportion of polymer at high molecular weight[19] so the light scattering technique must be responsible, indeed it is M_w which shows the more significant increase, not $[\eta]$. Aromatised polymer chains may also be subject to intramolecular aggregation if the chain contains more than one aromatised block, and these molecules being more compact than non-aggregated chains would reduce intrinsic viscosity without unduly affecting the measured value of M_w further pushing down α.

In conclusion the viscometric results show that poly(DHCD-DMC) is a typical randomly coiled polymer in the unaromatised state and at 10% aromatisation. Experimentally derived parameters, persistence length and Mark-Houwink coefficient α suggest some stiffening between 0 and 10% conversion, and further, more significant stiffening between 10 and 20% reaction, so that the polymer now behaves as a semiflexible wormlike chain rather than a random coil, at least over the weight range studied.

At 30% reaction the polymer was subject to some degree of aggregation, which caused a reduction in the M-H coefficient as the polymer became more compact. Determination of unperturbed dimensions was only possible in the case of polymer solutions obeying random coil behaviour, those at 0 and 10% aromatisation.

5.6 References

1, Huggins,M.L.,*J.Phys.Chem.*,**42**,911,(1938).

2, Houwink,R.,*J.Prakt.Chem.*,**157**,15,(1940).

3, Einstein,A.,*Ann.Phys.*,[4],**34**,591,(1911).

4, Taylor,G.I.,*Proc.Roy.Soc*,**A138**,41,(1932).

5, Kirkwood,J.G.,Riseman,J.,*J.Chem.Phys.*,**16**,565,(1948).

6, Auer,P.L,Gardner,C.S.,*J.Chem.Phys.*,**23**,1549,(1955).

7, Konishi,T.,Yamakawa,H.,Yoshizaki,T.,*Macromolecules*,**24**,5614,(1991).

8, Yamakawa,H.,'*Modern Theory of Polymer Solutions*',Harper and Row,New York,1971.

9, Flory,P.J.,Fox,T.G.,*J.Am.Chem.Soc.*,**73**,1904,(1951).

10, Kurata,M.,Stockmayer,W.H.,*Fortschr.Hochpolymer.Forsch.*,**3**,196, (1963).

11, Berry,G.C.,*J.Chem.Phys.*,**46**,1338,(1967).

12, Fixman,M.,Stockmayer,W.H.,*J.Polym.Sci.*,**C1**,137,(1963).

13, Inagaki,H.,Kurata,M.,Suzuki,H.,*J.Polym.Sci*,**C15**,409,(1966).

14, Flory,P.J.,'*Statistical Mechanics of Chain Molecules*',Wiley Interscience,New York,1969.

15, Hoftyzer,P.J.,Van Krevelan,D.W.,'*Properties of Polymers*', Elsevier,Amsterdam,1991.

16, Yamakawa,H.,*Ann.Rev.Phys.Chem.*,**35**,23,(1984).

17, Fujita,H.,Murakami,H.,Norisuye,T., ,*Macromolecules*,**13**,345,(1980).

18, Iwama,M.,Kamada.K.,Kurata,M.,Tsunashima,Y.,Ch IV in '*Plastics Handbook*',Ed Brandrup,J.,Immergut,E.H.,Wiley ,New York,1974.

19, Cotts,P.M.,Paul,C.W.,*Macromolecules*,**19**,692,(1986).

CHAPTER 6

QUASI-ELASTIC LIGHT SCATTERING

6.1 Introduction

Quasi-elastic light scattering (QELS), like intensity light scattering, involves the study of macromolecules in solution by measurement of the scattered light. The technique however is technologically more intense, and introduces a time element into the measurement, so that molecular motion can be determined. The technique is also known as photon correlation spectroscopy or dynamic light scattering.

6.2 Theoretical considerations

As discussed in chapter 4 a solution of particles will cause light to be scattered. The occurrence of random changes in concentration was also briefly touched upon, and these lead to the Debye equation for time averaged scattering. QELS allows a treatment of the dynamic behaviour of the light scattered by the fluctuating concentration to characterise the behaviour of the scattering particles.

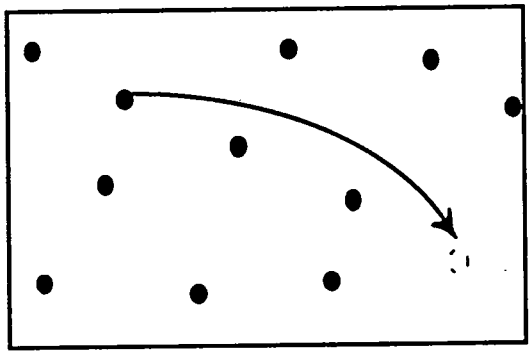

Figure 6.1: Schematic representation of Brownian motion.

A normal solution of polymer is homogenous on the macroscopic scale as it is thermodynamically unfavourable for solute to concentrate in one vicinity in the absence of exterior forces. However on the microscopic scale homogeneity is not to be implied. Brownian motion causes the random movement of the solute particles, so that if a particle in one location moves, as in fig.6.1, it is by no means certain that a second particle will take it's place, and a concentration gradient is the result. Brownian motion is

a random, thermally induced process which cannot be mathematically described. However the overall process may be approximated by the Onsager regression hypothesis, that is the particles in a solution are aware of their position, but do not know how they came to be there. Random thermal motion therefore has a similar effect to externally induced motion, and concentration gradients resulting must similarly relax. Induced concentration gradients are known to relax according to Ficks law;

$$J_i = D_i(dc_i/dx) \tag{6.1}$$

Where the flux J_i of a species i through unit area of concentration gradient dc_i/dx has the diffusion coefficient D_i. So it is assumed the same behaviour will be observed for random thermal motion. For a solution at scattering vector Q the fluctuation can be described in terms of the diffusion coefficient;

$$c_Q(t) = c_Q(0)e^{-DQ^2t} \tag{6.2}$$

Where c_Q is the amplitude of the Q'th spatial Fourier component of the concentration, that is the concentration fluctuation will decay to the time weighted average value with an exponential decay, with decay constant $2DQ^2$.

As seen in chapter 5 when a beam of coherent, polarised light interacts with a particle of size $>\lambda/20$ scattered light from different parts of the particle may reach the observer after having travelled different pathlengths, so they will be out of phase, resulting in interference, and an angular dependence on intensity is introduced. If the particle being observed is in motion then there will also be a time dependence, and at a fixed angle the intensity will be seen to fluctuate. Because the movement of the molecule causes the concentration fluctuation, which in turn leads to, and is directly proportional to the intensity fluctuation then c_Q can be replaced with I_Q and the intensity fluctuation decays with decay constant $2DQ^2$.

A typical profile of intensity with time for a polymer solution around a time weighted average, $\langle I \rangle$ is shown in figure 2.

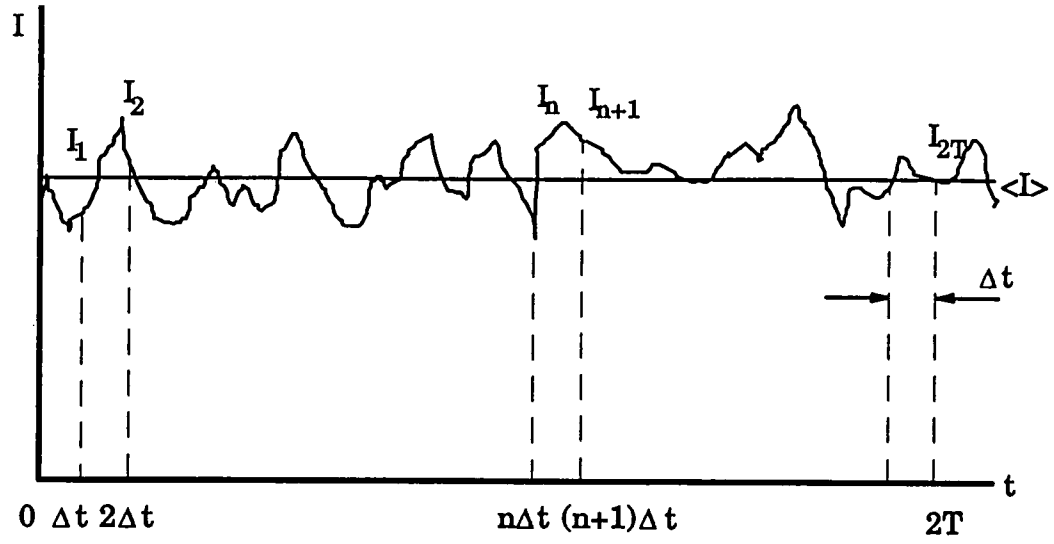

Figure 6.2: Typical light intensity fluctuations from polymer solution.

Suppose the intensity is sampled at discrete periods of Δt up to time 2T. The time weighted average $\langle I \rangle$ will be given by;

$$\langle I \rangle = \lim_{T\to\infty} \frac{1}{2T}\int_{-T}^{T} I(t).dt \qquad (6.3)$$

2T and 0 are replaced by T and -T for the sake of normalisation. At this point we introduce the intensity-intensity autocorrelation function, $G^2(\tau)$, $=\langle I(t)I(t+\tau)\rangle$, where τ =time between two given measurements. We then have;

$$G^{(2)}(\tau) = \lim_{t\to\infty} \frac{1}{2T}\int_{-T}^{T} I(t)I(t+\tau).dt \qquad (6.4)$$

The correlation function may be considered as a mathematical representation of the time for a particular fluctuation to decay to the average. For a random process without a time dependence the correlation function is independent of t.

At $\tau=0$, $\langle I(t+\tau)I(t)\rangle$ becomes $\langle |I(t)| \rangle^2$

$\tau=\infty$, $\langle I(t+\tau)I(t)\rangle$ becomes $\langle I\rangle^2$

The autocorrelation function decays from $\langle |I(t)| \rangle^2$ to $\langle I\rangle^2$ as $\tau\to\infty$.

The autocorrelation function, $G^2(\tau)$, is the unnormalised form of the second order intensity correlation function, $g^2(\tau)$. The frequency broadening giving rise to the power spectrum is caused by the random motion of the particle acting as an oscillating dipole, which gives a distribution of frequencies around a point ω_0. The broadening due to be completely random motion will be symmetrical (fig. 6.3).

The first order field correlation function is related to the second order intensity correlation function, $g^2(\tau)$, by the Siegert equation;

$$g^{(2)}(\tau) = 1 + \left|g^{(1)}(\tau)\right|^2 \tag{6.5}$$

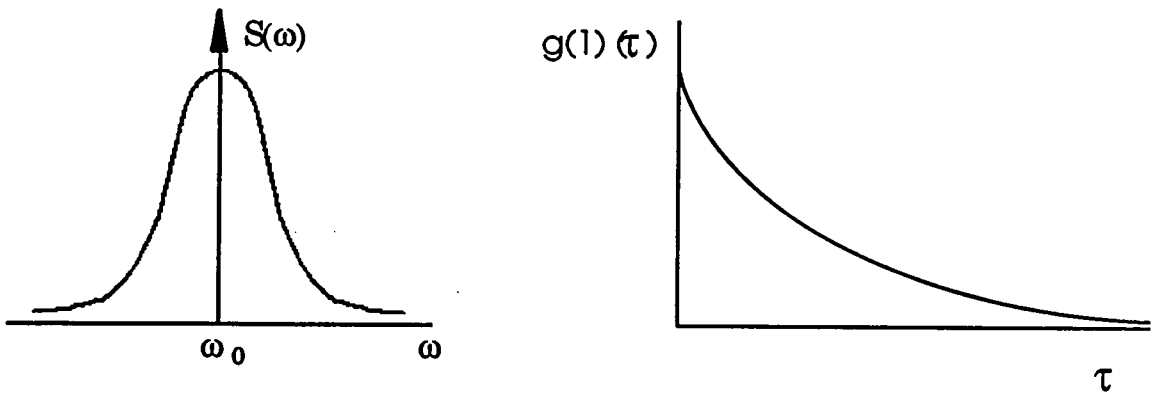

Figure 6.3: Optical spectrum of scattered light with associated electric field correlation function.

$g^1(\tau)$ is the Fourier transform of the field autocorrelation function, $G^{(1)}(\tau)$. These four functions are given below;

$$g^{(1)}(\tau) = \frac{1}{2\pi}\int_{-\infty}^{\infty} G^{(1)}(\tau)e^{-I\omega\tau}.d\tau \tag{6.6}$$

$$g^{(2)}(\tau) = \frac{1}{2\pi}\int_{-\infty}^{\infty} G^{(2)}(\tau)e^{-I\omega\tau}.d\tau \tag{6.7}$$

$$G^{(1)}(\tau) = \langle E_s(t)E_s(t+\tau)\rangle \tag{6.8}$$

$$G^{(2)}(\tau) = \langle I(t)I(t+\tau)\rangle \tag{6.9}$$

Where the scattered intensity ,I_s ,is a function of the scattered electric field, E_s ;

$$i_s = \langle |E_s|^2 \rangle \tag{6.10}$$

Equations 6-9 can be related by the expressions;

$$g^{(1)}(\tau) = G^{(1)}(\tau)/G^{(1)}(0) \tag{6.11}$$

$$g^{(2)}(\tau) = G^{(1)}(\tau)/G^{(1)}(0)^2 \tag{6.12}$$

6.3 Measurement of diffusion coefficient from QELS

In homodyne QELS the continuous signal from the detector is fed into a digital correlator, which measures an experimental correlation function, $G_E^{(2)}(\tau)$, and from this $g_E^{(2)}(\tau)$. The experimental $g_E^{(2)}(\tau)$ is related to $g^{(1)}(\tau)$ by a modified Seigert equation;

$$g_E^{(2)}(\tau) = B\left[1+\left|g^{(1)}(\tau)\right|^2\right] \tag{6.13}$$

For a monodisperse solution of polymers diffusion theory[1] gives;

$$g^{(1)}(\tau) = be^{(-2Q^2Dt)} \tag{6.14}$$

where b is a geometric factor dependant on detector area, and is typically ≈ 0.6. This is similar in form to (6.2), and relates the optical spectrum to the diffusion coefficient. Equation (6.14) gives;

$$g_E^{(2)}(\tau) = B\left[1+be^{(-2DQ^2t)}\right] \equiv B\left[1+be^{-\Gamma t}\right] \tag{6.15}$$

where $\Gamma = 2DQ^2$. Hence it becomes possible to determine diffusion coefficient from the spectrum of the scattered light.

A further useful quantity that may be determined from QELS is the hydrodynamic radius, R_h, that is the radius of a hypothetical impenetrable sphere having the same frictional effect in a hydrodynamic field as the polymer molecule. Hydrodynamic radius is calculated from the diffusion coefficient using the Stokes-Einstein equation;

$$R_h = \frac{kT}{6\pi\eta D} \tag{6.16}$$

where k is the Boltzmann constant, T is absolute temperature, η is the viscosity of the solvent, D the diffusion coefficient.

Hydrodynamic radius differs in definition and generally in value from the radius of gyration, and the ratio of the two, $\rho=\langle s^2\rangle^{1/2}/R_h$, affords some information to the structure of the scattering species.

6.4 Experimental determination of diffusion coefficient

There are two basic techniques in QELS, homodyne and heterodyne, the former involves simply the measurement of the scattered light from a solution and is used to measure $G_E^{(2)}(\tau)$, the latter is a split beam technique which involves the recombination of the scattered light with an unscattered incident and measures $G_E^{(1)}(\tau)$. The technique used in this case is homodyne QELS and no further description of heterodyne QELS is necessary.

The instrument used for these measurements is the same as that used for ILS, and is shown in figure 6.4. Unlike ILS where the light source simply requires sufficient intensity to give a good count rate, QELS requires the coherent source of illumination from a laser source. The digital correlator and computer are also essential in order to process the signal, however geometry of the set-up is less critical than for ILS.

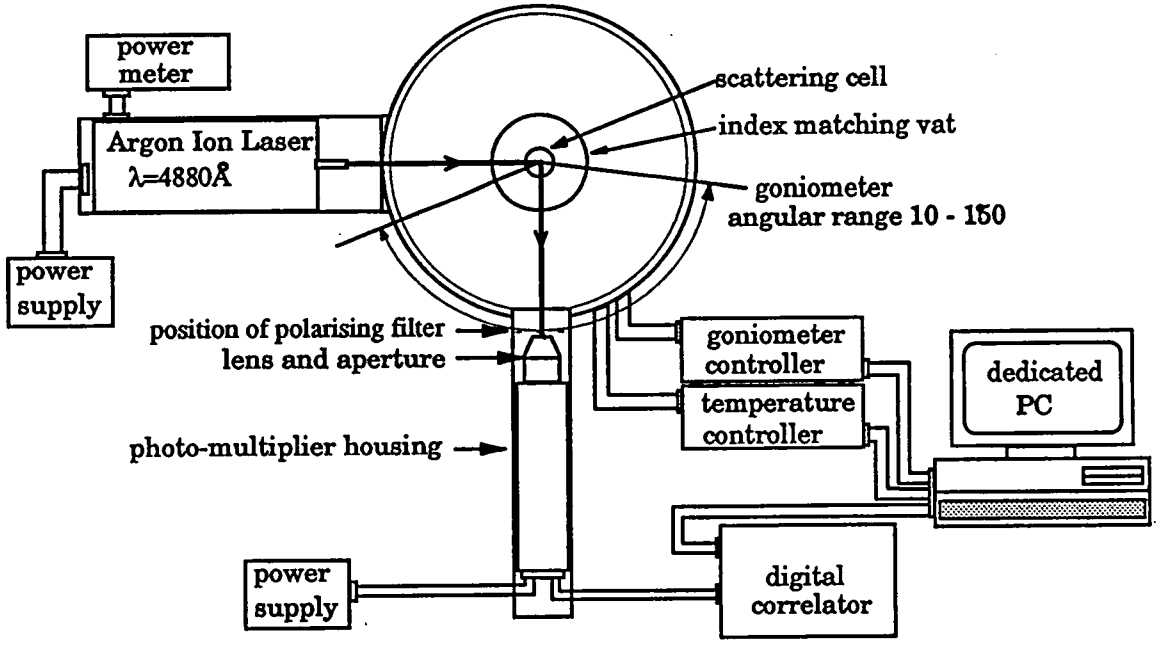

Figure 6.4: Instrumentation used for QELS measurements.

The inlet aperture was set to 150μm diameter, corresponding to one coherence area, as opposed to ILS where the aperture was set to maximum to gather as much scattered light as possible.

The scattering from dilute solutions was measured and the data obtained in the form of a correlation function $G_E^{(2)}(\tau)$(figure 6.5).

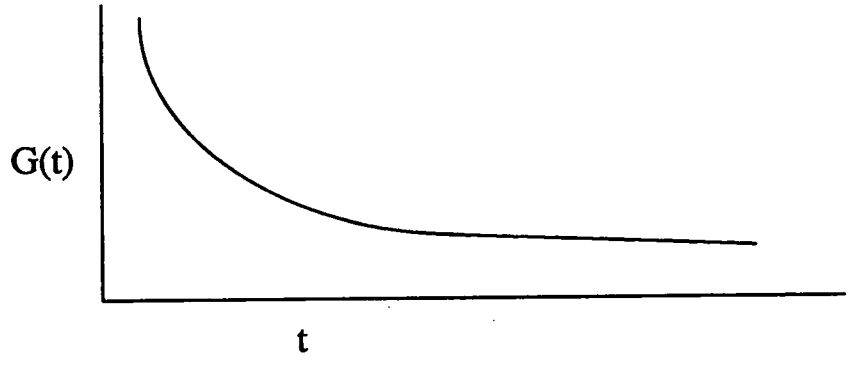

Figure 6.5: typical experimental correlation function.

To extract the diffusion coefficient it is necessary to fit equations to this function. The simplest method is to fit an exponential expression;

$$C(\tau) = Ae^{-\Gamma t} + B \qquad (6.17)$$

where $C(\tau)$ is the experimentally determined correlation function, B the background level, and A a constant. This method applies only to monodisperse polymers, which is rarely the experimental situation. A polydisperse sample produces a correlation function composed of a distribution of exponentials. Thus for $G^{(1)}(\tau)$ the expression is;

$$g^{(1)}(\tau) = \int G(\Gamma)\exp(-\Gamma t)d\Gamma \qquad (6.18)$$

where $G(\Gamma)$ is the distribution of decay rates. Equation (6.17) is in the form of a Laplace transform and in order to determine $G(\Gamma)$ it is necessary to invert the transform, this can produce problems, as the transform is mathematically ill conditioned, and very small changes in $G^{(1)}(\tau)$ can produce very large changes in $G(\Gamma)$. Therefore in order to analyse experimental data satisfactorily an approximate solution must be known so that the less likely solutions can be excluded. The analysis of $G(\Gamma)$ gives valuable data, not only on the value of the diffusion coefficient, D, but from the distribution of D it gives information on the polydispersity.

The method of cumulants[2] is a relatively straightforward method which extracts the z-average diffusion coefficient, D_z, and the second moment of $G(\Gamma)$, μ_2. A polynomial of

the second or possibly third order is fitted to the correlation function by a least squares fit;

$$\ln\left|g^{(1)}(\Gamma,t)\right| = A - \bar{\Gamma}t + \frac{\mu_2 t^2}{2} + \ldots \qquad (6.19)$$

where A is the background, $\bar{\Gamma}$ is $\int \Gamma G(\Gamma)d\Gamma$, and $\mu_2 = \int (\Gamma - \bar{\Gamma})^2 G(\Gamma)d\Gamma$. A measure of the polydispersity can be obtained from the variance, $\mu_2/\bar{\Gamma}^2$. For narrow dispersions it is defined as[3];

$$\frac{\mu_2}{\bar{\Gamma}^2} \approx \frac{1}{4}\left[\frac{M_z}{M_w} - 1\right] \qquad (6.20)$$

The variance tends to lose its significance at values above ≈ 0.3, and becomes simply a comparative value. There are serious limitations to the method of cumulants, especially if the sample is bimodal, which can lead to a slow convergence, or even a divergence of the cumulant fit, and because the fit is generally limited to three cumulants there is a limit to the uniqueness of the fit, indeed three distributions, quite different from each other, will have the same three cumulants (mean, variance and skewness)[4]

In order to obtain a consistent reliable measure of $G(\Gamma)$ it is necessary to extend the analyses beyond the least squares fit. CONTIN[5,6] is a FORTRAN program developed by S.W.Provencher which performs a non-linear least squares fit to solve the inverse Laplace transform of, in this case, the correlation function from a QELS experiment. The transformation is a mathematically ill conditioned problem to which there is a very large number of solutions. With noisy data, as is usually the case with QELS, an unfeasible solution with a very large number of peaks will often give a better fit than a smooth solution with a limited number of peaks which would provide the correct solution. To overcome this CONTIN uses parsimony and some prior restraints, rejecting all negative solutions for example, to limit the number of possible solutions. This means that the smoothest fit, consistent with the experimental data will be the chosen solution. Another feature of CONTIN is it's ability to cope with data containing an element of the signal contributed by dust in the solution, by incorporating a dust term into the program. Although CONTIN is able to resolve multi-peak solutions it is reported that it will not resolve those less than a factor of two in hydrodynamic radius apart[7], tending to smooth

them together. Two peaks approaching this limit will tend to be smoothed further apart, together these tend to make the study of distribution functions by QELS difficult. Nevertheless CONTIN does furnish a method to calculate the distribution of diffusion coefficients, providing number- and weight average values, which are more useful for comparison with data from other methods in contrast to the z-average value and less specific distribution index from the method of cumulants

6.5 Method

The samples used for QELS were those used for intensity light scattering, and preparation was therefore identical. The samples were contained in round optical cells of 10mm external diameter. The cells were thoroughly cleaned before use using permanganic acid, followed by rinsing with distilled water, and dried upside down, to exclude dust, in a glass drying oven. The solutions were filtered directly into the cells twice, the first time to rinse out remaining dust from the cells. It had originally been intended to centrifuge the solution in the cells to settle out remaining dust, however it was found that the cells were not sufficiently strong to withstand the forces exerted. The cells were closed using a polyethylene cap, and sealed using PTFE tape. Such solutions could be left standing for several days without detectable change in scattering intensity. All measurements were made at 25°C the cell being placed in a thermostated index matching bath. The solutions were illuminated with vertically polarised light, with a vertically polarised detector. Depolarised scattering was investigated using a polarising filter placed before the detector. Scattering for the pure solvent was compared to that for 5% concentration solutions at 0, 10, 20 and 40% aromatisation, no excess depolarised scattering from the solutions over the solvent could be detected. All measurements were made at 90°, the angular range of measurements which might have desirable would have been prohibitively time consuming.

Measurements were made on the Malvern 4700 PCS apparatus as described in section 4.3, using an argon ion laser with a measured output of about 50mW. The autocorrelation was measured using a Malvern 7032 8 bit, 128 channel digital correlator with 4 delay channels to measure the mean base line value. Data was collected using Malvern Automeasure software[8] on a dedicated PC. The system was set to automatically optimise the sample time, and the 128 channels were split into 8 'sub-correlators', each of 16 channels. Each sub-correlator spanned times from $\tau=2^n t$ to $2^{n+4}t$, with n = 0,1,2,3...7 for sub-correlators 1,2,3...8 so the multiples of sample time, t, measured were; 1,2,3...16 , 2,4,6...32 , ... , 128,256,384...2048.

This has the advantage of covering a wide range of τ while retaining good resolution at low τ to aid fitting. In most cases nine data sets were collected from each sample, each of which was made up from 10 separate correlograms. These were automatically summed by the software, after rejecting those that fell outside of the limits of acceptability. As each correlogram was collected the ratio of the measured baseline to the calculated baseline was calculated, and once ten had been collected the mean and standard deviation of the set was determined, and those whose ratio differed by more than one standard deviation from the mean were rejected. In general the calculated and measured baseline differed by 2.5% or less, with a signal to noise ratio in the order ≈20-25%, though this could fall substantially for weakly scattering solutions.

In some cases where the samples were of low molecular weight and were of low refractive index increment (section 4.3.4 and table 4.2) scattering was very low and hence collection times needed to be very long, up to six hours per correlogram, in these cases the dataset may be that from a single measurement. For low molecular weight polymers in chloroform, solutions of which could not be satisfactorily filtered, counting times of several hours resulted in unacceptable interference from dust, and no results have been determined. It was generally the situation that the highly aromatised samples with the greater refractive index increment, that is those giving the most intense signal by dint of good contrast with the solvent, were also those giving a strong signal because they were larger particles. In direct contrast the less aromatised samples, those with the low refractive index increments and poor contrast tended to be smaller molecules, thus exacerbating the weak scattering of the sample.

Data from the polymer solutions was analysed by two methods, by the method of cumulants, using the Malvern software with a second order fit to determine D_z, and with CONTIN the data from the Malvern program was converted to a suitable format and transferred to a microVAX computer where the processing was done.

The results for the nine datasets from each sample were averaged after poor results had been rejected. The rejection criteria for the cumulants data was to reject those whose final term $\mu_2 t^2/2$ differed by greater than one standard deviation. For CONTIN data the

criteria were where the value of the fit parameter 'PROB1 TO REJECT'[6] differed substantially from the preferred value of 0.5 or where multiple peaks were present in the range 1.0×10^{-6} to 1.0×10^{-9}cm s^{-1}. However some data possessed a peak at the slow end of the distribution, due presumably to dust, or a small, spurious, peak at the extreme fast end of the distribution. Additionally for 40% aromatised samples there was a small peak of very low intensity (≈0.01%) corresponding approximately to non-aggregated polymer. In these circumstances the relevant peak was singled out.

There was frequent appearance of a small peak (≈1%) corresponding to high diffusion coefficient with very large errors, which could not be eliminated by the smoothing term or by changing limits, which would simply alter the position of the peak. The occurrence of this peak in QELS data has been noted by other authors[6,9]. Sorlie and Pecora consider this to be a spurious peak, incorporated into the solution to increase the goodness of the fit. The authors note that when simulated data without noise is analysed the spurious peak is absent, but when noise is added to the simulated data this spurious peak is liable to appear. The remedy suggested for this is to remove the first data point, unfortunately time constraints prevented re-analysis in this study. Sorlie and Pecora note that the peak has a negligible effects on the real peaks.

6.6 Results

The diffusion coefficients of the polymer solutions measured with QELS are tabulated in tables 6.1 to 6.9. Examples of the correlation functions are shown in fig 6.6, together with the fits obtained.

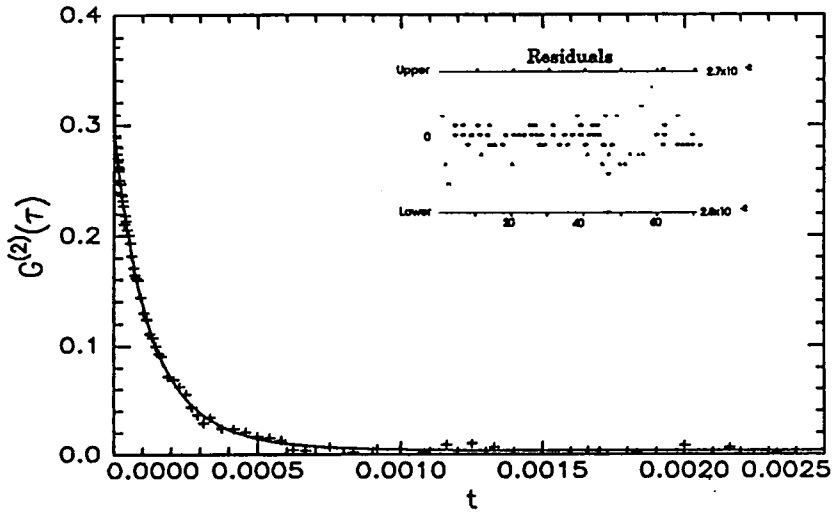

a0c41.res.

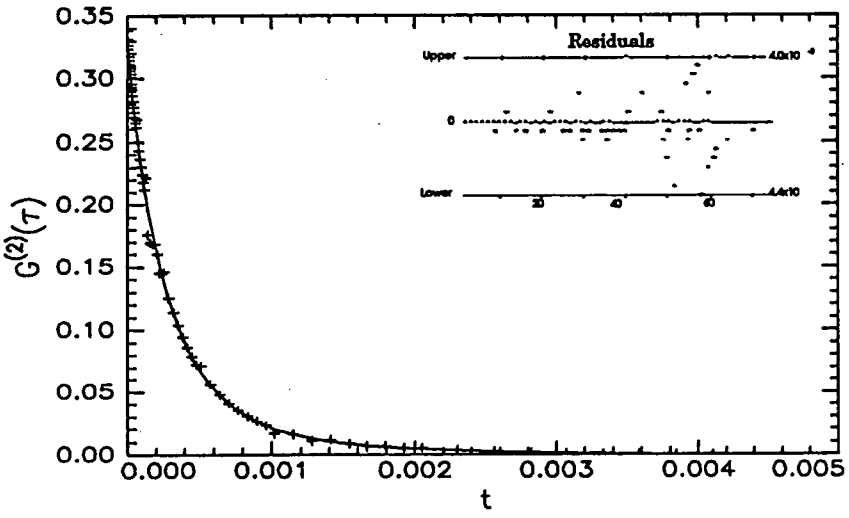

a40c33

Figure 6.6: CONTIN fits to QELS data.

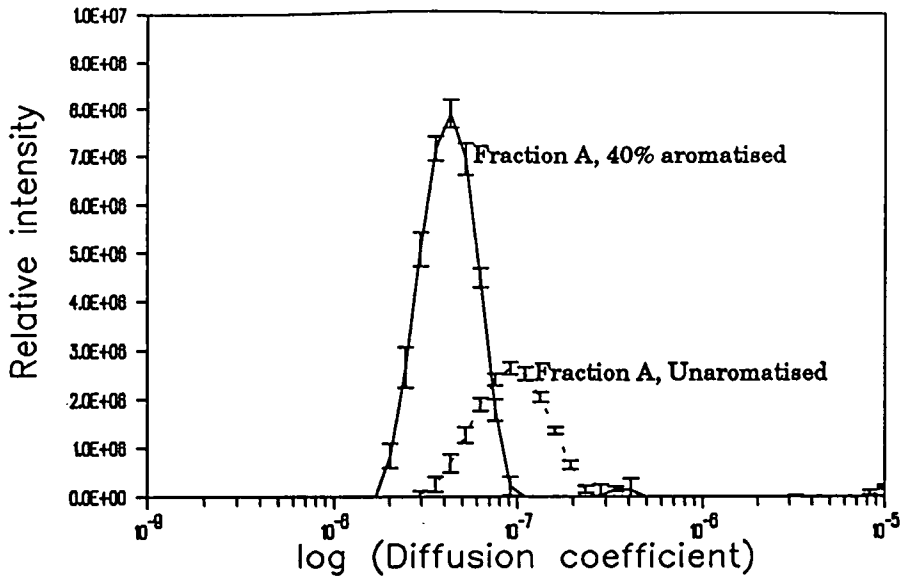

Figure 6.7: Distribution of diffusion coefficient from CONTIN from correlation functions in fig.6.6, showing small peak ≈ $6\times10^{-7}cm^2s^{-1}$ in highly aromatised polymer, and persistent high D tail ≈ $10^{-5}cm^2s^{-1}$ in both.

	CONTIN				cumulants	M_W	$\langle s^2\rangle^{1/2}$	M_w/M_n
	$D_n/10^{-7}$	$D_w/10^{-7}$	$D_z/10^{-7}$	D_w/D_n	$D_z/10^{-7}$	ILS	z-av.	SEC
	/cm² s⁻¹	/cm² s⁻¹	/cm²s⁻¹		/cm²s⁻¹		/Å	
H	0.36	0.44	0.51	1.23	0.49	1220000	978	1.89
A	0.89	0.96	1.05	1.08	0.91	242000	327	1.34
C	0.82	1.17	1.47	1.43	1.25	85000	192	1.32
F	1.38	1.97	2.56	1.43	1.58	65000	170	1.29
G	1.74	2.54	3.34	1.46	1.36	26000	88	1.14
L	2.49	3.65	4.97	1.47	---	10000	60	1.55

Table 6.1: Results of QELS from unaromatised poly(DHCD-DMC), solvent NMP.

	CONTIN				cumulants	M_W	$\langle s^2\rangle^{1/2}$	M_w/M_n
	$D_n/10^{-7}$	$D_w/10^{-7}$	$D_z/10^{-7}$	D_w/D_n	$D_z/10^{-7}$	ILS	z-av.	SEC
	/cm²s⁻¹	/cm²s⁻¹	/cm²s⁻¹		/cm²s⁻¹		/Å	
B	0.60	1.03	1.46	1.71	0.79	66000	235	1.79
E	0.53	1.09	1.44	2.06	0.82	59000	217	1.62
A	0.55	1.09	1.49	1.98	0.98	54000	205	1.59
C	0.41	1.04	1.33	2.55	1.06	45000	158	1.73
F	0.94	1.50	1.74	1.60	1.34	37000	146	1.48

Table 6.2: Results of QELS from 10% aromatised poly(DHCD-DMC), solvent NMP.

	CONTIN				cumulants	M_W	$\langle s^2 \rangle^{1/2}$	M_w/M_n
	$D_n/10^{-7}$	$D_w/10^{-7}$	$D_z/10^{-7}$	D_w/D_n	$D_z/10^{-7}$	ILS	z-av.	SEC
	/cm^{2}s^{-1}	/cm^{2}s^{-1}	/cm^{2}s^{-1}		/cm^{2}s^{-1}		/Å	
F	0.42	0.85	1.28	1.95	0.91	49000	211	2.26
B	0.66	0.94	1.11	1.43	0.91	48000	219	2.12
C	0.55	0.91	1.42	1.65	1.49	46000	214	2.51
D	0.58	0.92	1.29	2.12	0.82	35000	165	2.07
E	0.55	0.94	1.52	1.71	1.02	29000	179	2.04
H	0.62	1.22	1.77	1.64	0.73	27000	191	2.29
G	1.08	1.42	2.12	2.15	1.08	26000	135	1.73

Table 6.3: Results of QELS from 20% aromatised poly(DHCD-DMC), solvent NMP.

	CONTIN				cumulants	M_W	$\langle s^2 \rangle^{1/2}$	M_w/M_n
	$D_n/10^{-7}$	$D_w/10^{-7}$	$D_z/10^{-7}$	D_w/D_n	$D_z/10^{-7}$	ILS	z-av.	SEC
	/cm^{2}s^{-1}	/cm^{2}s^{-1}	/cm^{2}s^{-1}		/cm^{2}s^{-1}		/Å	
D	0.43	0.51	0.59	1.18	0.56	128000	244	6.7
H	0.36	0.55	0.71	1.52	0.56	110000	339	5.5
A	0.46	0.52	0.60	1.13	0.57	98000	267	8.3
C	0.45	0.52	0.67	1.16	0.52	70000	213	5.7
F	0.59	0.74	0.93	1.26	0.93	37000	135	4.3

Table 6.4: Results of QELS from 40% aromatised poly(DHCD-DMC), solvent NMP.

	CONTIN				cumulants	M_W	$\langle s^2 \rangle^{1/2}$	M_w/M_n
	$D_n/10^{-7}$	$D_w/10^{-7}$	$D_z/10^{-7}$	D_w/D_n	$D_z/10^{-7}$	ILS	z-av.	SEC
	/cm^{2}s^{-1}	/cm^{2}s^{-1}	/cm^{2}s^{-1}		/cm^{2}s^{-1}		/Å	
A	2.00	2.33	2.60	1.17	2.13	242000		1.34
B	2.79	3.18	3.28	1.14	1.63	159000	323	1.34
C	3.56	3.75	3.97	1.05	1.76	116000	261	1.32
D	2.81	3.23	3.64	1.15	2.85	78000	220	1.25

Table 6.5: Results of QELS from unaromatised poly(DHCD-DMC), solvent $CHCl_3$.

	CONTIN				cumulants	M_W	$\langle s^2 \rangle^{1/2}$	M_w/M_n
	$D_n/10^{-7}$	$D_w/10^{-7}$	$D_z/10^{-7}$	D_w/D_n	$D_z/10^{-7}$	ILS	z-av.	SEC
	/cm^{2}s^{-1}	/cm^{2}s^{-1}	/cm^{2}s^{-1}		/cm^{2}s^{-1}		/Å	
B	1.86	2.45	3.35	1.32	2.16	85000	222	1.79
D	1.83	3.04	3.49	1.66	1.33	80000	271	1.62
C	1.15	3.12	4.50	2.76	1.10	71000	184	1.75
F	1.28	1.94	3.16	1.52	1.37	44000	194	1.48

Table 6.6: Results of QELS from 10% aromatised poly(DHCD-DMC), solvent $CHCl_3$.

	CONTIN				cumulants	M_W	$\langle s^2\rangle^{1/2}$	M_w/M_n
	$D_n/10^{-7}$	$D_w/10^{-7}$	$D_z/10^{-7}$	D_w/D_n	$D_z/10^{-7}$	ILS	z-av.	SEC
	/cm^{2}s^{-1}	/cm^{2}s^{-1}	/cm^{2}s^{-1}		/cm^{2}s^{-1}		/Å	
A	0.78	2.26	3.33	2.90	1.71	156000	356	2.11
C	1.41	1.67	3.50	1.18	1.17	111000	285	2.07
D	1.54	2.26	2.83	1.77	1.47	105000	312	2.04
B	1.73	1.98	2.16	1.14	2.13	102000	278	2.51
E	0.95	1.75	3.80	1.84	2.46	96000	252	2.26
F	1.45	2.45	3.23	1.69	2.05	45000	179	1.66
G	2.39	3.00	3.65	1.26	3.59			

Table 6.7: Results of QELS from 20% aromatised poly(DHCD-DMC), solvent $CHCl_3$.

	CONTIN				cumulants	M_W	$\langle s^2\rangle^{1/2}$	M_w/M_n
	$D_n/10^{-7}$	$D_w/10^{-7}$	$D_z/10^{-7}$	D_w/D_n	$D_z/10^{-7}$	ILS	z-av.	SEC
	/cm^{2}s^{-1}	/cm^{2}s^{-1}	/cm^{2}s^{-1}		/cm^{2}s^{-1}		/Å	
A	1.32	1.36	1.47	1.03	1.30	289000	339	3.9
B	1.06	1.09	1.12	1.03	1.21	221000	295	3.0
C	1.06	2.79	3.63	2.63	1.50	206000	268	2.5
D	1.10	1.44	1.63	1.31	1.32	162000	208	2.9
F	1.90	2.78	3.69	1.46	2.53	75000	256	2.4
E	1.96	2.88	3.66	1.47	2.92	71000	223	2.4

Table 6.8: Results of QELS from 30% aromatised poly(DHCD-DMC), solvent $CHCl_3$.

	CONTIN				cumulants	M_W	$\langle s^2\rangle^{1/2}$	M_w/M_n
	$D_n/10^{-7}$	$D_w/10^{-7}$	$D_z/10^{-7}$	D_w/D_n	$D_z/10^{-7}$	ILS	z-av.	SEC
	/cm^{2}s^{-1}	/cm^{2}s^{-1}	/cm^{2}s^{-1}		/cm^{2}s^{-1}		/Å	
D	1.25	1.59	2.04	1.27	1.48	407000	288	6.7
C	1.36	1.75	2.07	1.29	1.85	215000	212	5.7
A	1.71	1.73	1.77	1.01	1.25	205000	257	8.3
H		2.16			1.19	199000	285	5.5
G	2.06	2.36	2.80	1.15	2.14	142000	201	4.7
F	1.56	2.32	3.23	1.48	2.13	114000	193	4.3

Table 6.9: Results of QELS from 40% aromatised poly(DHCD-DMC), solvent $CHCl_3$.

Hydrodynamic radii were calculated from the Stokes Einstein equation (6.16), using viscosities of 0.542 cps for chloroform (text[10]) and 1.610 cps for NMP (measured with Ubbelohde viscometer). The results of R_h are given in tables 6.10 together with the values for ρ in parenthesis. Determination of ρ has been done using $\langle s^2\rangle_z^{1/2}$, rather than

$\langle s^2 \rangle_w^{1/2}$, because the w-average figure was not available in all cases. This means that the value of ρ will be over-estimated.

NMP							
Unaromatised		10%Aromatised		20%Aromatised		40%Aromatised	
Fraction	R_h/Å	Fraction	R_h/Å	Fraction	R_h/Å	Fraction	R_h/Å
H	307(3.2)	B	131(1.8)	F	159(1.3)	D	265(0.9)
A	141(2.3)	E	124(1.8)	B	144(1.5)	H	245(1.4)
C	115(1.7)	A	124(1.7)	C	148(1.4)	A	260(1.0)
F	69(2.5)	C	130(1.2)	D	148(1.1)	C	260(0.8)
G	53(1.7)	F	90(1.6)	E	144(1.2)	F	182(0.7)
L	37(1.6)			H	111(1.7)		
				G	95(1.4)		

Table 6.10a; Hydrodynamic radii of partially aromatised poly(DHCD-DMC) in NMP (figures in parenthesis represent $\rho=\langle s^2 \rangle_z^{1/2}/R_{hz}$).

$CHCl_3$					
0% Aromatisation		10%Aromatisation		20%Aromatisation	
Fraction	R_h/Å	Fraction	R_h/Å	Fraction	R_h/Å
A	173(2.5)	B	164(1.4)	A	178(2.0)
B	127(2.5)	D	133(2.0)	C	241(1.2)
C	107(2.4)	C	129(1.4)	D	178(1.8)
D	125(1.7)	F	208(0.9)	B	204(1.3)
				E	230(1.1)
				F	164(1.1)

$CHCl_3$			
30%Aromatisation		40%Aromatisation	
Fraction	R_h/Å	Fraction	R_h/Å
A	296(1.2)	D	253(1.1)
B	370(0.8)	C	230(0.9)
C	144(1.8)	A	233(1.1)
D	280(0.7)	H	187(1.5)
F	145(1.8)	G	171(1.2)
E	140(1.6)	F	174(1.1)

Table 6.10b; Hydrodynamic radii of poly(DHCD-DMC) in chloroform.

Aromatisation	solvent	K''	γ
0%	NMP	0.30	0.51
10%	NMP	0.37	0.53
20%	NMP	0.16	0.64
40%	NMP	10.27	0.28
40%	Chloroform	3.45	0.34

Table 6.11: Fits to R_h *vs* M_w plots.

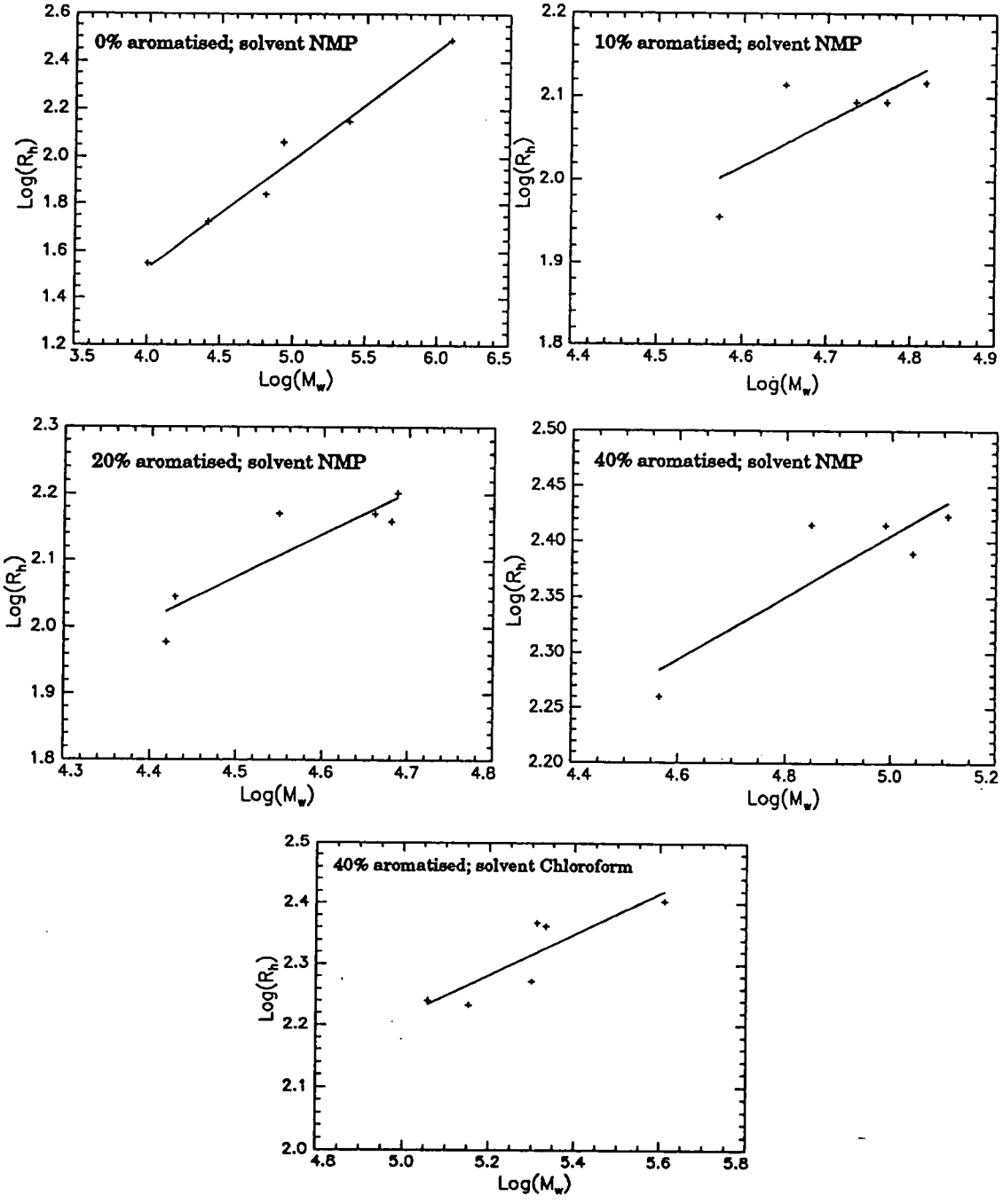

Figure 6.8: Plots of hydrodynamic radius *vs* molecular weight for partially aromatised poly(DHCD-DMC).

Figure 6.8 and table 6.11 show the molecular weight dependency of hydrodynamic radius according to the equation

$$R_h = K'' M_w^{\gamma}$$

There are no fits for the chloroform, excepting 40% aromatisation, because at low degrees of aromatisation no satisfactory correlation function could be obtained because of weak scattering and dust, causing a spurious increase in R_h values at the low M_w's, and at 20% and 30% aromatisation because scatter in the values of R_h was too great.

6.7 Discussion

Information obtained from quasi-elastic light scattering tends to support general observations from other techniques, although there are some differences. The value of γ for the unaromatised polymer in the molecular weight dependency of R_h is 0.51. The value of the exponent should follow the relation;

$$1+\alpha = 3\gamma$$

where α and γ are the respective exponents in the Mark-Houwink and the R_h *vs.* M_w relationships. Therefore the range of α, 0.5 to 2.0, from a theta coil to a true rigid rod corresponds to 0.5 to 1.0 for γ, as in the corresponding relationship for $\langle s^2 \rangle^{1/2}$. The unaromatised polymer fractions have reasonably narrow distribution of diffusion coefficient, although they differ from the SEC values being diffusion coefficient rather than molecular weight distribution. The diffusion coefficient has a positive concentration dependency (fig 6.9), indicating that A_2 is high. The unaromatised polymer in solution in NMP would therefore appear to have the configuration of a random coil molecule, in a reasonably good solvent.

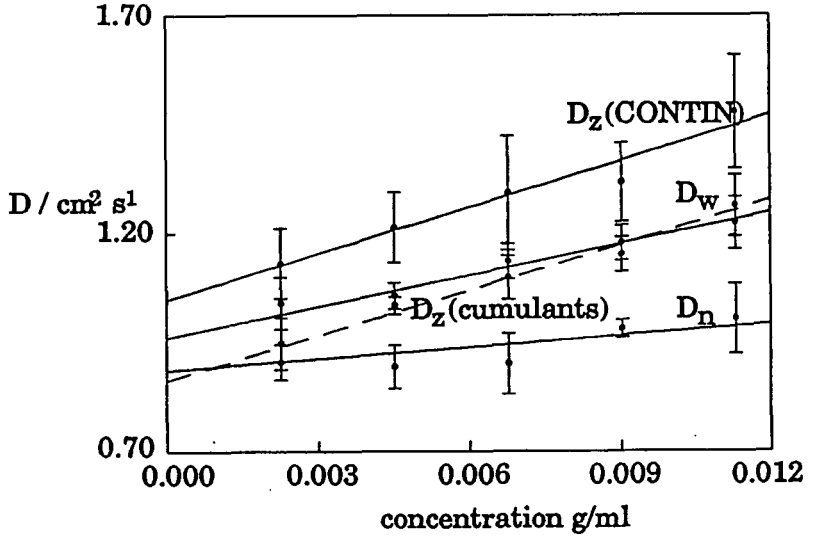

Fig 6.9: Concentration dependency of diffusion coefficients of fraction A unaromatised.

As the polymer is aromatised to low degrees of aromatisation a number of changes can be observed. There is a randomisation of the results, the polydispersities increase, and

the initial order with the molecular weights of the fractions is lost as the diffusion coefficients converge(fig 6.10).

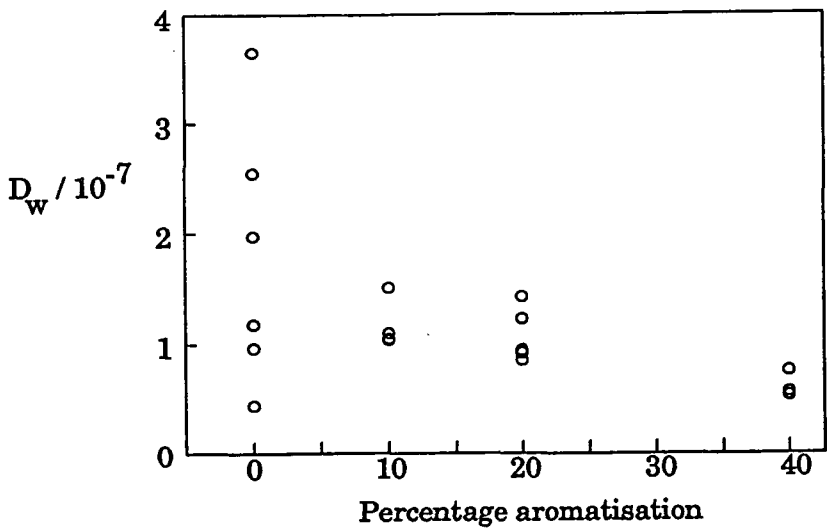

Figure 6.10: Change in diffusion coefficient with aromatisation.

This is caused by the chain scission process observed in ILS causing molecular weights to fall below that due to stoichiometry alone. Because of the convergence the chain degradation must be more severe in the larger molecular weight fractions. From figure 6.11 it can be seen that the hydrodynamic radius of a given molecular weight increases as aromatisation increases, from 0% through to 20%, this suggests that the molecules are stiffening, increasing the hydrodynamic volume, this is borne out by the increase in the exponent of the Rh *vs.* Mw relationship. As aromatisation increases 0 to 10 to 20% aromatisation, the exponent increases from 0.51 to 0.53 to 0.64, following the results from ILS, although the values are somewhat lower. The polymer at 40% aromatisation has become much less sensitive to increases in molecular weight, so that it's R_h changes less with increasing molecular weight. The polymer aromatised to 40% conversion in solution in NMP displays distinctly different properties in QELS from those at lower degrees of aromatisation, also observed by the other techniques.

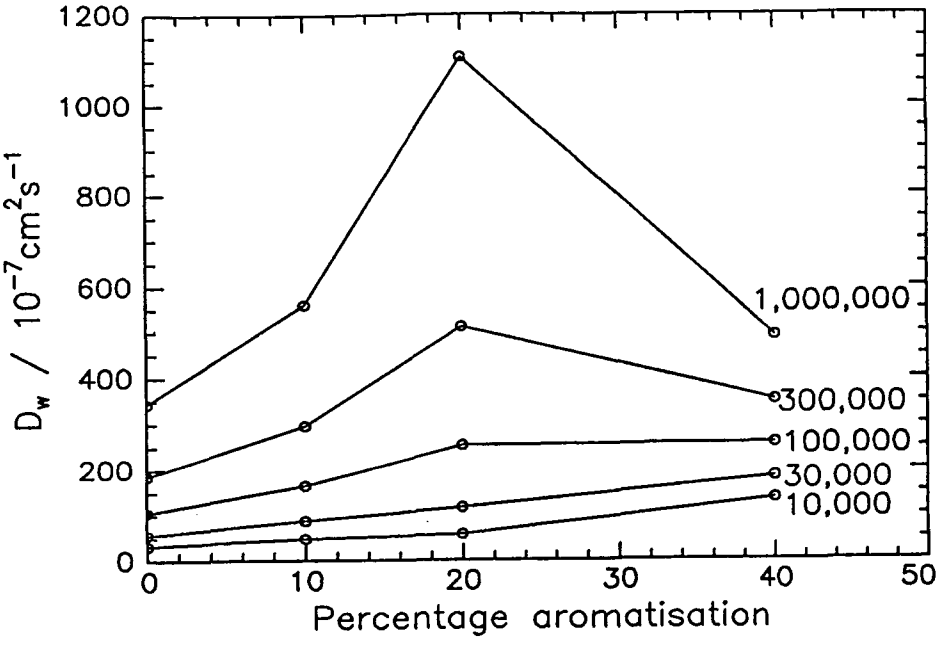

Figure 6.11: Fitted diffusion coefficients of partially aromatised polymer.

Somewhat unexpectedly the polydispersity of the samples has fallen below that of the unaromatised polymer, and the dependency of R_h on M_w has fallen sharply. The dependency of D on concentration has reversed (fig 6.12).

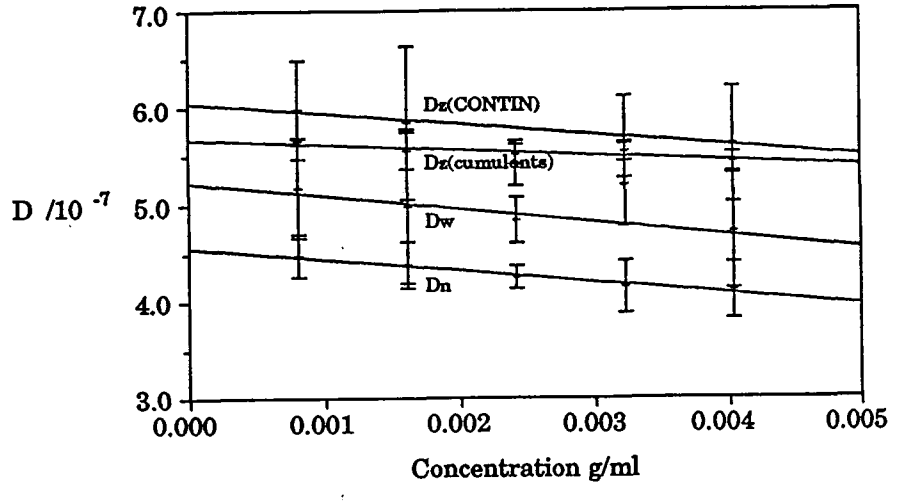

Figure 6.12: concentration dependency of diffusion coefficients of fraction A at 40% aromatisation.

This is because the aggregates which form have constrained the polymer chains to an extent that expansion with lower concentration becomes negligible, and physical entanglement becomes the controlling factor on D.

The change in the exponent of the R_h *vs.* M_w relationship, which rises from 0.51 at 0%, to 0.64 at 20% aromatisation falls to 0.29 at 40%. This is in common with the fall of the other exponents from the molecular weight dependency of other quantities, $[\eta]$ and $\langle s^2 \rangle^{1/2}$, and is caused by aggregation, the size of a tightly packed cluster will vary much less with molecular weight than an exanded polymer coil would. No values for such a relationship have been located, however the approximation of a sphere would give;

$$r = \frac{\pi\rho'}{3} M^{1/3} \qquad \text{hence} \qquad r \propto M^{1/3}$$

where r is radius and ρ' is density.

This is close to the exponent which was obtained, both for NMP and chloroform as solvent. These observations would support the suggestion that the aromatised polymer forms an aggregate, possibly of the fringed-micelle type at 40% aromatisation, with a dense core of polyphenylene segments and a corona of predominantly poly(DHCD-DMC) segments, somewhat more tightly packed than in the wholly unaromatised polymer. The low value of polydispersity of the 40% aromatised polymer indicates that the aggregates of a given sample are of a regular size, therefore possibly containing a similar number of chains. How these narrow distribution aggregates can form from highly polydisperse polymer molecules is unclear, unless each chain eventually degrades to the same size before recombining, or that there is an optimum size where the corona maintains sufficient solubility to prevent precipitation. The latter could explain why the R_h of 4 of the 5 fractions were virtually the same.

In some cases there is a peak in the diffusion coefficient distribution possibly corresponding approximately to residual unaggregated polymer (fig. 6.7), however the peaks are very small (≤0.5%), SEC (chapter 5) showed the opposite situation when the refractive index detector was used with the unaggregated polymer dominating. However dn/dc is colligative, and sensitive to the number of particles, the UV detector, sensitive to amount of phenyl rings showed the aggregated peak to be larger, therefore containing more polyphenylene. but did not provide information on the distribution of the residual 60% poly(DHCD-DMC).

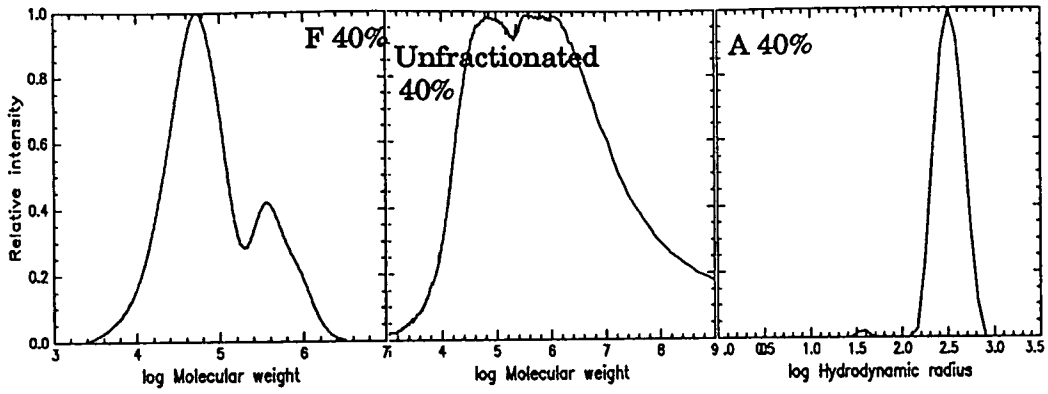

Figure 6.13: Comparative distributions of polymer in 40% aromatised polymer by;

A: SEC-refractive index detector, B: SEC-UV detector, C: QELS/CONTIN.

It would seem that the bimodality observed in SEC, whose existence was supported by the fact that separation of such a sample by fractionation into fractions corresponding to each peak was possible, is real and not an artifact. The results from QELS ought therefore resolve the two parts into peaks in the distribution, much less unequal in size than was found, that is ≥99% for the larger particles and ≤0.5% for the smaller. It maybe that bimodality is present and has been masked by the limits of resolution of the method, that is peaks with different by less than a factor of two cannot be resolved, or that the sensitivity of the method is biased too far towards the larger particles.

The results from chloroform solutions show a similar trend to that in NMP. If the mean values of the ratio ρ are plotted a similar trend is observed.

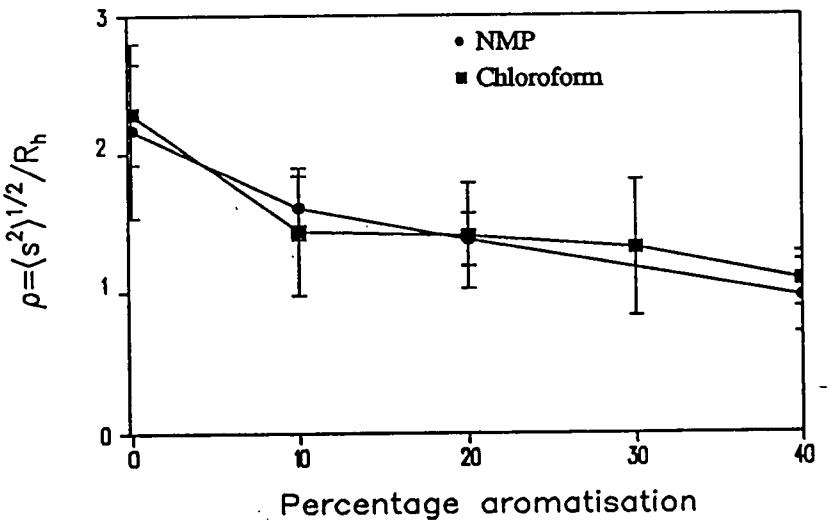

Figure 6.14: Comparison of mean values of factor ρ in NMP and chloroform.

	0%	10%	20%	30%	40%
NMP	2.17±0.63	1.61±0.23	1.38±0.19	——	0.98±0.26
$CHCl_3$	2.29±0.36	1.44±0.46	1.43±0.38	1.32±0.49	1.16±0.20

Table 6.12: Mean values of the parameter ρ, = $\langle s^2 \rangle^{1/2}/R_h$.

The values of ρ are determined by the configuration of the molecule. A random coil polymer in the theta condition has a value of 1.505, values for more compact molecules are lower, for example 12-armed polystyrene star molecules were found to have values in the range 0.89 to 1.2[11], and a compact sphere has the value 0.75. Less compact structures have higher values, so that stiffer molecules will have a value of ρ greater than a random coil. It is notable therefore that the polymers aromatised to 10% and 20%, which should be stiffer, as they contain the more rigid phenylene unit, and observed in the increased persistence length measured by ILS and viscometry, as well as by the increase in γ in QELS shows no such increase. However ρ is not wholly dependent on configuration, and will be affected by the polydispersity of the polymers. The values of ρ observed in both solvents were much higher than that of the theta coil, and polydispersity is a contributing factor to these elevated values as well as chain expansion The most polydisperse of the precursor polymers, fraction H, was also that with the highest ρ, 3.2, compared with the mean of 2.2. The decrease in ρ for the partially aromatised polymers may be caused by an greater sensitivity of QELS to the aggregated species present in these solutions than ILS.

6.8 Conclusion

Quasi-elastic light scattering did not provide any additional information on the configurational changes of poly(DHCD-DMC) during the aromatisation reaction beyond that provided by other methods.

The relationship between R_h and M_w for the polymer in NMP solutions follows the same trend as that between $\langle s^2 \rangle^{1/2}$ and M_w, as would be expected. The unaromatised polymer is an expanded coil, which further expands as the polymer is aromatised to 10 and 20% conversion, and is stiffened by the polyphenylene nuclei formed. There is a significant change in configuration between 20 and 40% aromatisation as the chains start to aggregate and form compact structures. Although it was not possible to derive the corresponding relationships for chloroform solutions a cursory examination of the data would suggest a similar situation.

Comparison of the configuration parameter ρ, $(=\langle s^2 \rangle^{1/2}/R_h)$, shows the structure for the polymer to be the similar in chloroform and NMP solutions, although ILS shows aggregation to be more severe in chloroform. The changes in ρ are sensitive on factors besides configuration, including polydispersity which shows significant fluctuation during aromatisation. The changes in ρ however suggest that aggregation could be present in the polymer solutions of low aromatisation, would would not necessarily be apparent in ILS. This was noted in size exclusion chromatography with the presence in some samples of a second, high molecular weight peak in the molecular weight distribution of samples even at 10% conversion (section 3.4). QELS data analysed using CONTIN, to give a distribution of diffusion coefficient, showed no bimodality corresponding to that in SEC, although there was some evidence of low molecular weight material in the results for some highly aromatised polymers. At low degrees of aromatisation the aggregates may simply be part of a broad distribution, at higher degrees of aromatisation a second peak may be masked by the lack of resolution. Two peaks with the average ratio of M_p's from SEC of 7.5(table 3.10) would give a ratio of

peak R_h's of 1.9 when $R_h \propto M_w^{0.33}$. This is below the limit of resolution, that is a ratio of 2.

The lack of useful information gathered from the technique of QELS is not due to the short-comings of the technique, but to the method of study. With hindsight better use of the equipment would have been made by concentrating on a more thorough study of fewer samples, over a range of angles. However the problems associated with weak scattering and the deleterious effect of residual dust were not apparent at the onset, and the seeming randomness of the aromatisation process has meant that large quantities of data are required to obtain representative samples.

6.9 References

1, Berne,B.J.,Pecora,R.,'*Dynamic Light Scattering with Applications to Chemistry, Biology, and Physics*', 1976, Wiley-Interscience, New York.

2, Koppel,D.E., *J.Chem. Phys.*, 57,4814(1972).

3, Brown,J.C., Pusey,P.N., *J.Phys.,D:Appl.Phys.*, 7,L31(1974).

4, Provencher,S.W., *Makromol.Chem.*, 180,202(1979).

5, Provencher,S.W., *CONTIN users manual*, Version 2, 1984.

6, Provencher,S.W., *Comput.Phys.Commun.*,27.

CHAPTER 7

SMALL ANGLE NEUTRON SCATTERING

7.1 Introduction

Small angle neutron scattering (SANS) has been used to measure the size of partially aromatised poly(DHCD-DMC) in solution. The data collected has been analysed by a number of fitting techniques to determine the configurational properties of the polymers.

7.2 Theoretical considerations

The technique of small angle neutron scattering[1] is broadly analogous to that of light scattering, and data generated can be treated in a similar manner, for example using the Zimm and Debye equations. There are however two essential differences, the range of the scattering vector, Q, that can be probed in light scattering is very small,

$$Q = \frac{4\pi}{\lambda} \sin\frac{\theta}{2} \qquad (7.1)$$

for light scattering λ is limited to ≈3000 to 7000Å, and θ to π radians, ∴ the extreme values of Q available are 1×10^{-4} to 5×10^{-3} Å^{-1}. In SANS much lower wavelengths are available, down to ≈2Å, so that Q, even at low angles is very much higher (for example at 10° when λ=2Å, Q=0.55Å^{-1}, when λ=3000Å, Q=3.7×10^{-4}Å^{-1}). This allows the investigation of a very much wider range of the scattering function, out to higher Q where in general differences become more pronounced, allowing structure to be investigated to shorter length scales. The length scale that can be probed by a scattering technique is related to the scattering vector by $2\pi/Q$, hence with a sufficiently large Q length scales down to a few monomers can be probed.

Light scattering is caused by the interaction of photons with molecular dipoles and the contrast factor is the difference in refractive index of the scattering species from the background matrix. Neutron scattering is the result of neutron-nucleus interaction, and the contrast factor is the difference in scattering length density between the scattering molecule and its supporting matrix, scattering length density is a property of the nuclear material of the constituent atoms, and this leads to the possibility of contrast

manipulation by isotopic enrichment. This gives rise to studies inaccessible to electromagnetic scattering methods, for example specific parts of the monomer or molecule can be isotopically marked so that they can be differentiated from the rest of the molecule which can be made to blend in with the background. It is also possible to tag a small proportion of a particular species, producing in effect a solid solution which can be used to study bulk properties.

7.2.1 SANS Theory

The incident neutron can interact with a nucleus in two ways, elastically and inelastically. Inelastic scattering involves a transfer of energy between the two bodies, and no further treatment will be made of it. Elastic scattering involves no transfer of energy, and provides valuable data on polymer configuration. The situation in neutron scattering is represented in figure 1. An incident beam of neutrons of intensity I_0, and wave vector K_0 is scattered by the sample S. The scattered beam of wave vector K describes an angle of 2θ from the normal. The change in wave vector is equivalent to the scattering vector Q

$$\mathbf{Q} = \mathbf{K}_0 - \mathbf{K} \tag{7.2}$$

from figure 7.1*b* we can redefine the scattering vector thus

$$\mathbf{Q} = \left(\mathbf{K}_0^2 + \mathbf{K}^2 - 2\mathbf{K}_0\mathbf{K}\cos 2\theta\right)^{1/2} \tag{7.3}$$

In elastic scattering where $K_0=K$, since $|K_0|=2\pi/\lambda$ equation (3) reduces to

$$\mathbf{Q} = |\mathbf{Q}| = \frac{4\pi}{\lambda}\sin\frac{\theta}{2} \tag{7.4}$$

In scattering experiments the quantity measured is partial differential scattering cross section, $d^2\sigma/d\Omega dE$, that is the fraction of neutrons of incident energy E_0 scattered into an element of solid angle $d\Omega$, equal to $\sin\theta d\theta.d\phi$, having an energy between E and E+dE. If only elastic collisions are considered the number of neutrons that will be scattered into $d\Omega$ per unit time is $I_0(d\sigma/d\Omega)d\Omega$ (number area^{-1} time^{-1}). From first order perturbation theory the probability of the scattering of a neutron, with wave vector $\underline{K}_0$ to $\underline{K}$ is expressed as the square of the matrix element;

$$\int d\mathbf{r}\Psi_{\mathbf{K}}^{*}(\mathbf{r})\hat{V}\Psi_{\mathbf{K}_0}(\mathbf{r}) = \left\langle \underline{\mathbf{K}}\middle|\overline{\mathbf{V}}\middle|\underline{\mathbf{K}}_0\right\rangle \tag{7.5}$$

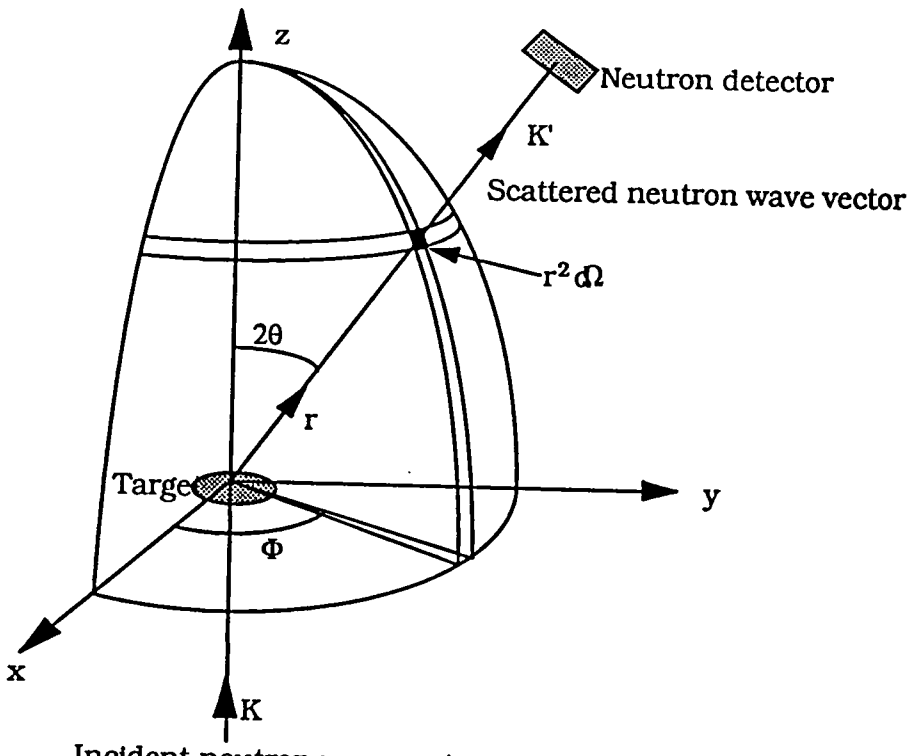

a

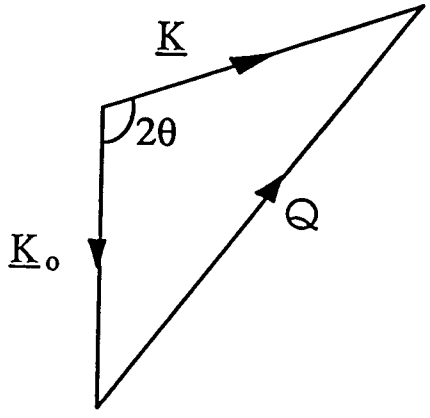

b

Figure 7.1*a:* Diagrammatic representation of neutron scattering process

b: Vector representation of neutron scattering process

where $\hat{V}$ is the interaction potential, and Ψ_{K0} and Ψ_K are the wave functions of the incident and scattered beam.

The cross section, $d\sigma$, is the product of the probability with the density of the final state divided by the incident flux;

$$d\sigma = \left(\frac{m}{2\pi\hbar^2}\right)^2 \left|\underline{K}\middle|\hat{V}\middle|\underline{K}_0\right|^2 d\Omega \qquad (7.6)$$

where m is the neutron mass, $\hbar = h/2\pi$, where h is Planck's constant, and $d\Omega$ is the element of solid angle into which the neutron is scattered. The double differential scattering cross section must include all possible scattering processes, so (7) is summed over all final states of the nuclei and spin states of the neutron;

$$\frac{d^2\sigma}{d\Omega dE} = \frac{K}{K_0}\left(\frac{m}{2\pi\hbar^2}\right)^2 \sum_{\sigma\lambda} p_\sigma p_\lambda \sum_{\sigma'\lambda'} \left|\left\langle \underline{K}\sigma'\lambda' \middle| \hat{V} \middle| \underline{K}_0\sigma\lambda \right\rangle\right|^2 \delta(\hbar\omega + E_\lambda - E_{\lambda'}) \qquad (7.7)$$

where σ, σ', λ, and λ' are the initial and final neutron spin and scattering nuclei states respectively, and p_σ and p_λ the probability of states σ and λ.

E_λ and $E_{\lambda'}$ are the initial and final energies of the scattering nuclei. Bearing in mind the conservation of energy in the elastic scattering process;

energy gained by nuclei = energy lost by the neutron

$$= E_0 - E\frac{\hbar^2}{2m}\left(K_0^2 - K^2\right)$$

The neutron-nucleus interaction is very short range, and known to contain only the S-wave component, with no angular momentum, it is therefore isotropic. The scattering can then be described in terms of a single parameter, b, the scattering length. Values of b are dependent on the relative orientation of neutron and nuclear spins, and on the isotope. The neutron-nucleus interaction may be described by the Fermi pseudo potential;

$$\overline{V}(r) = \frac{2\pi\hbar^2}{m} b\,\delta(\underline{r} - \underline{R}) \qquad (7.8)$$

where $\underline{r}$ and $\underline{R}$ are the positions of the neutron and the nucleus. If the nucleus is regarded as the origin ($\underline{R} = 0$), substituting (8) into (6) gives;

$$\frac{d\sigma}{d\Omega} = \left(\frac{m}{2\pi\hbar^2}\right)^2 \left(b\frac{2\pi\hbar^2}{m}\right)^2 \left(\int d\underline{r}\, e^{-i\underline{K}\underline{r}}\delta(\underline{r})e^{-i\underline{K}_0\underline{r}}\right)^2 \qquad (7.9)$$

since for elastic scattering $\underline{K} = \underline{K}_0$;

$$\frac{d\sigma}{d\Omega} = |b|^2 \qquad (7.10)$$

Because scattering is isotropic the total cross section $\sigma = 4\pi|b|^2$. If an array of scattering nuclei are considered the pseudo potential becomes;

$$\hat{V}(\mathbf{r}) = \frac{2\pi\hbar^2}{m}\sum_L b_L \delta(\underline{r} - \underline{R}_L) \qquad (7.11)$$

where $\underline{R}_L$ is the position of the L^{th} nucleus of scattering length b_L, substituting (11) into (7) gives;

$$\frac{d^2\sigma}{d\Omega dE} = \frac{K}{K_0}\sum_{\sigma\lambda} p_\sigma p_\lambda \sum_{\sigma'\lambda'}\left|\left\langle \sigma'\lambda'\left|\sum_L b_L e^{i\underline{K}\underline{R}_L}\right|\sigma\lambda\right\rangle\right|^2 \delta\left(\frac{\hbar^2}{2m}\left(K_0^2 - K^2\right) + E_\lambda - E_{\lambda'}\right) \qquad (7.12)$$

where $Q = \underline{K}\text{-}\underline{K}_0$. Equation (12) is the basis for elastic neutron scattering theory.

The treatment above can be extended to a rigid array of nuclei. The interaction of the neutron is assumed to have no effect but to redistribute nuclear spins without loss of energy, this means the δ function in (12) can be ignored , so (12) may be summed over σ and λ to;

$$\frac{d^2\sigma}{d\Omega} = \sum_{L,L'} p_\sigma p_\lambda e^{i\underline{Q}\cdot\underline{R}_L - \underline{R}_{L'}}\overline{b_L^* b_{L'}} \qquad (7.13)$$

where $\overline{b_L^* b_{L'}}$ is the mean over all random spin orientations and isotope distributions of $b_L^* b_{L'}$;

$$\overline{b_L^* b_{L'}} = \sum_\lambda p_\lambda \left\langle \lambda \left| b_L^* b_{L'} \right| \lambda \right\rangle \qquad (7.14)$$

b_L and $b_{L'}$ are uncorrelated, therefore if;

$L \neq L' \quad \Rightarrow \quad \overline{b_L^* b_{L'}} = \left|\overline{b}\right|^2$

$L = L' \quad \Rightarrow \quad \overline{b_L^* b_{L'}} = \overline{|b|^2}$

and in general;

$$\overline{b_L^* b_{L'}} = \left|\overline{b}\right|^2 + \left(\overline{|b|^2} - \left|\overline{b}\right|^2\right) \qquad (7.15)$$

substituting (14) into (12) gives

$$\frac{d^2\sigma}{d\Omega} = \overline{b}^2\left|\sum_{L,L'} e^{i\underline{Q}\cdot\underline{R}_L - \underline{R}_{L'}}\right|^2 + N\left[\left|\overline{b}\right|^2 + \left(\overline{|b|^2} - \left|\overline{b}\right|^2\right)\right] \qquad (7.16)$$

where N is the number of scattering nuclei. This can be divided into two sections, one with a Q dependence and one simply dependent on the number of scattering nuclei. These are termed the coherent and incoherent scattering respectively.

$$\frac{d\sigma}{d\Omega} = \left[\frac{d\sigma}{d\Omega}\right]_{coh} + \left[\frac{d\sigma}{d\Omega}\right]_{incoh} \qquad (7.17)$$

Coherent scattering is the Fourier transform of the scattering length correlation and contains all the structural information of the sample. Incoherent scattering is simply a

featureless background from which no configurational information is obtained and is simply subtracted for experimental purposes.

The scattering lengths can be obtained from published tables, those used here are tabulated below.

Nucleus	Mass / amu	b / 10^{12}cm	σ_{coh} / barns	σ_{incoh}/barns
$^{1}_{1}H$	1	-0.374	1.76	79.91
$^{2}_{1}H$	2	0.667	5.59	2.04
$^{12}_{6}C$	12	0.665	5.56	0
$^{14}_{7}N$	14	0.940	11.4	0.49
$^{16}_{8}O$	16	0.580	4.23	0

Table 7.1: Neutron scattering properties of common nuclei.

Polymer	Molar mass /amu	ρ / 10^{10} cm^{-2}
poly(DHCD-DMC)	228	1.639
poly(DHCD-DMC)-d12	240	5.006
PPP	76	2.432
PPP-d4	80	6.165

Table 7.2: Scattering length densities of polymers used in this study.

The scattering length of a molecule (or a segment of a molecule) is the sum of b over n atoms;

$$b_m = \sum_{i=1}^{n} n_i b_i \qquad (7.18)$$

The scattering length density, ρ of a molecule is the scattering length per unit molecular volume;

$$\rho = \frac{N_A b d}{m} \qquad (7.19)$$

where d is the density of the material and m is the molecular weight, in the case of polymers the molecular weight of the repeating unit.

In a dilute solution of a polymer the coherent scattering will be given by;

$$\frac{d\sigma}{d\Omega} = \left| V(\rho - \rho_s)\frac{1}{V}\int e^{i\underline{Q}\cdot\underline{R}_0 - \underline{R}} dR \right|^2 \qquad (7.20)$$

where ρ and ρ_s are the scattering length densities of the polymer and solvent and V is the volume containing the scattering particles.

The single particle form factor F(Q) contains the structural information about the scattering particle and is defined;

$$F(Q) = \frac{1}{V}\int_{v}^{0} e^{i\underline{Q}.\underline{R}_0 - \underline{R}}.dR \qquad (7.21)$$

so

$$\frac{d\sigma}{d\Omega} = V^2(\rho - \rho_s)^2 F^2(Q) \qquad (7.22)$$

$F^2(Q)$ is determined by the shape of the scattering particle, and is known as the scattering law P(Q). A wide variety of scattering laws have been described for particles of various shapes[2], together with a very large number which have been proposed to model the various configurations which polymer molecules can describe, a number of which are outlined in this work. Essentially this is the same as the scattering functions used as the basis for the Zimm plot in ILS (section 4.2.1) but in ILS only a small range of Q is accessible and in general the scattering function has converged to a single function close to $Q^2\langle s^2\rangle = 0$, P(Q) = 1, in SANS an extended Q-range is accessible and the scattering functions diverge, therefore greater information on configuration is available.

Describing polymer molecules by these models of scattering behaviour over a wide Q-range provides the means from which data can be extracted from the coherent component of neutron scattering data.

7.2.2 Determination Of Molecular Parameters From SANS Data

In the previous section the concept of the scattering law is introduced. This is related to the measured coherent intensity, $(d\sigma/d\Omega)_{ex.}$ by a number of factors. Intensity per unit volume, I(Q) is defined by

$$I(Q) = \left(\frac{d\sigma}{d\Omega}\right)_{ex} \frac{cN_A}{m} \qquad (7.23)$$

where c is concentration of scattering species and m the molecular weight. At the intercept Q = 0, the molecular weight of the scattered species can be derived from the ratio of the measured intercept to that of $P(Q)_{(0)}$;

$$\frac{I(0)}{P(Q)_{(0)}} = \frac{M}{k^* c} \qquad (7.24)$$

where $k^*=(\rho_D-\rho_H)^2 N_A/m^2$, where m = segment molecular mass. Since $P(Q)_{(0)} = 1$ then;

$$I(0) = \frac{M}{k^* c} \qquad (7.25)$$

From which molecular mass of the scattering polymer is determined.

Over a sufficiently wide range of Q it is possible to identify a number of distinctive regions of scattering behaviour for typical polymer molecules, demonstrated in the idealised Kratky plot in figure7.2.

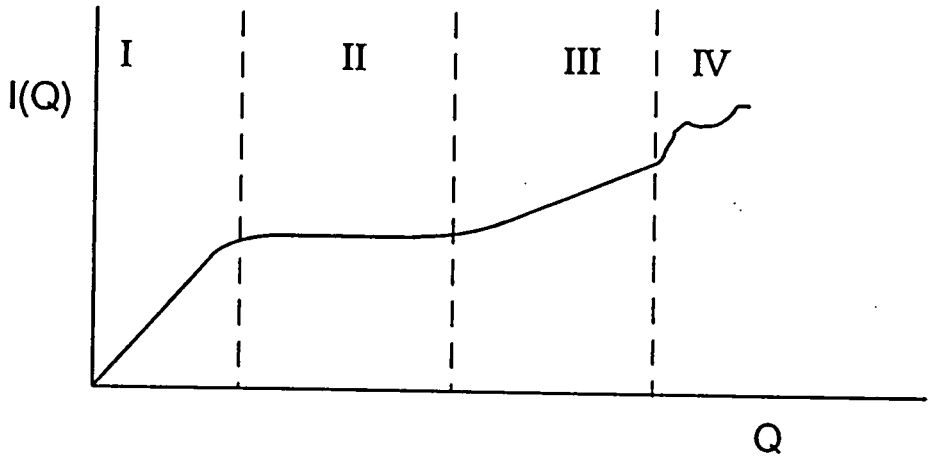

Figure 7.2: Idealised Kratky plot of scattering from a polymer.

I The Guinier region $0 \leq Q \leq 1/\langle s^2\rangle^{1/2}$

While scattering laws vary considerably, they all converge, as $Q \rightarrow 0$ then $P(Q) \rightarrow 1$ (section 4.2), and within the range $0 \leq Q \leq 1/\langle s^2\rangle^{1/2}$ their behaviour can be described by a single law, the Guinier approximation[3];

$$I(Q) = I(0) e^{\frac{Q^2\langle s^2\rangle}{3}} \qquad (7.26)$$

Hence if a sufficiently small range of Q can be probed the radius of gyration and the molecular mass can be extracted. This should hold for a molecule of any configuration. A second equation describing the scattering within this range is the Zimm approximation[4] used in ILS analysis;

$$\frac{1}{I(Q)} = \frac{1}{I(0)}\left[1 + \frac{Q^2\langle s^2\rangle}{3}\right] \qquad (7.27)$$

In the analysis of polydisperse polymers it is found that the values of radius of gyration will be overestimated by the Zimm approximation and underestimated by the Guinier[5]

II Plateau region $1/\langle s^2\rangle^{1/2} \leq Q \leq a^{-1}$

In this intermediate Q-range the scattering approaches the asymptotic value where $I(Q) \propto Q^{-2}$. In this region it becomes possible to resolve details of polymer configuration, scattering can be described by the Debye equation for isolated Gaussian coils;

$$P(Q) = \left[\frac{2}{u^2}\right]\left(u - 1 + e^{-u}\right) \qquad (7.28)$$

where $u=Q^2\langle s^2\rangle$. In terms of scattered intensity this becomes;

$$I(Q) = I(0)\left[\frac{2}{u^2}\right]\left(u - 1 + e^{-u}\right) \qquad (7.29)$$

and it is possible to fit (29) to obtain values for I(0) and $\langle s^2\rangle$.

III Upturn region $a^{-1} < Q < l^{-1}$, where l is the statistical step length

The scattered intensity now becomes that of a rigid-rod of length lxn where n is the number of statistical units in the chain.

$$P(Q) = \frac{2}{u}\int \frac{\sin u}{u} \cdot du\left[\frac{\sin(u/2)}{u/2}\right]^2 \qquad (7.30)$$

IV Local conformation $Q > l^{-1}$

The scattered intensity depends on the internal structure of the statistical step lengths of the chain.

7.2.3 Data analysis

Corrected data[6] from neutron scattering experiments can be manipulated in a number of ways. A straightforward method is to fit the data to a number of equations describing the scattering of Gaussian coils in terms of the scattered intensity, the scattering vector, and the radius of gyration. Three such equations are commonly used, those of Debye[7], Guinier[8] and Zimm[4].

Debye equation: $$I(Q) = I(0)\left(\frac{2}{u^2}\right)\left[e^{-u} + u - 1\right] \quad (7.28)$$

plotted as I(Q) *vs* Q

Guinier equation $$I(Q) = I(0)\, e^{-\frac{u}{3}} \quad (7.26)$$

plotted as ln[I(Q)] *vs* Q^2

Zimm equation $$\frac{1}{I(Q)} = \frac{1}{I(0)}\left[1 + \frac{u}{3}\right] \quad (7.27)$$

plotted as $I(Q)^{-1}$ vs Q^2

in each case $u = Q^2\langle s^2\rangle$, I(0) is intensity I(Q) at Q=0

For data fitted at a single concentration a correction for $\langle s^2\rangle^{1/2}$ is required to replicate the result from a full Zimm plot where concentration is extrapolated to zero. This requires a value for A_2, and takes the form;

$$\langle s^2\rangle_{true} = \langle s^2\rangle_{meas}(1 + 2A_2M_wc) \quad (7.31)$$

Each equation was fitted in the region where the equation holds true, described in section 7.2.2. Data sets from the scattering experiments have been fitted to each equation using a least squares fit using the GENPLOT computer software package.

7.3 SANS Instrumentation

Experiments have been performed on 3 instruments, LOQ at the Rutherford-Appleton Laboratory, and D16 and D17 at the Institute von-Laue-Langevin.

7.3.1 LOQ Spectrometer

LOQ is a small angle spectrometer using the ISIS pulsed spallation source[9]. The source is based on an 800MeV high intensity proton synchrotron, producing 200μA pulses of protons at 50Hz. The proton beam hits a uranium or tantalum target producing ≈$4x10^{16}$ fast neutrons/sec, these are moderated using liquid hydrogen at 25K and the thermal neutrons produced pass through a hole in the shielding to the LOQ beam guide. The neutrons' path includes a super-mirror bender removing those of wavelength below 2Å, an aperture, a chopper removing alternate pulses to prevent consecutive neutron pulses from merging, a frame overlap mirror to remove neutrons of wavelength above 12Å, collimation and an exit aperture before the sample. The incident wavelength is 2 to 10Å at 25Hz. The scattered neutrons are detected on a multiwire BF_3 detector of 64x64 $1cm^2$ cells to give a Q range of 0.006 to 0.22$Å^{-1}$. Data is analysed using a time of flight technique using the COLLETTE software[10]. Data is corrected for wavelength, thickness, transmission, background and detector efficiency to produce a scattering cross section in the form of Q, I(Q), and error in I(Q).

7.3.2 D16

Instruments at the ILL use a reactor as a source of continuous neutron radiation. The neutrons produced in the core are moderated with liquid deuterium at 25K to produce thermal neutrons. D16[11] uses a pyrolytic graphite monochromator to give a wavelength of 4.55Å. The neutron beam is collimated with adjustable slits before hitting the sample. The sample-detector distance is 50-100cm with a multiwire ^3_2He detector of 64 wires of 2.5mm spacing high by 16 wires of 5mm spacing wide. The detector and sample can be rotated to give an overall detector angle from 0 to 180°, giving a Q-range of 0.05 to 2$Å^{-1}$. Data is collected and analysed using a microVAX 11 computer using the ILL suite of

programs. Data is normalised against a known incoherent scatterer and output is absolute scattering cross section, in the form Q, I(Q), and error in I(Q).

7.3.3 D17

D17[11] uses the same neutron source as D16. Wavelength is selected using a velocity selector. The maximum intensity is at 12Å wavelength. After collimation the beam passes through a beam guide and the collimation before the sample. Sample detector distance can be varied from 0.8 to 3.46m. The detector can be rotated between 0 and 90° to give a Q-range of 0.003 to 1Å^{-1}. Data is collected and analysed using the ILL suite of programs on a microVAX 11 computer, correcting against a known standard (water) to give scattering in absolute scattering cross section, in the form Q, I(Q), and error in I(Q).

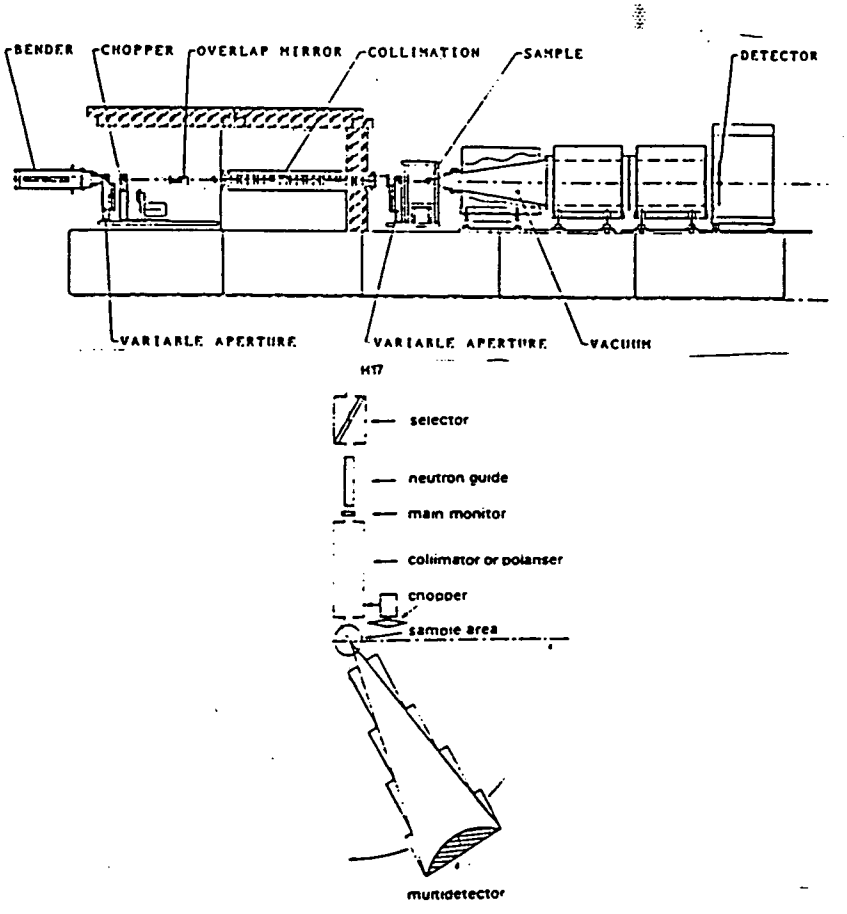

Figure 7.3: LOQ and D17 small angle neutron scattering spectrometers

7.4 Experimental

LOQ

A total of four experiments were performed on the LOQ spectrometer, these are identified thus;

LOQ-Aug90 - solutions of partially aromatised polymer

LOQ-Nov90 - solid solutions of partially aromatised polymer

LOQ-Nov91 - solutions of partially aromatised polymer

LOQ-May92 - solutions of partially aromatised polymer in shear cell

LOQ Aug90

This experiment was the first performed on the aromatised polymer, and was to assess the general suitability of the method for this study. Samples were prepared from 3 molecular weight fractions of a deuterated polymer. The polymer was aromatised in NMP, and the samples run as NMP solutions. Where possible (0-40% aromatisation) the polymer was precipitated and redissolved as necessary, allowing 24 hours for equilibriation before use. The highly aromatised samples were used as prepared, although this meant the solvent had undergone some degree of decomposition, producing a yellow colour unacceptable in light scattering however the elemental composition would not significantly change, therefore neither would the SANS signal.

A selection of samples were prepared for the experiment, covering 0 to ≈50% aromatisation, some at a range of concentrations to construct full Zimm plots (section 4.2.1). It was subsequently found that insufficient data was collected in the low Q region to allow these plots to be drawn. however the data did reveal changes in scattering with aromatisation indicating configurational changes and it was felt this merited further investigation using this technique. Results from this experiment are tabulated in table 7.3.

LOQ Nov90

This experiment was a study of solid solutions of deuterated polymer in a molecular weight-matched hydrogenous matrix, in order to assess the suitability of the method.

The samples were prepared by casting discs of the precursor polymer from chloroform solutions of mixed H/D polymer, then pyrolysing them as necessary at 250°C in a tube furnace under an inert atmosphere. The aromatisation of the polymers caused substantial problems as outlined in section 2.5.1, hence the aromatised samples were of poor quality and contained considerable voidage. It is possible there may also have been voids in the precursor polymer caused by the solvent evaporation.

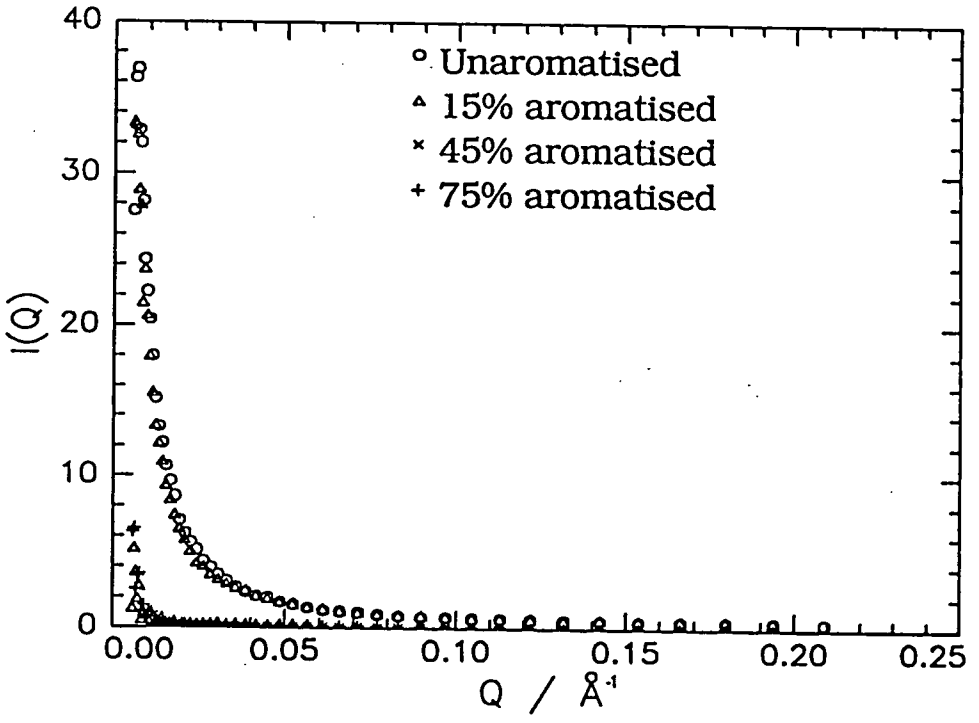

Figure 7.4: Scattering form solid state aromatised polymers.

The SANS data was collected from 3 molecular weight fractions, over a range of aromatisation. One fraction was made up at a range of concentration to construct Zimm plots, but again the Q-range meant this was not feasible. It can be seen in figure 7.4, where I(Q) vs Q plots for a polymer as it is aromatised are shown, that there is a very large decrease in signal intensity with aromatisation, suggesting a substantial fall in molecular weight (this is mentioned briefly in section 1.1.1).

It was concluded that because of the difficulties encountered of poor quality samples and the substantial drop in molecular weight with aromatisation, with the attendant fall in signal intensity, that further pursuing the solid state was not worthwhile and no further experiments were conducted. Results from this experiment are tabulated in 7.4.

LOQ Nov91

A series of samples from four molecular weight fractions were aromatised systematically, from 0% up to the point of precipitation, which became possible once the aromatisation reaction was mastered (section 2.5.2). As before the polymer was precipitated and redissolved where possible, or used as aromatised. A single concentration of each sample was prepared, 5% w/v, in hydrogenous NMP. The higher concentration was chosen to maintain a reasonable signal to noise ratio. Results from this experiment are tabulated in 7.5.

LOQ Mar92

This experiment was performed using a Couette type shear cell[12] (figure 7.5). This was to induce anisotropy in the sample to measure the dimensions of aromatised segments from the degree of anisotropy. This technique has been successfully applied to micelles of surfactants[6].

Samples were prepared from an unfractionated deuterated polymer (this was necessary to provide the large mass of polymer such a series of experiments required. Samples were prepared at 20%, 40%, 60% and 80% aromatisation following the usual procedure. The solutions were run under a range of shear rates, from zero to the maximum possible (where the meniscus became unstable) increasing speed with consecutive experiments. The sample name refers to the degree of aromatisation and the rotor speed in RPM. This can be converted to shear rate by multiplying the rotor speed by 5.28 s^{-1}. A few samples of a subsidiary experiment were also run, using 1% deuterated polymer in an overall 5% polymer solution to attempt to observe single chain configurations, however the experiment was severely curtailed by lost beam time and the fully hydrogenous background samples were not run. Results from this experiment are tabulated in 7.6.

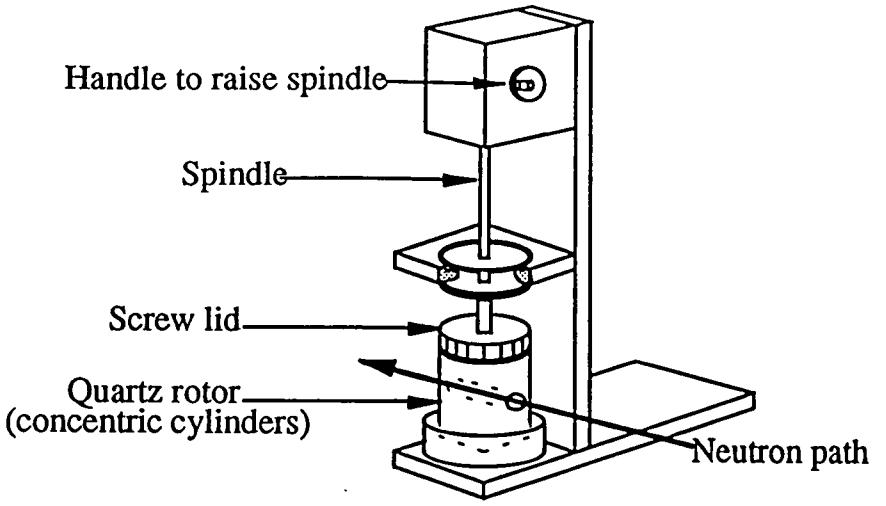

Figure 7.5: Coeutte shear cell used on LOQ.

D17-Oct90

Samples used in this experiment were prepared in the same manner as those for LOQ-Aug90. It had originally intended to produce samples at 10%, 20%, and 40% aromatisation for two fractions, however at this stage it was not possible to produce samples as accurately as for subsequent experiments, and the samples used are more randomly distributed. Samples were run in Hellma 1mm pathlength cells, at a range of concentrations in order to construct Zimm plots. The detector was set at 4.96°, allowing maximum Q while retaining the transmitted beam on the detector, with a sample to detector distance of 3.46m. The wavelength of neutron radiation was 12Å. The range of Q was 0.0066 to 0.095$Å^{-1}$.

7.5 Results

Results of fits to equtions 7.26-7.28 are tabulated below. Sample names are given as follows

Tables 7.3/4: letters refer to fraction(table 2.4), followed by percentage aromatisation, and concentration, eg., AE14-3%;fraction AE, 14% aromatised, 3% w/v concentration.

Table 7.5 letter refers to fraction(table 2.5), followed by percentage aromatisation, eg., A20; fraction A, 20% aromatised

Table 7.6 numbers following D(=deuterated) are percentage aromatisation, numbers following R(=rotation) are rotor speed in revolutions per minute(= shear rate/5.28)

Table 7.13 letter refers to fraction number to percentage aromatisation

7.5.1a LOQ Results- Debye, Guinier and Zimm fits

Sample	Debye		Guinier		Zimm	
	I(0)	$\langle s^2 \rangle^{1/2}$ /Å	I(0)	$\langle s^2 \rangle^{1/2}$ /Å	I(0)	$\langle s^2 \rangle^{1/2}$ /Å
AE0 5%	2.14	43	2.16	46	2.41	60
AE14 3%	2.07	56	2.35	61	2.43	69
AE25 5%	2.18	53	2.50	60	1.23	52
AE45 5%	10.9	60	9.53	59	12.4	105
AF0 5%	3.26	51	3.56	61	3.52	58
AF13 5%	1.74	38	2.40	57	1.75	39
AF45 5%	14.6	105	15.5	103	18.3	142
AG0 5%	2.92	48	3.03	49	3.16	56
AG27 1%	2.21	105	2.07	87	2.68	137
AG27 2%	2.30	75	2.25	68	2.45	89
AG27 5%	2.74	70	3.00	71	2.61	64
AG38 1%	5.98	180	4.86	134	7.70	244
AG38 2%	3.49	130	3.52	121	4.40	179
AG38 5%	4.59	68	4.86	71	5.12	82
AG39 1%	1.48	99	1.74	107	1.30	95
AG39 2%	3.54	108	3.77	108	3.33	109
AG39 3%	3.32	87	3.26	76	3.75	106
.AG39 5%	3.77	84	4.01	84	3.81	87
AG45 2%	12.1	78	21.7	72	14.4	102

Table 7.3: Fitted values from LOQ-Aug90 experiment

Percentage aromatised	0 %		15 %		45 %		75 %	
Sample	I(0)	$\langle s^2 \rangle^{1/2}$ /Å	I(0)	$\langle s^2 \rangle^{1/2}$ /Å	I(0)	$\langle s^2 \rangle^{1/2}$ /Å	I(0)	$\langle s^2 \rangle^{1/2}$ /Å
AD 5%	10.4	315	7.1	210	0.17	40	2.9	450
AF 2%	4.8	180	4.1	225	-	-	-	-
AF 4%	2.8	187	4.9	209	-	-	-	-
AF 5%	6.7	195	5.5	169	-	-	-	-
AH 5%	4.7	163	3.0	150	-	-	-	-

Table 7.4: Fitted values from LOQ-Nov90 experiment, Debye equation

Sample	Debye		Guinier		Zimm	
	I(0)	$\langle s^2 \rangle^{1/2}$ /Å	I(0)	$\langle s^2 \rangle^{1/2}$ /Å	I(0)	$\langle s^2 \rangle^{1/2}$ /Å
A0	4.45	55	5.25	62	4.48	50
A10	2.34	42	2.34	41	2.58	51
A20	2.67	49	2.78	54	2.72	56
A30	4.04	74	3.60	62	4.21	84
A40	5.76	74	5.95	76	5.95	85
A50	62.7	149	33.3	85	61.9	168
A60	68.6	132	60.0	107	79.6	164
A80	400	278	350	225	620	420
B0	3.19	50	3.29	54	3.19	56
B10	2.70	46	2.77	51	2.70	53
B20	2.86	54	3.13	66	2.86	66
B30	3.21	58	3.19	55	3.21	70
B60	66.6	124	63.6	110	77.0	150
B80	2100	700	545	270	2100	900
C0	2.68	45	2.97	58	2.76	54
C10	2.53	39	2.70	48	2.59	45
C20	5.76	74	6.02	79	5.76	83
C30	4.91	73	5.13	69	5.01	75
C50	27.0	95	27.7	79	32.8	120
C60	71.7	134	66.1	114	77.0	156
C80	2666	780	537.1	265	1750	750
D0	1.47	36	1.69	23	1.97	37
D10	1.41	32	1.41	29	1.41	30
D20	1.47	34	1.43	33	1.48	37
D30	3.54	64	3.53	63	3.62	72
D40	19.5	87	18.4	73	29.2	130
D60	110	160	123	180	113	190
D80	2050	660	630	280	2020	780

Table 7.5: Fitted values from LOQ-Nov91 experiment

Sample	Debye		Guinier		Zimm	
	I(0)	$\langle s^2\rangle^{1/2}$ /Å	I(0)	$\langle s^2\rangle^{1/2}$ /Å	I(0)	$\langle s^2\rangle^{1/2}$ /Å
D20R0	1.77	47	2.37	44	1.84	52
D20R10	1.83	49	2.15	42	1.75	47
D20R100	1.75	44	2.12	46	1.98	54
D20R1000	1.77	44	2.46	54	1.82	46
D20R2000	1.78	48	2.12	33	1.95	49
D40R0	5.13	74	5.47	49	5.19	78
D40R100	2.64	49	3.25	49	2.65	51
D40R1000	2.44	46	3.41	51	2.68	54
D40R2000	4.82	73	5.11	49	5.07	82
D40R3000	4.78	73	5.45	49	5.18	86
D60R0	38.1	128	40.2	80	39.7	148
D60R10	37.5	124	38.9	77	39.5	146
D60R100	36.8	125	38.9	78	37.3	140
D60R1000	13.9	77	16.2	71	12.6	75
D60R2000	13.0	72	17.6	78	12.5	77
D80R0	80.8	130	82.6	75	87.6	157
D80R10	72.8	121	80.2	79	76.0	142
D80R100	69.0	116	77.2	73	73.0	138
D80R500	78.0	131	93.3	89	64.0	128
D80R1000	74.7	131	93.5	92	58.9	127
D80R2000	75.5	140	93.9	95	70.7	136

Table 7.6: Fitted values from LOQ-Nov91 experiment

Molecular weights values (weight average) can be obtained from the intensity at zero-Q. For the time of flight data obtained on LOQ this is done by converting scattering into absolute intensity by comparison to a well defined standard, in this case a solid solution of deuteropolystyrene(PSD) in molecular weight matched hydrogenous polystyrene(PSH). Molecular weights can be obtained *via* the equation;

$$\frac{1}{M_w} = \frac{1}{I(0)}\left(K_m c_D (1-c_D)(\rho_D - \rho_H)^2\right) \qquad (7.31)$$

where K_m is a machine constant which should remain the constant during the experiment. K_m is calculated from the polystyrene standard, and whence used to calculate M_w for polymers subsequently run. standard polystyrene runs are tabulated in 7.7. True values[13] for the calibrant are M_w(PSD)=77,400, M_w(PSH)=75,000, $\langle s^2\rangle^{1/2}$=73.2±2Å, c=19.8%PSD in PSH.Values of $\langle s^2\rangle^{1/2}$ and I(0) for the

It is also necessary to correct radii of gyration using the equation;

$$\langle s^2 \rangle = \langle s^2 \rangle (1 + 2M_w A_2 c) \qquad (7.32)$$

Corrected values of M_w and $\langle s^2 \rangle^{1/2}$ for the samples from experiment LOQ-Nov91 are given in table 7.8, along with the molecular weights from SEC in table 7.9 where these have been measured. The three fitting methods give widely varying values for the parameters I(0) and $\langle s^2 \rangle^{1/2}$. It is suggested by Glatter and Kratky that a mean of the values from the Zimm and Guinier fits are taken as a representative value for polymer chains. It is also suggested that of these methods the Guinier approximation best represents structures with dense cores, and could therefore be regarded as the better method for analysing the data from the aggregated highly aromatised polymers.

Experiment	Debye		Guinier		Zimm	
	I(0) K_m	$\langle s^2 \rangle^{1/2}$ /Å	I(0) K_m	$\langle s^2 \rangle^{1/2}$ /Å	I(0) K_m	$\langle s^2 \rangle^{1/2}$ /Å
LOQ-Aug90	33 *3.87× 10⁻⁵*	67	34 *3.99× 10⁻⁵*	62	35 *4.11× 10⁻⁵*	76
LOQ-Nov90	30 *3.52× 10⁻⁵*	70	35 *4.11× 10⁻⁵*	63	32 *3.75× 10⁻⁵*	71
LOQ-Nov91	65 *7.63× 10⁻⁵*	73	82 *9.62× 10⁻⁵*	70	67 *7.86× 10⁻⁵*	77
LOQ-May92	70 *8.21× 10⁻⁵*	72	88 *1.03× 10⁻⁵*	71	71 *8.33× 10⁻⁵*	75

Table 7.7: Fitted parameters from standard polystyrene sample

Sample	Debye		Guinier/Zimm	
	M_w	$\langle s^2 \rangle^{1/2}$ / Å	M_w	$\langle s^2 \rangle^{1/2}$ / Å
A0	73 000	330	63000	340
A10	37 000	112	33 000	118
A20	42 000	116	36 000	125
A30	62 000	255	49 000	233
A40	85 000	169	74 000	179
A50	860 000	---	360 000	---
A60	830 000	---	620 000	---
A80	4 000 000	---	3 200 000	---
B0	52 000	180	53 000	200
B10	43 000	126	37 000	139
B20	45 000	130	39 000	153
B30	49 000	185	40 000	188
B60	800 000	---	650 000	---
B80	20 000 000	---	5 000 000	---
C0	44 000	120	47 000	160
C10	41 000	108	38 000	127
C20	90 000	216	35 000	183
C30	75 000	268	76 000	265
C50	370 000	---	300 000	---
C60	870 000	---	680 000	---
C80	26 000 000	---	4 900 000	---
D0	24 000	70	27 000	60
D10	23 000	74	40 000	82
D20	23 000	69	41 000	82
D30	54 000	211	98 000	118
D50	270 000	---	200 000	---
D60	1 300 00	---	1 300 000	---
D80	20 000 000	---	5 800 000	---

Table 7.8: Corrected molecular weight data from LOQ-Nov91 experiment (In table 7.8 the correction to molecular weights is done with the absolute value(table 7.9) where possible, otherwise the SANS value is used)

Sample	$M_{w\text{-SEC}}$	$M_{w\text{-Absolute}}$	$M_{w\text{-corrected SANS}}$	$\langle s^2 \rangle^{1/2}_{Abs.}$ / Å	$\langle s^2 \rangle^{1/2}_{Abs.}$ / Å
A0	640 000	350 000	73 000	390	330
B0	225 000	100 000	52 000	190	180
C0	120 000	50 000	44 000	125	120
D0	50 000	20 000	24 000	73	70

Table 7.9: Absolute molecular weights corresponding to values from SEC measurements

Sample	Debye	
	M_w	$\langle s^2 \rangle^{1/2}$ /Å
D20R0	24 000	97
D40R0	62 000	157
D60R0	860 000	---
D80R0	1 900 000	---

Table 7.10: Corrected data from experiment LOQ-May92

The values for M_w from SANS differ significantly from the SEC molecular weights, and the corresponding absolute values given in table 7.9, especially at high molecular weight. The reason for this is not clear, incorrect levels of deuteration was one possibility, therefore the level of deuteration of the monomer and the aromatised polymer after the SANS experiment was verified by NMR(section 2.6). This was performed by comparing the quantity of ^1H nuclei in a known mass of sample against that in a known mass of ethylene dichloride. Both samples were found to be in excess of 99% deuterated as has been assumed. The error may therefore be due to the data relying on measurement at a single concentration. The values from D17 using similar samples(section 7.5.1b), but at a range of concentration to construct full Zimm plots, do not show the same errors. Full Zimm plots were not possible on LOQ because of the limited number of points in the necessary Q-range.

There is no reason to doubt the validity of the SEC results, and these can be corrected against the M_{wSEC}/M_{wILS} relationship(Section 4.7) to give true values. The molecular weights calculated from SANS, at least those of higher molecular weight where the deviation is greatest, are therefore not correct. The error is not a proportional error which could be corrected but also contains some molecular weight dependency. Polymers of low molecular weight, those of $M_w \approx 50{,}000$ or less appear to have the correct values, those above are progressively undervalued as M_w rises. This may be due to an insufficient Q range being available for higher molecular weight polmers, molecular weight is obtained from the Guinier region, from Q = 0 to $1/\langle s^2 \rangle^{1/2}$, although this can be extended to $Q=2/\langle s^2 \rangle^{1/2}$ for polydisperse polymers. Figure 7.19 shows the range of data over which Fits have been made. These molecular weights therefore are of value for purposes of comparison with one another to determine behaviour with

aromatisation, especially if a wide range of molecular weight is covered, but not as the basis for firm relationships.

Bearing this in mind it can be seen that the molecular weights follow a pattern similar to that observed in the ILS measurements. Aromatisation from 0 to 10% causes a fall in molecular weight, more pronounced for higher molecular weight fractions, so that the fractions tend to converge. The fall in M_w is also greater than would be expected from stoichiometry alone, following the pattern in SEC and ILS measurements, and was probably due to thermal chain degradation. The randomness of the aromatisation process is also seen once again as the original molecular weight order of the fractions is lost.

Between 10 and 20% aromatisation the molecular weights rose slightly, here the behaviour is more like that seen in ILS with solutions of polymer in $CHCl_3$ rather than that in NMP, the solvent used for the SANS experiments. The solutions used for SANS were more concentrated (5%) than the solutions used in ILS (~0.2-1%) to achieve a good signal to noise ratio, and these more concentrated solutions aggregated more readily. Further increase in molecular weight occurred as conversion to polyphenylene increased 20-30-40%, and the increasing aromaticity of the chain led to greater aggregation. Forty percent is the maximum extent of conversion where the polymer can be precipitated and redissolved, because of the extent of aggregation, and above 40% a very sharp increase in molecular weight was seen, continuing up to 80% where the aromatised polymer was close to precipitating from the solution, and the solution gel-like, corresponding to a network forming between aggregates.

In contrast the corrected values of the radii of gyration measured for the polymers compare favourably with the values from correction of SEC data. With the exception of fraction A (distortion here was due to the low value of M_w used for the correction) the SANS radii of gyration are ≈5% less than those from ILS. The difference may arise from the higher concentration of the solutions used. The same pattern was followed by the aromatised polymers, where the radii of gyration were slightly below what might be

expected from ILS. Table 7.11 shows the molecular weight dependency of the radii of gyration according to the equation;

$$\langle s^2 \rangle^{1/2} = \delta M_w^{\gamma},$$

for the corrected Debye values only (averaged values from the Guinier and Zimm fits did not give linear plots). Fits are shown in figure 7.18.

Percentage aromatisation	δ	γ
0	0.00007	1.37
10	0.029	0.78
20	0.016	0.84
30	0.014	0.88
60*	0.019	0.48
80*	0.061	0.55

Table 7.11: Parameters of molecular weight dependency of radii of gyration of partially aromatised poly(DHCD-DMC) from SANS(c.f. table 4.16 for ILS)
* *:values for* $\langle s^2 \rangle^{1/2}$ *were uncorrected*

The value of γ for the unaromatised polymer, which is a measure of chain extension, is a spurious value because of the molecular weight discrepancies discussed above, M_w for the unaromatised polymer covers a wide range, greater than one decade the margin of error is therefore large. The values of γ for 10 to 30% aromatisation progressively increase, indicating an increase in chain stiffness as the polymer is aromatising. The values of the exponent γ for SANS are in contrast to those from ILS where the initial increase caused by extension as the polymer stiffened is outweighed by aggregation, and γ starts to decrease after 10% aromatisation. This suggests that SANS is less sensitive to the presence of aggregates in the solution than ILS, although the increase in molecular weight with aromatisation shows that their presence is detected. This is because larger particles scatter in a lower Q region, outside the range of LOQ.

The value of γ reaches a peak at 30% aromatisation, and then decreases, in comparison with a maximum at 10% for ILS and 20% for viscometry. Beyond this each technique shows a fall, attributed to the agglomeration of highly aromatised chains forming large more compact structures than the single chain, and by 60% aromatisation the value of γ has fallen to 0.48, that is below that of a coil in the theta condition.

Solid state experiment - LOQ-NOV91

Experiment LOQ-Nov91 was a study on solid samples of the polymer to assess changes in the configuration when the aromatisation reaction was performed in the solid state. Samples of 0%, 15%, 45%, and 75% aromatisation were prepared and the scattering function measured, a set of scattering functions for one fraction are shown in figure 7.4. The results from the solid state experiment, LOQ-Nov91, show a dramatic change in the polymer to occur during aromatisation. The scattering from the unaromatised polymer is that of a typical Gaussian chain. The relationship between M_w and $\langle s^2 \rangle^{1/2}$,

$\langle s^2 \rangle^{1/2} = 0.31\ M_w^{0.51}$

typical of that for a Gaussian chain. This is close to the relationship derived by Ballard *et al*[14],

$\langle s^2 \rangle^{1/2} = 0.26\ M_w^{0.5}$

As the polymer is aromatised to 15% little change is observed, there is a slight fall in intensity as the molecular weight falls, the fall in molecular weight is greater than would be expected from the reaction stoichiometry, indicating some chain scission has occurred. The molecular weight dependency on radius of gyration is;

$\langle s^2 \rangle^{1/2} = 0.19\ M_w^{0.55}$

A significant change is seen as the polymer is aromatised to 45%. The intensity has dropped very sharply, These samples of polymer contained a large amount of voidage, due to the blowing action of the gases evolved in the reaction, and so the high scattering at low Q is due to void scattering, while the very low scattering at higher Q is from the polymer, it is therefore not possible to obtain fits of the Debye equation, for example. There is also much greater uncertainty in the data as the low signal to noise ratio would require much greater counting times than was possible.

The problem can be illustrated by comparing the Kratky plots of the scattering functions. At the low aromatisation the scattering function is a smooth curve, which, although not displaying the classical scattering function of the wormlike chain is typical of the

scattering functions obtained from other polymers. The scattering from the highly aromatised polymers shows no obvious features.

The fall in intensity is due to excess loss of mass caused by chain scission, and it is known that at full aromatisation the chain lengths of the polymers are reduced to a mean of 8 or so[15]. In view of this and the poor results which were obtained, together with the difficulty in preparation of the samples it was decided not to continue the investigation of solid state aromatised polymers

Shear experiment - LOQ-May 92

The experiment LOQ-May92 was intended to determine whether the partially aromatised polymer displayed anisotropy under shear conditions, The presence of a shear field can cause micelles to align, and it then becomes possible to measure their dimensions from the degree of anisotropy of the signal. If the cores of the micelles formed by the aromatising poly(DHCD-DMC) solutions consist solely of poly(paraphenylene) then it is likely that they will pack in cylindrical form (figure 7.6) it is also possible therefore that in a shear field the cylindrical

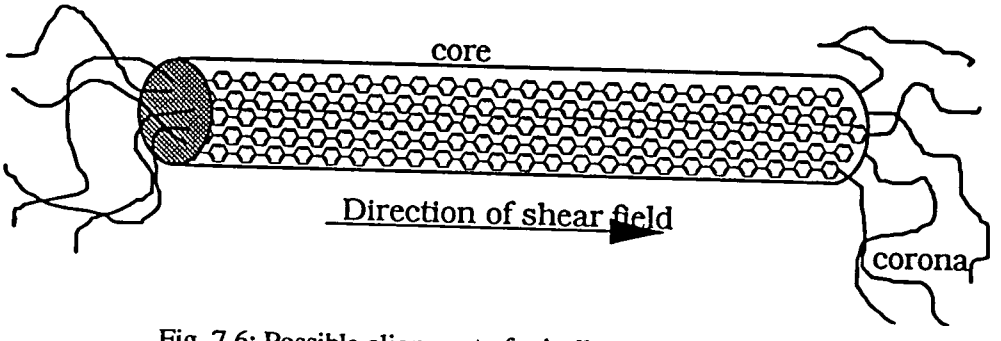

Fig. 7.6: Possible alignment of micelle core in shear field

domains could align. The experiment was performed using a range of rotor speeds from zero to the maximum possible. No anisotropy was observed during the experiment. This may mean that the supposition of cylindrical cores is incorrect, or that the shear rate obtained was insufficient to cause them to align. For very small cores a very high shear field would be required to cause alignment, this was not possible using the Couette cell as the meniscus of the solutions became unstable.

It would also be expected that if the solutions contained aggregates then the application of an external force would cause them to break up, and would be seen as a decrease in intensity($I(0) \propto M_w$). It is seen in figure 7.7 that this was not necessarily the case, with the exception of the 60% aromatised sample. There was an initial fall in intensity at low shear rate, but this was recovered at higher shear rates. Therefore there is some initial shear induced dissociation at low shear, but higher shear rate either causes the aggregates to reassociate, or return to their original condition. This may be the result of the strong aggregation tendency of the aromatised polymer, which is sufficient to resist the shear forces at low rotation, while at higher rotation the aggregation may be aided by the shearing action on the micelle exposing the aromatised core.

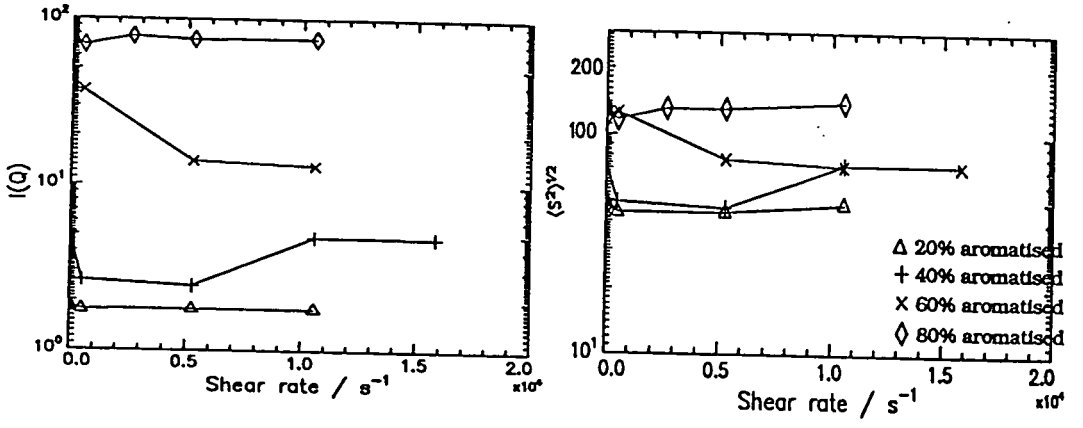

Figure 7.7: Change in i.scattered intensity, and ii.radii of gyration in shear field

7.5.1b Experiment on D17 - Oct 90

An experiment was conducted on the D17 spectrometer identified as;

D17-Oct90.

The samples were solutions of partially aromatised polymer. This experiment was performed at a sufficiently low Q-range to allow full Zimm plots to be constructed, and molecular weights, radii of gyration and second virial coefficient to be determined. It was therefore unnecessary to fit equations (26)-(28).

The Zimm plotting method is similar to that employed in ILS (section 4.2.1). The data was plotted as c(1-c)/I(Q) vs Q^2+c/10, where c is the concentration in g/ml, with four concentrations per sample. The data was extrapolated to Q=0 and c=0, and the intercepts of the extrapolated lines measured, and their common intercept determined. The molecular dimensions were the extracted using the equations,

$M_w = 1/K^*I_0$, $\langle s^2 \rangle = 3K^*M_wG_{c=0}$ $A_2 = G_{Q=0}/20$

where I_0 is the common y-intercept, $G_{c=0}$ the gradient as $c \rightarrow 0$, $G_{Q=0}$ the gradient as $Q \rightarrow 0$ and $K^* = 4\pi ft(\rho_p-\rho_m)^2T_s / t_w(1-T_w)N_A$

where f; correction factor for incoherent scattering of water, t/t_w; thickness of sample/water, T_s/T_w; transmission of sample/water, and ρ_s/ρ_m; scattering length density of scattering species/matrix

The Zimm plots obtained are shown in figures (7.8*a-h*), and the results are tabulated in 7.13.

Sample	M_w	$\langle s^2 \rangle^{1/2}$ / Å	A_2 / $cm^3\ g^{-1}$
D 0%	1,230,000	620	0.00065
E 0%	571,000	340	0.00079
G 0%	415,000	190	0.00084
H' 0%	377,000	240	0.00092
H' 13%	346,000	170	0.00076
H' 25%	281,000	140	0.00103
G 28%	218,000	130	0.00065
G 38%	495,000	260	0.00026

Table 7.13: Results from Zimm plots, D17Oct90.

The pattern shown in the molecular weights from this experiment are once more similar to those already seen in the light scattering measurements, there is an initial fall in molecular weight, followed by an increase at higher aromatisations as the polymer begins to aggregate.

The partially aromatised polymers measured by SANS have higher molecular weights than those hydrogenous polymers measured in either NMP or chloroform solutions by ILS. This may be due in some part to increased aggregation, but it is also possible that it is due to a true higher molecular weight of the deuterated aromatised polymers. This

would be an isotopic effect, it is seen in chapter two that a deuterated polymer is of a much higher molecular weight than a hydrogenous one polymerised under the same conditions, and has a lower polydispersity. This is attributed to lower extent of chain transfer, therefore fewer 1,2-bonds in the in deuterated polymer chain. Since these weaker links are thought to break during the aromatisation, leading to greater than stoichiometric fall in molecular weight, a polymer with fewer 1,2 bonds will degrade less, as is observed here. This does not appear to be the case with the deuterated polymers used in the LOQ-NOV91 experiment, however the polymer for this experiment were deliberately prepared at a higher temperature to increase the rate of chain termination reactions(section 2.3), producing a polymer of broader polydispersity and lower molecular weight (see tables 2.4/5). This may also have increased the rate of chain transfer sufficiently to overcome the isotopic effect, and incorporate a sufficient number of 1,2-bonds into the main chain to replicate the behaviour of the hydrogenous polymer. In this case the results of the LOQ-NOV91 experiment should be closer to the rest of the results in the study than those of the D17-OCT90 experiment.

When compared to the corresponding figures from ILS the values of $\langle s^2 \rangle^{1/2}$ are ≈60% of the corresponding values from ILS, due to the higher concentrations of the solutions used for SANS (2-5%) against those for ILS (0.1-1%). Values of second virial coefficient are ≈85% of the corresponding SANS values. Again this is due to the increased concentration.

7.5.2 Configuration of aromatised polymers

The configuration of aromatised polymers in solution can be determined by comparison of the SANS scattering function to those of model configurations. In this case fitting has been done to the models of the Gaussian coil, the Debye equation (7.28), the results of which are given in tables 7.4-6, and to various scattering functions of the wormlike chain (eqs. 1.55/56/62). The Gaussian coil model is defined in terms of the radius of gyration, and takes no account of chain stiffness, the wormlike models are defined in terms of the persistence length and the mass per unit contour length, and so incorporate chain stiffness. The Debye equation therefore only applies as far as the plateau region of the typical scattering behaviour (fig. 7.3), the wormlike models apply over a greater range of the scattering vector including the upturn from the plateau (region C in fig. 7.3). The wormlike models fitted are those of i.Yamakawa[16], ii.Muroga[17], and iii.Sharp & Bloomfield[18]. These are described in section (1.2.4.e) and are not reproduced here.

Scattering functions from SANS data were been fitted by normalising the dataset, using I(0) from the Debye fit, and for i. and ii. fitting the model by manual iteration, it was not possible to incorporate them into a computer fitting routine because of their complexity. Equation iii. is less complex and was fitted using a least squares routine.

Datasets from experiments D17-OCT90, LOQ-NOV91 and LOQ-NOV92 were fitted since these are the best quality data

7.5.2a D17-OCT90

In section 7.6.4 it is stated that the data collected on D17 was the highest quality SANS data obtained in the low Q region, the data quality is also good in the intermediate Q region. The range of aromatisation at which data was collected is however rather limited, samples of 0, 13, 25, 28 and 38% aromatisation were measured together with a single 'highly aromatised' sample at 44% aromatisation, but this should be sufficient to provide an illustration of the configurational changes during the early stages of aromatisaton. The fits of D17 data, using the 5% polymer concentration samples, are

tabulated in 7.13. The fits are shown plotted in the Kratky format, as this method best illustrates the small differences between data and model.

Sample	Yamakawa		Koyama		Sharp & Bloomfield	
	a / Å	L / Å	a / Å	L / Å	a / Å	L / Å
D - 0%	23	405	15	550	4	2070
E - 0%	24	420	18	510	5	1880
G - 0%	22	480	12	790	4	2450
H - 0%	22	420	18	480	5	1740
H - 12%	26	330	20	380	4	1670
H - 25%	28	360	18	650	6	1910
G - 27%	25	500	20	600	19	640
G - 38%	32	600	30	900	28	660
E - 44%	35	1550	35	1500	21	2380

Table 7.13: Fitted parameters from Kratky-Porod type models.

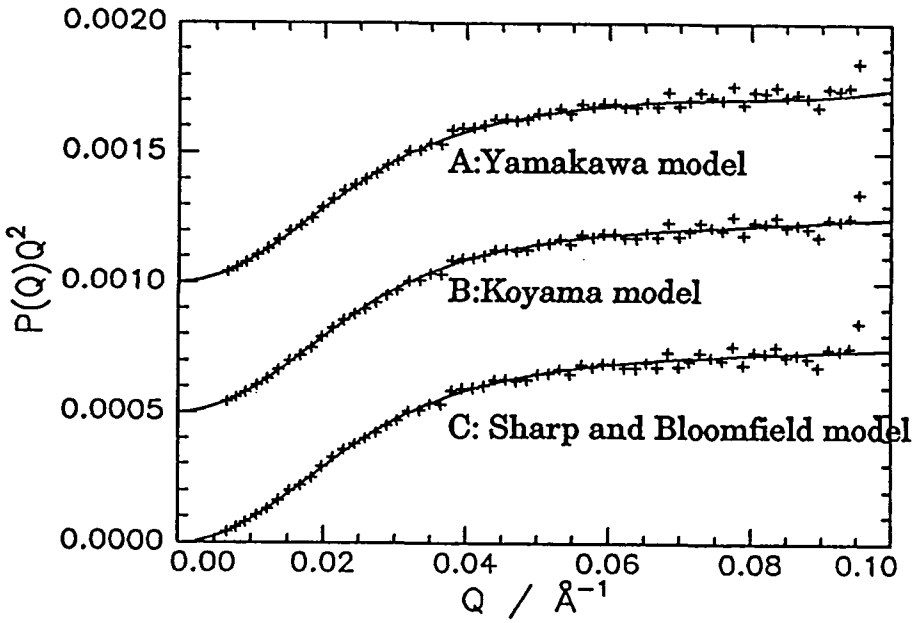

Fig. 7.9*a*: Best iterative fits to Fraction D, 0%.

Yamakawa; a=23Å, L=405Å, Koyama; a=15Å, L=550Å, S-B; a=4Å, L=2040Å.

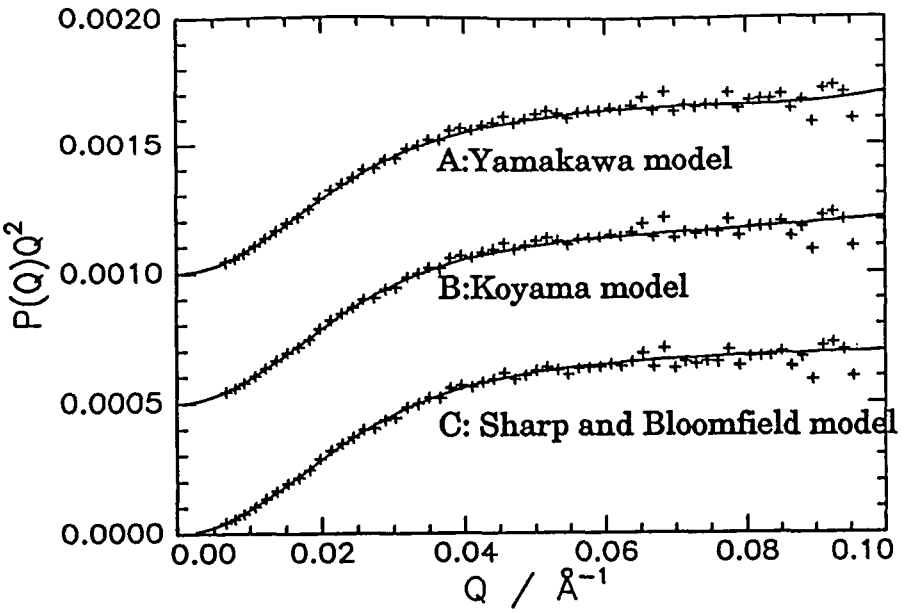

Fig. 7.9*b*: Best iterative fits to Fraction E, 0%.

Yamakawa; a=24Å, L=420Å, Koyama; a=18Å, L=510Å, S-B; a=5Å, L=1880Å.

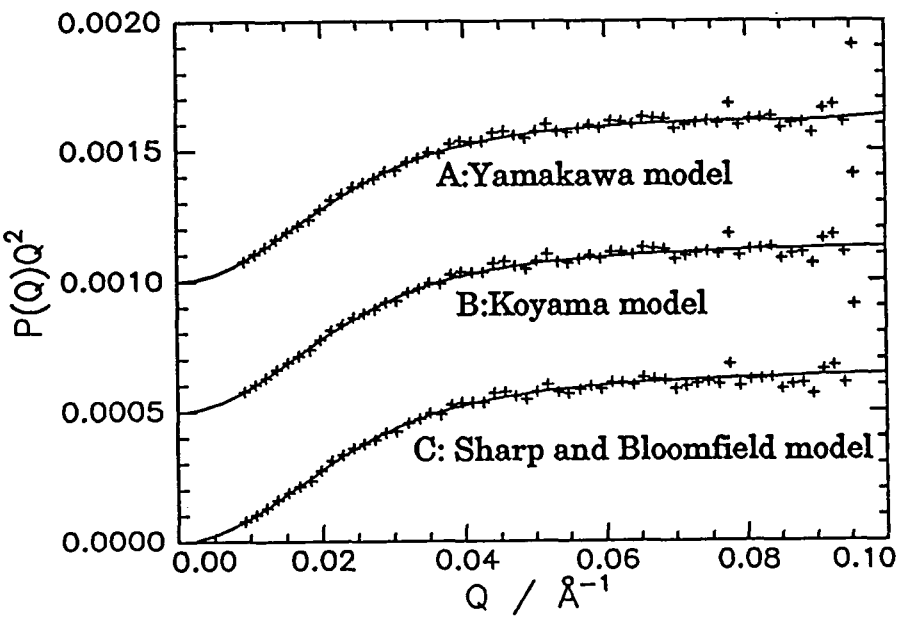

Fig. 7.9*c*: Best iterative fits to Fraction G, 0%.

Yamakawa; a=22Å, L=480Å, Koyama; a=12Å, L=790Å, S-B; a=4Å, L=2450Å.

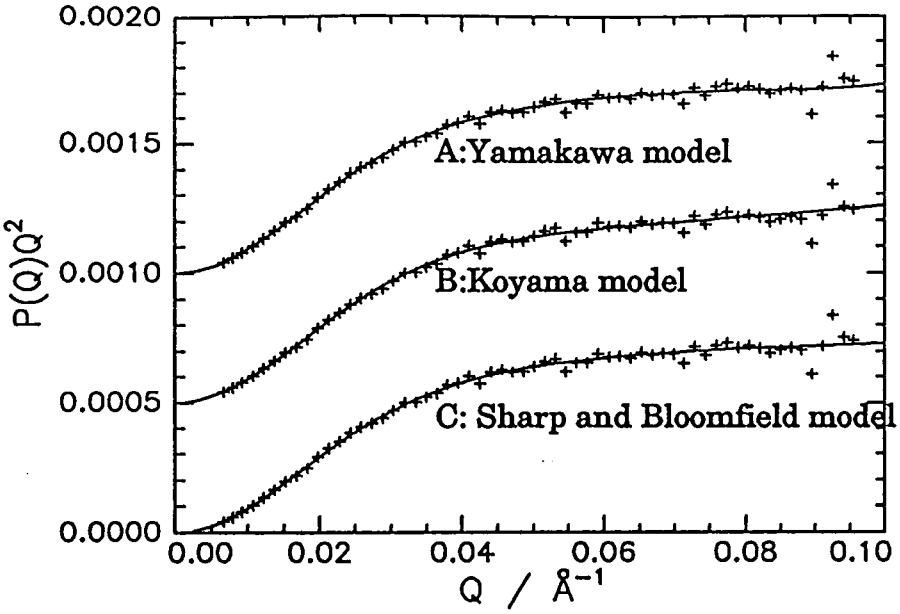

Fig. 7.9*d*: Best iterative fits to Fraction H, 0%,

Yamakawa; a=22Å, L=420Å, Koyama; a=18Å, L=480Å, S-B; a=5Å, L=1740Å.

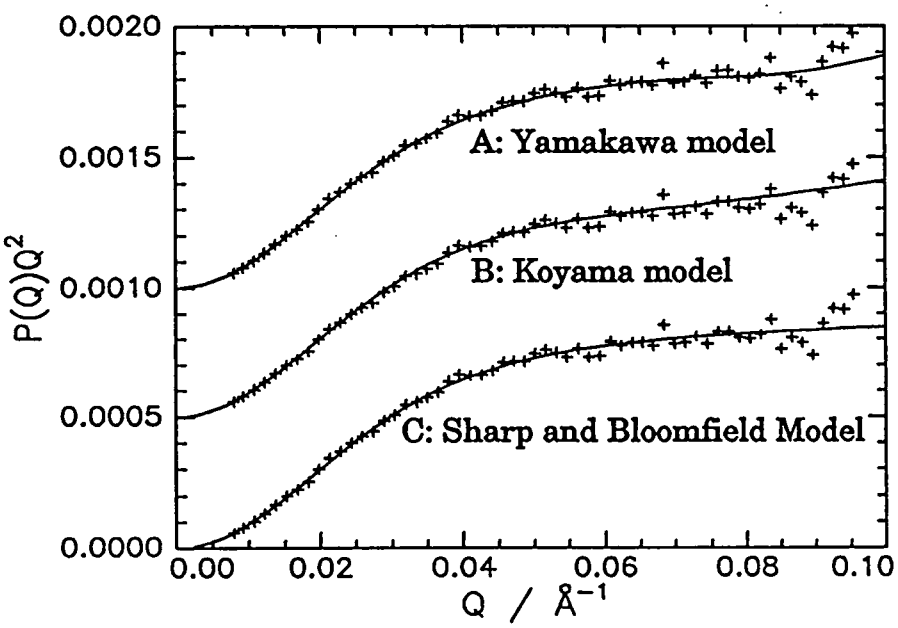

Fig. 7.9*e*: Best iterative fits to Fraction H, 12%.

Yamakawa; a=26, L=330Å, Koyama; a=20Å, L=380Å, S-B; a=4Å, L=1670Å.

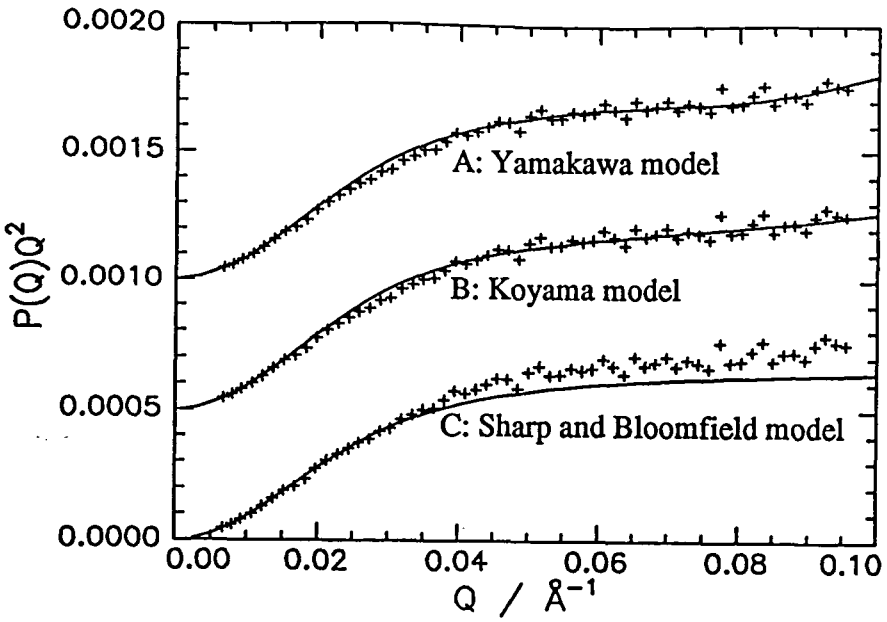

Fig. 7.9*f*: Best iterative fits to Fraction H, 25%.

Yamakawa; a=28Å, L=360Å, Koyama; a=20Å, L=450Å, S-B; a=6Å, L=1910Å.

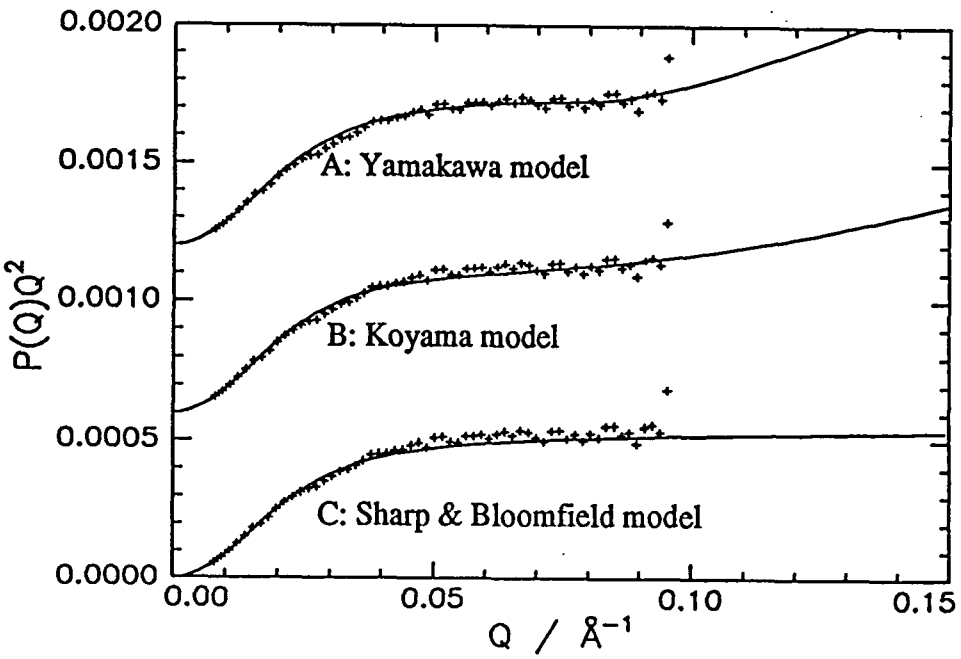

Fig. 7.9*g*: Best iterative fits to Fraction G, 27%.

Yamakawa; a=25Å, L=500Å, Koyama; a=20Å, L=600Å, S-B; a=19Å, L=640Å.

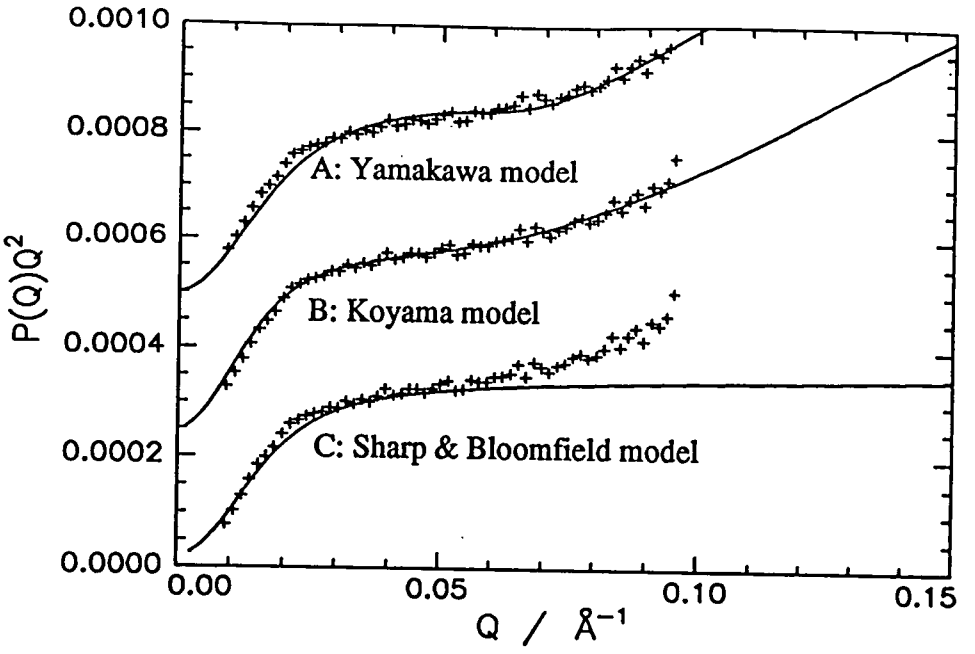

Fig. 7.9*h*: Best iterative fits to Fraction G, 38%.

Yamakawa; a=32Å, L=600Å, Koyama; a=30Å, L=900Å, S-B; a=28Å, L=660Å.

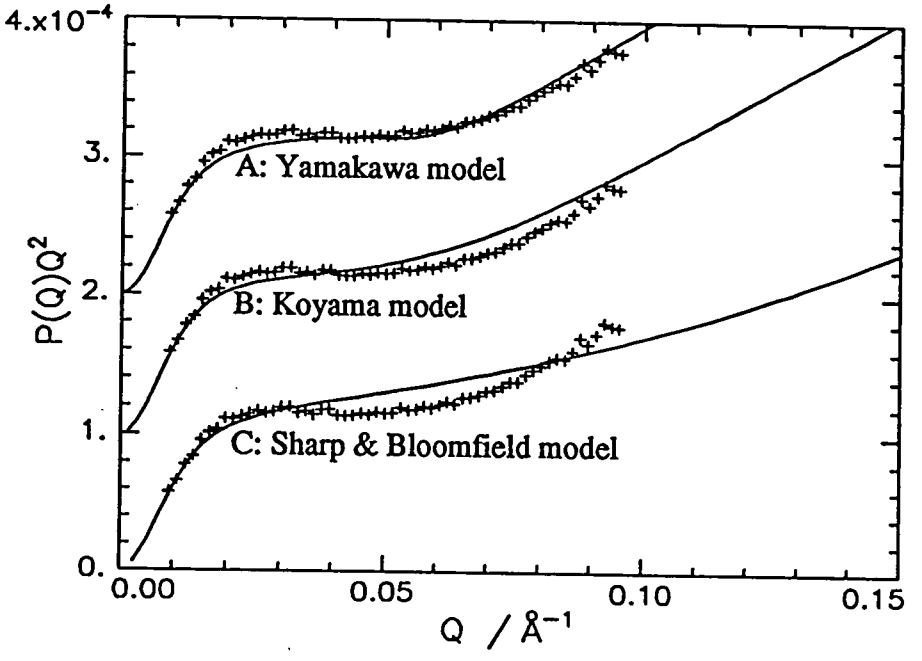

Fig. 7.9*i*: Best iterative fits to Fraction G, 44%.

Yamakawa; a=35Å, L=1550Å, Koyama; a=35Å, L=1500Å, S-B; a=21Å, L=2380Å.

From the plots in figure 7.9 it is seen that the Sharp and Bloomfield model is not generally a good model for the polymers, it does not display the pronounced upturn at Q* which is clearly evident in the scattering data of the more highly aromatised

polymers, and therefore under-estimates the value of a. This difference is more pronounced for the unaromatised polymers. The S-B model was fitted by a least squares fitting routine, and was weighted in favour of the low Q region, because of the greater concentration of data in this region. The scattering function of the SB model(eq.1.62) is relatively straightforward, therefore the model is simplistic, the models of Yamakawa and Koyama are more complex, and give a better approximation to the data, especially for those at higher degrees of aromatisation where the upturn was clearly defined. The models differ slightly in the 'best fit' values which are obtained because of the different form of the model curves. Fitting for the unaromatised polymers in these cases was less certain because a clear upturn from the plateau is not observed, and a number of other sets of parameters could have been given, in these cases the values shown relied on the accuracy of the few data points at the upper Q range, which appear to turn upwards to rod-like behaviour, however these data points are those with the greatest uncertainty. The fitted parameters in these cases are therefore somewhat erratic. The best fit for each individual sample varies between the two fitting routines, for example the Yamakawa model appears to give the best fit for 38% aromatised fraction G, while the Koyama model gives a better fit for the same polymer aromatised to 27%.

The overall trend shown by the fitting of a Kratky-Porod type model to partially aromatised polymers is of an increase in persistence length with aromatisation, although it is more gradual than that measured by other techniques, and the values are of lesser magnitude(tables 4.22 and 5.11).

7.5.2b LOQ data

A set of comparative plots of LOQ data from the experiment LOQ-NOV91 with D17-Oct 90 data is shown in figure 7.10a. It can be seen that the D17 data has a clear plateau region, but no clearly defined plateau is seen in the LOQ data, instead there is a convex bulge in the plateau region. This may be due to slight errors in calibrating the detector on LOQ, which have led to a non linear response in that region of Q. The Kratky plot of the standard polystyrene is also shown in figure 7.10b, and neither does this display the plateau region which might be expected from a Gaussian polymer chain, although the curve is less scattered than the data for poly(DHCD-DMC), due to the much greater scattered intensity and the corresponding higher signal to noise ratio of the standard polystyrene.

These differences present some problem in using a model fitting method to determine configurational parameters, it is obviously difficult to fit the wormlike equations if the transition from the plateau behaviour of the coil to the upturn of the rod, which is a vital feature of the model, cannot be distinguished. These samples fitted are 5% solution of partially aromatised fraction A, from 0 to 40% aromatised, and samples from the shear cell experiment of the same concentration. The solutions were at rest and had not been previously sheared. These cover a limited range of aromatisation, 20% and 40%. The samples from the uncompleted experiment with 1% overall of deuteropolymer in a 5%polymer solution. The data for these is very scattered as the counting times were short. The fits to these are shown in figure 7.11*a-i*, and tabulated in 7.15.

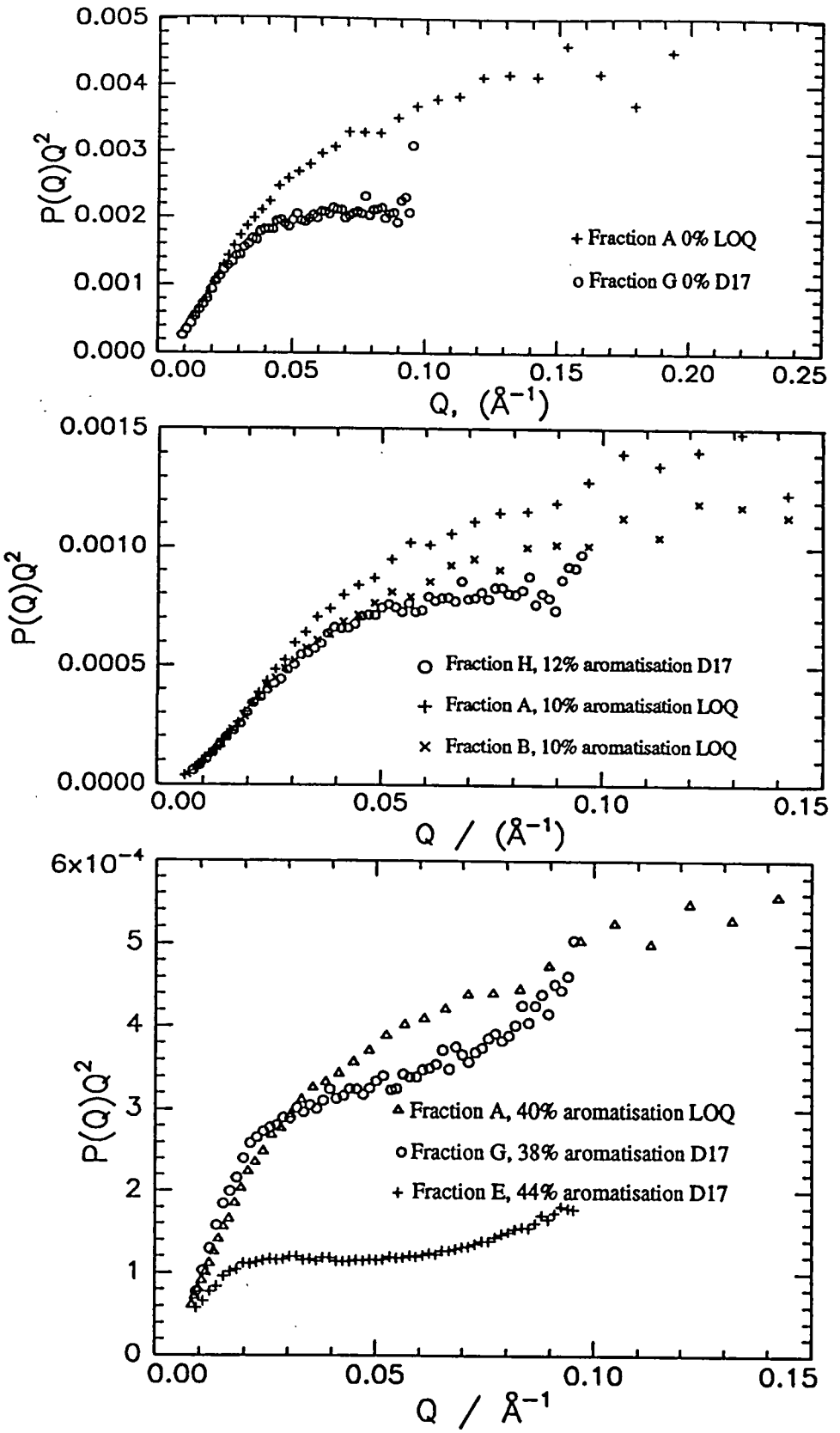

Figure 7.10*a*: Comparison of scattering from unaromatised polymers (5% solution in NMP) from LOQ and D17 instruments.

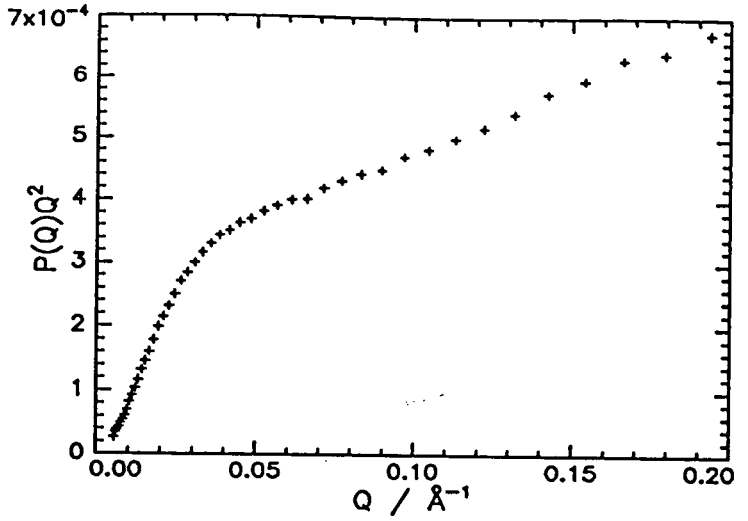

Figure 7.10*b*: Scattering from standard polystyrene LOQ-Nov 91

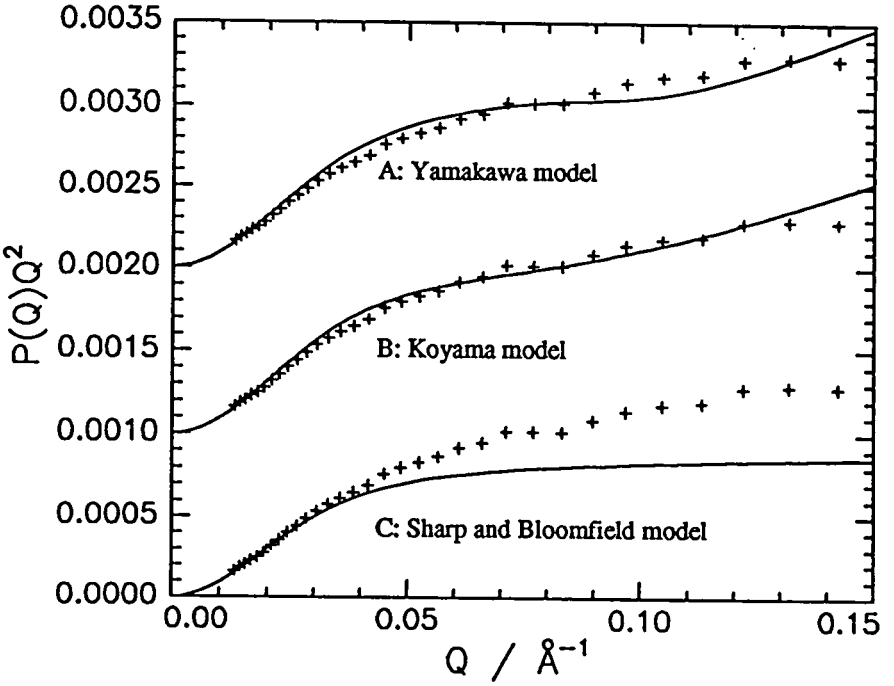

Figure 7.11*a*: Iterative fits to fraction A-0%.

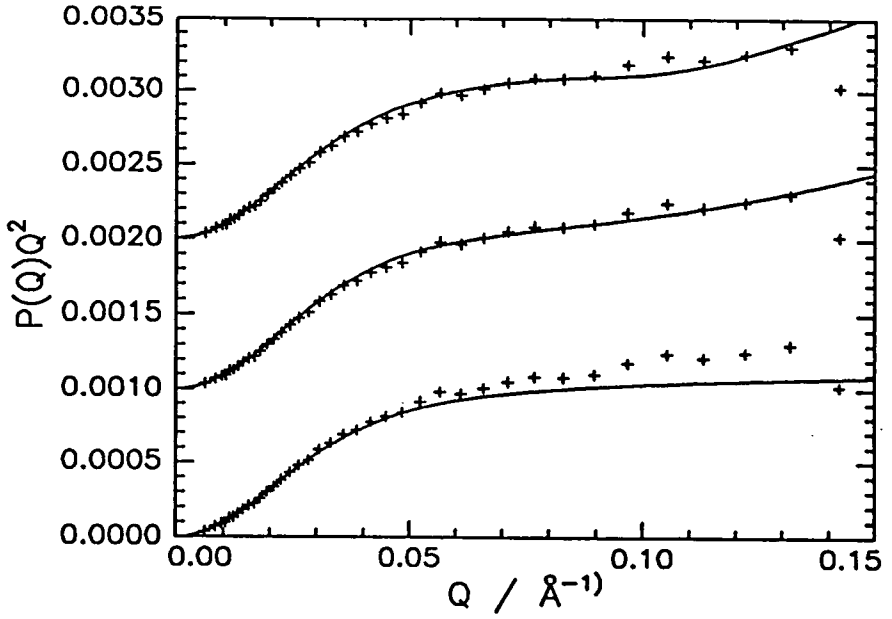

Figure 7.11*b*: Iterative fits to fraction A-10%.

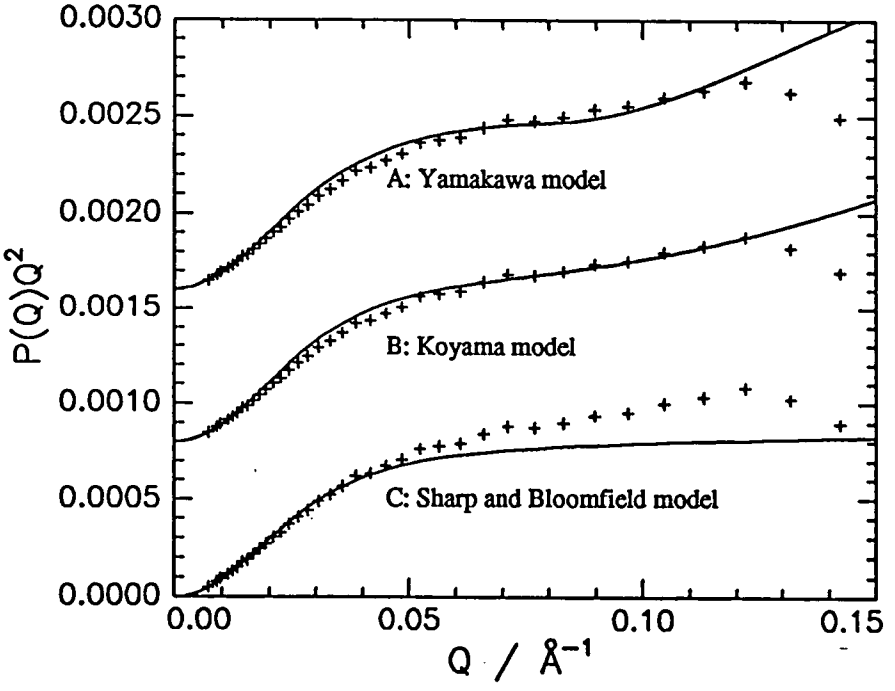

Figure 7.11*c*: Iterative fits to fraction A-20%.

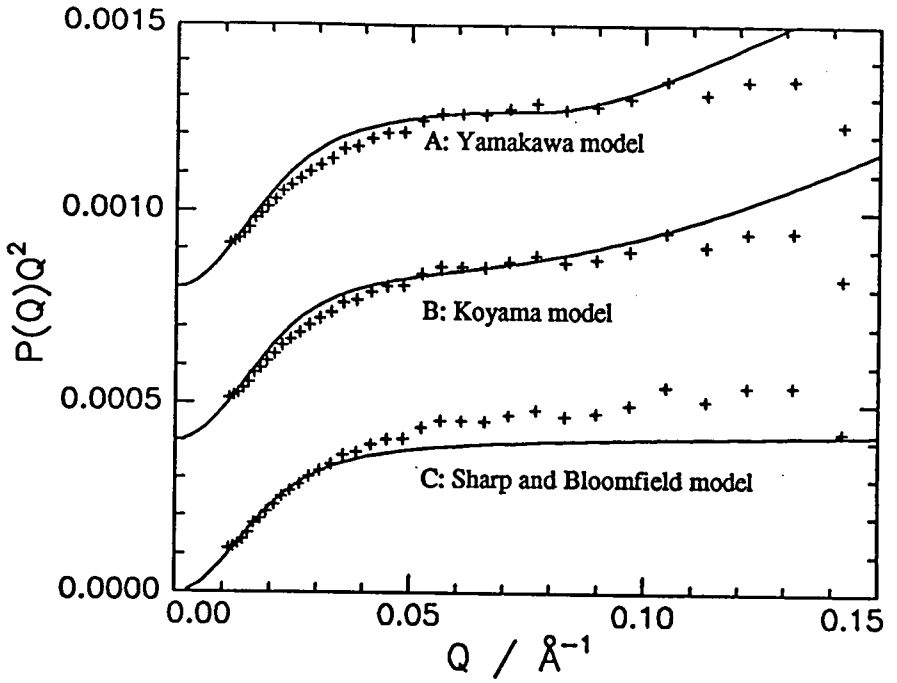

Figure 7.11*d*: Iterative fits to fraction A-30%.

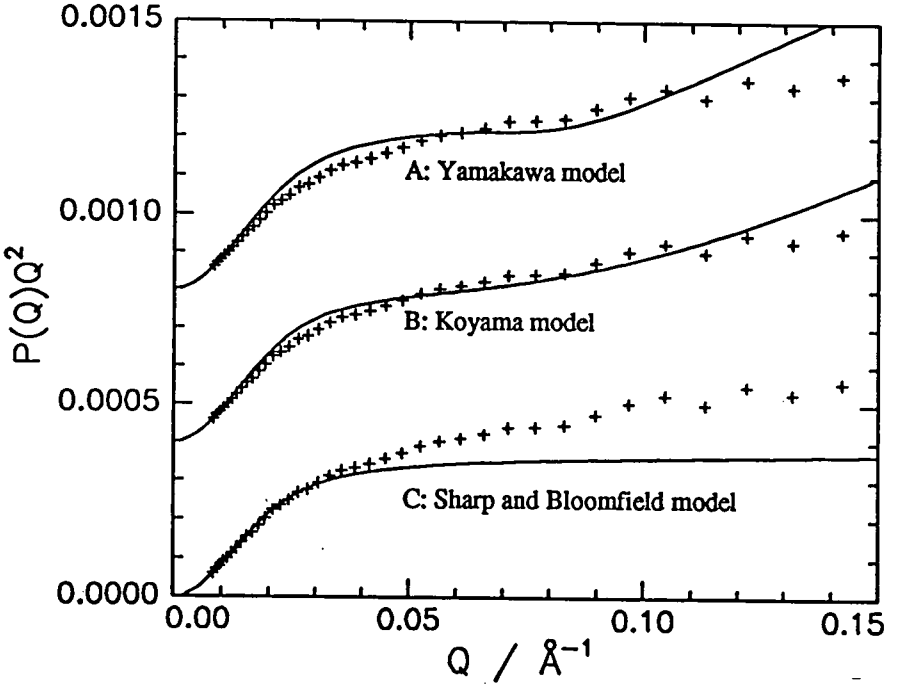

Figure 7.11*e*: Iterative fits to fraction A-40%.

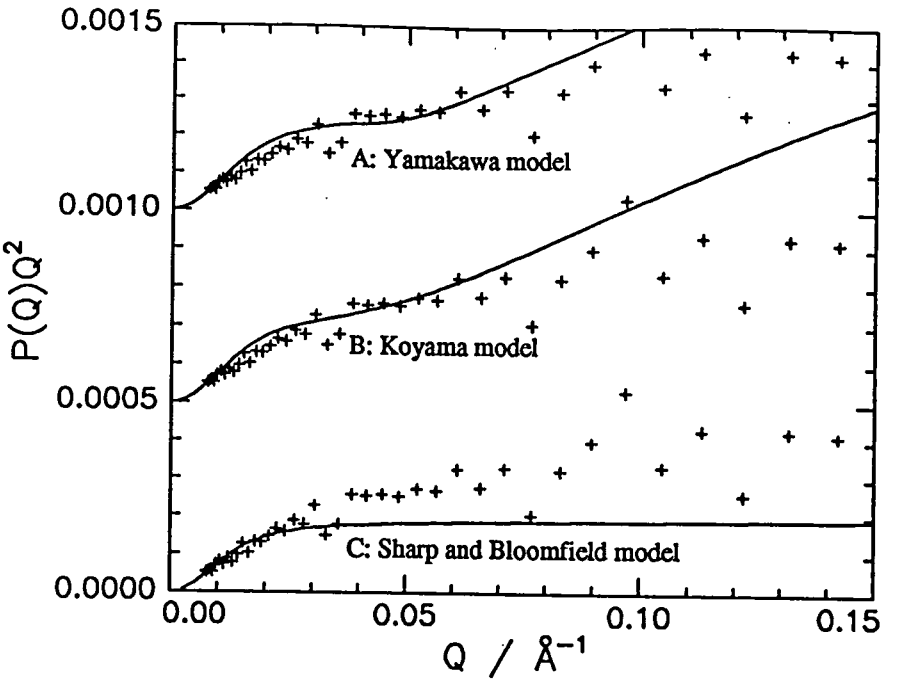

Figure 7.11*f*: Iterative fits to unfractionated polymer 1% deuterated polymer in 5% polymer solution, 20% aromatised

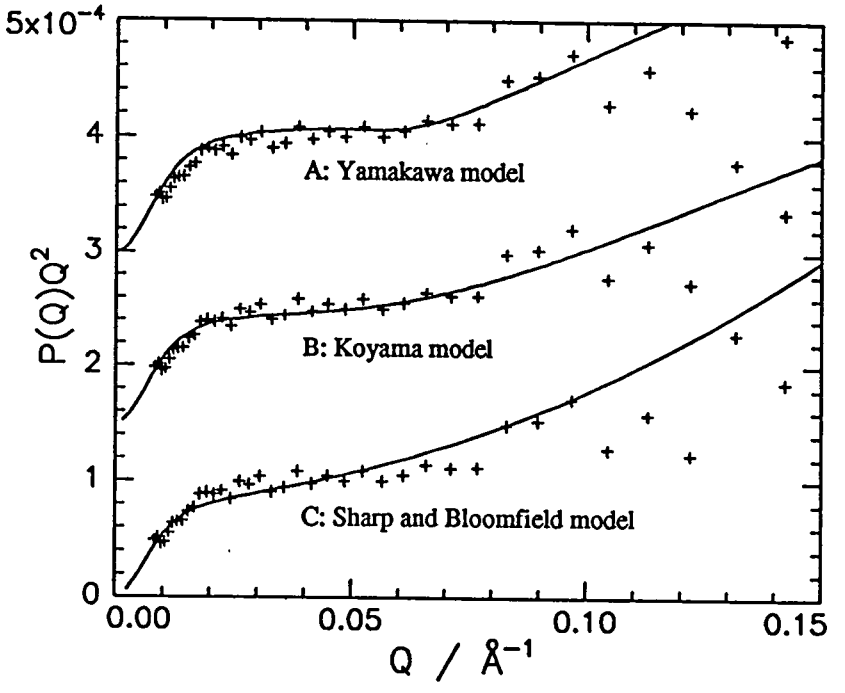

Figure 7.11*g* Iterative fits to unfractionated polymer 1% deuterated polymer in 5% polymer solution, 40% aromatised.

Sample	Yamakawa		Koyama		Sharp and Bloomfield	
	a / Å	L / Å	a / Å	L / Å	a / Å	L / Å
A-0%	22	300	20	340	3	1540
A-10%	22	285	18	320	4	1450
A-20%	26	310	20	360	8	960
A-30%	28	560	23	600	12	1170
A-40%	26	600	24	650	12	1450
D20R0	50	200	50	200	11	530
D40R0	40	520	36	550	17	940
HD20	50	600	50	600	22	1900
HD40	32	1800	33	1900	55	1300

Table 7.15: Fits of Kratky-Porod type models to LOQ scattering data.

The model plots shown in figure 7.11 do not fit the data particulary well, and this is caused by the distorted shape of the scattering function, caused by the non linear response of the detector. The data was fitted to overlay the Guinier region, and the Q* upturn if possible, taking less account of the plateau region. The fitted parameters do show a general increase in persistence length with increasing aromatisation, as would be expected for a stiffening chain. As with the values obtained from D17 data the magnitude of a from SANS is less than from ILS and viscometry, especially for the more highly aromatised polymers.

The data from LOQ experiments has a Q range extending some way beyond that of D17. The scattering for the low aromatisation polymers on LOQ shows the upturn at Q* at around 0.1Å^{-1}, the limit of D17's range. This supports the position of the fit of KP models on D17 data made in section 7.5.2 on the evidence of an upturn in the few highest-Q data-points .

7.6 Scattering from highly aromatised polymers

The scattering from polymers with a lower degree of polymerisation, i.e. up to the point where the polymer precipitated from the aromatised solution will no longer dissolve, around 40% aromatisation is distinctly different from those for highly aromatised polymers above 40% aromatisation. Figure 7.12 shows the scattering from two samples of the same fraction at different degrees of aromatisation, presented in the intensity (I(Q) *vs* Q) and Kratky ($I(Q)Q^2$ *vs* Q) formats.

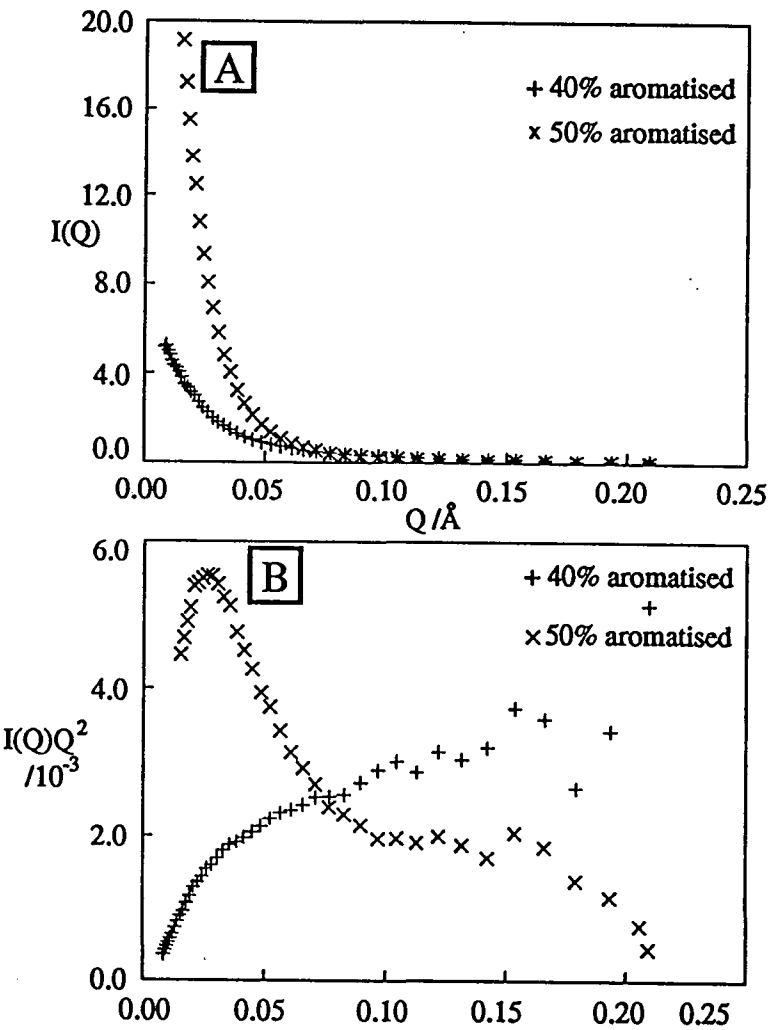

Figure 7.12: Scattering from fraction A at 40% and 50% aromatisation

A; Intensity plot, B; Kratky plot.

In the intensity plot it can be seen that there is a sharp upturn in the scattering at low Q values for the more highly aromatised polymers, indicating the scattering particles are

much larger, and therefore presumably aggregates as has previously been suggested from light scattering and SEC results. The Kratky plot shows an even more marked change, here the highly aromatised sample shows a prominent peak at low Q, compared with the more conventional wormlike type scattering seen at 40% aromatisation. This type of scattering has been reported to occur in structures with compact cores, for example star polymers[19,20], aggregates of conjugated polymers[21,22] and micelles[23].

This type of scattering behaviour is most conveniently modelled in terms of the star polymer described by Benoit[24] to describe a polymer of *f* Gaussian arms with a common core. For a star polymer with monodisperse arms the equation is;

$$P(Q) = \left(\frac{2}{fV^2}\right)\left[V - \left(1 - e^{-V}\right) + (f+1)\left(\frac{(1-e^{-V})}{2}\right)\right] \qquad (7.33)$$

where $V = fu^2/(3f-2)$, and $u=Q^2\langle s^2\rangle$. A second form of the equation covers such a polymer with polydisperse arms[25];

$$P(Q) = \frac{1+\left(\frac{u^2}{3f}\right)}{\left(1+\frac{u^2(f+1)}{6f}\right)} \qquad (7.34)$$

where the same variables apply.

The comparison between the two equations is shown in figure 7.13, it can be seen that the polydisperse polymer has a broader peak for the maximum, which is also shifted to higher Q, from 0.005Å to 0.0125Å. The position of the peak from the Benoit monodisperse model is predicted to occur at $Q\langle s^2\rangle^{1/2} \approx 1$, for the polydisperse peak $Q\langle s^2\rangle^{1/2}$ is considerably greater. The scattering functions from the highly aromatised polymers have been fitted to the star like models, and best matches, judged subjectively and not fitted, are shown. This is because the weighting of the non-linear squares fitting routine strongly favoured either the region from the origin to the peak, which can be seen from figure(7.14) is where the Debye equation is obeyed, or from the peak down, depending on the weighting procedure employed. A balance was struck therefore between the peak position, peak height, and the general shape of the function.

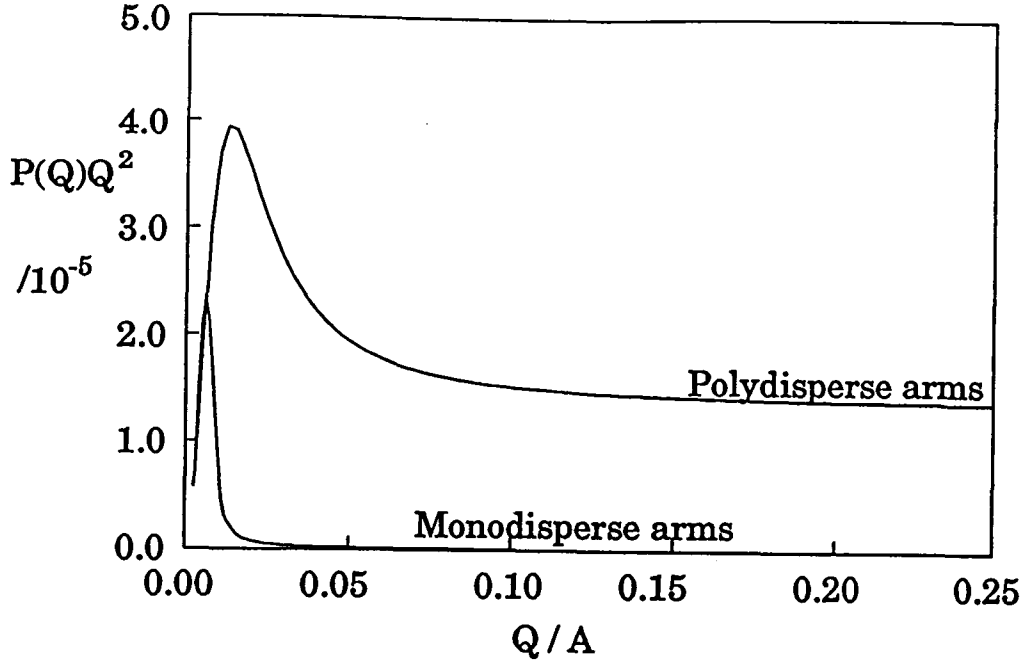

Figure 7.13: Comparison of scattering from star polymers (eqn.(7.33)&(7.34)) 20 arms and $\langle s^2 \rangle^{1/2} = 200$Å.

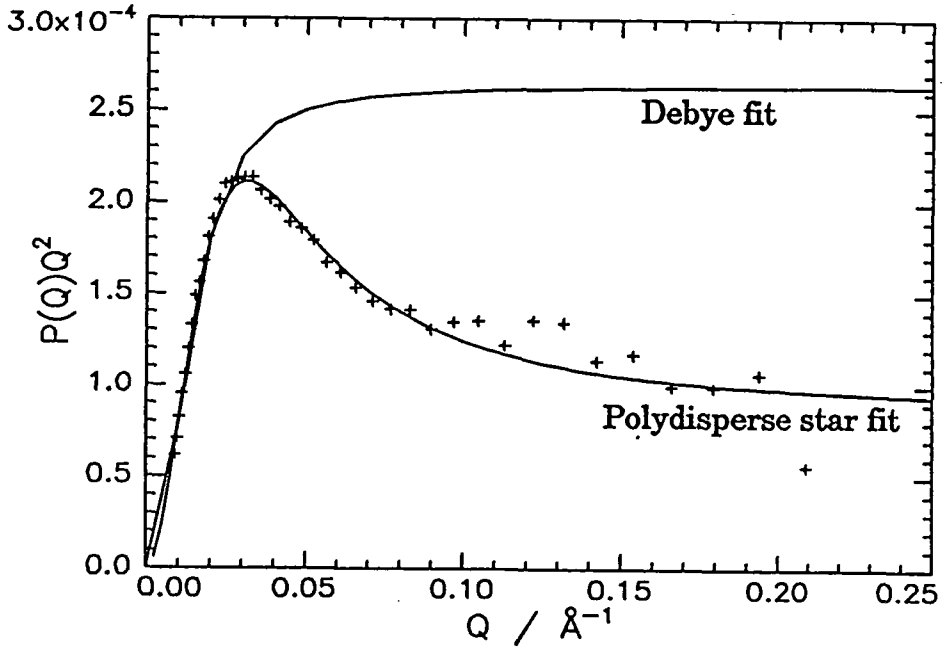

Figure 7.14: Comparison of star model and Debye model fits for highly aromatised polymer, fraction C at 50% aromatisation showing short range of coincidence of Debye model fit.

Sample	$\langle s^2 \rangle^{1/2}_{star}$ / Å	$\langle s^2 \rangle^{1/2}_{Debye}$ / Å	Number of arms
A-50%	125	148.7	35
C-50%	94	95	35
D-50%	87	87	16
A-60%	110	131.5	500
B-60%	115	124.3	100
C-60%	118	134	110
D-60%	130	161	500
A-80%	100	278	50000
B-80%	--	702	--
C-80%	--	785	--
D-80%	--	658	--

Table 7.16: Fits of the polydisperse star scattering function(eq.7.34) to SANS data.

A number of the fits to equation 7.34 are shown in figures 7.15*a-h*.

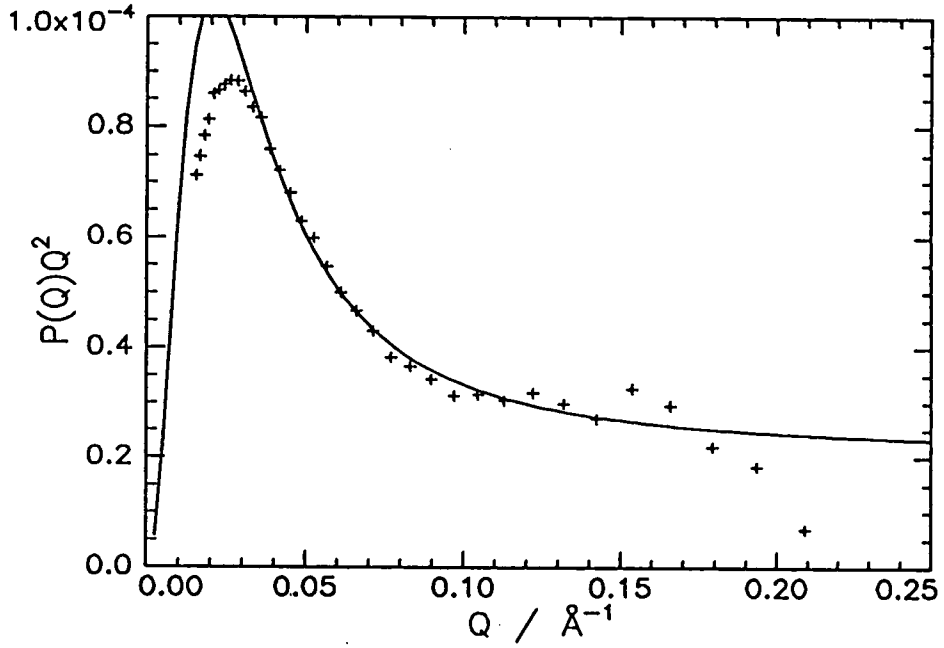

Figure 7.14*a*: Fit of polydisperse star model to fraction A-50% aromatisation.

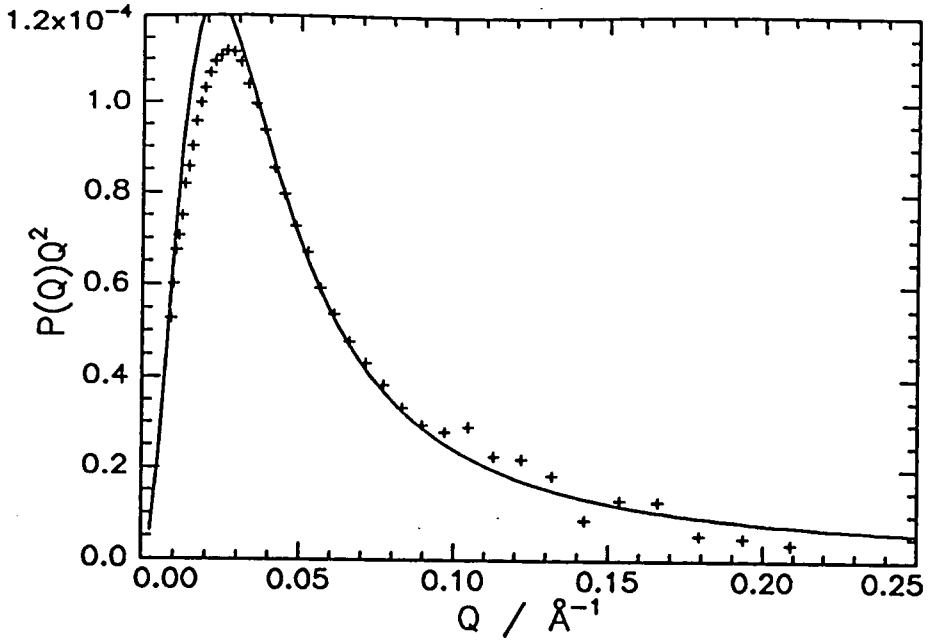

Figure 7.14*b*: Fit of polydisperse star model to fraction A-60% aromatisation.

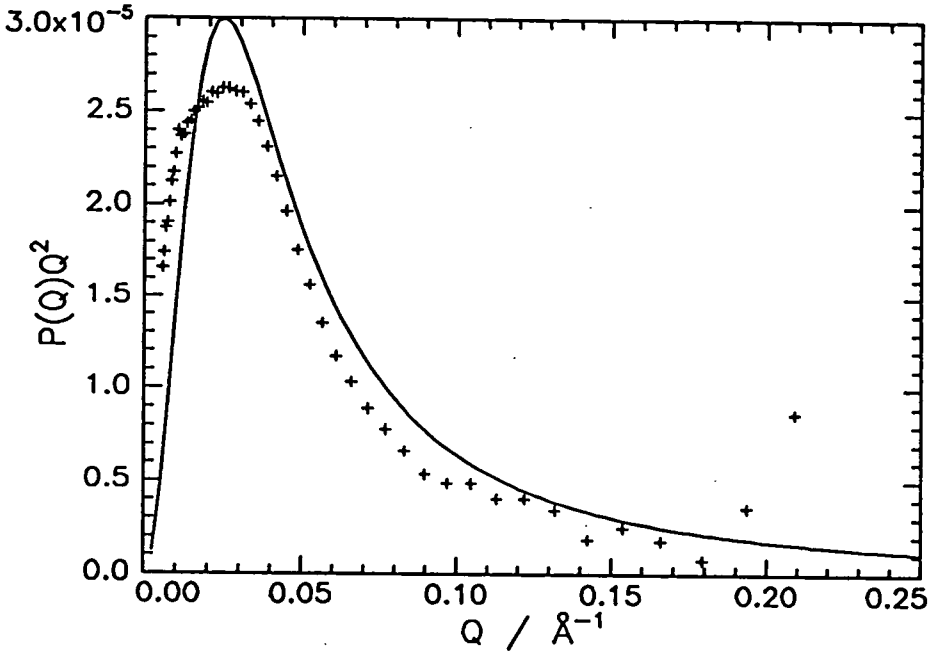

Figure 7.14*c*: Fit of polydisperse star model to fraction A-80% aromatisation.

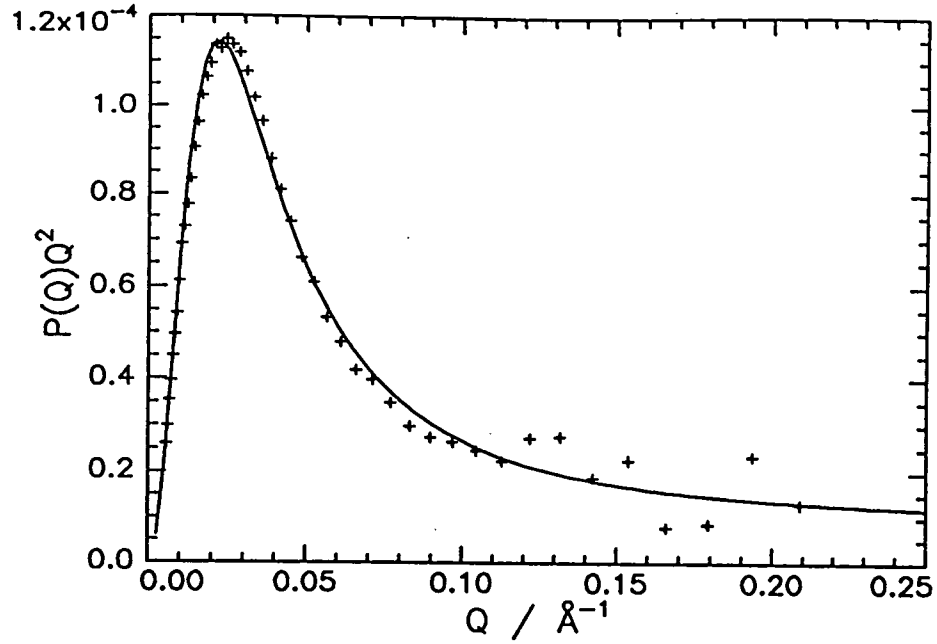

Figure 7.14*d*: Fit of polydisperse star model to fraction B-60% aromatisation.

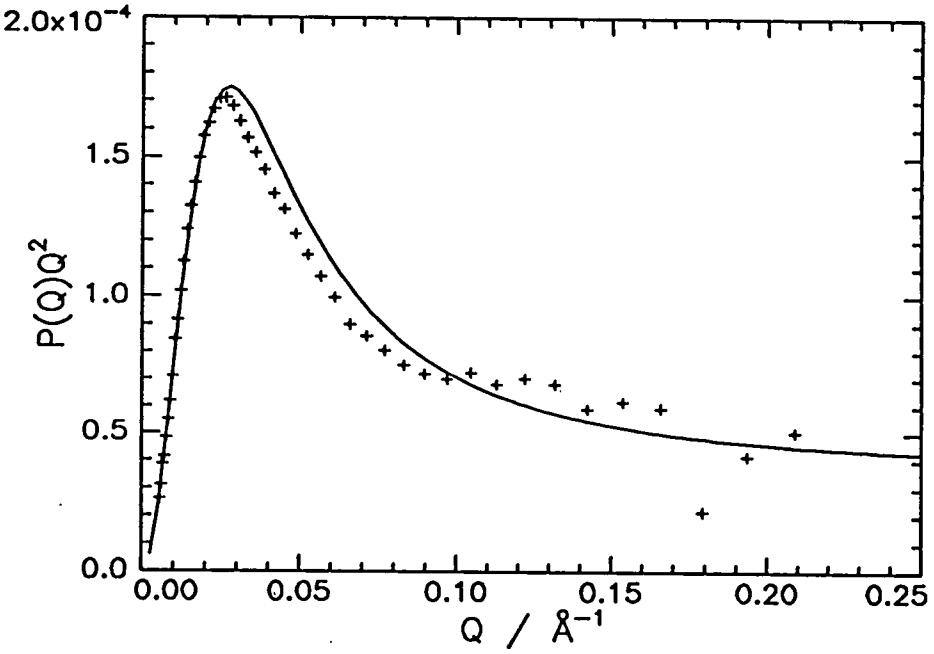

Figure 7.14*e*: Fit of polydisperse star model to fraction C-50% aromatisation.

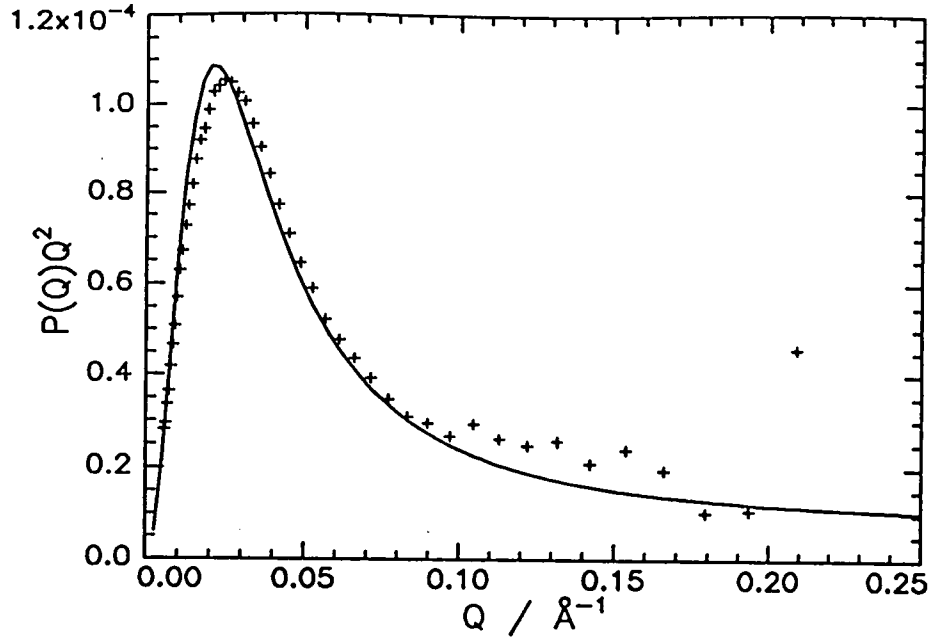

Figure 7.14*f*: Fit of polydisperse star model to fraction C-60% aromatisation.

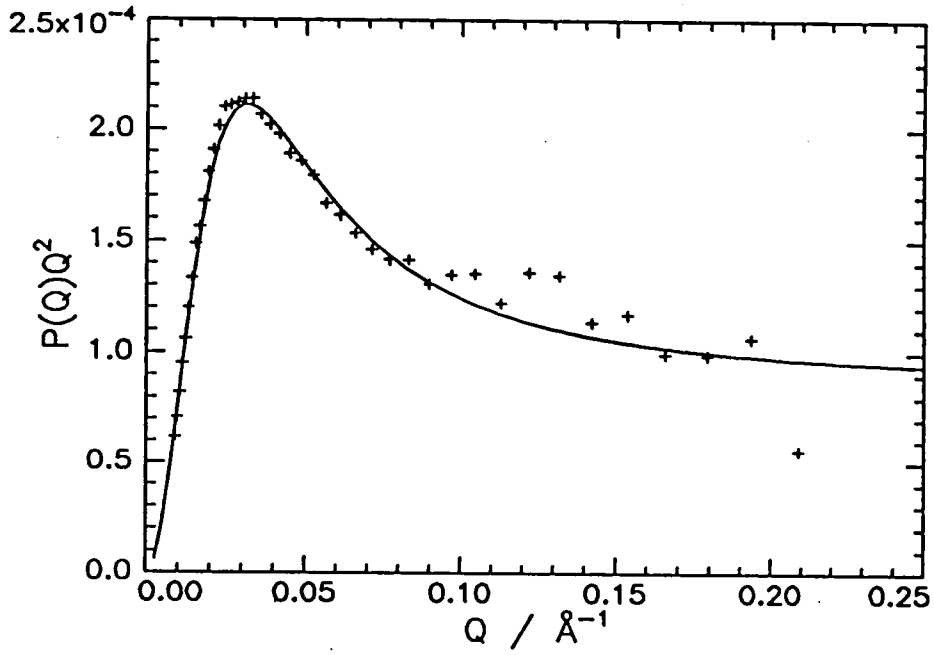

Figure 7.14*g*: Fit of polydisperse star model to fraction D-50% aromatisation.

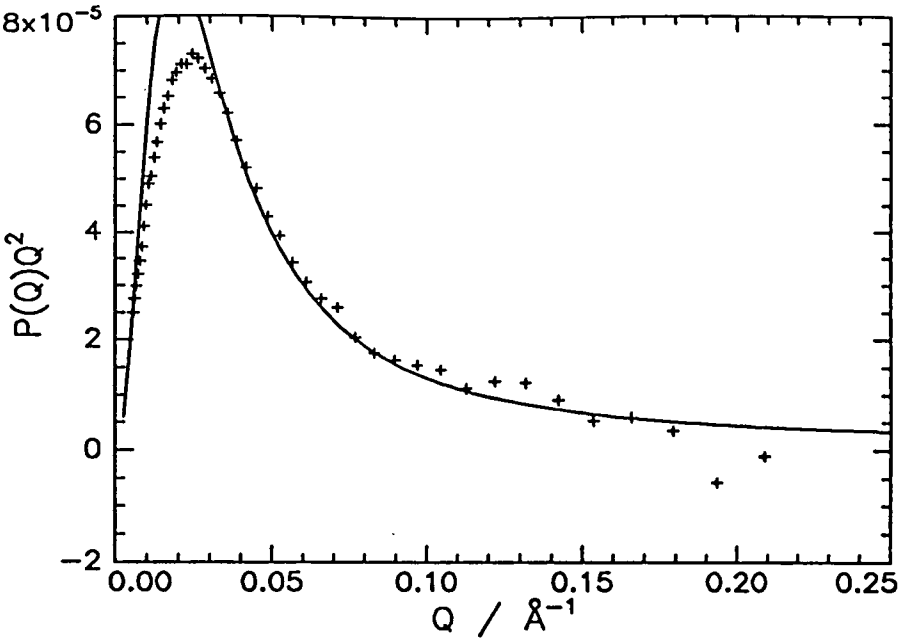

Figure 7.14*h*: Fit of polydisperse star model to fraction D-60% aromatisation.

The fits obtained are reasonable for 50% and 60% aromatised polymers, with the Guinier region, the peaks, and the descending slope more or less corresponding. The extremely broad peaks for the 80% aromatised polymers could not be fitted adequately, and this is probably due to the formation of a network structure in the solution, which is close to the point of precipitation (≈85% aromatisation). The fit given for A-80% is not a particularly good fit, but it included to show that the peak in the Kratky plot corresponds to a much smaller radius of gyration than the fit from the Debye equation, and that the number of arms is very much greater than those of the lesser aromatised polymers.

It is interesting to note the great increase in the number of arms from 50% to 60%, while the intensity values I(0), roughly proportional to M_w, only double, and the radius of gyration changes only slightly.

7.7 Conclusion

The technique of small angle neutron scattering has proved a powerful and useful tool for studying the behaviour of poly(DHCD-DMC) as it is aromatised to polyphenylene. It has been possible to extract the parameters of the wormlike chain from the polymer at lower degrees of aromatisation, and the molecular dimensions obtained broadly correlate with those already measured, and support the observations thus far. SANS has also uniquely provided a method to study the behaviour of the highly aromatised polymer in solution, which provides a better insight into the behaviour to the limit of solubility, and how the polymer aggregates. If the star model is a reasonable approximation to the structure of the aggregated polymer it would support the notion of fringed micelle structures in the solution as this model is used as an approximation to the behaviour of fringed micelles of block copolymers in selective solvents[26,27,28]. Workers in this field often produce scattering functions of the same shape as those in figure 14 for these structures.

There is some discrepancy between the values for persistence length obtained for the polymers by SANS from those obtained by light scattering and viscometry. For the unaromatised polymer *a* from SANS is in the order of 20Å, which is similar to that from viscometry, and slightly lower than ILS, at ≈10% aromatisation the value increases slightly, and is still comparable to viscometry, though much lower than ILS with values >100Å. At 20% aromatisation the SANS value is much lower than that from either of the other methods. The values for the unaromatised polymer at 20Å are comparable to that of Gaussian chains, for example syndiotactic polystyrene(19Å)[29] or isotactic polymethyl methacrylate(18Å). It would be expected that the 44% aromatised chain, would have a persistence length greater than 35Å, which only compares to other fairly flexible chains, for example syndiotactic polyvinyl chloride(39Å) or syndiotactic PMMA(33Å), however this could be the result of the chain discontinuities at the 1,2-bonded sites. The reason for the difference in values derived from the various methods is not clear, but the SANS method is the most direct, for example the same valuefor *a* for

38 or 44% aromatised polymers could be obtained by a drawing method extrapolating the plateau and upturn lines. If the other methods give erroneous values it could be the result of aggregation phenomena, and the differing sensitivites of each technique to aggregated species.

7.8 References

1 Allen,G.,Higgins,J.S.,*Rep.Prog.Phys.*,**36**,1073,(1973).

2 Burchard,W., Ch 10 in '*Applied Fibre Science*', Vol 1, ed F.Happey, Academic Press, London, 1978.

3 R.W.Richards, Ch 6 in *'Determination of Molecular Weight'* ed. A.R.Cooper, Wiley, New York, 1989.

4 Zimm ,B.H.,*J.Chem.Phys.*,16,1093,(1948).

5 Kirste,R.G. and Oberthür,R.C., Ch.12 in '*Small Angle X-Ray Scattering*, ed. Glatter,O., and Kratky,O, Academic Press, New York, 1982.

6 Bates,F.S.,Wignall,G.D.,*J.Appl.Cryst.*,**20**,28,(1987).

7 Debye,P.,*J.Phys.Colloid.Chem.*,**51**,18,(1947).

8 Kirste,R.G. and Oberthür,R.C., Ch.12 in '*Small Angle X-Ray Scattering*, ed. Glatter,O., and Kratky,O, Academic Press, New York, 1982.

9 Neutron scattering instruments at the ISIS Facility: User Guide, RAL,Chilton,1990.

10 King,S.M.,'*LOQ Data Analysis*',RAL,Chilton,1991.

11 'Neutron beam facilites at the high flux reactor available for users',ILL,Grenoble,1985.

12 Cummins,P.G.,Penfold,J.,Staples,E.,*Adv.Colloid.Interface.Sci.*,**34**,451, (1991).

13 *Polymer*, **22**, 886 (1981).

14 Ballard,D.G.H.,Courtis,A.,Shirley,I.M.,Taylor,S.C.,Macromolecules,**21**, 294,(1989).

15 ICI PLC, Internal report.

16 Yamakawa,H.,Yoshizaki,T.,*Macromolecules*,**13**,1518,(1980).

17 Koyama,S.,*J.Phys.Soc.Japan*,**34**,1029(1974).

18 Bloomfield,V.A.,Sharp,P.,*Biopolymers*,**6**,1201(1968).

19 Benoit,H., *J.Polym.Sci.*, **11**,507(1953).

20 Richter,D. *et al*, *Macromolecules*, **23**,1845(1990).

21 Shukla,P. *et al*, *Macromolecules*, **24**,5606(1991).

22 Rawiso,M. *et al*, *J.Phys.France*, **49**,861(1988).

23 Capel,M.,Cogan,K.A.,Gast,A.P., *Macromolecules*, **24**,6512(1991).

24 Benoit,H,*J.Polym.Sci*',**11**,507,(1953).

25 Burchard,W., Ch 10 in '*Applied Fibre Science*', Vol 1, ed F.Happey, Academic Press, London, 1978.

26 Lally,T.P.,McAdam,J.D.G.,Price,C.,Woods,D.,*Polymer*,**15**,228,(1973).

27 Frank,C.W,Yeung,A.S.,*Polymer*,**31**,2089(1990).

28 Tuzar,Z. *et al*,*Polymer*,**31**,2118,(1990).

29 Yamakawa,H.,*Ann.Rev.Phys.Chem*,**35**,23,(1984).

5.9 Plots of SANS data

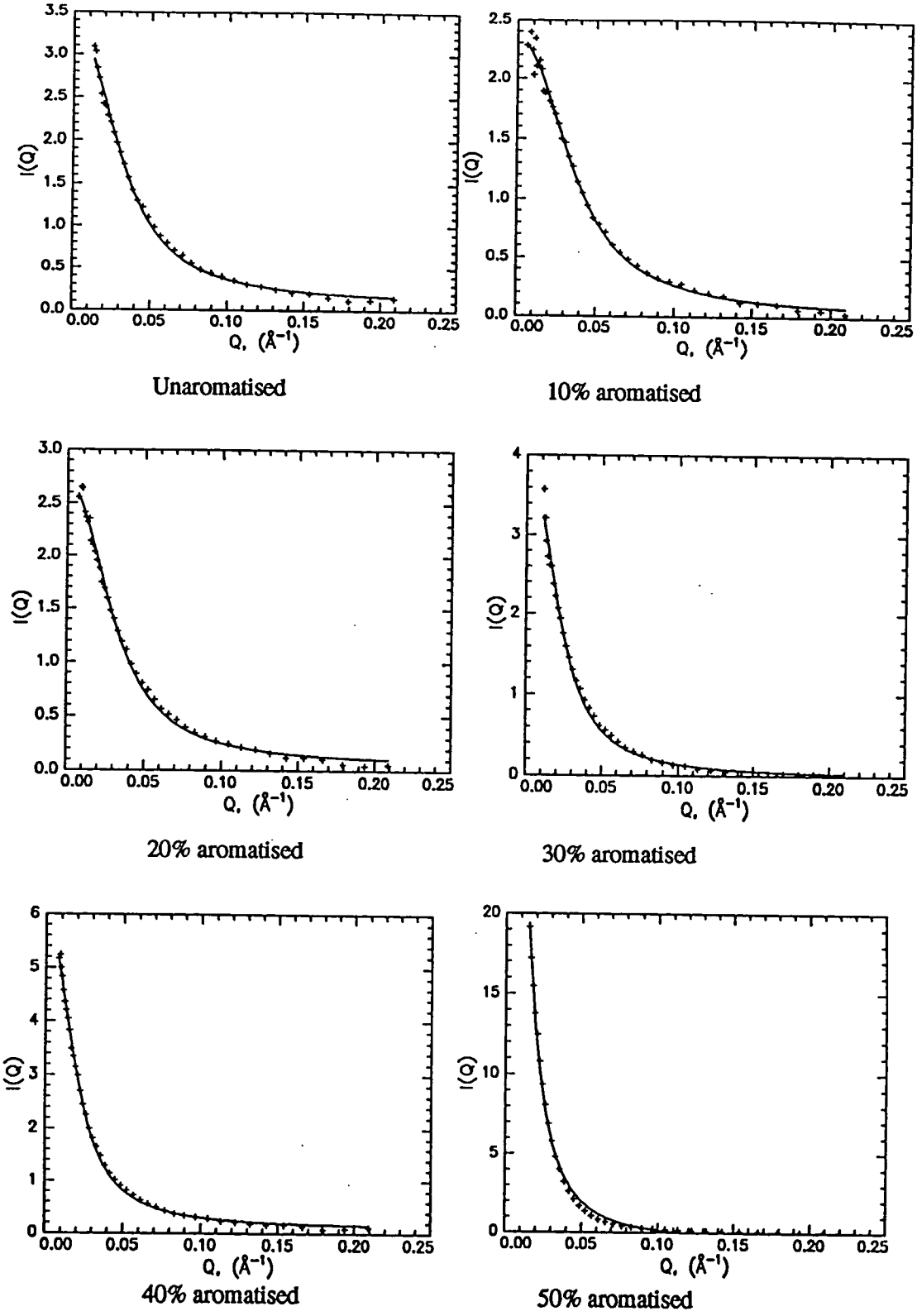

Figure 7.15a: Debye fits to fraction A at a range of aromatisation, LOQ-Nov91.

5% w/v deuterated polymer solution in NMP.

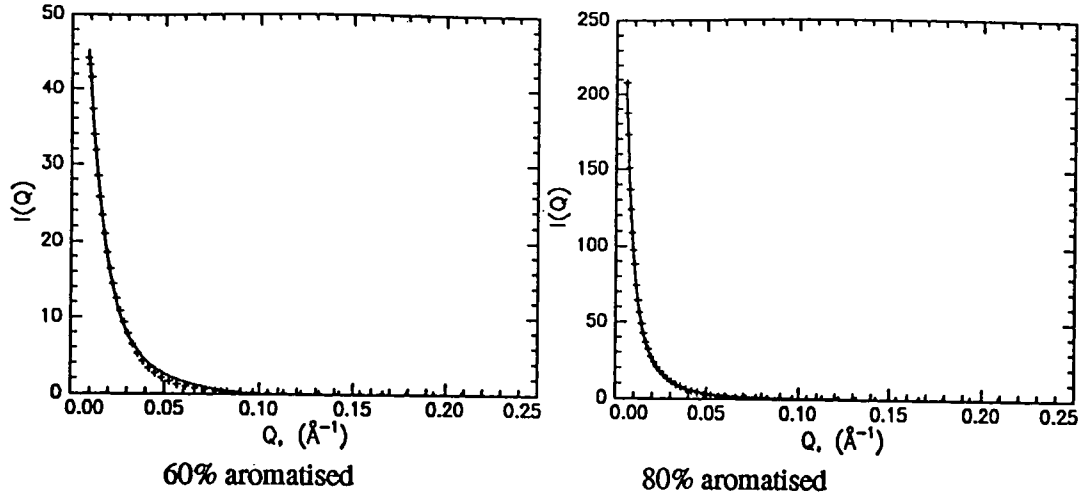

Figure 7.15b: Debye fits to fraction A at a range of aromatisation, LOQ-Nov91. 5% w/v deuterated polymer solution in NMP.

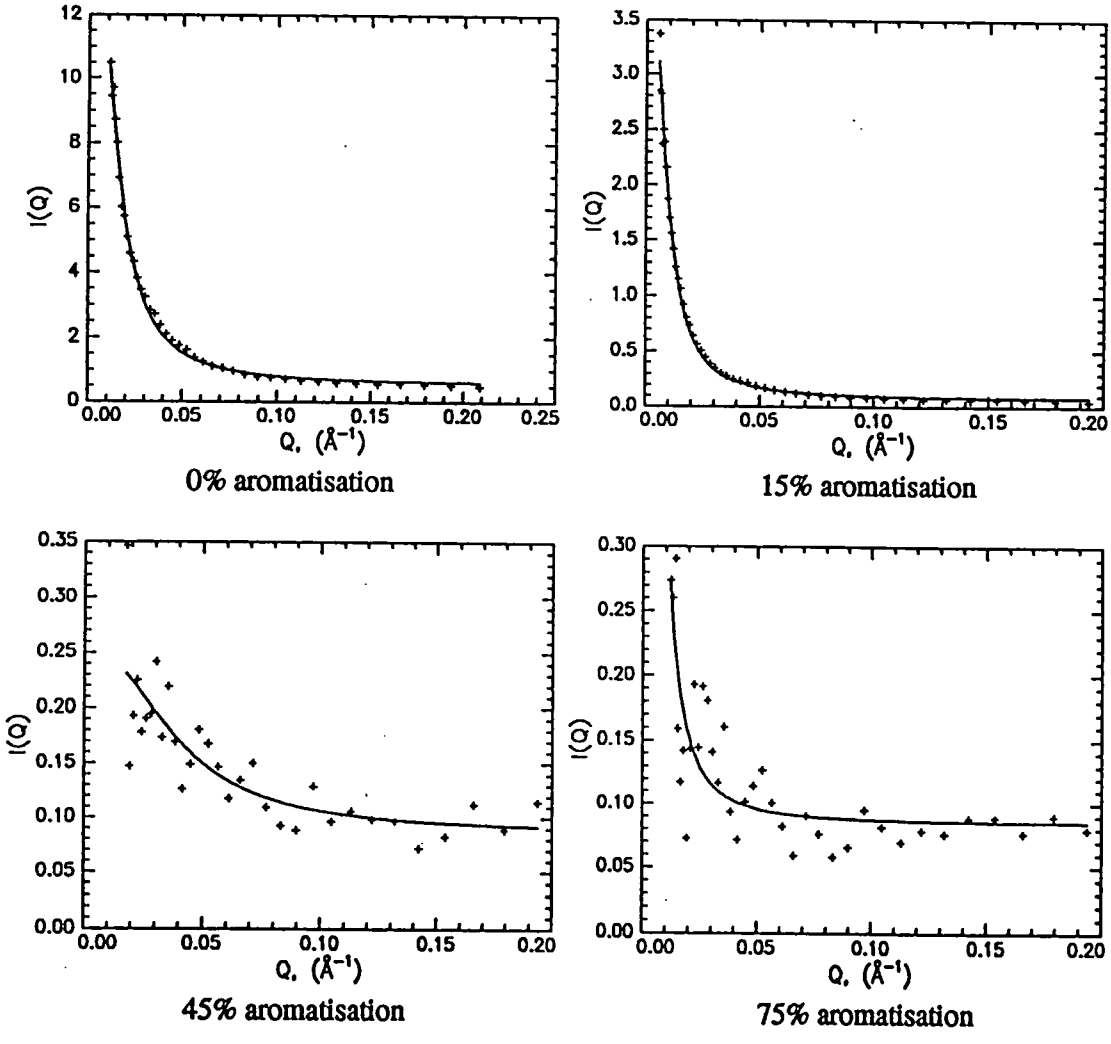

Figure 7.16: Debye fit to fraction F at a range of aromatisations, LOQ-Nov90. 5%w/v deuterated polymer solid samples

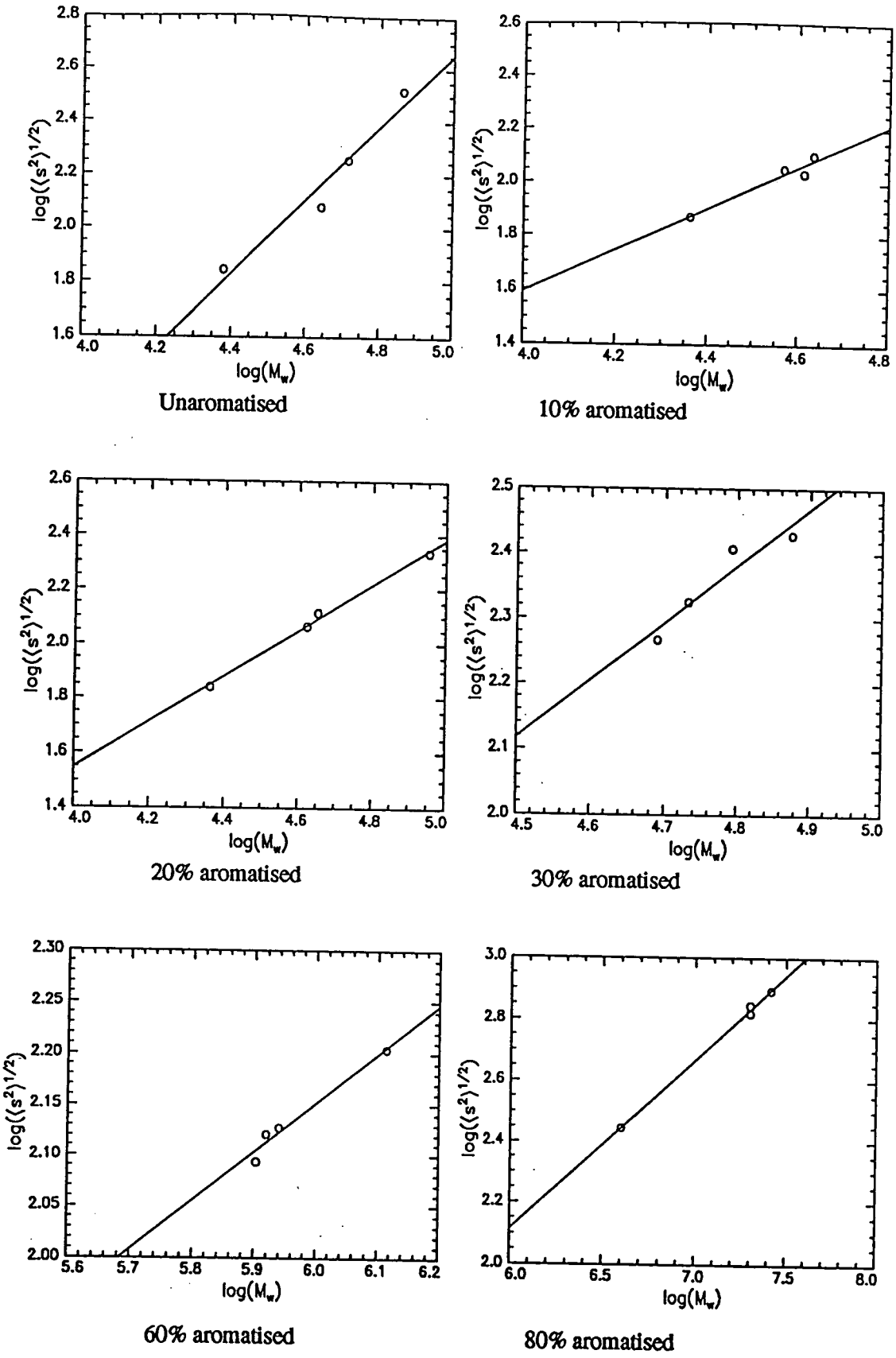

Figure 7.17: Power law fit to corrected LOQ data(table 7.5). 0%, 10%,20%,and 30% 60%,and 80% aromatisation respectively. LOQ-Nov91.

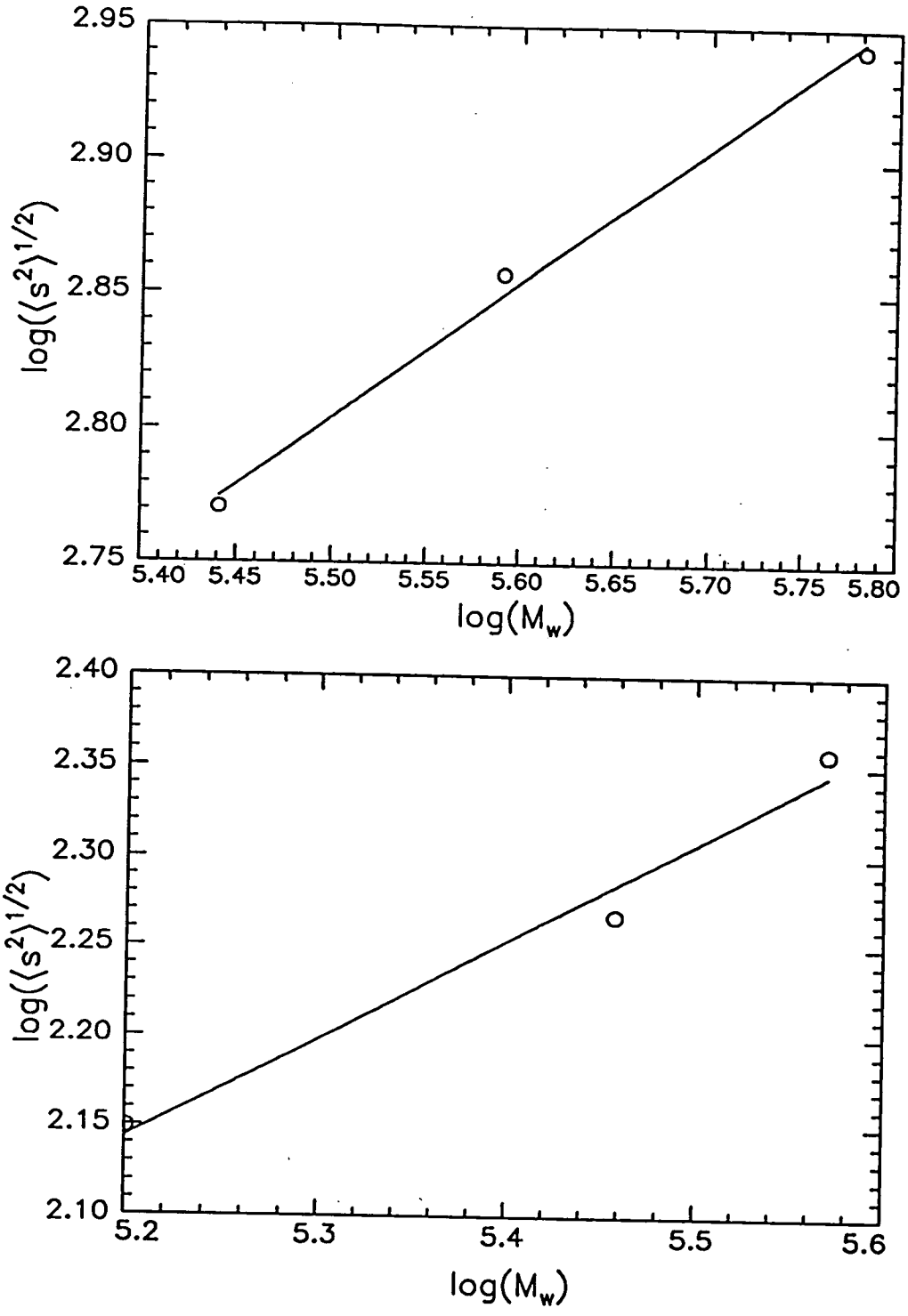

Figure 7.18: Power law fits to corrected LOQ data(table 7.5). 0% and 15% aromatisation respectively. LOQNov90.

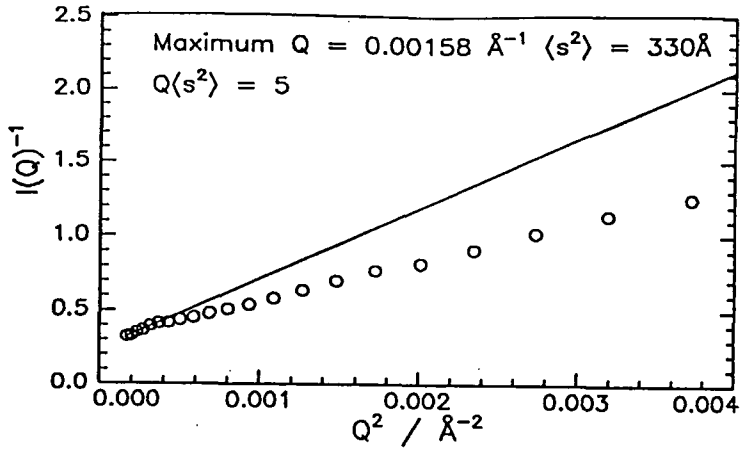

Fraction A, unaromatised, Q $\langle s^2 \rangle^{1/2}$ too high ∴ molecular weight incorrect.

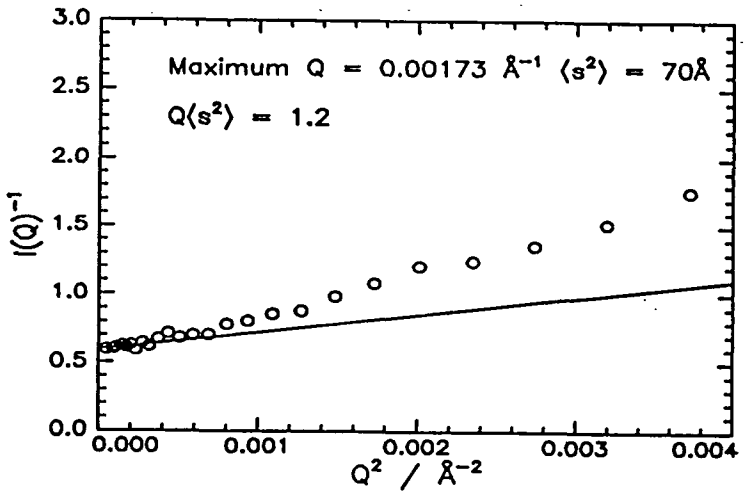

Fraction D, unaromatised, Q $\langle s^2 \rangle^{1/2}$ acceptable for polydisperse polymer ∴ molecular weight correct.

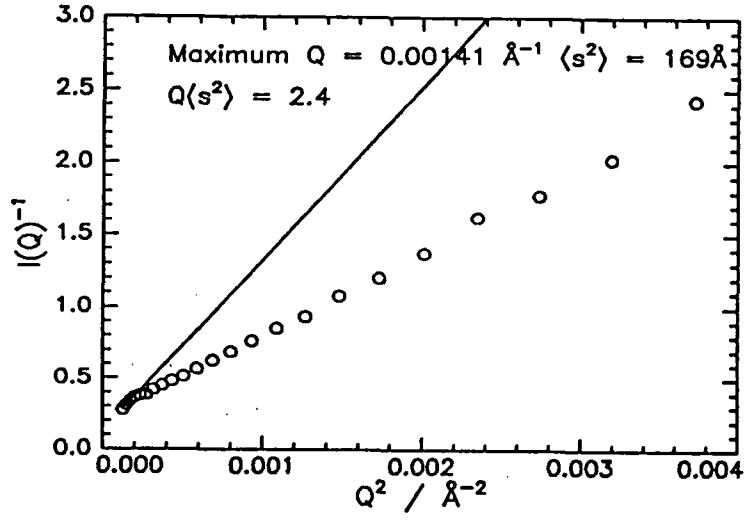

Fraction A, 30% aromatised, Q $\langle s^2 \rangle^{1/2}$ high, but may still be acceptable for polydisperse sample. Molecular weight correct.

Figure 7.19: Zimm plots of SANS data(LOQ-Nov91) showing effect of increasing size on validity of molecular weight measurement where Q range is fixed.

Zimm Plot Of Fraction DG At 0% Aromatisation

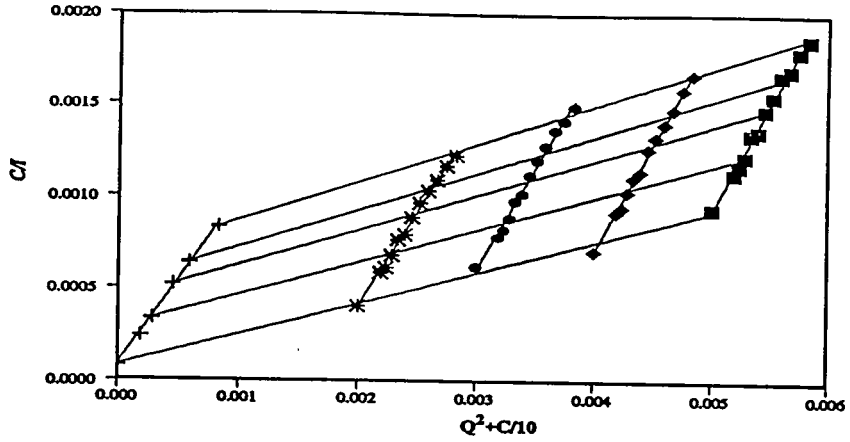

Zimm Plot Of Fraction dG At 25% Aromatisation

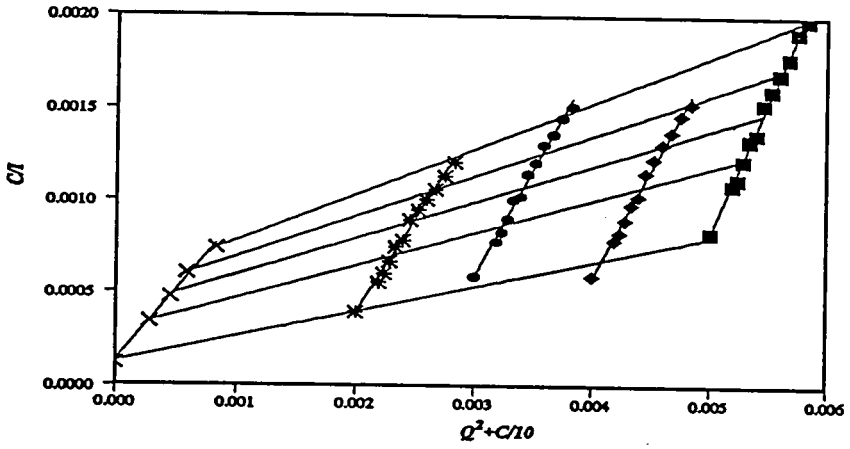

Zimm Plot Of Fraction dG At 38% Aromatisation

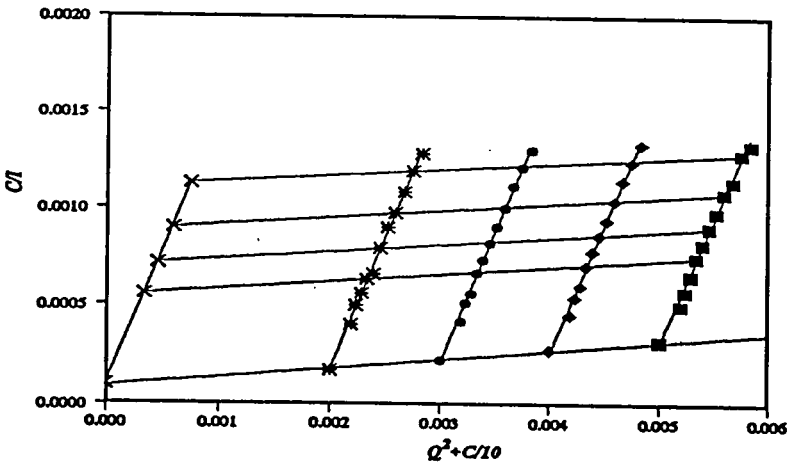

Figure 7.@: Zimm plots of fraction G in NMP, D17Oct.90

Zimm Plot Of Fraction DH At 0% Aromatisation

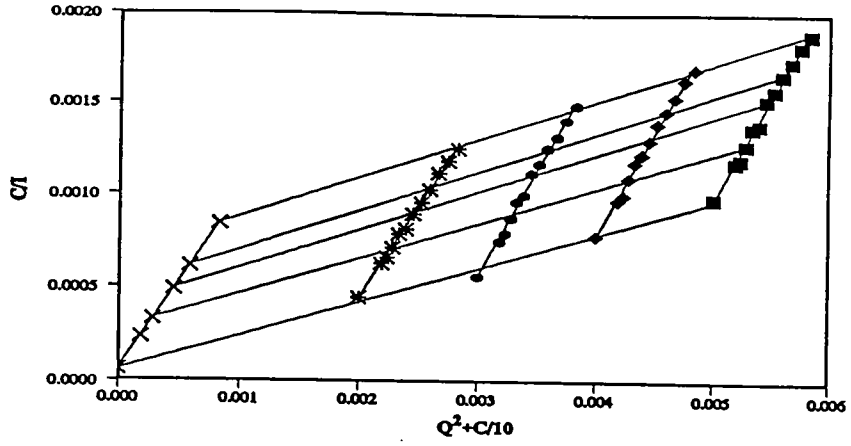

Zimm Plot Of Fraction DH At 12.5% Aromatisation

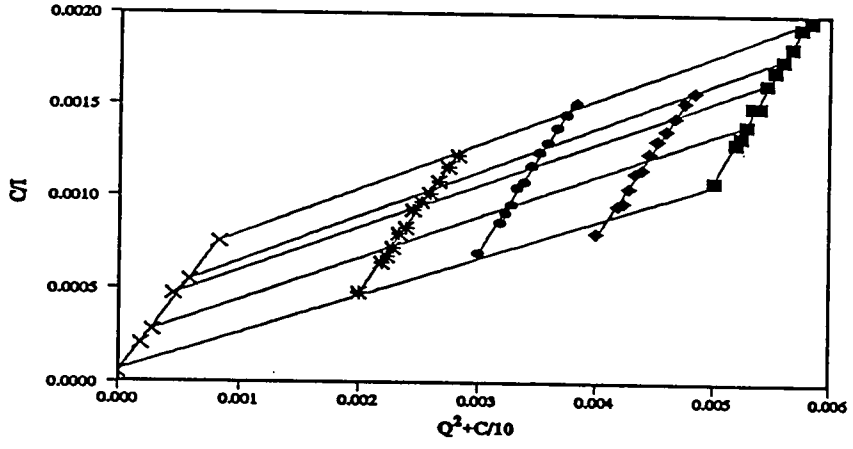

Zimm Plot Of Fraction dH At 25% Aromatisation

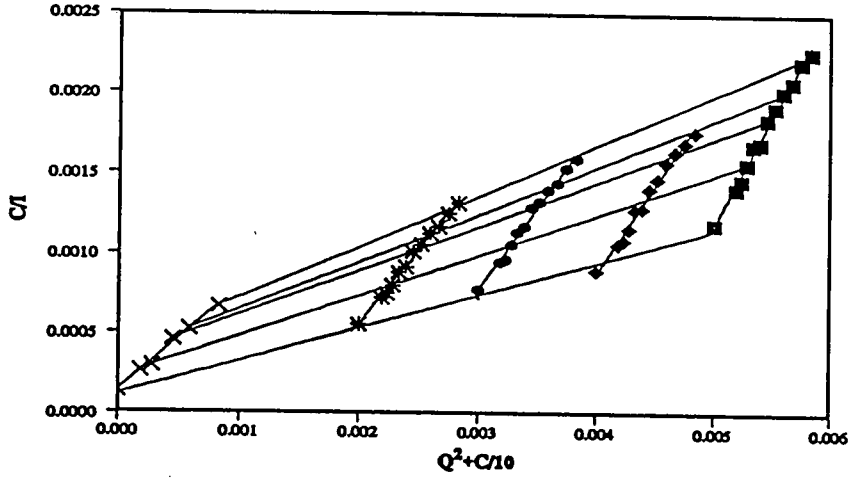

Figure 7.@: Zimm plots of fraction H in NMP, D17Oct.90

CHAPTER 8

CONCLUSION

This study has produced results from a number of techniques size exclusion chromatography, viscometry, intensity- and quasi-elastic-light scattering and neutron scattering which, with some differences, reveal the same trend in behaviour of solutions of poly(DHCD-DMC) as it is aromatised. The configurational transition which occurs is one of ;

RANDOM COIL → WORMLIKE CHAIN → AGGREGATE

The rigid nature of the poly(paraphenylene) caused by π-delocalisation causes it to become insoluble, therefore the partially aromatised polymer becomes liable to aggregation.

The degree of stiffening of the wormlike chain measured varies with the technique used (table 8.1). The most reliable values ought to be those from SANS, where the measurement is obtained directly from the scattering function.

Method	Solvent	Persistence Length /Å					
		0%	10%	20%	27%	38%	44%
Viscometry/Bohdanecky	NMP	21	27	127	-	-	-
ILS/Murikami or Zhang	NMP	35	238	318	-	-	-
ILS/Murikami or Zhang	$CHCl_3$	68	97	195	-	-	-
ILS/Characteristic ratio	NMP	53	138	227	-	-	-
ILS/Characteristic ratio	$CHCl_3$	-	-	-	-	-	-
SANS/Yamakawa	NMP	23	26(12%)	28(25%)	25	32	35

Table 8.1: Comparison of persistence lengths from different techniques.

This yields very low values for the aromatised polymer, both in comparison with the values from other measurements, and from values of typical stiff macromolecules, for example PHIC in hexane is 420Å, and in dichloromethane 185Å, poly(p-phenyleneterephthalamide) in H_2SO_4 is 290Å, and poly(phenylhydroquinone terephthalate) in dichlorobenzene/ chlorophenol is 72Å. Biopolymers tend to be stiffer, for example DNA ranges from 450 to 1500Å, and PBLG from 900 to 1600Å[1]. Under any circumstances it might be expected that a polymer containing 40% of 1,4-phenylene

nuclei would be considerably stiffened. The reason for this may be connected with the kinking of the rigid segments by 1,2-bonded units. Statistically one in seven units might be thus bonded, and the average length of PPP segments would therefore be seven, corresponding to approximately 30Å for either monomeric unit, close to the maximum persistence length from SANS.

In each technique the transition from free chains to aggregate appears around 40% aromatisation. This corresponds to the limit of solubility of the polymer as would be expected, although in most cases aggregation was noted before this point. The changes in configuration can be clearly illustrated by the change in the power law indices for the various molecular weight/molecular dimension relationships of the form $x=\alpha M_w^i$ where x is the dimension and i is the index (table 8.2).

Method	Dimension	Solvent	0%	10%	20%	30%	40%
ILS	$\langle s^2\rangle^{1/2}_z$	NMP	0.59	0.87	0.82	0.40	0.60
ILS	$\langle s^2\rangle^{1/2}_z$	Chloroform	0.53	0.71	0.48	0.18	0.29
Viscometry	$[\eta]$	NMP	0.61	0.70	1.15	0.35	-
QELS	$R_{h\,w}$	NMP	0.51	0.53	0.64	-	0.28
QELS	$R_{h\,w}$	Chloroform	-	-	-	-	0.34
SANS	$\langle s^2\rangle^{1/2}_z$	NMP	1.37†	0.78	0.84	0.88	0.48‡

†*Distorted value - too high* ‡ *60% aromatisation*

Table 8.2: Comparison of power law indices from different techniques.

In each case the precursor polymer has the property of a typical random coil in a reasonably good solvent. Some increase in the index is then seen with small degrees of aromatisation to around 20/30%. Beyond this i falls as aggregation becomes more significant, to fall below the value for a random coil in the unperturbed state (= 0.5), suggesting the formation of a species more compact than the flexible chain, that is some form of inter- or intra-molecular aggregate. The former is more likely as the transition is accompanied by significant increases in molecular weight. The presence of intramolecular aggregation is possible, but would be difficult to distinguish. The response of the remaining single chains is masked by the behaviour of the larger aggregates.

Evidence form SEC, and from fractionation of a partially aromatised polymer shows that for a polymer at 30% aromatisation, and by extension from 0% to 40%, the type of aromatisation a chain experiences is random, it could cause short sequences or long sequences of PPP to form, and at a given degree of aromatisation it is the nature of the aromatisation, and not the extent of it which determines whether the chain aggregates or not. SEC also shows that as high as 50% there is still free chain material in the polymer, although the aggregates predominate in the behaviour of the solutions.

The nature of the aromatisation does present a number of problems within the study. The mechanism of the reaction is assumed to be autocatalytic[2], that is the presence of a phenylene nucleus catalyses the aromatisation of the neighbouring cyclohexene rings, which would lead to a zipping reaction, with the formation of segments of stiff polyphenylene in a poly(DHCD-DMC) chain. This is supported to some extent by the reaction profiles (fig. 2.5). This leads to the formation of insoluble segments in chains, inevitably causing aggregation to reduce solvent-polymer(PPP) interaction. A more random reaction with spontaneous formation of single phenylene nuclei dispersed throughout the chain would not cause formation of aggregates as a contiguous segment of PPP is required for aggregation to occur, "it is common textbook knowledge that substituents randomly distributed on a chain will strongly prevent lateral aggregation "[3]. The presence of aggregates in solution, detected by SEC to occur in many cases as low as 10% conversion, may therefore be taken as proof of the existence of blocks of phenylene, and therefore evidence of a 'zipping' type reaction during aromatisation. A second feature which interferes with measurement of the aromatisation process is chain degradation. This leads to a decrease in molecular weight beyond that expected from stoichiometry alone, and an increase in polydispersity as smaller fragments are formed, further aggravated by the formation of high molecular weight species. A further feature of chain scission is the randomisation of results, so that the initial order of a set of fractions is lost as they are aromatised. It is possible that the 1,2-bonded 'kinks' in the chain cause this scission, borne out to some extent by the SANS measurements on fully aromatised polymer showing an average chain length of ≈7/8 phenylene units,

comparing well to a 1,2-bonded content of 14%, that is one in seven monomer units. Chain scission at kinks in the chain also effectively increases the stiffness of the polymer, as it contains fewer kinks per unit of contour length, albeit in shorter chains.

The measurements are therefore performed against a background of not only increasing stiffness, but also increasing polydispersity and aggregation, and decreasing molecular weight. The net result is an increase in scatter of values measured as aromatisation proceeds, therefore a greater uncertainty in fitting any theoretical relationship to the data. This has been the case with each of the experimental technique used.

The theoretical relationships which exist in the main apply to random coil polymers, therefore extraction of molecular parameters for the unaromatised polymer is straightforward and the data of higher quality, a lesser number of relationships exist for wormlike chains, and those for random coils are on the whole inapplicable (section 5.5). There appears to be virtually no work done on determining theoretical relationships for aggregated polymers, hardly surprising given the potential scope and complexity of the field. This means the bulk of the analysis has been performed on the less aromatised polymer, while the aggregated polymer has been necessarily neglected- even to the extent that the nature of the aggregates is uncertain. It has been stated in the text that the aggregates are micelles, of the fringed micelle variety (fig. 3.8). This is based on three factors, firstly the regularity of the aggregates, seen in the narrow distribution observed in SEC and QELS leading to the assumption of a degree of order in the aggregates. Secondly the goodness of fit of SANS data from the aggregates to a star type structure with arms of Gaussian statistics is evidence that the precursor polymer is not involved in the aggregation, but remains solvated to the maximum extent possible as the arms of the star, the halo of a fringed micelle. Finally the presence of blocks of poly(paraphenylene) would cause the formation of tightly packed, even partially crystallised domains within the aggregate solution, ideal cores for fringed micelles.

The study of polymeric aggregates is on the whole a rather neglected field, probably because of the inherent complexity of the subject. Those studies which have been made tend to concentrate on well defined, monodisperse polymer samples, reducing the

number of variables in the study. A study of the aggregates described in this study, where they are composed of polymers of only approximately known structures of unknown size will naturally be far more complex.

In a recent review Burchard[4] defines six classes of polymeric aggregates of three types, of these four would be applicable to synthetic polymers. These are illustrated in figure 8.1

1) Random associates, associates of flexible molecules by point contacts

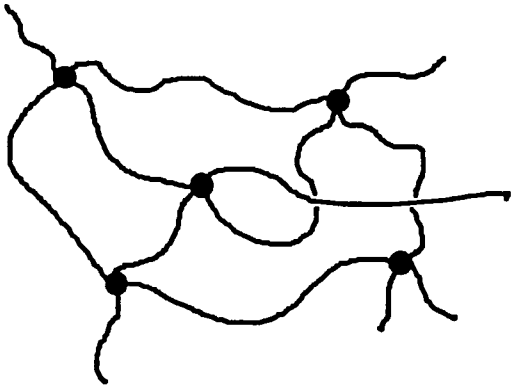

2) End to end associates of linear flexible chains

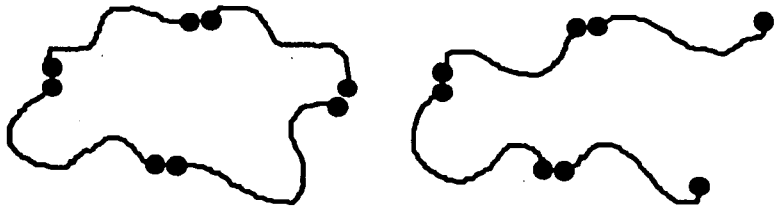

3) Micelles

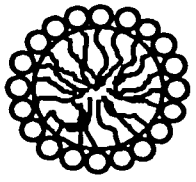

i. spherical

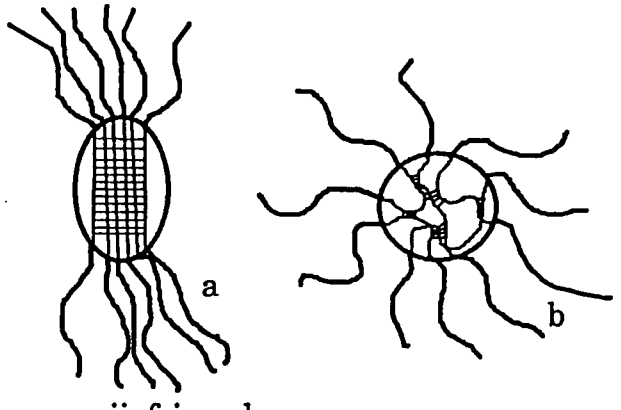

ii. fringed

Figure 8.1: Types of polymeric aggregates

With regard to the study of aromatised poly(DHCD-DMC) 1 is unlikely, as it is assumed that sequences of poly(paraphenylene) form, single or a few contiguous units of PPP

would be soluble, therefore less likely to aggregate. Type 2 is also unlikely, it is improbable that only the end units of polymer would aromatise, then even more unlikely that they would aggregate end to end. This leaves the micelle as a possible structure for the aggregates in this study , and indeed this has been suggested previously (section 3.5). However two types of micelles are presented, spherical and fringed. The spherical micelle is that formed by concentrated surfactant solutions, with a hydrophobic head and a hydrophilic tail, the tails cluster, minimising interactions with water to form an aggregate the surface of which consists of the hydrophilic heads. These are spherical and have well defined aggregation numbers. This structure can form from diblock copolymers in selective solvents by microphase separation of the insoluble blocks, but requires a greater degree of regularity from the substituent molecules than could be expected from partially aromatised poly(DHCD-DMC). This leaves the fringed micelle, with a core of oriented segments, and disordered chains at the end forming a halo. This structure is frequently assumed for multiblock copolymers in selective solvents, as well as biopolymers with ordered(helical) and disordered(random coil) sections. The fringed micelle itself might have a structure of either a or b, a compact linear core with disordered chains emerging from the ends, or a more random microgel type structure with a less ordered core, and disordered chains emergent from all around the core. In the micelles of block copolymers of two random coil polymers the core may be swollen to some extent with solvent molecules, and the chains within the core will not form supra-molecular structures. The situation within the rod-coil block copolymer micelle is likely to be somewhat different. The rodlike structure, such as poly(paraphenylene), will have a great propensity for coalescing in an ordered, perhaps even crystalline, manner. This tendency will be further increased when as with PPP the polymer is extremely insoluble and will exclude solvent from the core. A degree of order for the chains within a micellar core will cause the core to be of quite considerable density in relation to the solvated halo, and is responsible for the peak seen in the Kratky plots of the SANS data for such aggregates (figure 7.14).

The instrumental methods used in this work have varied degrees of applicability to the study of the aggregates that were formed. Studies of micelles using size exclusion chromatography appear to be rare. At first glance it might seem an ideal method of study, molecules are partitioned solely in terms of hydrodynamic radii, and can then be analysed in a number of ways, including true molecular weight or a selective technique(such as monochromatic UV), and presented as a size distribution. Using the combination of a LALLS detector and a R_h *vs* elution time calibration curve it is possible that results could be obtained in the form of a M_w or $\langle s^2 \rangle^{1/2}$ *vs* R_h distribution. The distribution of particle size obtained in this study showed clearly the presence of high molecular weight species within the samples, a similar result has been observed in a study of a rod-coil copolymer, again with a PPP rod segment with a PS coil segment[5]. The authors report the size distribution of a molecule containing a PS sequence of molecular weight 25000, and a PPP block of molecular weight 3000, but kinked, with a mean sequence length of 11 units in the para-conformation gives a peak at around 25000, attributed to P(DHCD)-co-PS precursor, and 10×10^6, corresponding to aggregates, which were found to be isotropic.

Price studied a PS-co-(PE-co-PP) copolymer over a range of temperatures[6]. At 50°C the authors report an elution time of 5hrs, and the micelles elute as a sharp peak, suggesting the rate of micelle dissociation is very slow with strong shielding of the core by the halo. However Duplessix and Jalal studying micelles of an ionomer obtained the molecular weight of the free polymer chains for micellar solutions[7], and suggest the shear gradient within the column is responsible for their disintegration.

This uncertainty may be the reason for the paucity of SEC studies of micelles, scattering techniques cause no perturbation of the polymer solution, and viscosity techniques minimum perturbation, but depending on the flow rate and the column packing density SEC may subject the aggregate to considerable external forces. These could cause dissociation, depending on the cohesive forces in the micelle, or possibly even further aggregation.

Intensity light scattering presents a much less ambiguous method of study, simply measuring molecular weight, radius of gyration and virial coefficients. This method has been widely used to measure aggregates. A phenomena which is commonly observed with micelle solutions however is a non-linear concentration dependence of (Kc/R_θ) as $\theta \rightarrow 0$[8]. This occurs with coil-coil block copolymers in selective solvents, for example PS-co-PI in n-decane[9], PS-co-(PE-co-PP) in heptane[10], PVB in methanol[11], and PS-co-PE-co-PS in heptane[12]. These polymer/solvent systems display the critical micelle concentration behaviour of soap micelles, below the CMC the polymer exists largely as free chains, above it they exist as micelles. This behaviour was not observed for the polymers in this study (section 4.4.4). Non CMC behaviour, or limited CMC behaviour in poor or selective solvents is observed in other studies, Francois and Zhong[5] report that there was no CMC for PPP-co-PS, although high temperature(100°C) increased the solvation sufficiently to disperse the aggregates partially. The use of high temperature was not used in this study as it would have caused further aromatisation. Non CMC behaviour was also observed for solutions of polydiacetylenes in poor solvents[13] (in which PDA is supposed to adopt a rodlike configuration) even at concentrations as low as 5ppm. It is notable that those polymers displaying CMC behaviour are coil-coil copolymers, while those with non CMC behaviour contain rigid rod segments. This suggests a fundamental difference in the aggregates of rods. It is suggested by some authors that aggregates of polysilanes[14], polydiacetylenes[13,15]and PBT[16]are due to a crystalline-like arrangement with rods aligned in parallel arrays, For thermodynamic reasons these would be reluctant to dissociate, even at vanishingly low concentrations, hence the lack of CMC behaviour. This is likely to be the case for partially aromatised poly(DHCD-DMC) especially if, as is conjectured, the aromatisation reaction produces long sequences of PPP, between which polymer-polymer interactions are vastly more favourable than those of polymer-solvent. From the evidence of this study and those of other authors it would appear that polymers with significant electron delocalisation along the chain will always be insoluble, unless modified as block copolymers which form micelles, or with sufficiently side groups attached.

Neutron and X-ray scattering techniques also prove useful tools for studying micelle-like polymer aggregates. Small angle scattering methods probe a wide range of length scales that include the overall dimensions of the polymer, together with the internal structure. This does lead to a greater scope for studying the micelles than ILS. The use of SAXS and SANS with coil-coil block copolymers can determine the dimensions of the core and halo of the spherical micelles formed[17,18] and the internal structure of the core[19] and the halo[18] of the micelles. These studies used polymer of well defined and narrow polydispersity, in contrast to the studies made on micelle forming rigid rod polymers.

The studies of PDA[13] PSi[14], in which the polymer exists as a free chain in good solvent and polyconjugated aggregates in poor solvent, were achieved with a single solvent over a temperature range, heating improving solvent power. It had been speculated that the changes in the UV/visible spectra of these polymers were due to the formation of rigid rod polymers[20,21]. SANS and SAXS studies showed both polymers to adopt a wormlike configuration in the good solvent, however in neither case was the rigid rod configuration found in the poor solvent, and the true nature of the polymer in both cases was found to be an aggregate. In the case of PDA it is suggested that the aggregate is of the fringed micelle type. Aggregation is caused by the formation of sections of rigid structure, while some of the polymer remains in a random coil configuration, in a manner similar to the behaviour of biopolymers such as poly(γ-benzyl-l-glutamate)[22] and is analogous to the situation of partially aromatised poly(DHCD-DMC).

A notable feature of the scattering functions of such aggregates is a sharp upturn in scattering at low Q, corresponding to the peak in the Kratky plots. This is seen in this study(section 7.7) and for coil-coil[18] and rod-coil[13,14] block copolymer aggregates. This represents an enhancement in the radial segment density over the random coil halo.

Analysis of SANS data from aggregates can be usefully extended by fitting models to the experimental scattering functions. The most simple model is that of the star polymer, used in section 7.7. More complex models have been developed, enlarging on the star polymer to include such factors as the core radius, and configuration of the arms in the halo[23,24]. These more complex models were not used in this study as they require well

defined, narrow molecular weight distribution polymer samples. The model of the star polymer excludes such variables as chain stiffness in the arms, or contrast between the core and the halo, however in this work it was found to produce an approximate fit.

The study of the aggregates formed between 40% and 80% aromatisation is difficult to study, but is worthy of some consideration. The building blocks are the aromatised polymer chains. It has been previously suggested that chain scission occurs at ortho bonded units in the backbone, some possibly during the 'zipping' aromatisation, so that for a molecule that has undergone considerable aromatisation, and therefore considerable scission, it may be imagined that it contains long PPP sequences, some of which may be terminal. Remaining poly(DHCD-DMC) may also be assumed to be mainly in contiguous sequences, hence the overall chain is a block copolymer, di-, tri-, or even poly-block. If this situation is compared to literature studies of similar synthetic polymers there appears to be few similar cases. Halperin describes theoretical aspects of such polymers[3], and states that immiscible blocks tend to pack with their axes aligned and their tips forming a plane surface to minimise their surface free energy. Depending on the regularity of the PPP blocks the core of the aggregate will tend towards a flat ended sphere, the soluble arms emerging from the ends. The possibility of a polyblock copolymer would cause either multiple entry to a single core for a single chain, forming loops in the halo region, or a microgel type core with several cylindrical sub-cores. Given the sharp increase in size from 40% to 80% aromatisation it may be that there is a change from single to multiple cores as aromatisation increases.

8.1 Suggestions for further study

If this study were to be continued along the lines of the original proposal, that is to study a coil to rod transition for a poly(phenylene) precursor polymer it would be necessary to remove some of the variables which blur the configurational changes. The major problems are degradation and aggregation, with increasing polydispersity symptomatic of both. The only solution would be to choose another form of the polymer. Model block copolymers could be synthesised using the method of François and Zhong[5],

preparing a range of PS/PPP copolymers representing a range of percentage aromatisation, with PS in the rôle of poly(DHCD-DMC). This would eliminate the effects of polydispersity, but constrains the copolymer structure to a diblock, and would be liable to aggregation, unless random copolymers could be synthesised.

Aggregation of partially aromatised poly(DHCD-DMC) could be reduced if DHCD-DMC were copolymerised with a different DHCD derivative, the acetate for example, which would aromatise less readily, and therefore interrupt block sequences of PPP. This could also increase the limit of solubility above 40%. This still leaves the problem of chain scission, although this might be less if 'zipping' reactions are eliminated.

Chain scission could be reduced if a lower molecular weight polymer were used, in the region $2 \rightarrow 50 \times 10^3$ for example, as the amount of chain scission was less for lower molecular weight fractions. This would also reduce the convergence of molecular weights with aromatisation which hampered the determination of molecular weight dependencies as the range of M_w available decreased.

Any further study would therefore need to focus on which aspect were of interest, and then to produce samples as necessary, so that if the stiffest possible non-aggregated chains were required a reactive/non reactive DHCD derivative copolymer would be suitable, and if the precise structure of chains or aggregates was required narrow dispersity model compounds were be of greater use.

Application of instrumental methods could be altered, if SANS were to be used to measure persistence alone, using dilute solutions with very long counting times on a suitable machine for which time is limited, measurement of M_w and $\langle s^2 \rangle^{1/2}$ for a range of fractions could be restricted to ILS, for which ample machine time is available.

8.3 References

1, Brelsford,G.L.,Krigbaum,W.R.,Ch.2 in '*Liquid Crystallinity in Polymers Principles and Fundamental Properties*',Ed Cifferri,A.,VCH Publishers, New York,1991

2, Ballard,D.G.H,Courtis,A.,Shirley,I.M.Taylor,S.C.,*Macromolecules*,**21**,294,(1989).

3, Halperin ,A.,*Macromolecules*,23,2724,(1990).

4, Burchard,W.,*Trends in Polymer Science*,**1**,192,(1993).

5, François,B., Zhong,X.F., *Synth. metals.*, **28**,E35,(1989).

6, Booth,C.,Hudd,A.L.,Price,C.,Wright,B.,*Polymer Comm.*, **23**,650,(1982).

7, Duplessix,R.,Jalal,N.,*J.Phys.France.*,**49**,1775,(1988).

8, Elias,H.G., Ch.9 in '*Light Scattering From Polymer Solutions*',Ed Huglin, M.B.,Academic press, London,1972.

9, Lally,T.P.,McAdam,J.D.G.,Price,C.,Woods,D.,*Polymer*,**15**,228,(1973).

10, Frank,C.W,Yeung,A.S.,*Polymer*,**31**,2089(1990).

11, Cotts,P.M.,Paul,C.W.,*Macromolecules*,**19**,692,(1986).

12, Tuzar,Z. *et al,Polymer*,**31**,2118,(1990).

13, Aimé J.P. *et al, J.Phys.France.*,**49**,891,(1988).

14, Shukla,P. *et al,Macromolecules*,**24**,5606,(1991).

15, Müller,M.A.,Schmidt,M.,Wegner,G.,Wenz,G.,*Macromolecules*,**17**,837,(1984).

16, Berry et al, *J.Polym.Sci.,Polym. Phys.Ed.*,**21**,913(1983).

17, Brown,D.S.,Dawkins,J.V.,Farnell,A.S.,Taylor,G.,*Eur.Polym.J.*,**23**,463,(1987).

18, Cogan,K.A.,Gast,A.P.,Capel,M.,*Macromolecules*,**24**,6512(1991).

19, Dawkins,J.V.,Higgins,J.S.,Maghami,G.G.,Shakir,S.A.,*Polymer*,**27**,931,(1986).

20, Patel,G.N.Khanna,Y.P.,Witt,J.D.,*J.Polym.Sci.,Polym.Lett.Ed.*,**18**,1383,(1980).

21, Harrah,L.A.,Ziegler,J.M.,*J.Poly.Sci.,Polym Lett. Ed.*,**23**,209,(1985).

22, Muroga,Y. et al,*Macromolecules*,**21**,2756,(1985)

23, Cotton,J.P.,Daoud,M.,*J.Phys.(Paris)*,**43**,531,(1982).

24, Hirata,M.,Tsunashima,Y.,*Macromolecules*,**22**,249,(1989).

Appendices

1: Units used in text and SI equivalents

The units used in this work follow the usual practice within the polymer literature, and do not follow the SI units for clarity's sake. A list is therefore given of the units used together with their SI equivalent.

Unit	Abbreviation	SI equivalent	conversion factor
Angstrom	Å	metre	$\times 10^{-10}$
Degree Celsius	°C	degree Kelvin	+ 273.15
Cubic centimetre	cm^3	cubic metre	$\times 10^{-9}$
Millilitre	ml	cubic metre	$\times 10^{-9}$
Gram	g	kilogram	$\times 10^{-3}$
Centipoise	cps	Pascal-second	$\times 10^{-3}$

No units have used for molecular weights of polymers, values quoted are relative molecular masses, ie;

$$\text{mass quoted} = \frac{\text{molar mass of polymer (Daltons)}}{\text{mass of } {}^{12}C \text{ nuclei (Daltons)}}$$

2: Definition of molecular weight averages

Molecular masses (and other properties) of synthetic polymers are necessarily averages values, and a number of different averages are used. For a system containing N_i molecules of the *i*th species of molecular weight M_i then the averages used are defined as;

Number average: $$M_n \equiv \sum_i x_i M_i \equiv \frac{\sum_i N_i M_i}{\sum_i N_i}$$ where x_i = mole fraction

Weight average: $$M_w \equiv \sum_i y_i M_i \equiv \frac{\sum_i N_i M_i^2}{\sum_i N_i}$$ where y_i = mass fraction

Z-average: $$M_z \equiv \frac{\sum_i N_i M_i^3}{\sum_i N_i^2}$$

Similar relationships define the averages for radii of gyration, hydrodynamic radii, and diffusion coefficients.

3: Radius of gyration

The radius of gyration is a quantity to characterise the size of a body of any shape. It is defined as;

$$\left\langle s^2 \right\rangle^{1/2} = \frac{\left\langle \sum_i m_i r_i^2 \right\rangle^{1/2}}{\left(\sum_i m_i \right)^{1/2}}$$

where m is the mass of an element distance r from the centre of mass

4: Constants

Below are given the constants used within the text;

Name	Symbol	Value	Units
Avogadro's number	N_A	6.0226×10^{23}	mol^{-1}
Boltzmann's constant	k	1.3805×10^{-23}	$J K^{-1}$
Planck's constant	h	6.6255×10^{-34}	$J Hz^{-1}$
	$\hbar$	1.0546×10^{-34}	$J s^{-1}$
Pi	π	3.1416	
Base of natural log	e	2.7183	

5: Abbreviations

A number of undefined abbreviations have been used in the text. Most of these are in common usage within polymer science and refer to polymer types. A list of such abbreviations, together with those defined within the text but frequently used and are given below.

CMC: critical micelle concentration

ILS: intensity light scattering

LALLS: low angle laser light scattering

M_w: weight average molecular weight

NMP: N-methyl pyrrolidinone

PBLG: poly(γ-benzyl-l-glutamate)

PBT: polybenzothiazole

PD: polydispersity, M_w/M_n

PDA: polydiacetylene

PE-co-PP: poly(ethylene-co-propylene) (hydrogenated polyisoprene)

PHIC: poly(hexyl isocyanate)

poly(DHCD-DMC): poly(5,6-cis-dimethylcarboxycyclohexa-1,3-diene)

PPP: poly(paraphenylene)

PS: poly(styrene)

PSi: polysilane

PVB: poly(vinyl butyrate)

Q: scattering vector

QELS: quasi-elastic light scattering

$\langle s^2 \rangle^{1/2}$: mean square radius of gyration

$\langle r^2 \rangle^{1/2}$: mean square end to end distance

SANS: small angle neutron scattering

SAXS: small angle X-ray scattering

SEC: size exclusion chromatography

UNIVERSITY OF DURHAM

Board of Studies in Chemistry

COLLOQUIA, LECTURES AND SEMINARS GIVEN BY INVITED SPEAKERS 1ST AUGUST 1989 TO 31ST JULY 1990

BADYAL, Dr. J.P.S. (Durham University) Breakthoughs in Heterogeneous Catalysis	1st November, 1989
BECHER, Dr. J. (Odense University) Synthesis of New Macrocylic Systems using Heterocyclic Building Blocks	13th November, 1989
BERCAW, Prof. J.E. (California Institute of Technology) Synthetic and Mechanistic Approaches to Ziegler–natta Polymerization of Olefins	10th November, 1989
BLEASDALE, Dr. C. (Newcastle University) The Mode of Action of some Anti–tumour Agents	21st February, 1990
BOWMAN, Prof. J.M. (Emory University) Fitting Experiment with Theory in Ar–OH	23rd March, 1990
BUTLER, Dr. A. (St. Andrews University) The Discovery of Penicillin: Facts and Fancies	7th December, 1989
CHEETHAM, Dr. A.K. (Oxford University) Chemistry of Zeolite Cages	8th March, 1990
CLARK, Prof. D.T. (ICI Wilton) Spatially Resolved Chemistry (using Natures's Paradigm in the Advanced Materials Arena)	22nd February, 1990
COLE–HAMILTON, Prof. D.J. (St. Andrews University) New Polymers from Homogeneous Catalysis	29th November, 1989
CROMBIE, Prof. L. (Nottingham University) The Chemistry of Cannabis and Khat	15th February, 1990
DYER, Dr. U. (Glaxo) Synthesis and Conformation of C–Glycosides	31st January, 1990
FLORIANI, Prof. C. (University of Lausanne, Switzerland) Molecular Aggregates – A Bridge between homogeneous and Heterogeneous Systems	25th October, 1989
GERMAN, Prof. L.S. (USSR Academy of Sciences – Moscow) New Syntheses in Fluoroaliphatic Chemistry: Recent Advances in the Chemistry of Fluorinated Oxiranes	9th July, 1990
GRAHAM, Dr. D. (B.P. Reserch Centre) How Proteins Absorb to Interfaces	4th December, 1989
GREENWOOD, Prof. N.N. (University of Leeds) Novel Cluster Geometries in Metalloboron Chemistry	9th November, 1989

HOLLOWAY, Prof. J.H. (University of Leicester) — 1st February, 1990
Noble Gas Chemistry

HUGHES, Dr. M.N. (King's College, London) — 30th November, 1989
A Bug's Eye View of the Periodic Table

HUISGEN, Prof. R. (Universität München) — 15th December, 1989
Recent Mechanistic Studies of [2+2] Additions

KLINOWSKI, Dr. J. (Cambridge University) — 13th December 1989
Solid State NMR Studies of Zeolite Catalysts

LANCASTER, Rev. R. (Kimbolton Fireworks) — 8th February, 1990
Fireworks – Principles and Practice

LUNAZZI, Prof. L. (University of Bologna) — 12th February, 1990
Application of Dynamic NMR to the Study of Conformational Enantiomerism

PALMER, Dr. F. (Nottingham University) — 17th October, 1989
Thunder and Lightning

PARKER, Dr. D. (Durham University) — 16th November, 1989
Macrocycles, Drugs and Rock 'n' roll

PERUTZ, Dr. R.N. (York University) — 24th January, 1990
Plotting the Course of C–H Activations with Organometallics

PLATONOV, Prof. V.E. (USSR Academy of Sciences – Novosibirsk) — 9th July, 1990
Polyfluoroindanes: Synthesis and Transformation

POWELL, Dr. R.L. (ICI) — 6th December, 1989
The Development of CFC Replacements

POWIS, Dr. I. (Nottingham University) — 21st March, 1990
Spinning off in a huff: Photodissociation of Methyl Iodide

ROZHKOV, Prof. I.N. (USSR Academy of Sciences – Moscow) — 9th July, 1990
Reactivity of Perfluoroalkyl Bromides

STODDART, Dr. J.F. (Sheffield University) — 1st March, 1990
Molecular Lego

SUTTON, Prof. D. (Simon Fraser University, Vancouver B.C.) — 14th February, 1990
Synthesis and Applications of Dinitrogen and Diazo Compounds of Rhenium and Iridium

THOMAS, Dr. R.K. (Oxford University) — 28th February, 1990
Neutron Reflectometry from Surfaces

THOMPSON, Dr. D.P. (Newcastle University) — 7th February, 1990
The role of Nitrogen in Extending Silicate Crystal Chemistry

UNIVERSITY OF DURHAM

Board of Studies in Chemistry

COLLOQUIA, LECTURES AND SEMINARS GIVEN BY INVITED SPEAKERS
1ST AUGUST 1988 to 31st JULY 1989

AVEYARD, Dr. R. (University of Hull) Surfactants at your Surface	15th March, 1989
AYLETT, Prof. B.J. (Queen Mary College, London) Silicon-Based Chips:- The Chemist's Contribution	16th February, 1989
BALDWIN, Prof. J.E. (Oxford University) Recent Advances in the Bioorganic Chemistry of Penicillin Biosynthesis	9th February, 1989
BALDWIN & WALKER, Drs. R.R. & R.W. (Hull University) Combustion: Some Burning Problems	24th November, 1988
BUTLER, Dr. A.R. (St. Andrews University) Cancer in Linxiam: The Chemical Dimension	15th February, 1989
CADOGAN, Prof. J.I.G. (British Petroleum) From Pure Science to Profit	10th November, 1988
CASEY, Dr. M. (University of Salford) Sulphoxides in Stereoselective Synthesis	20th April, 1989
CRICH, Dr. D. (University College London) Some Novel Uses of Free Radicals in Organic Synthesis	27th April, 1989
DINGWALL, Dr. J. (Ciba Geigy) Phosphorus-containing Amino Acids: Biologically Active Natural and Unnatural Products	18th October, 1988
ERRINGTON, Dr. R.J. (University of Newcastle-upon-Tyne) Polymetalate Assembly in Organic Solvents	1st March, 1989
FREY, Dr. J. (Southampton University) Spectroscopy of the Reaction Path: Photodissociation Raman Spectra of NOCl	11th May, 1989
* GRADUATE CHEMISTS. (Polytechs and Universities in North East England) R.S.C. Symposium for presentation of papers by postgraduate students	12th April, 1989
* HALL, Prof. L.D. (Addenbrooke's Hospital, Cambridge) NMR - A Window to the Human Body	2nd February, 1989
* HARDGROVE, Dr. G. (St. Olaf College, U.S.A.) Polymers in the Physical Chemistry Laboratory	December, 1988
HARWOOD, Dr. L. (Oxford University) Synthetic Approaches to Phorbols Via Intramolecular Furan Diels-Alder Reactions: Chemistry under Pressure	25th January, 1988

ROGER, Dr. [illegible] (Friedrich-Schiller University GDR) NMR Investigations of Fast Ion Conductors of the NASICON Type	5th December, 19[illegible]
JENNINGS, Prof. R.R. (Warwick University) Chemistry of the Masses	26th January, 19[illegible]
JOHNSON, Dr. B.F.G. (Cambridge University) The Binary Carbonyls	23rd February, 19
LUDMAN, Dr. C.J. (Durham University) The Energetics of Explosives	18th October, 19[illegible]
MACDOUGALL, Dr. J. (Edinburgh University) Vibrational Spectroscopy of Model Catalytic Systems	22nd February, 19
MARKO, Dr. I. (Sheffield University) Catalytic Asymmetric Osmylation of Olefins	9th March, 1989
McLAUCHLAN, Dr. K.A. (University of Oxford) The Effect of Magnetic Fields on Chemical Reactions	16th November, 19
MOODY, Dr. C.J. (Imperial College) Reactive Intermediates in Heterocyclic Synthesis	17th May, 1989
PAETZOLD, Prof. P. (Aachen) Iminoboranes XB≡NR: Inorganic Acetylenes?	23rd May, 1989
PAGE, Dr. P.C.B. (University of Liverpool) Stereocontrol of Organic Reactions Using 1,3-dithiane-1-oxides	3rd May, 1989
POLA, Prof. J. (Czechoslovak Academy of Sciences) Carbon Dioxide Laser Induced Chemical Reactions - New Pathways in Gas-Phase Chemistry	15th June, 1989
REES, Prof. C.W. (Imperial College London) Some Very Heterocyclic Compounds	27th October, 1988
SCHMUTZLER, Prof. R. (Technische Universitat Braunschweig) Fluoropnosphines Revisited - New Contributions to an Old Theme	6th October, 1988
* SCHROCK, Prof. R.R. (M.I.T.) Recent Advances in Living Metathesis	13th February, 1989
SINGH, Dr. G. (Teesside Polytechnic) Towards Third Generation Anti-Leukaemics	9th November, 1988
SNAITH, Dr. R. (Cambridge University) Egyptian Mummies: What, Where, Why and How?	1st December, 1988
STIBR, Dr. B. (Czechoslovak Academy of Sciences) Recent Developments in the Chemistry of Intermediate-Sited Carboranes	16th May, 1989
VON RAGUE SCHLEYER, Prof. P. (Universitat Erlangen Nurnberg) The Fruitful Interplay Between Calculational and Experimental Chemistry	21st October, 1988
WELLS, Prof. P.B. (Hull University) Catalyst Characterisation and Activity	10th May, 1989

UNIVERSITY OF DURHAM
Board of Studies in Chemistry
Colloquia,Lectures and Seminars given by Invited Speakers

1990

October 11	Dr.W.A.MacDonald, (ICI, Wilton). Materials for the Space Age.
October 24	Dr.M.Bochmann, (University of East Anglia). Synthesis, Reactions and Catalytic Activity of Cationic Titanium Alkyls.
October 26	Prof.R.Soulen, (South Western University, Texas). Preparation and Reactions of Bicycloalkenes.
October 31	Dr.R.Jackson, (Newcastle University). New Synthetic Methods: α-Amino Acids and Small Rings.
November 1	Dr.N.Logan, (Nottingham University). Rocket Propellants.
November 6	Dr.P.Kocovsky, (Uppsala University) Stereo-Controlled Reactions Mediated by Transistion and Non-Transistion Metals.
November 7	Dr.D.Gerrard, (British Petroleum). Raman Spectroscopy for Industrial Analysis.
November 8	Dr.S.K.Scott, (Leeds University). Clocks. Oscillations and Chaos.
November 14	Prof.T.Bell, (SUNY, Stoney Brook, USA). Functional Molecular Architectures and Molecular Recognition.
November 21	Prof.J.Pritchard, (Queen Mary & Westfield College, London University). Copper Surfaces and Catalysts.
November 28	Dr.B.J.Whitaker, (Leeds University). Two-Dimensonal Velocity Imaging of State-Selected Reaction Products.
November 29	Prof.D.Crout, (Warwick University). Enzymes in Organic Synthesis.
December 5	Dr.P.G.Pringle, (Bristol University). Metal Complexes with Functionlised Phosphines.
December 13	Prof.A.H.Cowley, (University of Texas). New Organometallic Routes to Electronic Materials.

1991

January 15	Dr.B.J.Alder, (Lawerence Livermore Labs. California). Hydrogen in all its Glory.
January 17	Dr.P.Sarre, (Nottingham University). Comet Chemistry.

January 24	Dr.P.J.Sadler, (Birkbeck College London). Design of Inorganic Drugs: Precious Metals, Hypertension and HIV.
January 30	Prof.E.Sinn, (Hull University). Coupling of Little Electrons in Big Molecules. Implications for the Active Site of (Metalloproteins and other) Macromolecules.
January 31	Dr.D.Lacey, (Hull University). Liquid Crystals.
February 6	D.R.Bushby, (Leeds University). Biradicals and Organic Magnets.
February 14	Dr.M.C.Petty, (Durham University). Molecular Electronics.
February 20	Prof.B.L.Shaw, (Leeds University). Syntheses with Coordinated, Unsaturated Phosphine Ligands.
February 28	Dr.J.Brown, (Oxford University). Can Chemistry Provide Catalysts Superior to Enzymes?
March 6	Dr.C.M.Dobson, (Oxford University). NMR Studies of Dynamics in Molecular Crystals.
March 7	Dr.J.Markam, (ICI Pharmaceticals). DNA Fingerprinting.
April 24	Prof.R.R.Schrock, (Massachusettes Institute of Technology). Metal-Ligand Multiple Bonds and Metathesis Initiators.
April 25	Prof.T.Hudlicky, (Virginia Polytechnic Institute). Biocatalysts ans Symmetry Based Approaches to the Efficient Synthesis of Complex Natural Products.
June 20	Prof.M.S.Brookhart, (University of N.Carolina). Olefin Polymerisations, Oligomerisations and Dimerisations using Electrophilic Late Transistion Metal Catalysts.
July 29	Dr.M.A.Brimble, (Massey University, New Zealand). Synthetic Studies Towards the Antibiotic Griseusin-A.
October 17	Dr.J.A.Salthouse, (University of Manchester). Son et Lumiere-A Demonstration Lecture.
October 31	Dr.Keeley, (Metropolitian Police Forensic Science). Modern Forensic Science.
November 6	Prof.B.F.G.Johnson, (Edinburgh University). Cluster-surface Analogies.
November 7	Dr.A.R.Butler, (St.Andrews University). Traditional Chinese Herbal Drugs: A Different Way of Treating Disease.
November 13	Prof.D.Gani, (St.Andrews University). The Chemistry of PLP Dependent Enzymes.

November 20	Dr.R.More O'Ferrall, (University College, Dublin). Some Acid-Catalysed Rearrangements in Organic Chemistry.
November 28 **SCI Lecture**	Prof.I.M.Ward, (IRC in Polymer Science, Leeds University). The Science and Technology of Orientated Polymers.
December 4	Prof.R.Grigg, (Leeds University). Palladium-Catalysed Cyclisation and Ion-Capture Processes.
December 5	Prof.A.L.Smith, (Ex. Unilever). Soap, Detergents and Black Puddings.
December 11	Dr.W.D.Cooper, (Shell Research). Colloid Sceiene: Theory and Practice.

1992

January 22	Dr.K.D.M.Harris, (St.Andrews University). Understanding the Properties of Solid Inclusion Compounds.
January 29	Dr.A.Holmes, (Cambridge University). Cycloaddition Reactions in the Service of the Synthesis of Piperidine and Indolizine Natural Products.
January 30	Dr.M.Anderson, (Sittingbourne, Shell Research). Recent Advances in the Safe and Selective Chemical Control of Insect Pests.
February 12	Prof.D.E.Fenton, (Sheffield University). Polynuclear Complexes of Molecular Clefts as Models for Copper Biosites.
February 13	Dr.J.Saunders, (Glaxo Group Research Limited). Molecular Modelling in Drug Discovery.
February 19	Prof.E.J.Thomas, (University of Manchester). Applications of Organostannanes to Organic Synthesis.
February 20 **Musgrave Lecture**	Prof.E.Vogel, (University of Cologne). Porphyrins: Molecules of Interdisciplinary Interest.
February 25 **Tilden Lecture:**	Prof.J.F.Nixon, (University of Sussex). Phosphaalkynes: New Building Blocks in Organic and Organometallic Chemistry.
February 26	Prof.M.L.Hitchman, (Strathcylde University). Chemical Vapour Deposition.
March 5	Dr.N.C.Billingham, (University of Sussex). Degradable Plastics-Myth or Magic.
March 11	Dr.S.E.Thomas, (Imperial College). Recent Advances in Organoiron Chemistry.
March 12	Dr.R.A.Hann, (ICI Imagedata). Electronic Photography-An Image of the Future.

March 18	Dr.H.Maskill, (Newcastle University). Concerted or Stepwise Fragmentation in a Deamination-type Reaction.
April 7	Prof.D.M.Knight, (University of Durham). Interpreting Experiments: The Beginning of Electrochemistry.
May 13	Dr.J-C.Gehret, (Ciba Geigy, Basel). Some Aspects of Industrial Agrochemical Research.
October 15	Dr.M.Glazer and Dr.S.Tarling, (Oxford University and Birbeck College). It Pays to be British!- The Chemist's Role as an Expert Witness in Patent Litigation.
October 20	Dr.H.E.Bryndza, (Du Pont Central Research). Synthesis.Reactions and Thermochemistry of Metal(alkyl)cyanide Complexes and Their Impact on Olefin Hydrocyanation Catalysts.
October 22 **Ingold-Albert Lecture**	Prof. A.G.Davies, (University College, London). The Behaviour of Hydrogen as a Pseudometal.
October 28	Dr.J.K.Cockroft, (Durham University). Recent Developments in Powder Diffraction.
October 29	Dr.J.Emsley, (Imperial College, London). The Shocking History of Phosphorus.